



TECHNISCHE
UNIVERSITÄT
WIEN

Dissertation

Development and Dynamic Simulation of a Variable-Ratio Transmission System for the UH-60 Helicopter

carried out for the purpose of obtaining the degree of Doctor technicae (Dr. techn.),
submitted at TU Wien, Faculty of Mechanical and Industrial Engineering,
by

Dipl.-Ing. Pierre Paschinger

e00726669

Schaichgasse 19, 3804 Allentsteig, Austria

under the supervision of

Univ.Prof. Dipl.-Ing. Dr.-Ing. Michael Weigand

Institute for Engineering Design and Product Development, E307

reviewed by

Prof. Dr.-Ing. Berthold Schlecht
Institut für Maschinenelemente und
Maschinenkonstruktion
Technische Universität Dresden
Münchner Platz 3,
01187 Dresden,
Germany

Prof. Giorgio Guglieri, Ph.D.
Dipartimento di Ingegneria
Meccanica e Aerospaziale
Politecnico di Torino
Corso Duca degli Abruzzi, 24,
10129 Torino TO,
Italy



Die approbierte gedruckte Originalversion dieser Dissertation ist an der TU Wien Bibliothek verfügbar.
The approved original version of this doctoral thesis is available in print at TU Wien Bibliothek.

This work was supported by Österreichische Forschungsförderungsgesellschaft FFG within the framework of the project VARI-SPEED (grant number 850442).

I confirm, that going to press of this thesis needs the confirmation of the examination committee.

Affidavit

I declare in lieu of oath, that I wrote this thesis and performed the associated research myself, using only literature cited in this volume. If text passages from sources are used literally, they are marked as such. I confirm that this work is original and has not been submitted elsewhere for any examination, nor is it currently under consideration for a thesis elsewhere.

Wien, Wednesday 26th June, 2019



Die approbierte gedruckte Originalversion dieser Dissertation ist an der TU Wien Bibliothek verfügbar.
The approved original version of this doctoral thesis is available in print at TU Wien Bibliothek.

Acknowledgements

First of all, I want to thank my supervisor Prof. Michael Weigand and Helga Havlik, representative for the staff of the Institute of Engineering Design and Product Development, for their support. My particular thanks go to Hanns Amri, Tobias Pflumm and Willem Rex. Hanns took care that everything worked fine in the project VARI-SPEED and Toby and Willem at TU München patiently answered all my questions regarding helicopters and rotors.

Most of the time of my PhD study, I was part-time employee of Zoerkler Gears GmbH & Co KG. At this point, I would like to take the opportunity to say "thank you" to Bernhard Wagner, Helmut Mad, Verena Graf and my former colleagues.

Throughout the years, the VARI-SPEED team was supported by numerous students who contributed to the research in the course of seminar papers and final theses. Their findings and new ideas – but also their merciless criticism – contributed to the successful completion of the project. Representative, I want to thank Florian Donner & Felix Huber for checking thousands of lines of Matlab code and Clemens "Orty" Ortmayr, from whom I learned that in the field of epicyclic gearing only abstraction leads to success.

I owe particular thanks to Hannes Brandstätter for his useful remarks on the curve fits of hydraulic motors. I also thank Stefan Löffler for proofreading a paper manuscript.

Besides academia, I had the chance to discuss my work and ideas with a lot of people at various occasions: in bars, at weddings and manoeuvres or in the gym. At this point I would like to thank all the people who endured my explanations and contributed to the completion of this thesis – sometimes more than they are aware of. I also owe special thanks to Christian Spieß, whose \LaTeX template is a masterpiece in itself.

I also thank Peter Wiesmair (Bosch Rexroth GmbH) and his colleagues for the support regarding the use of images published by Bosch Rexroth.

Last but not least, I thank my family for their support throughout the years of my studies and especially my wife Katharina for her patience and love.



Die approbierte gedruckte Originalversion dieser Dissertation ist an der TU Wien Bibliothek verfügbar.
The approved original version of this doctoral thesis is available in print at TU Wien Bibliothek.

Kurzfassung

Aktuelle Studien und Versuchsreihen haben gezeigt, dass die Änderung der Drehzahl des Hauptrotors des UH-60 (*Black Hawk*) Mehrzweckhubschraubers in manchen Flugzuständen die Möglichkeit einer signifikanten Reduktion der erforderlichen Antriebsleistung bietet. Da aber der Drehzahlbereich der Wellentriebwerke des Hubschraubers begrenzt ist und außerdem einige Hilfs-Aggregate, insbesondere die beiden Haupt-Generatoren, eine konstante Antriebsdrehzahl benötigen, wurde der Einsatz von stufenlos verstellbaren Getrieben (Continuously Variable Transmissions – CVTs) in Form von Compound-Split-Getrieben zur Anpassung der Drehzahl des Hauptrotors vorgeschlagen.

Zweck der vorliegenden Arbeit ist es, darauf aufbauend einen geeigneten Antriebsstrang für den UH-60 zu entwickeln. Dazu werden Zuverlässigkeit, erwartete Gesamtmasse und Drehzahlen der Komponenten des Antriebsstranges mehrerer möglicher Lösungen verglichen. Wegen der begrenzten Mittel dieser Studie, mussten einige Einschränkungen hinsichtlich der zulässigen Architekturen gemacht werden. Diese werden im Detail beschrieben und begründet. Als vielversprechendste Variante erweist sich eine Anordnung mit zwei Compound-Split-Modulen, je eines im Leistungspfad eines Triebwerks.

Der sogenannte Variator; ein stufenloses Getriebe, das Übersetzungen zwischen Null und unendlich realisieren kann; bildet eine Schlüssel-Baugruppe des Antriebsstrangs. Wegen ihrer hohen Leistungsdichten sind dafür Axialkolbenmotoren mit veränderlichem Hub vorgesehen. Die entsprechenden Konstruktions- und Leistungsdaten werden auf Grundlage von Hersteller-Katalogen geschätzt. Ein wesentlicher Nachteil hydraulischer Leistungsübertragung ist der geringe Wirkungsgrad im Vergleich zu Zahnradgetrieben. Aus diesem Grund wird der Gesamt-Wirkungsgrad der gefundenen Lösung untersucht. Obwohl dieser deutlich unter dem Wert des Getriebes mit konstanter Übersetzung liegt, lassen die Ergebnisse erwarten, dass die Vorteile der variablen Rotordrehzahl dennoch überwiegen.

In Vorbereitung einer dynamischen Simulation des Antriebsstranges im Flug, werden die wesentlichen Parameter des Getriebes konstruktiv festgelegt und die Ergebnisse in das Simulationsmodell eingepflegt. Anschließend wird in mehreren Simulationen das Betriebsverhalten des Getriebes untersucht.

Zusammenfassend beinhaltet die vorliegende Arbeit

- den grundlegenden Entwurf eines Stufenlos-Getriebes für den UH-60,
- die konstruktive Festlegung der Eckdaten von Variator und mechanischem System,
- den Nachweis, dass der Gesamtwirkungsgrad zwar reduziert, aber in Anbetracht der zu erwartenden Vorteile ausreichend ist,
- die Ergebnisse dynamischer Simulationen, die die einwandfreie Funktion des entwickelten Getriebes im Flug zeigen, und

- eine Auseinandersetzung mit zulassungsrechtlichen sowie mit Sicherheits-Aspekten in Form eines einfachen Safety Assessments.

Obwohl im Laufe der Untersuchungen einige technische Herausforderungen, die noch zu meistern sein werden, zum Vorschein gekommen sind und noch einiges an Entwicklungsarbeit zu leisten ist, scheint das beschriebene Getriebe geeignet zu sein, im UH-60 Verwendung zu finden. Auf dieser Grundlage ist eine weitere wissenschaftliche und technische Auseinandersetzung mit Compound-Split-Getrieben für Hubschrauber jedenfalls gerechtfertigt.

Abstract

Recent studies and test campaigns have shown that the variation of the main rotor speed of the Sikorsky UH-60 (*Black Hawk*) utility helicopter offers the opportunity to significantly reduce the propulsive power demand in some flight conditions. Since the speed range of the turboshaft engines of the helicopter is limited and several accessories, especially the two main electric generators, require constant rotational speed of their input shafts, Continuously Variable Transmissions (CVTs) in the form of so-called Compound-Split (CS) transmissions have been proposed to vary the main rotor speed whilst keeping the angular velocity of the engines unchanged.

The aim of this thesis is to develop a feasible drivetrain architecture for the UH-60 helicopter based on this principle. This is done by comparing the reliability, expected mass and rotational speeds of the drivetrain components of different possible solutions. Due to limited resources, the possible solutions must be restricted, which is explained in detail. The most promising solution contains two Compound-Split modules, one in the power path of each turboshaft engine.

The so-called variator, an infinitely variable transmission as sub-system of the Compound-Split, poses a key component of the drivetrain. Because of the high power density of axial piston hydraulic machines with variable displacement, these were chosen to build up the variator. Their properties are estimated based on the required corner power and catalogue data published by a manufacturer. A major drawback of hydraulic power transfer is the poor efficiency compared to gear drives. Therefore, the expected efficiency of the whole drivetrain is rated. Although lower than for the baseline transmission system of the UH-60, the results indicate that it will be sufficient, and the advantages of reduced power demand of the main rotor may outweigh the drawback of reduced drivetrain efficiency.

As preparation for the dynamic simulation of the transmission system in flight, the main parameters of the drivetrain are derived in a design study. The results are integrated into a simulation model of the whole rotorcraft. In several simulation runs, the operation of the proposed transmission system at different transmission ratios and during change of main rotor speed is studied.

In summary,

- a basic design layout for a CVT system for the UH-60 is developed,
- the main parameters of the variator machines and the mechanical transmission are defined,
- it is shown, that the overall drivetrain efficiency is reduced, but still sufficient,
- in dynamic simulations the proper function of the transmission system is shown, and
- certification aspects are discussed, and a safety assessment is performed.

Although several issues raised during the study still have to be resolved and a lot of engineering is still to be done, the proposed transmission system seems suitable for the use in the UH-60 heli-

copter. Based on these findings, further research on Compound-Split transmissions for rotorcraft is justified.

Contents

Abbreviations and Symbols	V
List of Figures	XV
List of Tables	XVII
Introduction	3
1. Introduction	3
1.1. State-of-the-art of helicopter propulsion	3
1.2. Variable rotor speed	3
1.3. Previous approaches to achieve rotor speed variation	4
1.3.1. Variable-Speed Power Turbines	4
1.3.2. Blade tip drives	5
1.3.3. Electric and Hybrid Electric Rotorcraft	6
1.3.4. Drivetrain solutions	7
1.4. Aim of the thesis	8
I. Epicyclic gear trains and power-split transmissions	9
2. Basics of epicyclic gearing and power-split transmissions	11
2.1. Principles and basic equations	11
2.1.1. Planetary gear sets	11
2.1.2. Epicyclic gear sets	12
2.1.3. Kinematics of epicyclic gear sets	13
2.1.4. Torque and power	14
2.2. Power-Split Transmissions	14
2.2.1. Output-Split	15
2.2.2. Input-Split	18
2.2.3. Compound-Split	20
2.2.4. Summary of Power-Split transmissions	27
II. Design of a Compound-Split drivetrain for the UH-60	29
3. Basic Architecture	31
3.1. The UH-60's transmission system	31
3.2. Possible drivetrain architectures	31
3.3. Reliability – Decision on architecture	33
3.3.1. The exponential distribution	33

Contents

3.3.2. Comparison of the architectures	34
3.4. Planetary gear sets – Decision on Compound-Split arrangement	36
3.4.1. Mass of planetary gear sets	37
3.4.2. Rotational speeds	39
3.5. Resulting arrangement of CS modules and drivetrain	40
4. The Variator	43
4.1. Axial piston motors with variable displacement	43
4.1.1. Principle layout	43
4.1.2. Pump and motor operation	44
4.1.3. Open and closed circuits	45
4.2. Requirements on hydraulic machines	45
4.3. Approximation of hydraulic machine data	48
5. Assessment of drivetrain efficiency	53
5.1. Efficiency of hydraulic motors	53
5.2. Efficiency of A6VE Series 71 hydraulic motors	54
5.3. Efficiency of gear stages	57
5.4. Drivetrain efficiency	57
6. Design	63
6.1. Compound-Split modules	63
6.1.1. Definition of possible combinations of numbers of teeth	63
6.1.2. Calculation of strength	64
6.1.3. Calculation method	67
6.1.4. Final parameters of planetary gear sets <i>C</i> and <i>D</i>	69
6.2. Fixed-ratio helical gear stages connecting the variator to the mechanical path	72
6.3. Changes to combining bevel gear stage and main planetary gear stage	74
6.4. Remarks on the design of the variable-ratio drivetrain	75
III. Dynamic Simulation	77
7. Modelling	79
7.1. T700 turboshaft engine	79
7.2. Main rotor	80
7.2.1. Blade model	80
7.2.2. Lift and drag forces	82
7.2.3. Induced inflow model	83
7.3. Tail rotor	86
7.4. Fuselage	86
7.5. Transmission system	87
7.5.1. Variator and hydraulic system	87
7.5.2. Multi-body system	88
7.6. Controls	90
7.7. Simulation runs	90

8. Results	93
8.1. Validation of model at reference rotor speed	93
8.1.1. Main rotor speed and power coefficient	93
8.1.2. Control angles	94
8.1.3. Reaction moments	97
8.1.4. Flapping and lead/lag motion	99
8.1.5. Turboshaft engines	102
8.1.6. Summary of model validation	105
8.2. Results for different flight conditions	105
8.2.1. Mechanical point I	105
8.2.2. Mechanical point II	108
8.2.3. Operation with hydraulic power transmission	110
8.2.4. Change of main rotor speed	113
8.3. Power demand	117
8.4. Main rotor torque	120
8.5. Tail rotor power	121
8.6. Variator power	122
8.7. Summary of simulation results and discussion	124
IV. Certification & Safety Aspects	125
9. Certification according to CS-29	127
9.1. Certification requirements	127
9.1.1. Applicability	127
9.1.2. Weight limits	127
9.1.3. Main rotor speed range	127
9.1.4. One Engine Inoperative (OEI) resp. one engine disconnected by loss of variator	128
9.1.5. Flight and handling characteristics	129
9.1.6. Strength requirements	130
9.1.7. General aspects of design and construction	131
9.1.8. Rotor drive system	131
9.1.9. Hydraulic systems	133
9.1.10. Powerplant limitations	133
9.1.11. Emergency landing	134
9.1.12. Additional considerations	134
9.2. Acceptable Means of Compliance	134
9.2.1. Loss of lubrication tests	135
9.2.2. Vibration health monitoring system	135
9.3. Concluding remarks on certification	135
10. Design/Safety Assessment	137
10.1. Functional FMEA	137
10.1.1. Definition of functions	137
10.1.2. Possible failures, failure effects and severity	137
10.2. Results of FMEA	139
10.3. Concluding remarks of the Design/Safety Assessment	141

Contents

Summary	147
11. Summary	147
11.1. Results, discussion and conclusion	147
11.2. Future research and engineering	149
Bibliography	151
A. Appendix	159
A.1. Characteristics of hydraulic machines	159
A.2. Additional results of turboshaft engines	164
A.3. Supplementary	169
Index	171
Curriculum vitae	175

Die approbierte gedruckte Originalversion dieser Dissertation ist an der TU Wien Bibliothek verfügbar.
The approved original version of this doctoral thesis is available in print at TU Wien Bibliothek.

Abbreviations and Symbols

Acronyms

AC	Advisory Circular
AMC	Acceptable Means of Compliance
AoA	Angle of attack
BEMT	Blade Element Momentum Theory
CBGS	Combining Bevel Gear Stage
COG	Center Of Gravity
COTS	Commercial Off-The-Shelf
CS	Compound-Split
CS	Certification Specification
CSD	Constant Speed Drive
CVT	Continuously Variable Transmission
DIN	Deutsches Institut für Normung
DOF	Degree Of Freedom
DSTL	Defence Science and Technology Laboratory
EASA	European Aviation Safety Agency
EGS	Epicyclic Gear Set
EIS	Entry-Into-Service
ERF	European Rotorcraft Forum
FAA	Federal Aviation Administration
FADEC	Full Authority Digital Engine Control
FHA	Failure Hazard Analysis
FM	Figure of Merit
FMEA	Failure Mode and Effect Analysis
FVA	Forschungsvereinigung Antriebstechnik
FVA-Wb	FVA-Workbench
GE	General Electrics
HEV	Hybrid Electric Vehicle

Mathematical functions

HTS	High Temperature Superconductor
HUMS	Health and Usage Monitoring System
IDG	Integrated Drive Generator
IS	Input-Split
LCTR2	Large Civil Tiltrotor
MCP	Maximum Continuous Power
MDAO	Multi-Disciplinary Analysis and Optimization
MP	Mechanical point
MPGS	Main Planetary Gear Stage
NASA	National Aeronautics and Space Administration
O&S	Operational and Support
OEI	One Engine Inoperative
OS	Output-Split
PGS	Planetary Gear Set
PSE	Principal Structural Element
PSSA	Preliminary System Safety Assessment
PST	Power-Split Transmission
SAE	Society of Automotive Engineers
SSA	System Safety Assessment
TDP	Take-Off Decision Point
TPP	Tip Path Plane
TRL	Technology Readiness Level
TSE	Turboshaft Engine
UAV	Unmanned Aerial Vehicle
UH	Utility Helicopter
VARTOMS	Variable Rotor Speed and Torque Matching System
VDI	Verein Deutscher Ingenieure
VHM	Vibration Health Monitoring
VSPT	Variable-Speed Power Turbine

Mathematical functions

$f(\dots)$	Function (general)
$\gcd(.,.)$	Greatest common divisor of two positive integers
$. \bmod .$	Modulo operation

.]	Absolute value function (abs)
[.]	Round to next higher integer (ceil)
⌊.]	Round to next lower integer (floor)
⌊.]	Round to nearest integer (round)

Subscripts

1	Index of sun gear (shaft) of a planetary gear set / pinion of a gear stage
2	Index of ring gear (shaft) of a planetary gear set / wheel of a gear stage
C	Index of carrier shaft of a planetary gear set
C	Planetary gear set of CS module with epicyclic ratio $i_{..c}$
D	Planetary gear set of CS module with epicyclic ratio $i_{..d}$
B	Index for scuffing in gear calculations
F	Index for root in gear calculations
H	Index for flank in gear calculations
MR	Main rotor
TR	Tail rotor

Greek letters

Symbol	Description	Unit
α	Angle of Attack	deg
α	Pressure angle of the basic rack for cylindrical gears	deg
$\tilde{\alpha}$	Swivel angle of axial piston machine of bent-axis design	deg
α_{MR}	Tilt angle of main rotor relative to waterline	rad (deg)
α_{WL}	Tilt angle of fuselage relative to waterline	rad (deg)
β	Flapping angle	rad (deg)
β	Helix angle	deg
ε	Absolute value of ratio of variator power to total propulsion power	1.0
ε_{β}	Overlap ratio	10
ζ	Ratio between corner power and maximum power of a hydraulic motor	1.0

Greek letters

Symbol	Description	Unit
η_{hm}	Hydraulic-mechanical efficiency	1.0 (%)
η_p	Efficiency factor of hydraulic lines	1.0 (%)
η_t	Total efficiency of a hydraulic machine	1.0 (%)
η_v	Volumetric efficiency	1.0 (%)
Θ	Basic ratio at a mechanical point	1.0
ϑ_0	Collective pitch angle	deg
Θ_1 and Θ_2	Basic ratios at mechanical points I and II of a Compound-Split transmission	1.0
ϑ_{1c}	Lateral cyclic pitch angle	deg
ϑ_{1s}	Longitudinal cyclic pitch angle	deg
ϑ_{tw}	Twist angle of blade section	deg
λ	Induced velocity parameter	1.0
λ_{crit}	Critical value of film thickness	1.0
λ	Ratio of film thickness to surface roughness	1.0
λ	Non-dimensional parameter in efficiency model	1.0
μ	Advance ratio	1.0
μ	Dynamic viscosity	Pas
ν	Poisson's ratio	1.0
ν_{100}	Kinematic viscosity at 100 °C	mm ² /s (cSt)
ν_{40}	Kinematic viscosity at 40 °C	mm ² /s (cSt)
ξ	Ratio of hinge offset and main rotor radius	1.0
ρ	Density of hydraulic fluid	kg/m ³
ρ_{air}	Air density	kg/m ³
ρ_{fP}	Root fillet radius of the basic rack for cylindrical gears	mm
ρ_{fP}^*	Root fillet radius-factor of the basic rack for cylindrical gears	1.0
σ	Solidity	1.0
σ	Non-dimensional parameter in efficiency model	1.0
σ_{Flim}	Nominal stress number (bending)	N/mm ²
$\sigma_{Flim,99}$	Nominal stress number (bending) for 99 % reliability	N/mm ²
σ_{FE}	Allowable stress number (bending)	N/mm ²

Symbol	Description	Unit
$\sigma_{FE,99}$	Allowable stress number (bending) for 99 % reliability	N/mm ²
$\sigma_{H,lim}$	Allowable stress number (contact)	N/mm ²
$\sigma_{H,lim,99}$	Allowable stress number (contact) for 99 % reliability	N/mm ²
τ_t	Shear stress	N/mm ²
Φ	Transmission spread	1.0
Ψ	Azimuthal blade angle	rad (deg)
Ω	Main rotor angular velocity	rad/s
ω	Angular velocity	rad/s
ω_{max}	Maximum angular velocity of hydraulic motor	rad/s
$\omega_{max,0}$	Maximum angular velocity of hydraulic motor when no load is applied	rad/s
ω_{nom}	Nominal angular velocity of hydraulic motor	rad/s

Latin letters

Symbol	Description	Unit
A_{bl}	Area of blade section	m ²
A_{MR}	Main rotor disc area	m ²
A_{piston}	Cross-section area of a piston	mm ²
A_{TR}	Tail rotor disc area	m ²
c	Blade chord of main rotor	m
C_D	Drag coefficient	1.0
C_L	Lift coefficient	1.0
c_p	Tip clearance of basic rack of cylindrical gears	mm
c_p	Power coefficient	1.0
c_p^*	Tip clearance-factor of basic rack of cylindrical gears	1.0
C_{pv}	Loss factor taking the mechanical and hydraulic losses dependent on Δp into account	1.0
C_R	Reliability factor for pitting resistance acc. to AGMA 911-A94	1.0
C_{st}	Loss factor taking the volumetric losses dependent on ρ into account	1.0

Latin letters

Symbol	Description	Unit
C_{sv}	Loss factor taking the volumetric losses dependent on μ into account	1.0
c_T	Thrust coefficient	1.0
C_{tv}	Loss factor taking the mechanical losses dependent on ρ into account	1.0
C_{vv}	Loss factor taking the hydraulic losses dependent on μ into account	1.0
c_W	Weight coefficient	1.0
D_{piston}	Pitch diameter of axial piston motor	mm
E	Young's modulus	N/mm ²
e	Hinge offset	m
F_D	Drag force of a blade element	N
F_L	Lift force of a blade element	N
G	Shear modulus	N/mm ²
g	Gravity (9.81 m/s ²)	m/s ²
h_{aP}	Addendum of basic rack of cylindrical gears	mm
h_{aP}^*	Addendum-factor of basic rack of cylindrical gears	1.0
h_{fP}	Dedendum of basic rack of cylindrical gears	mm
h_{fP}^*	Dedendum-factor of basic rack of cylindrical gears	1.0
\tilde{h}	Stroke of a piston	mm
i_0	Epicyclic ratio	1.0
i_{12}	Planetary ratio	1.0
i_c	Ratio of gear stage connecting variator pump to mechanical path	1.0
i_d	Ratio of gear stage connecting variator motor to mechanical path	1.0
J_T	Torsion constant of a shaft section	m ⁴
k_0	Basic ratio of epicyclic gear set	1.0
k_{12}	Ratio when carrier is not grounded	1.0
K_A	Application factor	1.0
K_{AS}	Application factor (scuffing)	1.0
$K_{B\alpha}$	Transverse load factor (scuffing)	1.0
$K_{B\beta}$	Face load factor (scuffing)	1.0

Symbol	Description	Unit
$K_{F\alpha}$	Transverse load factor (root stress)	1.0
$K_{F\beta}$	Face load factor (root stress)	1.0
K_{γ}	Load sharing factor (mesh load factor)	1.0
$K_{H\alpha}$	Transverse load factor (contact stress)	1.0
$K_{H\beta}$	Face load factor (contact stress)	1.0
K_R	Reliability factor for bending strength acc. to AGMA 911-A94	1.0
K_v	Dynamic factor	1.0
L	Characteristic length	m
L_{bl}	Length of blade section	m
m_{bl}	Mass of blade section	kg
m_n	Normal module	mm
Ma	Mach number	1.0
ME	Quality grade acc. to ISO 6336-5 for represents requirements that must be realized when a high degree of operating reliability is required	n/a
N	Number of blades	1
n_{max}	Maximum rotational speed of hydraulic motor in RPM	RPM
$n_{max,0}$	Maximum rotational speed of hydraulic motor in RPM when no load is applied	RPM
n_{nom}	Nominal rotational speed of hydraulic motor in RPM	RPM
P	Power	kW
P_{corner}	Corner power of hydraulic motor	kW
Δp	Pressure difference	bar (Pa)
P_i	Induced power of a rotor	kW
P_{in}	Input power of power-split transmission	kW
P_{hydr}	Maximum power to be transmitted hydraulically via the variator	kW
P_{max}	Maximum power of hydraulic motor	kW
p_{max}	Maximum pressure of hydraulic motor	bar (Pa)
P_{MR}	Main rotor power	kW (W)
p_{nom}	Nominal pressure of hydraulic motor	bar (Pa)
P_{out}	Output power of power-split transmission	kW
P_{S3}	Static pressure at station 3 (turboshaft engine)	psi (bar)
P_{TR}	Tail rotor power	kW
P_{TSE}	Engine shaft power	kW

Symbol	Description	Unit
P_{var}	Power transmitted via the variator path	kW
Q	Torque	Nm
Q_{max}	Maximum torque of hydraulic motor	Nm
Q_S	Engine shaft torque (at MR)	ft – lb
Q_{TSE}	Engine shaft torque	Nm
n_{TSE}	Engine shaft speed	RPM
q_v	Hydraulic flow	m ³ /s
Q_x	Deliverable torque of hydraulic motor at maximum angular velocity	Nm
R	Main rotor radius	m
\tilde{r}	Generic radial position from hinge	1.0
r	Radial position on main rotor blade	m
r_{max}	Maximum radius of a shaft section	mm
R^2	Coefficient of determination	1.0
Ra_F	Arithmetic mean roughness (root)	um
Ra_H	Arithmetic mean roughness (flank)	um
$\%N_G$	Relative gas generator speed	%
$\%N_P$	Relative power turbine speed	%
Rz_F	Mean peak-to-valley roughness (root)	um
Rz_H	Mean peak-to-valley roughness (flank)	um
S_B	Safety factor scuffing (DIN 3990, contact temperature)	1.0
S_F	Safety factor root (ISO 6336)	1.0
$S_{\text{EFVA 389}}$	Safety factor root (FVA 389)	1.0
$S_{\text{EFVA 45}}$	Safety factor root (FVA 45)	1.0
$S_{\text{FVDI 2737}}$	Safety factor root (VDI 2737)	1.0
S_H	Safety factor pitting (ISO 6336)	1.0
$S_{\text{int S}}$	Safety factor scuffing (DIN 3990, integral temperature)	Nm
T_{45}	Interturbine gas temperature (turboshaft engine)	degR
T_{TR}	Tail rotor thrust	N
T	Main rotor thrust	N
\underline{u}	Control vector of turboshaft engine model	n.a.
V	Forward speed of the helicopter	m/s
V_{AS}	Airfoil section speed in wind axes	m/s
V_g	Displacement of axial piston motor	cm ³ (m ³)

Symbol	Description	Unit
$V_{g,max}$	Maximum displacement of axial piston motor	$\text{cm}^3 (\text{m}^3)$
V_P	Airfoil perpendicular speed in wind axes	m/s
V_R	Airfoil radial speed in wind axes	m/s
V_T	Airfoil tangential speed in wind axes	m/s
W_F	Fuel flow	lb/s
m_{ac}	Aircraft mass	kg (lb)
\underline{x}	State vector of turboshaft engine model	n.a.
x	Profile shift coefficient	1.0
\underline{y}	Output vector of turboshaft engine model	n.a.
Y_N	Life factor for tooth root stress	1.0
Z	Number of pistons of axial piston motor	1
\mathcal{Z}	Set of vectors containing the numbers of teeth of sun, planet and ring gears of planetary gear sets	n/a
\mathcal{Z}'	Set of vectors containing the numbers of teeth of sun, planet and ring gears and a related number of planets	n/a
\mathcal{Z}''_C	Set of vectors containing the numbers of teeth of sun, planet and ring gears and a related number of planets with planetary ratios required for PGS C	n/a
\mathcal{Z}''_D	Set of vectors containing the numbers of teeth of sun, planet and ring gears and a related number of planets with planetary ratios required for PGS D	n/a
\mathcal{Z}_{hC}	Set of vectors containing the numbers of teeth of pinion and wheel with ratios required for i_c	n/a
\mathcal{Z}_{hD}	Set of vectors containing the numbers of teeth of pinion and wheel with ratios required for i_d	n/a
Z_N	Life factor for contact stress,	1.0



Die approbierte gedruckte Originalversion dieser Dissertation ist an der TU Wien Bibliothek verfügbar.
The approved original version of this doctoral thesis is available in print at TU Wien Bibliothek.

List of Figures

2.1. Typical arrangement of a planetary gear set	12
2.2. Principal layout of an epicyclic gear set	13
2.3. Principal layout of an Output-Split transmission	16
2.4. Quantities for Output-Split transmissions	17
2.5. Principal layout of an Input-Split transmission	19
2.6. Quantities for Input-Split transmissions	20
2.7. Principal layout of Compound-Split transmissions	21
2.8. Quantities for Compound-Split transmissions	26
3.1. Layout of UH-60 transmission system (based on [120])	32
3.2. Probabilities of failure of Architectures I and II	35
3.3. Mass of the four Compound-Split arrangements according to figure 2.7	38
3.4. Maximum rotational speeds of the planet gears (absolute values)	39
3.5. Sketch of the final arrangement D	40
3.6. Sketch of UH-60 transmission system (taken from [74])	41
3.7. Sketch of transmission layout	42
4.1. Layout of A6VE axial piston motors (taken from [126, p. 18/60])	43
4.2. Characteristic curves of variable displacement axial piston motors	46
4.3. Power transferred via variator path and characteristic curves of different hydraulic machines	47
4.4. Fit of mass as a function of corner power for A6VE motors Series 63, 65 and 71	51
4.5. Fit of characteristic variables as a function of corner power for A6VE Series 71 motors	52
5.1. Total efficiency of hydraulic machines of the A6VE Series 71 type in pump and motor operation	56
5.2. Overall drivetrain efficiency η_{overall}	60
5.3. Pressure level at the pump	62
7.1. Main rotor blade of UH-60 (taken from [28, p. 6])	81
7.2. Lift and drag forces at a blade section (cf. [70, p. 65])	82
7.3. Induced velocity parameter λ at different advance ratios μ	85
7.4. Display of multi-body system in Simulink Mechanics Explorer	89
7.5. Detail view of Compound-Split in Simulink Mechanics Explorer	90
8.1. Angular velocity of main rotor	93
8.2. Angular velocity of main rotor rel. to target value	94
8.3. Main rotor power coefficient compared to reference data	95
8.4. Collective angle	95
8.5. Mean collective angle compared to reference data	96

List of Figures

8.6. Lateral cyclic angle	96
8.7. Mean lateral cyclic angle compared to reference data	97
8.8. Longitudinal cyclic angle	97
8.9. Mean longitudinal cyclic angle compared to reference data	98
8.10. Reaction torque in pitch axis rel. to $Q_{MR,max}$	99
8.11. Reaction torque in roll axis rel. to $Q_{MR,max}$	99
8.12. Flapping angle	100
8.13. Coning angle compared to reference data	101
8.14. Maximum flapping angle compared to reference data	101
8.15. Lead/lag angle	102
8.16. Mean lead/lag angle compared to reference data	102
8.17. Operation parameters of turboshaft engines at 27 rad/s	104
8.18. Speeds and yaw angle at MP I	107
8.19. Speeds and yaw angle at MP II	109
8.20. Speeds and yaw angle with hydraulic power transmission	111
8.21. Pressure in hydraulic system	112
8.22. Flow of hydraulic fluid	113
8.23. Variator efficiency	113
8.24. Speeds and yaw angle during change of main rotor speed	115
8.25. Pressure in hydraulic system	116
8.26. Flow of hydraulic fluid	116
8.27. Variator efficiency	117
8.28. Main rotor power demand	118
8.29. Main rotor power demand rel. to reference speed	118
8.30. Engine power	119
8.31. Engine power rel. to reference speed	119
8.32. Main rotor torque	120
8.33. Main rotor torque rel. to reference speed	121
8.34. Tail rotor power demand	122
8.35. Tail rotor power demand rel. to reference speed	122
8.36. Power flow in variator	123
8.37. Power flow in variator rel. to engine power	124
A.1. Volumetric efficiency of hydraulic machines of the A6VE Series 71 type in pump and motor operation	160
A.2. Hydraulic-mechanical efficiency of hydraulic machines of the A6VE Series 71 type in pump and motor operation	161
A.3. Torques of hydraulic machines of the A6VE Series 71 type in pump and motor operation	162
A.4. Mechanical powers of hydraulic machines of the A6VE Series 71 type in pump and motor operation	163
A.5. Operation parameters of turboshaft engines at MP I	165
A.6. Operation parameters of turboshaft engines at MP II	166
A.7. Operation parameters of turboshaft engines with hydraulic power transmission . . .	167
A.8. Operation parameters of turboshaft engines during change of main rotor speed . . .	168

List of Tables

2.1. Operating ranges and shafts transmitting the maximum absolute value of power . . .	24
4.1. Data of A6VE Series 63 variable displacement axial piston motors	48
4.2. Data of A6VE Series 65 variable displacement axial piston motors	49
4.3. Data of A6VE Series 71 variable displacement axial piston motors	49
4.4. Approximated data of the required hydraulic motors	52
5.1. Loss factors (taken from [97])	54
5.2. Assumptions regarding power supply and demand	58
6.1. Reference profile for gears of planetary gear sets <i>C</i> and <i>D</i>	65
6.2. Gear material	66
6.3. Manufacturing and finishing	66
6.4. Lubricant data	67
6.5. Operating data	67
6.6. Required minimum safety factors for the planetary gear sets within the CS modules	68
6.7. Chosen parameters and resulting safety factors for planetary gear set <i>C</i>	70
6.8. Chosen parameters and resulting safety factors for planetary gear set <i>D</i>	71
6.9. Chosen parameters and resulting safety factors for helical gear stage i_c	73
6.10. Chosen parameters and resulting safety factors for helical gear stage i_d	73
6.11. Data of combining bevel gear and main planetary gear stage (cf. [74, p. 7])	74
6.12. Data of modified combining bevel gear and main planetary gear stage	75
7.1. Operating points of turboshaft engine model (cf. [40, p. 64])	80
7.2. Data of UH-60's main rotor blades (based on [32, 35])	81
7.3. Blade loading for different advance ratios μ	86
7.4. Attitude of fuselage (cf. [133])	87
7.5. Main parameters of the different simulation runs	92
8.1. Mean reaction moments at fuselage	98
10.1. Severity of failure modes acc. to AC 29-2C (cf. [122])	138
10.2. Design assessment of hydraulic machines (see p. 142)	139
10.3. Design assessment of planetary gear sets (see p. 143)	139



Die approbierte gedruckte Originalversion dieser Dissertation ist an der TU Wien Bibliothek verfügbar.
The approved original version of this doctoral thesis is available in print at TU Wien Bibliothek.

Introduction



Die approbierte gedruckte Originalversion dieser Dissertation ist an der TU Wien Bibliothek verfügbar.
The approved original version of this doctoral thesis is available in print at TU Wien Bibliothek.

1. Introduction

1.1. State-of-the-art of helicopter propulsion

Almost all helicopters of CS-29 class currently at service are powered by one or more turboshaft engines. They are connected to the main and auxiliary rotors via fixed-ratio transmission systems which reduce the rotational speeds, connect all rotors necessary for safe flight and drive several accessories; such as electric generators, hydraulic and pneumatic pumps and cooling fans. Highest demands in terms of reliability are placed on helicopter drivetrains, because failures usually lead to hazardous or even catastrophic events. Besides that, high efficiency and power density are required to limit the mass of the transmission system and increase the payload of the rotorcraft. The certification requirements issued by the aviation authorities define several special requirements to ensure safe operation of helicopters.

For example, CS-29 and AC-29 require either that all rotors necessary for operation and control are driven by the main rotors (single-engine helicopters) or that the drive system arrangement continues to drive all rotors by the remaining engines (multi-engine helicopters). In almost all modern helicopters, these requirements are met by using cross-shafting and transmissions. (cf. [42, 122], paragraphs 29.917)

Another special request on transmissions in rotorcraft applications relates to their operation in case of a failure of the lubrication system, the so-called loss of lubricant. Several mandatory tests to show the compliance with these requirements are defined in the certification specifications. (cf. [42, 122])

1.2. Variable rotor speed

The angular velocity of the main rotor is kept constant for most helicopters, especially for large ones. Although for smaller rotorcraft a variation of main rotor speed has been tested to increase the endurance (cf. [87]), for CS-29 class helicopter only a reduction of rotor speed by decreasing engine speed during ground operation was implemented in the EC145/H145 (Variable Rotor Speed and Torque Matching System (VARTOMS), cf. [56]).

However, the possibility to change the angular velocity of the main rotor offers several benefits. For example, the noise generation can be affected, which was the main reason for the application of different speed levels in the EC145/H145. Also, the flight envelope can be expanded. Lower angular velocities of a rotor lead to lower Mach numbers at the tips of the advancing blade in forward flight and therefore, faster flight speeds are possible. This is of special interest in – but not limited to – military applications. On the other hand, increased rotor speeds allow the operation of a helicopter at higher altitude. A particular demand for different angular velocities occurs in tiltwing or tiltrotor aircraft, because the rotors are operated as helicopter rotors in hover mode and as propellers in forward flight mode. (cf., for example, [25])

Besides these advantages, the major benefit of a variation of rotor speed is the possible reduction of the power consumption of the main rotor, which has been shown in several studies. The rea-

1. Introduction

son is, simply speaking, that the variation of angular velocity allows to operate the rotor at more favourable lift to drag ratios of the used aerodynamic profiles. An overview of previous findings and the physical background is given in [25]. Because of the large amount of publicly available data, ranging from information on design to results of flight tests, a lot of studies deal with the UH-60 (*Black Hawk*), a medium utility helicopter mainly used by armed forces. A study conducted by Mistry and Gandhi [73] showed that, depending on gross mass and flight condition, up to 12 % power reduction is possible. Misté et al. [72] presented a methodology for determining the optimal rotational speed of the main rotor and showed that more than 10 % fuel saving is feasible in some flight conditions. Garre et al. [46] investigated the influence of variable rotor RPM on four different types of rotorcraft and found that within a range of 70 % to 110 % of nominal speed, power reductions of up to 15 % can be achieved. Additional information and results concerning a variable main rotor speed can be found in [34, 39, 70, 71, 85, 111].

1.3. Previous approaches to achieve rotor speed variation

Several concepts to obtain a variation of rotor angular velocity have been proposed. These include Variable-Speed Power Turbines (VSPTs), tip driven rotors, electric or hybrid electric drives and various transmission designs. An overview of different approaches with a discussion of advantages and drawbacks as well as a rating of the feasibility can be found in [24]. A short summary of proposed technologies is given below.

1.3.1. Variable-Speed Power Turbines

An important contribution to the research on changing main rotor speed by adapting engine speed was made by G. A. Misté et al. (cf. [70, 72]) and J. Steiner [111]. In [72], the optimum main rotor speed of the UH-60 in consideration of the engine efficiency and specific fuel consumption were determined. A comparison of these results to the operation at fixed engine speed but with using a continuously variable transmission (CVT) was done in [70]. This study showed that for intermediate advancing speeds, a fixed ratio transmission yields similar benefits as a CVT, but that in hover and fast forward flight the helicopter equipped with a CVT has a much better performance. However, the different weight and reliability of fixed ratio transmission and CVT were not considered and still have to be addressed. The thesis in hand deals with some of these issues.

In the National Aeronautics and Space Administration (NASA) Heavy Lift Rotorcraft Systems Investigation project, Johnson et al. [55] came to the conclusion, that the Large Civil Tiltrotor (LCTR2) concept has the best potential to meet the NASA technology goals. As already mentioned, tiltrotor and tiltwing aircraft have a particular demand for different rotor speeds. For this reason, the NASA conducted research on this topic for the LCTR2 concept, which is part of the Fundamental Aeronautics Program, Subsonic Rotary Wing Project. A reduction of rotor speed of 50 % was identified as necessary. The work was carried out in cooperation with Boeing and Rolls Royce. Snyder, Robuck et al. [19, 91, 92, 106, 132] compared engine and multi-speed gearbox technology as well as combinations of both, but not continuously variable transmissions. Each concept was studied at three technology levels: Commercial Off-The-Shelf (COTS), Entry-Into-Service (EIS) in 2025 and EIS in 2035. It was assumed that Variable-Speed Power Turbines which work efficiently at 50 % to 100 % of the design speed will be ready for the market in the coming decades. The resulting gross mass was

1.3. Previous approaches to achieve rotor speed variation

specified as the most important characteristic of a concept. The results did not yield a clear preference for a single solution. A follow-up study [105] assessed the VSPT technology on Civil Tiltrotor size and performance. Again, multi-speed gearboxes were also considered. The assumed 10 % weight penalty for the multi-speed gearbox had much more influence on the resulting mass of the propulsion system than the anticipated weight penalties of the different engines. However, because of some unexpected results, the authors suggested a deeper look on VSPT technologies. Subsequently, detailed requirements of the LCTR2 on the turbine engines have been defined in [107] and further studies on the design of propulsion and drive system, their sub-systems and arrangement were carried out (cf. [90, 108, 109]). The results presented in [108] indicated, that the EIS 2035 engine with a single-speed gearbox would lead to a minimum gross weight of the propulsion system. However, the benefits compared to concepts using a two-speed gearbox are not that significant and strongly depend on the assumptions made for the 2035 engine technology. Based on these findings, sub-systems of the propulsion and drive system were studied and optimized in [109]. In addition, Operational and Support (O&S) costs were evaluated. The results presented in this publication represent the final outcome of the series of research projects carried out for the LCTR2 propulsion and drive system. In summary, it turned out that fixed geometry VSPT EIS 2035 with two-speed transmission yield the lowest gross mass of all studied options. However, the results strongly rely on the assumed technical progress concerning engine weight and fuel consumption. Regarding operational costs, the two-speed transmission provides significant advantages compared to a wide-range speed variation. For the EIS 2035 engine with a two-speed gearbox possible arrangements in the pod nacelle were studied in [90]. A Multi-Disciplinary Analysis and Optimization (MDAO) approach for transmission sizing was also part of the project.

1.3.2. Blade tip drives

Driving the main rotor by means of an internal combustion engine and a transmission system is not the only technically feasible way of propulsion. It is also possible, to use the repulsion of a device acting on the blade tip perpendicular to blade axis. This device can be a nozzle emitting compressed air (cold tip jets), a reaction chamber where a fuel-air mixture is combusted (hot tip jets), ramjets, pulsejets or rockets.

Cold tip jets have been used in the Sud-Ouest Djinn and the VFW-Fokker H2 and H3. The most famous example of a rotorcraft equipped with a hot tip jet is the WNF-342, developed by Friedrich Doblhoff and built at the Wiener Neustädter Flugzeugwerke during the Second World War. The principle and ideas to overcome some technical issues can be found in [36, 37, 38]. Another example is the Fairey Rotodyne. The rotor of the Hiller YH-32 Hornet was driven by two ramjets. Pulsejets and rockets have not been widely used in series rotorcraft. [49]

In principle, blade tip drives offer several benefits. The heavy transmission system can be omitted and there is no need for a torque compensating device such as a tail or second main rotor. Also, angular velocity of the rotor can be theoretically adapted by controlling the thrust of the tip drives. For some reasons though, these technologies have not been pursued. A major issue with hot tip jets and other concepts using fuel is the transport of the fuel from a tank in the fuselage – i.e., the non-rotating system – to the rotor. Besides that, the fuel consumption is much higher than for helicopters equipped with turboshaft engines and a transmission. Other important drawbacks are the high noise level and the big masses at the blade tips which lead to large centrifugal forces.

1. Introduction

1.3.3. Electric and Hybrid Electric Rotorcraft

In the last decades, the electrification of drive systems has become a big issue. To some extent driven by environmental legislation, hybrid or even fully electric vehicles are nowadays common in the automotive sector and their market share is still increasing. Also in other areas of applications, such as marine propulsion or wing airplanes, these technologies have found use. Increasing power-to-mass ratios may offer the opportunity to use hybrid electric propulsion in rotorcraft. (cf., for example, [53, 69, 88, 130])

By varying the output speed of electric machines, which is usually done by a frequency inverter, hybrid electric drive technologies offer the opportunity to change main rotor speed in flight. Although many architectures of hybrid electric drive systems strongly affect the transmission design and a fully electric propulsion system is comparable to adapting the angular velocity of an internal combustion engine, these technologies have been summarized in a special section. Serial hybrid architectures without a dedicated energy storage and electric transmissions are also included, although they pose no hybrid technologies in a strict sense.¹ The reason is, that all of these concepts use the same technology to vary the rotor speed and all of them face similar problems, which prevent a implementation with state-of-the-art technology.

Several patents and publications are a proof of the research and development activities on hybrid electric propulsion for rotorcraft. The following examples make no claim to be a comprehensive summary of the developments.

A good overview of different possible approaches is given in [69]. This study concludes that although so-called microhybrids with an electric power of about 50 kW as emergency electric power sources are feasible with state-of-the-art electric drive technology, the additional mass still poses a major disadvantage. Especially under economic considerations, the drawbacks outweigh the benefits clearly. For hybrid architectures requiring more electric power significant progress is needed in electric machine technology and especially in the field of electric energy storages.

The NASA also dealt with different kinds of more electric propulsion systems for rotorcraft. A summary is given in [104]. The findings were similar to the ones of [69]. Technology projection lead to the expectation that within 15 years (that would be in 2030) only small helicopters could be equipped with electric propulsion. It is predicted, that in 2045, these helicopters will obtain similar performance as the baseline small helicopters.

Airbus Group took out several patents [116, 117, 118] for a hybrid drive for rotorcraft. The inventions include electric machines directly driving the main and tail rotors. For these drives, low-inertia electric motors shall be used. A possible design has been disclosed in [65]. Besides a thermal engine driving a generator and a battery as electro-chemical energy storage, the helicopter disclosed in one of the patents has also a fuel cell. Battery and fuel cell are intended to provide the whole power required in take-off and landing whilst the thermal engine is in idle operation during these manoeuvres. The system is intended to reduce noise emission near heliports. Besides that, the possibility to increase the efficiency of main and tail rotor is explicitly underlined. However, to the present day it has not been implemented by Airbus Helicopters in a series rotorcraft.

A promising application for electric drive technology is the tail rotor. Because of the lower demand of power, it is probably easier to implement. Information on this field of development can

¹As a consequence, a Compound-Split with an electric variator falls into this group whilst the Compound-Split with hydraulic variator is considered a transmission technology.

1.3. Previous approaches to achieve rotor speed variation

be found, for example, in [21, 41, 68, 115]. However, no electric tail rotor has been implemented to a series helicopter by now.

A serial hybrid drive for Unmanned Aerial Vehicles (UAVs) has been invented by SWISS UAV GmbH [76]. Another concept for a hybrid propulsion system has been published in [93]. A study on possible applications of High Temperature Superconductor (HTS) technology in aircraft propulsion systems is described in [64]. Detailed considerations on the electric system in a hybrid electric rotorcraft can be found [54].

This short summary is not intended to provide a comprehensive overview of the field of (more) electric drive technology in rotorcraft applications, but points out some main development trends. What they all have in common is, that with state-of-the-art technologies no economically competitive series helicopter can be build. The main challenges are the power density of electric machines and especially the poor energy density of batteries. Furthermore, the cooling of the electric system raises technical issues which still have to be solved. If the electric drive system is intended to vary the rotor speed, the rotorcraft has to be equipped with heavy frequency inverters, which further increases the empty weight and raises additional questions concerning cooling and reliability. However, the continued research and development in the field of hybrid electric vehicles and future environmental legislation may lead to the realization of (more) electric helicopters.

1.3.4. Drivetrain solutions

The last approach to obtain a variable rotor speed which will be discussed in this introduction is the field of drivetrains. As already mentioned, the classification of research work to one of the sections is arbitrary to some extent. For example, the work on the LCTR2 [19, 90, 91, 92, 105, 106, 107, 108, 109, 132] always included single- and two-speed transmissions and has already been discussed in section 1.3.1. Also, hybrid electric powertrains usually affect the design of the drivetrain. However, in this section developments, which vary the rotor speed by making use of mechanical principles will be discussed. A comprehensive analysis on these concepts can also be found in [24, 84]. These studies also included different mechanical principles; such as chain gears, friction and belt drives; which are clearly unsuitable to transmit power in the scale of a helicopter powertrain. These systems will not be discussed in detail here, but it is concentrated on developments expressly made for rotorcraft. Studies on the influence of using different types of transmissions on a rotorcraft with variable rotor speed can be found in [47, 70, 71].

Besides the studies carried out for the LCTR2, which have already been discussed, the NASA searched several technologies to obtain a variable rotor speed (cf. [112, 113]). These included dual-clutch and power-split transmissions (including a variator with a toroidal friction concept). The authors recommended an *Inline Two-Speed With Double Star/Idler Reversing Stage* and the so-called *Offset Compound Gear*, patented in [114], as promising concepts for future research on two-speed transmissions. If a continuously variable transmission should be required, a *Planetary Differential With Variable Controlled Ring Gear* was assessed as the simplest and most viable solution. The concepts derived in these studies were tested and the results were published in [61, 62]. The reasons which lead the author of the thesis in hand to choose a more complicated variant of power-split transmission, the so-called Compound-Split, will be explained in chapter 2. Further information can be found in [82, 83, 84]. The idea has been adopted by Amri et al. [22, 23].

1. Introduction

A lot of additional published and patented designs of variable speed gearboxes for helicopters are based on the principles of epicyclic gearing, for example, [20, 26, 75]. A totally different approach was chosen by F. Buysschaert et al. [29, 30, 31]. They studied the use of a Ljungström turbine to drive a coaxial rotor. This development was not primarily intended to enable a variable rotor speed but is capable to do so and poses an unconventional approach to helicopter drivetrains.

Litt et al. [63] studied a sequential shifting algorithm for the control of a rotor with variable speed, but still a lot of work has to be done in this field before the first series helicopter equipped with the variable speed technology is ready for market.

1.4. Aim of the thesis

A lot of different ideas to realize a variable main rotor speed in various types of aircraft have been searched and Misté already studied the influence on the UH-60's powertrain including engines, rotors and a basic model of the transmission system. However, a detailed dynamic simulation of the propulsion system based on a sufficiently detailed model of the drivetrain has not yet been carried out. Therefore, the main objectives of this thesis, which are reflected by its structure, can be summarized as follows:

- I A comprehensive summary of the basics of epicyclic gearing and power-split transmissions shall be given. Based on this, a set of equations determining the operation of different Compound-Split architectures shall be derived.
- II With the fundamentals worked out in part I, the most promising architecture of a drivetrain containing one or more Compound-Split modules for the UH-60 shall be derived. In preparation for part III, a sufficiently detailed design of the specified transmission system, including the variator, shall be developed.
- III To show the feasibility of the derived transmission system, a dynamic simulation of the powertrain shall be performed.
- IV Safety and certification aspects play a major role in aviation. A transmission design which theoretically enables a variable rotor speed but does not fulfil basic requirements on reliability would not be an option for use in rotorcraft. This part of the thesis is dedicated to the discussion of these aspects.

Some of the research questions have been studied by the author in previous publications [82, 83, 84]. If information is taken from there – adapted or not – it is emphasized in the text.

Although a wide range of topics has been addressed in the research presented in this thesis, a lot of scientific and engineering work remains to be done. All parts of the powertrain need to be tailored for the application, before a series helicopter is ready for market. Rotor tolerant to a wide range of excitation frequencies, sufficiently efficient and reliable hydraulic machines as well as a mechanical drivetrain capable of fulfilling the requirements of rotorcraft operation still have to be developed, designed and tested.

Part I.

Epicyclic gear trains and power-split transmissions



Die approbierte gedruckte Originalversion dieser Dissertation ist an der TU Wien Bibliothek verfügbar.
The approved original version of this doctoral thesis is available in print at TU Wien Bibliothek.

2. Basics of epicyclic gearing and power-split transmissions

In this chapter a short overview of the field of epicyclic gearing is given and the basic equations are stated. Furthermore, the principles of power-split transmissions are described. Based on these foundations, the formulae will be abstracted in the following chapter in order to obtain a system of equations suitable for finding solutions of problems in the field of drive technology.

2.1. Principles and basic equations

2.1.1. Planetary gear sets

It shall be started with the description of the well-known Planetary Gear Set (PGS) consisting of three shafts and three different types of spur or helical gears. The term "planetary" will be only used for this kind of gear set, the general case will be referred to as "epicyclic". The three shafts are denoted by indices 1, 2 and C . The different types of gears which can be found in planetary gear sets are sun (shaft 1), ring (shaft 2) and planet gears (pivoted on carrier shaft C). One sun and one ring gear are combined with at least one (but usually more than two) planet gear(s). A typical arrangement is depicted in figure 2.1 The *planetary ratio* i_{12} is defined by the famous Willis¹ equation:

$$i_{12} := \frac{\omega_1}{\omega_2} \Big|_{\omega_C=0} = \frac{\omega_1 - \omega_C}{\omega_2 - \omega_C}, \quad (2.1)$$

where ω_1 , ω_2 and ω_C denote the angular velocities of the respective shafts. For gears, the planetary ratio i_{12} is the ratio of the numbers of teeth of sun and ring gear resp. the ratio of the working pitch diameter of the ring gear to the one of the sun gear. The range of the planetary ratio i_{12} of a planetary gear set as depicted in figure 2.1 is limited. By the very principle, $i_{12} < -1$ applies. Due to limitations in design and manufacturing of spur and helical gears, this range is further narrowed. In [77, p. 27] a range of $i_{12} \in [-11.3, -1.2]$ specified. The *basic ratio* of the angular speeds ω_1 and ω_2 in general operation conditions – i.e., $\omega_C \neq 0$ – is denoted k_{12} and defined as

$$k_{12} := \frac{\omega_1}{\omega_2}. \quad (2.2)$$

Apparently, $k_{12} = i_{12}$ applies for $\omega_C = 0$.

¹Robert Willis (1800-1875), English academic

2. Basics of epicyclic gearing and power-split transmissions

Analogous to definition (2.1), the planetary ratios can be defined as the ratio of the rotational speeds of two arbitrary shafts when the third one stands still (cf. [77, Arbeitsblatt 1]):

$$i_{21} := \frac{\omega_2}{\omega_1} \Big|_{\omega_C=0} = \frac{\omega_2 - \omega_C}{\omega_1 - \omega_C} = \frac{1}{i_{12}} \quad (2.3)$$

$$i_{1C} := \frac{\omega_1}{\omega_C} \Big|_{\omega_2=0} = \frac{\omega_1 - \omega_2}{\omega_C - \omega_2} = 1 - i_{12} \quad (2.4)$$

$$i_{C1} := \frac{\omega_C}{\omega_1} \Big|_{\omega_2=0} = \frac{\omega_C - \omega_2}{\omega_1 - \omega_2} = \frac{1}{i_{1C}} = \frac{1}{1 - i_{12}} \quad (2.5)$$

$$i_{2C} := \frac{\omega_2}{\omega_C} \Big|_{\omega_1=0} = \frac{\omega_2 - \omega_1}{\omega_C - \omega_1} = 1 - \frac{1}{i_{12}} \quad (2.6)$$

$$i_{C2} := \frac{\omega_C}{\omega_2} \Big|_{\omega_1=0} = \frac{\omega_C - \omega_1}{\omega_2 - \omega_1} = \frac{1}{i_{2C}} = \frac{i_{12}}{i_{12} - 1}. \quad (2.7)$$

Obviously, the six train ratios form three pairs of reciprocal values, each representing the same planetary gear set defined by i_{12} . The respective basic ratios can be easily defined analogous to (2.2) (cf. [77, Arbeitsblatt 1]).

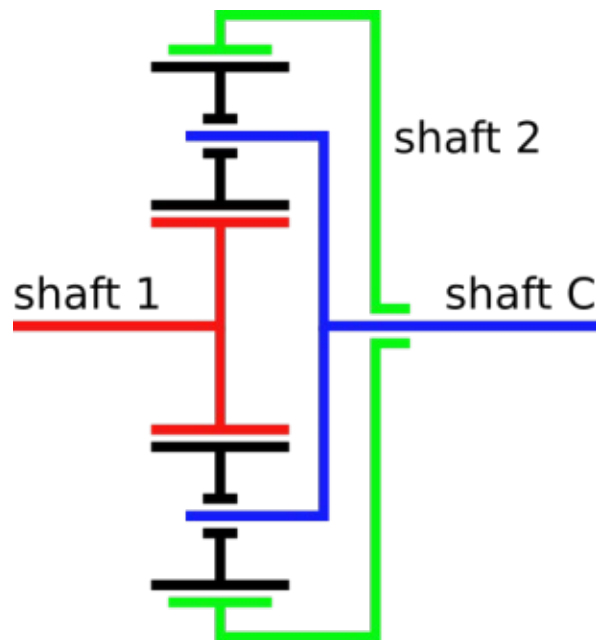


Figure 2.1.: Typical arrangement of a planetary gear set

2.1.2. Epicyclic gear sets

Epicyclic Gear Sets (EGSs) pose a generalization of planetary gear sets. The principal layout of an EGS with three shafts a , b and c is depicted in figure 2.2. Its *epicyclic ratio* i_{abc} of an EGS with shafts a , b and c can be defined as

$$i_{abc} := \frac{\omega_a}{\omega_b} \Big|_{\omega_c=0} = \frac{\omega_a - \omega_c}{\omega_b - \omega_c}. \quad (2.8)$$

The shafts can be – but are not restricted to – the three shafts of a planetary gear set. Analogous to (2.3), i_{acb} , i_{bac} , i_{bca} , i_{cab} , and i_{cba} can be defined. If the actual designation of the shafts does not matter or follows from the context, i_0 will be used for the epicyclic ratio. For the general considerations on one EGS, i_0 will be identified with i_{abc} . Of course, the respective *basic ratio* k_0 is

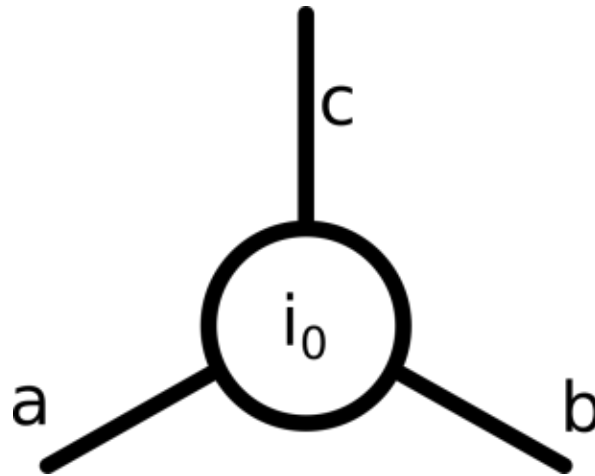


Figure 2.2.: Principal layout of an epicyclic gear set

$$k_0 := \frac{\omega_a}{\omega_b}. \quad (2.9)$$

The epicyclic ratio i_0 is an extension of (2.1), which takes different installation positions of planetary gear sets – e.g. ring gear as input and carrier shaft as output – into account but also includes epicyclic gear sets consisting of bevel gears or stepped planetary gears. Different to i_{12} , i_0 can be any real number. The epicyclic ratio is useful to study and compare different drivetrain architectures, but for the final design proposed later in this thesis, only planetary gear sets shall be used. The reason for this is, that planetary gears are widely used in rotorcraft transmissions and there are proven solutions for a multitude of design problems, which will be an advantage in the certification process. For this reason, a mapping from i_0 to i_{12} is needed. For $i_{12} \leq -1$ even a one-to-one mapping can be defined (cf. [77, pp. 35 & 249]):

$$i_{12}(i_0) = \begin{cases} i_0 & -\infty < i_0 \leq -1 & (i_0 = i_{12}) \\ 1/i_0 & -1 < i_0 \leq 0 & (i_0 = i_{21}) \\ 1 - 1/i_0 & 0 < i_0 \leq \frac{1}{2} & (i_0 = i_{C1}) \\ i_0/(i_0 - 1) & \frac{1}{2} < i_0 \leq 1 & (i_0 = i_{C2}) \\ 1/(1 - i_0) & 1 < i_0 \leq 2 & (i_0 = i_{2C}) \\ 1 - i_0 & 2 < i_0 \leq \infty & (i_0 = i_{1C}). \end{cases} \quad (2.10)$$

For the final planetary ratios, the discussed limitations of i_{12} have to be considered.

2.1.3. Kinematics of epicyclic gear sets

As a consequence of (2.8), an epicyclic gear set has two kinematic Degrees Of Freedom (DOFs), i.e., the angular velocity of two of the three shafts can be chosen independently, determining the speed

2. Basics of epicyclic gearing and power-split transmissions

of the third. In this thesis, shaft a will be identified with the input shaft of a transmission system and b with the output shaft. Indices c and d will refer to shafts which are connected to some kind of machine able to control their angular velocity. Therefore, ω_b will be regarded as the dependent variable (in a mathematical sense):

$$\omega_b = \frac{\omega_a + (i_0 - 1) \omega_c}{i_0}. \quad (2.11)$$

2.1.4. Torque and power

Angular velocity ω , torque Q and power P of a rotating shaft are interconnected via

$$P = Q \omega. \quad (2.12)$$

If the efficiency of gear meshes is neglected,

$$\sum_{i \in \{a,b,c\}} Q_i = 0 \quad (2.13)$$

and

$$\sum_{i \in \{a,b,c\}} P_i = \sum_{i \in \{a,b,c\}} Q_i \omega_i = 0 \quad (2.14)$$

have to be fulfilled. Therefore, the ratios between the torques at the three shafts are given by

$$Q_a : Q_b : Q_c = 1 : -i_0 : i_0 - 1. \quad (2.15)$$

This means, that an epicyclic gear set has one static degree of freedom, i.e., in states of balance, one torque can be chosen independently and the other two are determined by (2.15). The description of torques and powers of lossy meshes in general cases is possible but tedious and will not be discussed here. When describing the efficiency of the chosen drivetrain architecture for the UH-60, the efficiency of the used planetary gear sets will be discussed there. For a more general survey of the topic it is referred to [77, p. 59. sqq.].

2.2. Power-Split Transmissions

Epicyclic gear sets can be used to build up so-called Power-Split Transmissions (PSTs). In a transmission system of this kind the power provided by the main (thermal) engine is split into a mechanical and a so-called variator path. The latter can consist of two electric or hydraulic machines and the related system. Although this technology is widely used in Hybrid Electric Vehicles (HEVs), no energy storage such as a battery or a hydraulic accumulator is needed and thus the drivetrain can be operated as a Continuously Variable Transmission (CVT). Because of the high powers involved in a rotorcraft transmission system and the resulting weight of energy storages, this thesis will focus on the CVT case, i.e., without additional energy storage. Three main types of power-split transmissions can be distinguished: Output-Split (OS), Input-Split (IS) and Compound-Split (CS). In addition, transmission systems comprising more than two epicyclic gear sets are possible. The difference between the three main types is the connection of the variator machines to the mechanical path. In Output- and Input-split transmissions, one machine is connected to the mechanical

path by a gear train with constant ratio and the other by an epicyclic gear set. Input-Split means that the whole engine power is split into mechanical and variator power in the epicyclic gear set and brought together again via a fixed-ratio gear stage. In Output-Split transmissions it is just the other way around. In difference, Compound-Split transmissions use two nested epicyclic gear sets connected to the variator machines. All three main types of power-split transmissions have two kinematic degrees of freedom. [53, 88]

Since the efficiency of the variator path is usually lower than the one of mechanical transmission, the portion of propulsion power transmitted in the variator path has a strong influence on drivetrain efficiency. Therefore, the factor ε as the ratio of variator power P_{var} to input power P_{in} is introduced (cf. [53, p. 39]):

$$\varepsilon := \frac{P_{\text{var}}}{P_{\text{in}}}. \quad (2.16)$$

2.2.1. Output-Split

The detailed description of the three most important types of power-split transmissions will start with the Output-Split. It will also be used for describing the principles of power-split transmissions in general.

In figure 2.3 the layout of an Output-Split transmission system is depicted. Only the parts necessary to build up such a system are considered. In general, a drivetrain can contain additional gear stages, shafts and clutches. On the left-hand side of figure 2.3, the input power from the engine(s) is supplied via shaft a . A portion of power is taken off by a fixed-ratio gear stage and transmitted to one of the machines of the variator. This machine is depicted as hydraulic pump but could also be an electric generator. Here the mechanical power is transformed into hydraulic power which is transmitted to a second machine, a hydraulic or electric motor. The power is converted back to torque and angular velocity and transmitted to an epicyclic gear set with epicyclic ratio i_0 . Here the power from the variator and the remaining mechanical power on shaft a are brought together again and the output power P_{out} is further transmitted to the driven machine(s). As will be explained later, the operation modes of the variator machines – i.e., pump or motor – can be interchanged, but this operation condition is not desirable.

To be able to use an additional source of power, an energy storage device could be added to the variator path. Due to the high masses expected for these devices they will not be used in this thesis.

To vary the output speed of the Output-Split transmission system, the speed of the engine and the one of the hydraulic/electric motor can be adapted. To illustrate the characteristics of an Output-Split, angular speeds, torques and powers are calculated using equations (2.11) to (2.16), epicyclic ratios from 0.2 to 5.0 and basic ratios $k_0 \in [\frac{2}{3} i_0, 1.5 i_0]$. As will be explained later, it is very important, the range of k_0 includes the epicyclic ratio i_0 . It was chosen because according to [46], a transmission spread Φ , i.e., the ratio of maximum and minimum output speed, of 1.5 is desirable for the UH-60 helicopter. In principle, the range of k_0/i_0 can be extended to negative values, which can be used as reverse gear in hybrid electric vehicles. However, for rotorcraft a reversal of the sense of rotation is not needed. Since on both axes transmission ratios are plotted, the axes are scaled logarithmically so that sections of equal length refer to the same multiple of transmission

2. Basics of epicyclic gearing and power-split transmissions

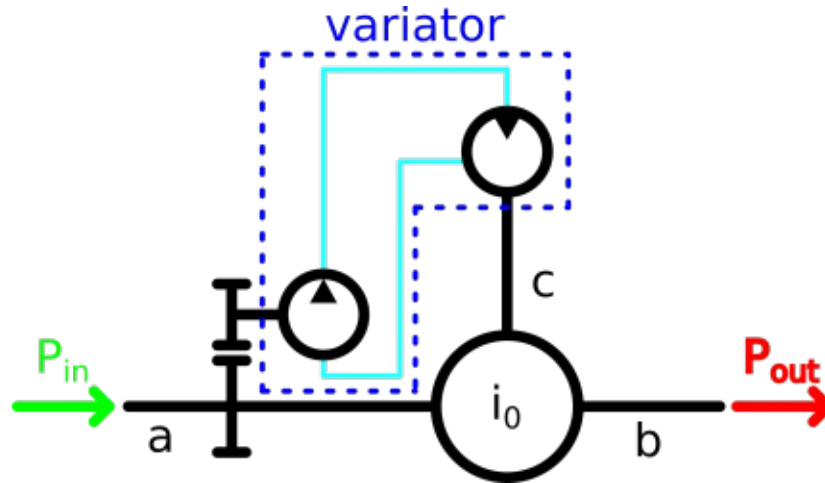


Figure 2.3.: Principal layout of an Output-Split transmission

ratio. Where applicable, the results are normalized to the input quantities ω_{in} , Q_{in} and P_{in} . In figure 2.4 (a), the relative angular velocity of shaft b is depicted. It is given by

$$\omega_b = \frac{\omega_a}{k_0}. \quad (2.17)$$

For epicyclic ratios near 1.0 and the given range of k_0 , the Output-Split transmission can reduce as well as increase the input speed. Values of i_0 below 1.0 generally lead to increased output speed whilst such above 1.0 reduce the input speed. Since for rotorcraft drivetrains an increase of speed is not of interest, values of i_0 larger than 1.0 are advantageous.

Subfigure (b) shows the angular velocity of shaft c in accordance with

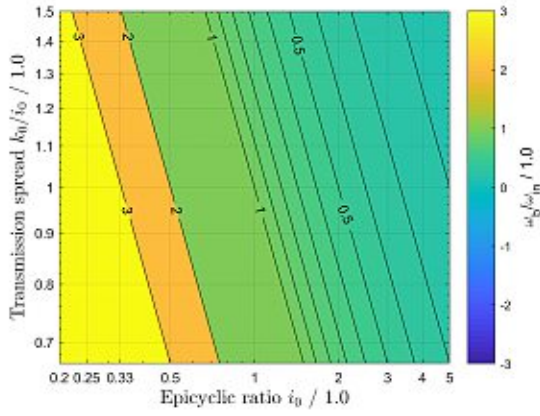
$$\omega_c = \omega_a \frac{1 - \frac{i_0}{k_0}}{1 - i_0}. \quad (2.18)$$

For $i_0 = 1.0$ and $k_0 \neq 1.0$, ω_c has a singularity and near these values angular velocities with high absolute values occur. However, there are wide ranges where ω_c has speeds below the input speed ω_a . For $k_0 = i_0$, shaft c stands still. As will be explained later, this is a very desirable operation condition of the OS transmission system.

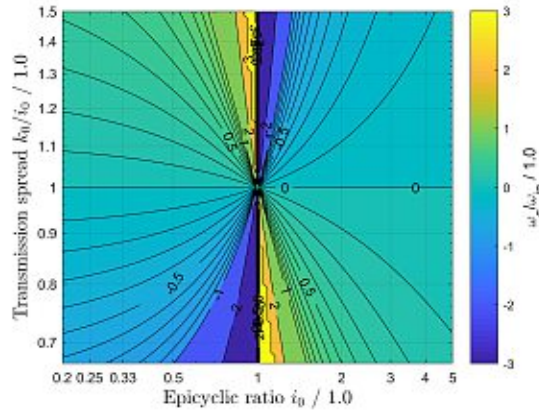
The following three subfigures (c), (d) and (f) depict the torques of the three shafts a , b and c which act on the EGS. They are calculated by

$$\begin{aligned} Q_a &= -\frac{Q_b}{i_0} &= \frac{P_{in} k_0}{i_0 \omega_a} \\ Q_b &= -\frac{P_{in}}{\omega_b} &= -\frac{P_{in} k_0}{\omega_a} \\ Q_c &= (i_0 - 1) Q_a &= \frac{(i_0 - 1) P_{in} k_0}{i_0 \omega_a}. \end{aligned} \quad (2.19)$$

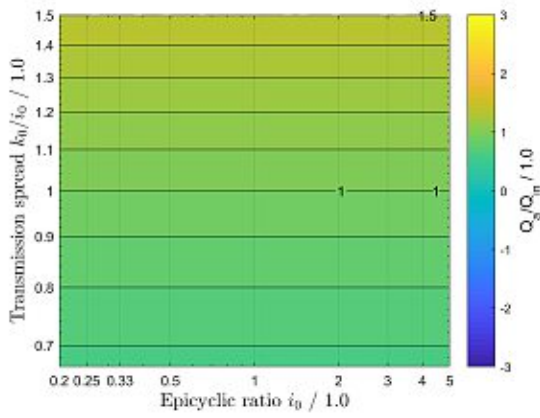
These equations are based on the assumption that no losses occur, i.e., $P_{in} = -P_{out}$. Apparently, Q_a is input torque times k_0/i_0 . At $k_0/i_0 = 1$, the whole input torque – and therefore the whole input power – is transmitted to the epicyclic gear set via shaft a . Since $P_{in} = -P_{out}$, the plot of Q_b in



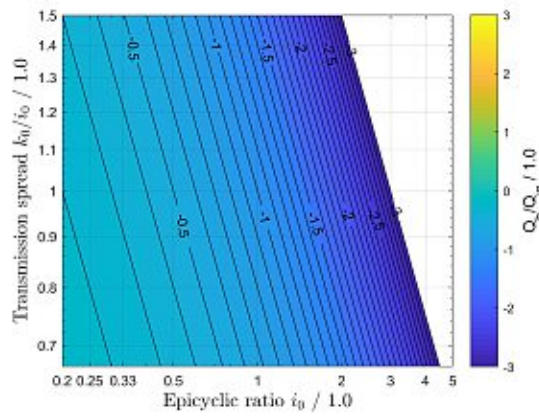
(a) Angular velocity of shaft *b* rel. to ω_{in}



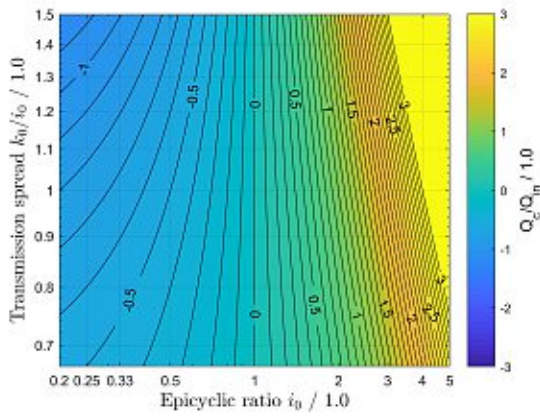
(b) Angular velocity of shaft *c* rel. to ω_{in}



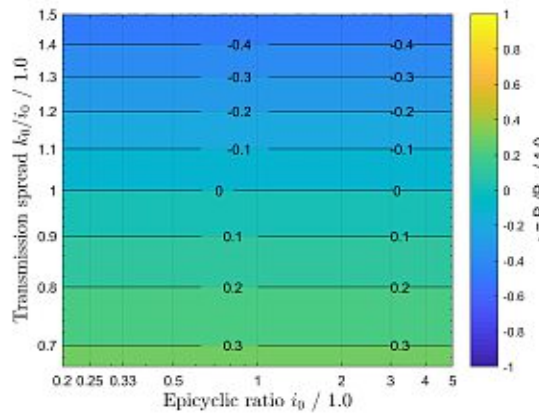
(c) Torque at shaft *a* rel. to Q_{in}



(d) Torque at shaft *b* rel. to Q_{in}



(e) Torque at shaft *c* rel. to Q_{in}



(f) Factor ϵ

Figure 2.4.: Quantities for Output-Split transmissions

2. Basics of epicyclic gearing and power-split transmissions

subfigure (d) is the inverse of the plot of ω_b in subfigure (a) and therefore the similar assertions apply. From (2.19) and (e) it can be seen that $Q_c = 0$ for $i_0 = 1$. However, at these epicyclic ratios the angular velocity ω_c has a singularity and goes towards infinite.

A very important characteristic of the Output-Split transmission is the ratio between the power to be transmitted via the variator path and the total propulsive power provided by the engine. The formulae already given yields

$$\varepsilon = \frac{P_c}{P_{\text{in}}} = \frac{Q_c \omega_c}{P_{\text{in}}} = 1 - \frac{k_0}{i_0}. \quad (2.20)$$

The results are plotted in figure 2.4 (f). For $k_0/i_0 = 1$, shaft c stands still and therefore no power is transmitted via the variator path. Since the whole propulsion power is transmitted mechanically, this transmission ratio is called a Mechanical point (MP) Θ . The operation is highly efficient, which is the reason why the range of transmission ratios k_0 ought to include i_0 . Below $i_0 = 1.0$, P_c is positive whilst above these values it is of negative sign. This means that in the first case power is supplied to the EGS by shaft c and in the second case it is taken off. Referring to figure 2.3, this means that for $k_0/i_0 > 1.0$, the direction of power flow in the variator changes and that the motor works as a pump and vice versa. With (2.19) and figure 2.4 (c) it can be seen that the power at shaft a , $P_a = Q_a \omega_a$, becomes larger than the input power in these operation conditions. Accordingly, power is circulating in the transmission system. Since the circulating power does not contribute to driving shaft b and the connected machines but causes losses, these operation conditions have to be avoided. Different to hybrid electric vehicles, which are operated in a range with circulating power (cf. [53, p. 39]), it shall be avoided in rotorcraft. The maximum value of ε in this case is 0.33, i.e., one third of the propulsive power is transmitted via the variator path. If circulating power flow is permissible, a range of k_0 from 0.8 to 1.2 would yield a maximum absolute value of $\varepsilon = 0.2$.

Of course, the range of i_0 in figure 2.4 can be extended to negative values. It follows from (2.17) that negative values of i_0 will yield output speeds with negative sign but the same absolute values as in figure 2.4 (a). This also applies for Q_b . Q_a and ε only depend on k_0/i_0 but not on i_0 explicitly. In contrast, ω_c and Q_c are strongly influenced by negative epicyclic ratios. As can be seen from (2.18), the absolute value of ω_c is smaller for $-|i_0|$ than for $|i_0|$. The effect is just inverse for the torque Q_c , whose absolute value is greater. For $i_0 < -1$, Q_c is the highest torque at the EGS for the given range of k_0 . Therefore, this range will be excluded in this thesis.

2.2.2. Input-Split

The second type of power-split transmission is the Input-Split sketched in figure 2.5. In some sense, the arrangement of the Output-Split is mirrored. Shaft a transmits the propulsive power to the epicyclic gear set, where it is split into one portion which flows directly to the output shaft b and one supplied to the pump/generator of the variator by shaft c . After being transformed in the variator the latter is transferred to shaft b via a fixed-ratio gear stage.

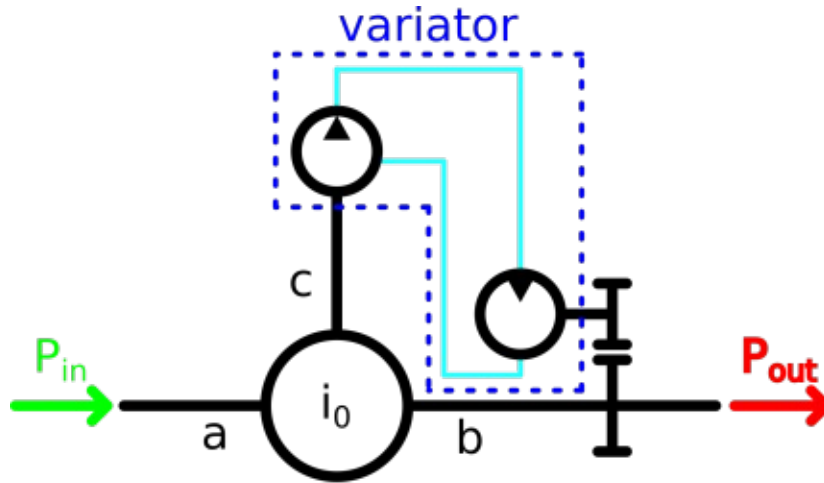


Figure 2.5.: Principal layout of an Input-Split transmission

When efficiency is neglected, the following formulae apply:

$$\begin{aligned}
 Q_a &= Q_{\text{in}} & \omega_b &= \frac{\omega_a}{k_0} \\
 Q_b &= -i_0 Q_{\text{in}} & \omega_c &= \omega_a \frac{1 - \frac{i_0}{k_0}}{1 - i_0} \\
 Q_c &= (i_0 - 1) Q_{\text{in}} & \varepsilon &= \frac{i_0}{k_0} - 1.
 \end{aligned} \tag{2.21}$$

Apparently, the angular velocities are the same as for the Output-Split and the torques are independent of the basic ratio k_0 . As for the OS, ε does not depend on i_0 explicitly but on the ratio k_0/i_0 . For $i_0 \in [0.2, 5]$ and $k_0 \in [\frac{2}{3}i_0, 1.5i_0]$, the resulting values of the torques and ε are depicted in figure 2.6. The torque at shaft a is the input torque for all epicyclic ratios. At $i_0 = 0.5$ the torques Q_b and Q_c are the same. For ratios below this value, Q_c is the torque with the biggest absolute value and for $i_0 > 0.5$ it is Q_b . In difference to the OS, circulating power flow occurs for negative values of ε . From figure 2.6 (b) it can be seen that circulating power flow occurs for $k_0 < i_0$. The maximum absolute value of ε is 0.33 if this is not permissible and 0.2 for $k_0 \in [\frac{5}{6}i_0, \frac{5}{4}i_0] \approx [0.83i_0, 1.25i_0]$. The Input-Split has one mechanical point at $k_0 = i_0$. At this basic ratio shaft c stands still and no power is transmitted via the variator path.

2. Basics of epicyclic gearing and power-split transmissions

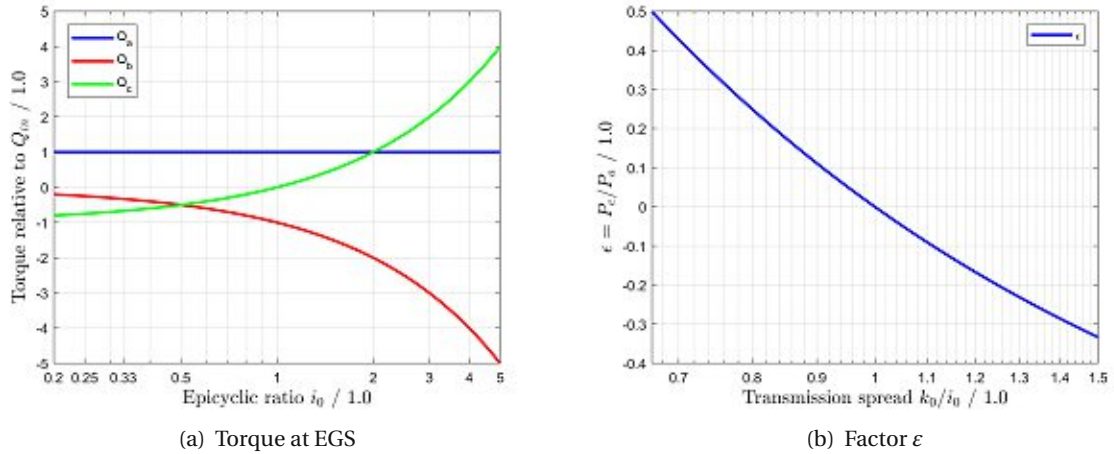


Figure 2.6.: Quantities for Input-Split transmissions

2.2.3. Compound-Split

The main drawback of Output- and Input-Split transmissions is the poor efficiency when operated at transmission ratios far off the mechanical point. One possibility to improve this characteristic is the use of a second epicyclic gear set with a different epicyclic ratio. If appropriately connected, the two epicyclic gear sets yield a transmission system with two kinematic degrees of freedom and two mechanical points. This type of power-split transmission is called Compound-Split. The principle is used in hybrid electric vehicles, as CVT in ships and in aircraft to provide constant input speed to electrical generators. In the latter case, the transmission is known as Constant Speed Drive (CSD) and is part of the so-called Integrated Drive Generator (IDG).

The four possible arrangements are depicted in figure 2.7. As for OS and IS, the input power is supplied to shaft a and the output is connected to b . In Arrangement **A**, the input power is split at shaft a . This can be achieved by a being a shaft (sun, ring, carrier) of each EGS or by means of additional fixed-ratio gear stages. Since a Compound-Split transmission comprises two EGS, a distinction between them has to be introduced. They shall be referred to according to (2.8). The shaft c of the EGS i_{abc} is connected to one machine of the variator (depicted as hydraulic pump) and d is driven by the other. When shaft c stands still, there is no power supply to the variator system and since there is no energy storage available, no torque from the motor acts on shaft d . The same applies when shaft d stands still. The corresponding basic ratios $k_0 := \frac{\omega_a}{\omega_b}$ are the two mechanical points Θ_1 and Θ_2 of the CS transmission, i.e.,

$$\Theta_1 := \left. \frac{\omega_a}{\omega_b} \right|_{\omega_c=0} = \frac{\omega_a - \omega_c}{\omega_b - \omega_c}, \quad \Theta_2 := \left. \frac{\omega_a}{\omega_b} \right|_{\omega_d=0} = \frac{\omega_a - \omega_d}{\omega_b - \omega_d}. \quad (2.22)$$

At shaft b the power is brought together again and further transmitted to the driven machines. The working principle is the same for the other three arrangements **B**, **C** and **D**. In all of them two shafts of each EGS are coupled which leads to two DOFs. They also have two MPs each. In the

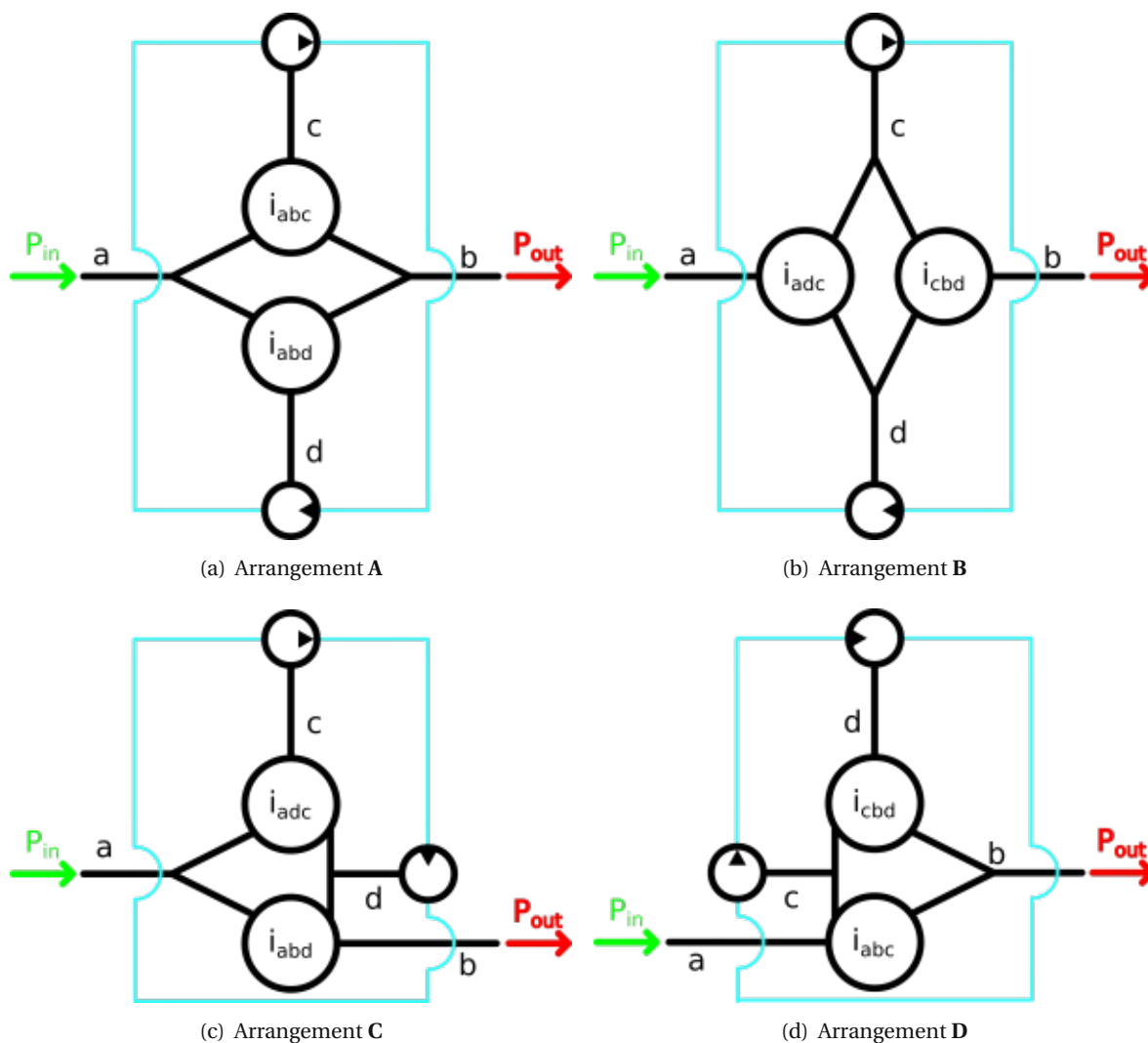


Figure 2.7.: Principal layout of Compound-Split transmissions

four arrangements four different epicyclic ratios i_{abc} , i_{abd} , i_{adc} and i_{cbd} occur. Their values can be determined with (2.22):

$$\begin{aligned}
 i_{abc} &:= \frac{\omega_a}{\omega_b} \Big|_{\omega_c=0} = \frac{\omega_a - \omega_c}{\omega_b - \omega_c} = \Theta_1, \\
 i_{abd} &:= \frac{\omega_a}{\omega_b} \Big|_{\omega_d=0} = \frac{\omega_a - \omega_d}{\omega_b - \omega_d} = \Theta_2, \\
 i_{adc} &:= \frac{\omega_a}{\omega_d} \Big|_{\omega_c=0} = \frac{\omega_a - \omega_c}{\omega_d - \omega_c} = \frac{\Theta_1 (1 - \Theta_2)}{\Theta_1 - \Theta_2}, \\
 i_{cbd} &:= \frac{\omega_c}{\omega_b} \Big|_{\omega_d=0} = \frac{\omega_c - \omega_d}{\omega_b - \omega_d} = \frac{\Theta_1 - \Theta_2}{\Theta_1 - 1}.
 \end{aligned}
 \tag{2.23}$$

2. Basics of epicyclic gearing and power-split transmissions

Furthermore, the kinematics of all four CS arrangements is the same and given by

$$\begin{aligned}\omega_b &= \frac{\omega_a}{k_0} \\ \omega_c &= \omega_a \frac{1 - \frac{\Theta_1}{k_0}}{1 - \Theta_1} \\ \omega_d &= \omega_a \frac{1 - \frac{\Theta_2}{k_0}}{1 - \Theta_2}.\end{aligned}\quad (2.24)$$

The conditions

$$\begin{aligned}\sum_{j \in \{a,b,c,d\}} Q_j &= 0 \\ P_a + P_b &= Q_a \omega_a + Q_b \omega_b = 0 \\ P_c + P_d &= Q_c \omega_c + Q_d \omega_d = 0\end{aligned}\quad (2.25)$$

and equation (2.24) yield the following formulae for the torques:

$$\begin{aligned}Q_a &= Q_{\text{in}} \\ Q_b &= -k_0 Q_{\text{in}} \\ Q_c &= Q_{\text{in}} (\Theta_1 - 1) \frac{k_0 - \Theta_2}{\Theta_1 - \Theta_2} \\ Q_d &= Q_{\text{in}} (\Theta_2 - 1) \frac{\Theta_1 - k_0}{\Theta_1 - \Theta_2}.\end{aligned}\quad (2.26)$$

In contrast to Output- and Input-Split, the torques Q_a and Q_b denote the input and output torques of the Compound-Split transmission and not the portion acting on one of the epicyclic gear sets. Because of the different epicyclic ratios according to (2.23), the latter depend on the CS arrangement and can be calculated from Q_c resp. Q_d by (2.15). With equations (2.24) and (2.26) the powers at shafts c and d are given by

$$\begin{aligned}P_c &= P_{\text{in}} \frac{(\Theta_1 - k_0)(k_0 - \Theta_2)}{k_0(\Theta_1 - \Theta_2)} \\ P_d &= -P_c.\end{aligned}\quad (2.27)$$

Depending on the mechanical points, the variator machine acting on shaft c is a pump or a motor:

$$P_c(k_0) = \begin{cases} > 0 \text{ (motor)} & |\Theta_1| > |\Theta_2|, \\ < 0 \text{ (pump)} & |\Theta_1| < |\Theta_2|. \end{cases}\quad (2.28)$$

Without loss of generality, the variator machine acting on c will be considered as a pump hereinafter. In the discussion of the flow of circulating power in the mechanical path, the advantage of this definition will become apparent. Furthermore, only positive values of Θ_1 and Θ_2 will be considered to limit the torque acting on shafts c and d .

With P_c , ε can be calculated by

$$\varepsilon = \frac{P_c}{P_{\text{in}}} = \frac{(\Theta_1 - k_0)(k_0 - \Theta_2)}{k_0(\Theta_1 - \Theta_2)} = \frac{\left(1 - \frac{k_0}{\Theta_1}\right) \left(\frac{k_0}{\Theta_1} - \frac{\Theta_2}{\Theta_1}\right)}{\frac{k_0}{\Theta_1} \left(1 - \frac{\Theta_2}{\Theta_1}\right)}.\quad (2.29)$$

With the assumptions made for Θ_1 and Θ_2 , the following statements apply:

$$\varepsilon \begin{cases} < 0 & \text{for } k_0 \in]\Theta_1, \Theta_2[\\ > 0 & \text{for } k_0 \notin [\Theta_1, \Theta_2], k_0 > 0 \\ = 0 & \text{for } k_0 \in \{\Theta_1, \Theta_2\}. \end{cases} \quad (2.30)$$

This means that no circulating power flow occurs for basic ratios between the mechanical points. Furthermore, $|\varepsilon|(k_0)$ has a single extreme value of

$$|\varepsilon|_{\max} := \left| \frac{\sqrt{\frac{\Theta_2}{\Theta_1}} - 1}{\sqrt{\frac{\Theta_2}{\Theta_1}} + 1} \right| \quad (2.31)$$

at $k_0 = \sqrt{\Theta_1 \Theta_2}$. The function $\varepsilon(\log(\cdot))$, restricted to the domain of the log function, is symmetric with respect to this value, i.e.,

$$\varepsilon\left(\log\left(\sqrt{\Theta_1 \Theta_2}\right) + \log(x)\right) = \varepsilon\left(\log\left(\sqrt{\Theta_1 \Theta_2} x\right)\right) = \varepsilon\left(\log\left(\frac{\sqrt{\Theta_1 \Theta_2}}{x}\right)\right) = \varepsilon\left(\log\left(\sqrt{\Theta_1 \Theta_2}\right) - \log(x)\right). \quad (2.32)$$

Consequently,

$$\varepsilon(k_0) = \varepsilon\left(\frac{\Theta_1 \Theta_2}{k_0}\right) \quad (2.33)$$

applies for $k_0 > 0$. Since the absolute value of $|\varepsilon|_{\max}$ increases with the ratio $\frac{\Theta_2}{\Theta_1}$, the mechanical points must be set $\Theta_2 = \Phi \Theta_1$ when the CS shall be operated with a transmission spread of Φ , without circulating power flow and a minimum of $|\varepsilon|_{\max}$. For $\Phi = 1.5$, this yields $|\varepsilon|_{\max} \approx 0.101$. If circulating power flow is permitted and a minimum of $|\varepsilon|_{\max}$ is desired, i.e.,

$$\begin{aligned} k_{0,\max} &\stackrel{!}{=} \Phi k_{0,\min} \\ \left| \frac{\sqrt{\frac{\Theta_2}{\Theta_1}} - 1}{\sqrt{\frac{\Theta_2}{\Theta_1}} + 1} \right| &\stackrel{!}{=} \left| \frac{(\Theta_1 - k_{0,\min})(k_{0,\min} - \Theta_2)}{k_{0,\min}(\Theta_1 - \Theta_2)} \right| \\ \left| \frac{\sqrt{\frac{\Theta_2}{\Theta_1}} - 1}{\sqrt{\frac{\Theta_2}{\Theta_1}} + 1} \right| &\stackrel{!}{=} \left| \frac{(\Theta_1 - k_{0,\max})(k_{0,\max} - \Theta_2)}{k_{0,\max}(\Theta_1 - \Theta_2)} \right|, \end{aligned} \quad (2.34)$$

this value can be significantly reduced. Solving (2.34) for $\Phi = 1.5$ yields

$$\begin{aligned} \Theta_1 &\approx 1.06 k_0 \\ \Theta_2 &\approx 1.41 k_0 \\ |\varepsilon|_{\max} &\approx 0.0716. \end{aligned} \quad (2.35)$$

Although the ε value is significantly lower if circulating power flow is permitted, this thesis focusses on the case of basic ratios between the mechanical points. The main reason is that the four-quadrant operation of hydraulic motors, which will be used in the variator, raises issues leading beyond the scope of this thesis.

2. Basics of epicyclic gearing and power-split transmissions

Besides the power circulation in the CS transmission if operated at basic ratios outside the interval between the mechanical points, power circulating in the mechanical path only can occur (cf. [77, p. 146 sqq.]). According to [77, p. 251], the shaft of an EGS transmitting maximum power can be determined depending on the epicyclic ratio and the basic ratio. The information presented there was adapted for a Compound-Split transmission in arrangement **A** and is summarized in table 2.1. In the first column the range of the two epicyclic ratios i_{abc} and i_{abd} (equivalent to the

i_{abc}, i_{abd}	k_0	$ P _{\max}$ of EGS i_{abc} at shaft	$ P _{\max}$ of EGS i_{abd} at shaft	Remark
$0 < i_{abc} < i_{abd} < 1$	$k_0 < 0$	c	d	circ. power flow
	$0 < k_0 < i_{abc}$	b	b	circ. power flow
	$i_{abc} < k_0 < i_{abd}$	a	b	no circ. power flow
	$i_{abd} < k_0$	a	a	circ. power flow
$0 < i_{abc} < 1 < i_{abd}$	$k_0 < 0$	c	d	circ. power flow
	$0 < k_0 < i_{abc}$	b	b	circ. power flow
	$i_{abc} < k_0 < i_{abd}$	a	b	no circ. power flow
	$i_{abd} < k_0$	a	a	circ. power flow
$1 < i_{abc} < i_{abd}$	$k_0 < 0$	c	d	circ. power flow
	$0 < k_0 < i_{abc}$	b	b	circ. power flow
	$i_{abc} < k_0 < i_{abd}$	a	b	no circ. power flow
	$i_{abd} < k_0$	a	a	circ. power flow

Table 2.1.: Operating ranges and shafts transmitting the maximum absolute value of power (cf. [77, p. 251])

two mechanical points Θ_1 and Θ_2) can be found. The ratio between them was chosen so that with equations (2.27) and (2.28), the machine acting on shaft c is the pump/generator for $k_0 \in [\Theta_1, \Theta_2]$. Furthermore, only positive mechanical points were studied. In the second column the different cases of $k_0 = k_{ab}$ are listed. Since the focus is on the shaft transmitting the maximum power and not on efficiency etc. or distribution of power, some cases listed in [77] were omitted. The following two columns contain the designation of the shaft transmitting the maximum power for both of the epicyclic gear sets. In three-shaft-operation, the power of two shafts are of the same sign whilst the power transmitted via the third shaft is of the different one. Since the sum of the three powers has to be zero, the latter is transmitting the maximum absolute value of power. To avoid flow of circulating power, this should be shaft a for the EGS connected to the pump/generator and shaft b for the EGS connected to the motor. It can be found that for $k_0 \in [\Theta_1, \Theta_2]$, no power flow occurs for any considered combination of i_{abc} and i_{abd} . The flow of idle power for basic ratios outside this interval has been discussed previously.

So far, these findings are only valid for arrangement **A**, but they can be easily extended to the other three arrangements. With figure 2.7 and equations (2.23), it can be understood, that the third column of table 2.1 is also valid for arrangement **D** and the fourth column is also valid for arrangement **C**. Turning to the latter, it can be seen that if the shaft transmitting maximum power is not b for i_{abd} , this means that either a or d do not supply power to EGS i_{abd} but take power off. If k_0 is restricted to $[\Theta_1, \Theta_2]$ – otherwise circulating power occurs anyway –, the machine acting on d is the motor. Also, the input power supplied to shaft a is positive. As a consequence of a or

d taking off power from i_{abd} , either a supplies a greater power than P_{in} to EGS i_{adc} or d supplies power to it instead of taking off. In both cases a flow of circulating power occurs. Therefore, b not being the shaft transmitting the maximum power of EGS i_{abd} ($k_0 \in [\Theta_1, \Theta_2]$) leads to a flow of idle power in EGS i_{adc} . Using the same line of argumentation, it is concluded that a not being the shaft transmitting the maximum power of EGS i_{abc} ($k_0 \in [\Theta_1, \Theta_2]$) leads to a flow of idle power in EGS i_{cbd} . Since the occurrence of the flow of circulating power only depends on the basic ratio k_0 and the mechanical points Θ_1 and Θ_2 , it can be concluded that it occurs in arrangement **B** if either i_{abc} or i_{abd} fulfil the conditions. This means, that i_{abc} fulfilling the condition leads to i_{cbd} being affected by circulating power which further leads to i_{adc} being affected by circulating power and finally, i_{abd} is also affected. This also works the other way around: $i_{abd} \rightarrow i_{adc} \rightarrow i_{cbd} \rightarrow i_{abc}$. Therefore, the flow of circulating power occurs for all or none of the four arrangements and, as explained previously, does not occur for $\text{sgn}(\Theta_1) = \text{sgn}(\Theta_2)$, $\Theta_1 < \Theta_2$ and $k_0 \in [\Theta_1, \Theta_2]$.

In figure 2.8 the main quantities at a Compound-Split transmission in dependence of the mechanical point Θ_1 and $\frac{k_0}{\Theta_1} \in [1, 1.5]$ are depicted. Due to the definition of ω_b , it is the same as for Output- and Input-Split. The angular velocities at the variator shafts, ω_c and ω_d , depicted in 2.8 (b) and (c) also have the characteristics shown in figure 2.4 (b). Subfigures 2.8 (d) and (e) present the torques at the two variator shafts. These differ strongly from the ones for OS and IS, which leads to lower powers in the variator path of the CS. The resulting ratio ε is depicted in Subfigure 2.8 (f). Clearly visible, its value is zero at the two mechanical points and has its minimum at the geometric mean of them. Also, the value of $|\varepsilon|_{\max} \approx 0.1$ can be read off.

2. Basics of epicyclic gearing and power-split transmissions

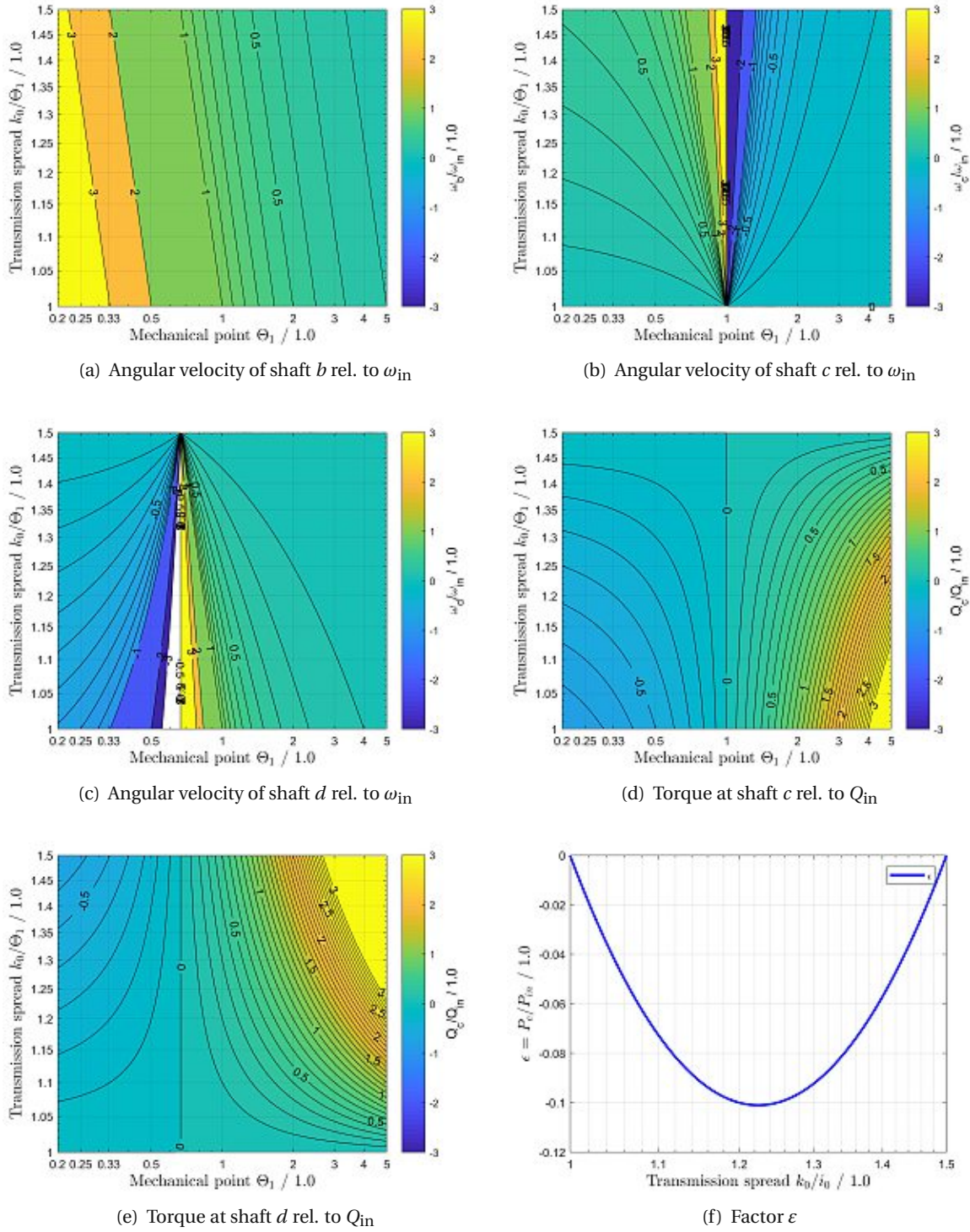


Figure 2.8.: Quantities for Compound-Split transmissions

2.2.4. Summary of Power-Split transmissions

In the previous sections the properties of the three most important architectures of power-split transmissions – Output-, Input- and Compound-Split – were described and compared. It was shown that the Compound-Split offers the opportunity to obtain a given transmission spread with a smaller portion of propulsive power to be transmitted via the less efficient variator path. The four different arrangements of a CS transmission system were described, and it was shown, that they are identical with respect to their kinematic properties. An important finding was that for $\text{sgn}(\Theta_1) = \text{sgn}(\Theta_2)$, $\Theta_1 < \Theta_2$ and $k_0 \in [\Theta_1, \Theta_2]$ no flow of idle power occurs for any arrangement. As a result of all of this, it is decided to analyse the possibilities of a CS transmission in rotorcraft in detail.



Die approbierte gedruckte Originalversion dieser Dissertation ist an der TU Wien Bibliothek verfügbar.
The approved original version of this doctoral thesis is available in print at TU Wien Bibliothek.

Part II.

Design of a Compound-Split drivetrain for the UH-60



Die approbierte gedruckte Originalversion dieser Dissertation ist an der TU Wien Bibliothek verfügbar.
The approved original version of this doctoral thesis is available in print at TU Wien Bibliothek.

3. Basic Architecture

This chapter deals with the definition of the principal layout of a rotorcraft transmission system containing one or more Compound-Split modules. Parts of the information presented have been published in [83].

3.1. The UH-60's transmission system

The Sikorsky UH-60 Black Hawk is a medium-lift, twin-engine Utility Helicopter (UH) developed and manufactured by Sikorsky Aircraft Corporation [119]. It is well-studied and therefore was chosen as a basis for showing the feasibility of a helicopter with a continuously variable transmission system.

The basic structure of the UH-60's transmission system as found in [120] is depicted in figure 3.1. The rotors and accessories are driven by two General Electrics (GE) T700 Turboshaft Engines (TSEs) rotating at 20900 RPM, each providing 1543 SHP (1151 kW) of intermediate power (cf. [121]). In the two input modules, the speed is reduced to 5750 RPM by a bevel gear stage. The bevel gear is connected to a shaft (*red*) connecting input module and main gearbox (MGB) via a free-wheeling unit. This shaft is also driving the accessories (not depicted in figure 3.1) and further leads into the main gearbox, where the powers of both turboshaft engines are brought together and speed is further reduced to 1207 RPM¹ by a bevel gear stage. From the output shaft of this stage the tail rotor (TR) drive (*green*) goes off and the main rotor (MR) power is transmitted into a planetary gear stage, the output shaft (carrier) of which is the main rotor shaft rotating at 258 RPM. The tail rotor power is further transmitted to the tail rotor via an intermediate gearbox and the tail gearbox.

3.2. Possible drivetrain architectures

There are virtually unlimited possibilities to implement a Compound-Split module as part of the UH-60's transmission system. To limit the possible drivetrain architectures, three constraints are imposed in this work:

1. For constant power consumption, a reduction of the main rotor RPM leads to increased torque and therefore to a higher power demand of the tail rotor. In [39] three different cases were examined:
 - a. Constant ratio of main and tail rotor speeds (TR following MR speed variation)
 - b. Continuously variable tail rotor speed (independent of MR)
 - c. Constant tail rotor speed

¹In [83, p. 20] the rotational speed of the connecting bevel gear resp. the sun gear is erroneously stated to be 1270 RPM.

3. Basic Architecture

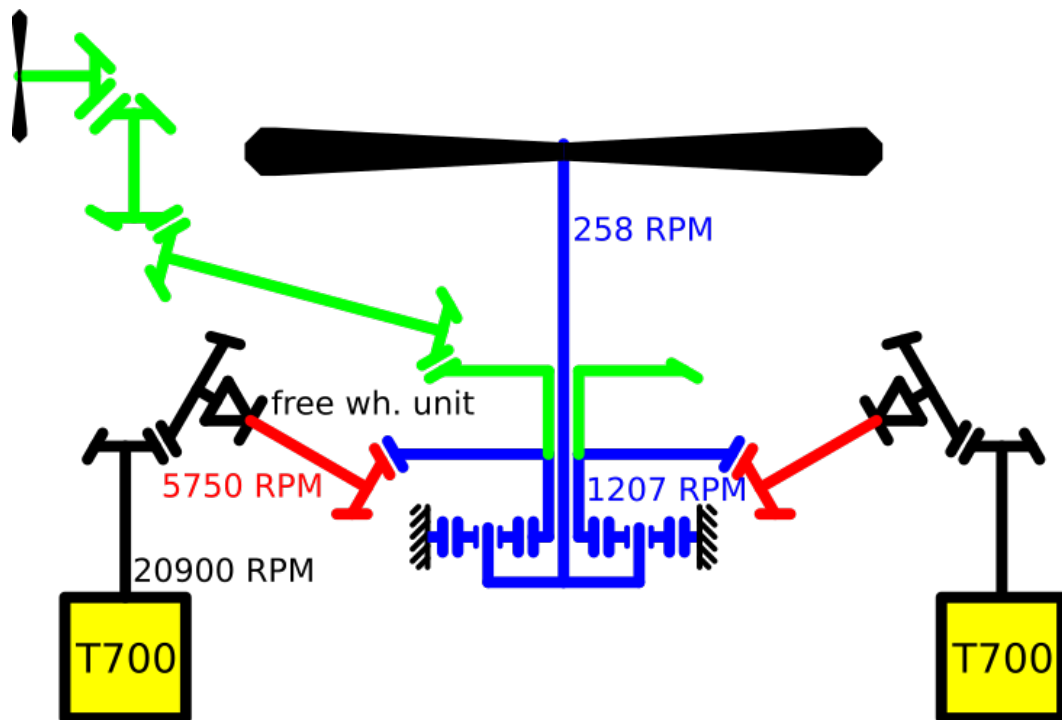


Figure 3.1.: Layout of UH-60 transmission system (based on [120])

It is shown, that in the first case for low main rotor speed ($\sim 80\%$ of the nominal speed) the tail rotor is not able to balance the MR torque in all flight conditions any more. Since the implementation of a continuously variable tail rotor speed is possible – with the same solution as for the main rotor – but entails further technical effort and safety issues, it is decided to restrict further analysis on tail rotors with constant speed. This means that the tail rotor power has to be taken off before the transmission ratio is varied.

2. A continuously variable helicopter transmission system will still need a device to decouple an engine from the rotors in case of failure of this engine. Since free-wheeling units are complex components, changes in the design also imply technical and safety issues. This is beyond the scope of this study and therefore the design of the free-wheeling unit will be kept as in the basic UH-60 drivetrain.
3. For reasons of redundancy, the accessories (electric generators and hydraulic pumps) are to be connected to the rotors any time. From the technical view, constant speed is a great advantage for these machines. As a consequence, their power take-off has to be between the free-wheeling unit and the speed variation module, i.e., the Compound-Split module.

Because of these constraints, all high-speed parts of the drivetrain, input modules, free-wheeling units and accessories will be kept unchanged. This means that their kinematic structure, principal design and especially rotational speed will stay the same, however, their positions may change. Hence, two possible basic architectures for a redesign of the UH-60 transmission system are envisaged:

- I. The connecting bevel gear stage and the tail rotor take-off are kept unchanged. The Compound-Split module is placed in the *blue* part of the drivetrain in figure 3.1. For this architecture, only one CS module is needed, but it has to transmit and vary the power of both engines (minus accessories and tail rotor).
- II. The connecting shaft (*red* in figure 3.1) is divided into input shaft *a* and output shaft *b* of the Compound-Split module. Accessories stay where they are on shaft *a*, the tail rotor take-off is moved to shaft *a* and the Compound-Split module is placed afterwards. This leads to two tail rotor drives, one on each side of the transmission system, and also two Compound-Split modules. Possible implementations of such a tail rotor drive system can be found in [60, 81].

3.3. Reliability – Decision on architecture

3.3.1. The exponential distribution

To reach a decision on which of the architectures I and II is the most promising solution for a helicopter transmission with variable ratio, the reliability of them will be evaluated in this section. The lifetime of technical devices with constant failure rate is distributed exponentially, i.e., the probability density function is given by

$$f(t) = \begin{cases} \lambda e^{-\lambda t} & t \geq 0, \\ 0 & \text{else} \end{cases} \quad (3.1)$$

and the related cumulative distribution function is

$$F(t) = \begin{cases} 1 - e^{-\lambda t} & t \geq 0, \\ 0 & \text{else.} \end{cases} \quad (3.2)$$

Herein $\lambda > 0$ is the number of failures per time interval, usually per 10^6 hours. The exponential distribution is a good approximation for matured components when teething troubles and effects of ageing and wear are not taken into account. It will be used in the following to compare the reliability of the two drivetrain architectures. The most important difference between the two architectures found in the previous section is the number of Compound-Split modules. Since these components have not been in service in helicopter propulsion so far, the focus of the reliability analysis will be on them. For the analysis of the reliability, some assumptions are made:

1. Although, by the very principle, a Compound-Split module is an aggregate of several technical components, it is assumed that its failure rate λ_{CS} is constant, i.e., the time to failure is distributed exponentially.
2. The failure rate λ_{CS} is independent of the size of the system, i.e., there is no difference whether it has to transmit and transform the power of two or only one engine.
3. It is presumed that fixed ratio gear trains (comprising gears, shafts, bearings and free-wheeling units) pose a proven solution for helicopter transmission systems and meet the certification requirements, i.e., they have no significant influence on the reliability of a transmission architecture. This means that the decisive aspect is the reliability of the Compound-Split module. This assumption is supported by the fact that major sections of the UH-60's transmission system will stay as they are.

3. Basic Architecture

4. The lifetimes of the two CS modules of architecture II are independent exponentially distributed random variables, i.e., a failure of one module does not influence the failure rate of the other.

3.3.2. Comparison of the architectures

Based on the assumptions described in section 3.3.1, the probability of failure of the helicopter drivetrain caused by a failure of the Compound-Split module of architecture I within t hours of operational life is

$$P(t) = F(t) = 1 - e^{-\lambda_{CS}t}. \quad (3.3)$$

A rating of the reliability of architecture II is more complex, because it has to be distinguished between failures of one module resp. both modules. The probability of failure of one module is the same as for architecture I. After a failure of one module, it will be replaced instead of continuing operation of the rotorcraft with the remaining one. Therefore, a failure of both modules can only occur if they fail within the time interval from the failure of the first module to the repair of the transmission system. Since the UH-60 is a twin-engine helicopter, operation of architecture II with a failed CS module is comparable to *One-Engine-Inoperative* (OEI) condition. According to AC 29 [122], there are three different OEI ratings: 30-second, 2-minute and 30-minute. Under the given assumptions, the probability that both of the modules, each with a operational life of t , fail within a time interval Δt is

$$\begin{aligned} P(t, \Delta t) &= \int \int_{|\tau_1 - \tau_2| < \Delta t} f(\tau_1) f(\tau_2) d\tau_1 d\tau_2 \\ &= 2 \cdot \int_0^t \int_0^{\tau_2} \lambda_{CS}^2 e^{-\lambda_{CS}(\tau_1 + \tau_2)} d\tau_1 d\tau_2 \\ &\quad - 2 \cdot \int_{\Delta t}^t \int_0^{\tau_2 - \Delta t} \lambda_{CS}^2 e^{-\lambda_{CS}(\tau_1 + \tau_2)} d\tau_1 d\tau_2 \\ &= 1 - e^{-\lambda_{CS}\Delta t} - e^{-\lambda_{CS}(2t - \Delta t)} + e^{-2\lambda_{CS}t}. \end{aligned} \quad (3.4)$$

At present, no information on failure rates of Compound-Split modules with a hydraulic variator in rotorcraft is available. However, under the assumption that λ_{CS} is the same for both possible architectures, probabilities that one single resp. both modules fail in the operational life of a transmission can be calculated for a range of failure rates and the results be compared. The computed probabilities $P(t)$ (*solid blue* line) and $P(t, \Delta t)$ (*dashed blue*) for $t = 15000\text{h}$ and $\Delta t = 30\text{min}$ as well as the ratio of them (*red*) are plotted as functions of λ_{CS} in figure 3.2. In addition, the permissible probabilities of failure of several probability classes according to [122] are depicted as *dashed black* lines. Note that different failures may lead to different effects and, therefore, λ_{CS} must be interpreted as the portion of the total number of failures leading to a specific failure mode. It is also important that $P(t, \Delta t)$ is not necessarily the probability of failure of architecture II, but the probability that both modules fail in the same way or show the same failure effect within Δt . During operation, the failure of only one CS module may also have consequences, but in general, they are less severe than for architecture I.

Apparently, the probability of failure of one CS module is higher than the probability of two CS

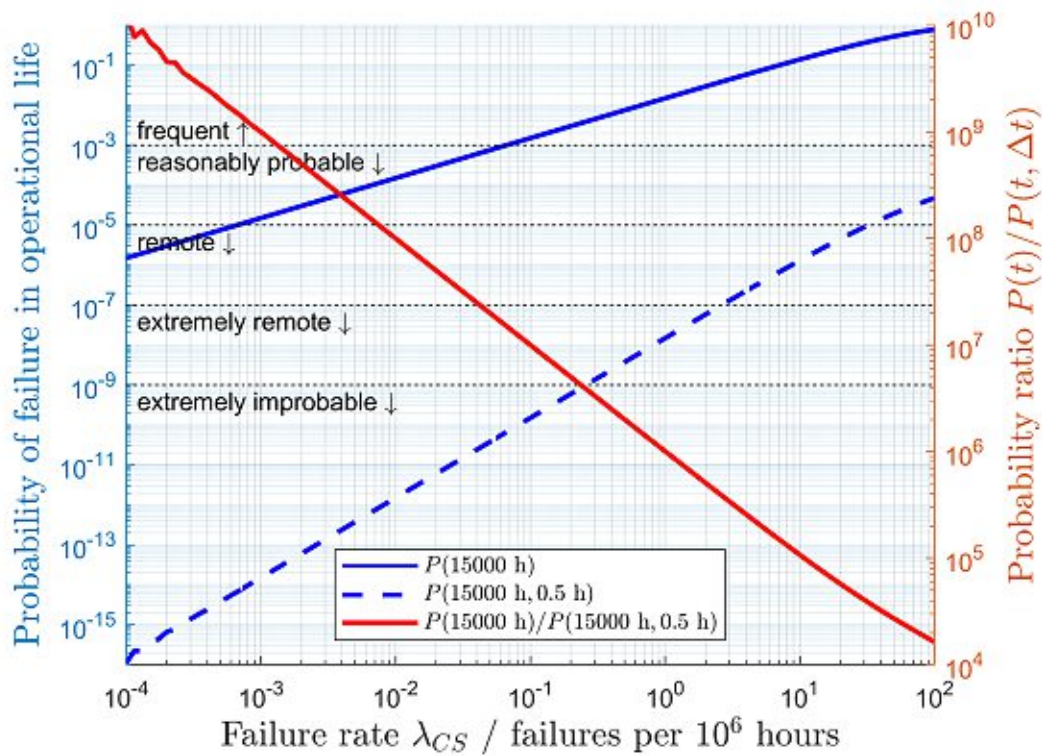


Figure 3.2.: Probabilities of failure of Architectures I and II

modules failing at almost the same time. $P(t, \Delta t)$ meets the requirements of all failure classes for failure rates λ_{CS} lower than $3 \cdot 10^{-1}$ (failures per 10^6 hours). The ratio of the probabilities is about $2 \cdot 10^4$ for $\lambda_{CS} = 10^2$ and is strongly increasing for lower failure rates, reaching a value of 10^9 for $\lambda_{CS} = 10^{-3}$. These results mean that it is more than $2 \cdot 10^4$ times more probable that architecture I fails than it is for the alternative design II.

Although the data situation is poor, example values for hydraulic pumps in helicopters taken from [89, p. 75] can be used as a guideline. From a source of four records and 365 pumps failed (reason type of failure unknown) in $0.924 \cdot 10^6$ hours, a maximum likelihood estimator of the failure rate of $\hat{\lambda} = 395.022$ (60 % confidence interval: [377.544, 413.448]) failures per 10^6 hours is quoted. Because a failure of each hydraulic machine would lead to a failure of the CS module, this value has to be taken twice (as an approximation), leading to $\hat{\lambda} = 790.044$. In this value, failures of gears, shafts or bearings of the CS module are not yet included. This failure rate is much too high for drivetrain components and of course is not directly applicable to hydraulic machines designed for the use in rotorcraft transmission systems and not every failure is to be classified in the same way. In addition, special measures (cf. [84]) may reduce the consequences of a specific type of failure and therefore increase the permissible possibility of failure. However, it shows that the reliability of hydraulic components is a mayor safety issue and that further efforts have to be made to reach acceptable failure rates. As a result, architecture II offers a better chance to reach the required reliability at reasonable cost and therefore it is chosen for further study.

3.4. Planetary gear sets – Decision on Compound-Split arrangement

Besides the decision for a drivetrain architecture, the one for one of the principal Compound-Split arrangements depicted in figure 2.7 is crucial for the final transmission design and its characteristics. To be able to compare the different arrangements, their structures depending on the two mechanical points Θ_1 and Θ_2 have to be known. Therefore, the epicyclic ratios $i_0 \in \{i_{abc}, i_{abd}, i_{adc}, i_{cbd}\}$ defined in (2.23) have to be converted into planetary ratios i_{12} . This can be done by using the one-to-one mapping defined in equation (2.10). This mapping also provides information on the installation position. This means that a permutation matrix $\underline{\underline{R}} \in \mathbb{R}^{3 \times 3}$ assigning three of the shafts a, b, c, d to sun, ring and carrier (1,2,C) can be defined:

$$\underline{\underline{R}}(i_0) = \begin{cases} \begin{bmatrix} 1 & 0 & 0 \\ 0 & 1 & 0 \\ 0 & 0 & 1 \end{bmatrix} & -\infty < i_0 \leq -1 & (i_0 = i_{12}) \\ \begin{bmatrix} 0 & 1 & 0 \\ 1 & 0 & 0 \\ 0 & 0 & 1 \end{bmatrix} & -1 < i_0 \leq 0 & (i_0 = i_{21}) \\ \begin{bmatrix} 0 & 1 & 0 \\ 0 & 0 & 1 \\ 1 & 0 & 0 \end{bmatrix} & 0 < i_0 \leq \frac{1}{2} & (i_0 = i_{C1}) \\ \begin{bmatrix} 0 & 0 & 1 \\ 0 & 1 & 0 \\ 1 & 0 & 0 \end{bmatrix} & \frac{1}{2} < i_0 \leq 1 & (i_0 = i_{C2}) \\ \begin{bmatrix} 0 & 0 & 1 \\ 1 & 0 & 0 \\ 0 & 1 & 0 \end{bmatrix} & 1 < i_0 \leq 2 & (i_0 = i_{2C}) \\ \begin{bmatrix} 1 & 0 & 0 \\ 0 & 0 & 1 \\ 0 & 1 & 0 \end{bmatrix} & 2 < i_0 \leq \infty & (i_0 = i_{1C}). \end{cases} \quad (3.5)$$

By use of $\underline{\underline{R}}$, speed vectors $\underline{\omega}_{abc} := [\omega_a, \omega_b, \omega_c]^T$ can be easily assigned to $\underline{\omega}_{12C} := [\omega_1, \omega_2, \omega_C]^T$ via

$$\underline{\omega}_{12C} = \underline{\underline{R}} \underline{\omega}_{abc}. \quad (3.6)$$

Based on the derived equivalences, the properties "mass of planetary gear sets" and "maximum relative speed of planet gears" will be used to find the best arrangement for the UH-60 with the assumptions made.

3.4.1. Mass of planetary gear sets

According to [79, pp. 262 sqq.] the reference diameter d_1 of a spur or helical pinion can be calculated as

$$d_1 = \sqrt[3]{\frac{2000 Q_1}{K^* (b/d_1)} \frac{u+1}{u}}, \quad (3.7)$$

where $u = \frac{z_{\text{gear}}}{z_{\text{pinion}}}$ is the gear ratio, Q_1 is the pinion torque and b/d_1 is the given ratio of face width and reference diameter of the pinion. K^* is a characteristic value for the Hertzian stress. For helicopters driven by gas turbines values of $K^* = 6.4 \text{ N/mm}^2$ and $K^* = 6.2 \text{ N/mm}^2$ for the first respectively the second stage are specified in [79, Tafel 22.1/2.]. Hereinafter the higher value will be used throughout the calculations. It has to be stressed that (3.7) is a numerical value equation, i.e., lengths have to be in mm and the torque in Nm. For planetary gear sets the gear ratio between the sun and the planet gears is

$$u = \frac{z_{pl}}{z_1} = \frac{-1 - i_{12}}{2}. \quad (3.8)$$

In a strict sense, (3.8) is only valid for $z_1 + 2z_{pl} + z_2 = 0$ ($z_2 < 0$), but poses a good approximation for other cases. If all gears – including the rotating ring gear – are approximated by cylinders, whose diameters are calculated with (3.7) and (3.8), and multiplied with volume utilization factors, the mass can be estimated via

$$m(i_{12}, Q_1) = \begin{cases} \rho_{\text{steel}} \frac{2000 K_\gamma Q_1}{4qK^*} \frac{u+1}{u} (0.8 + 0.5qu^2 + 0.1(1+2u)^2) \pi & u \geq \frac{1}{0.7}, \\ \rho_{\text{steel}} \frac{2000 K_\gamma Q_1}{4qK^* 0.7} \frac{u^{-1}+1}{u^{-1}} (0.5q + 0.8u^{-2} + 0.1u^{-2}(1+2u)^2) \pi & u < \frac{1}{0.7}. \end{cases} \quad (3.9)$$

The volume utilization factors 0.8, 0.5 and 0.1 for sun, planet and ring gears are taken from [57]. The formula distinguishes between the cases that the sun resp. the planet gear is critical. The factor 0.7 takes the reverse load at the planetary gears into account. K_γ is the load sharing factor [1, Table 8] and q is the number of planets. Since the analysis is based on the planetary ratio i_{12} and no further details are known, the maximum number of planets will be assumed and calculated as

$$q = \left\lfloor \frac{\pi}{1.10 \arcsin\left(\frac{u}{u+1}\right)} \right\rfloor. \quad (3.10)$$

In principle, the maximum integer of non-colliding planets is calculated. Therefore, the reference diameters are increased by 10 % to take addendum and clearance into account. At this point, the following restriction is made: planetary ratios, which are below -11.3 (cf. [77, p. 27]) or allow more than nine planets according to (3.10) will be neglected. This leads to a range of planetary ratios of about $i_{12} \in [-11.3, -1.78]$. As a consequence, there are pairs (Θ_1, Θ_2) for which some arrangements cannot be implemented with common planetary gear sets.

The relevant torque Q_1 is the torque at the sun gear. It is determined by

$$Q_1 = \begin{cases} \min(|Q_c|, |i_{abc}Q_c|, |(i_{abc}-1)Q_c|) & \text{for } i_{abc} \\ \min(|Q_d|, |i_{abd}Q_d|, |(i_{abd}-1)Q_d|) & \text{for } i_{abd} \\ \min(|Q_c|, |i_{adc}Q_c|, |(i_{adc}-1)Q_c|) & \text{for } i_{adc} \\ \min(|Q_d|, |i_{cbd}Q_d|, |(i_{cbd}-1)Q_d|) & \text{for } i_{cbd} \end{cases} \quad (3.11)$$

3. Basic Architecture

for the four different epicyclic gear sets. Note, that in (3.11) Q_c and Q_d denote the torque acting on the EGS via shafts c and d and not necessarily the ones defined in (2.26).

The resulting masses for the different arrangements are depicted as colour-levels in figure 3.3 along with logarithmically spaced levels of spread. To minimize the necessary changes in the UH-60 drivetrain, Θ_1 and Θ_2 were restricted to $[1.1, 2.5]$. These changes are caused by the increase of torque in the low-speed part of the drivetrain and the transmission ratio of the CS module, which will lead to a lower ratio in the remaining gear stages. This will primarily affect the number of teeth and the diametral pitch of the combining bevel gear stage and the planetary gear set and subsequently the diameters, bearings and housing. Where no solution for the calculated i_{12} could be found for at least one of the two planetary gear sets of each arrangement, the plot is blank. The colourbar on the right side of each subfigure indicates the mass of the colour-levels in kg. However, this is just a rough estimation based on cylindrical gears and neglecting shaft, bearing, carrier and housing masses. Based on [46], a main rotor speed range of 180 RPM to 285 RPM (70 % to 110 % of

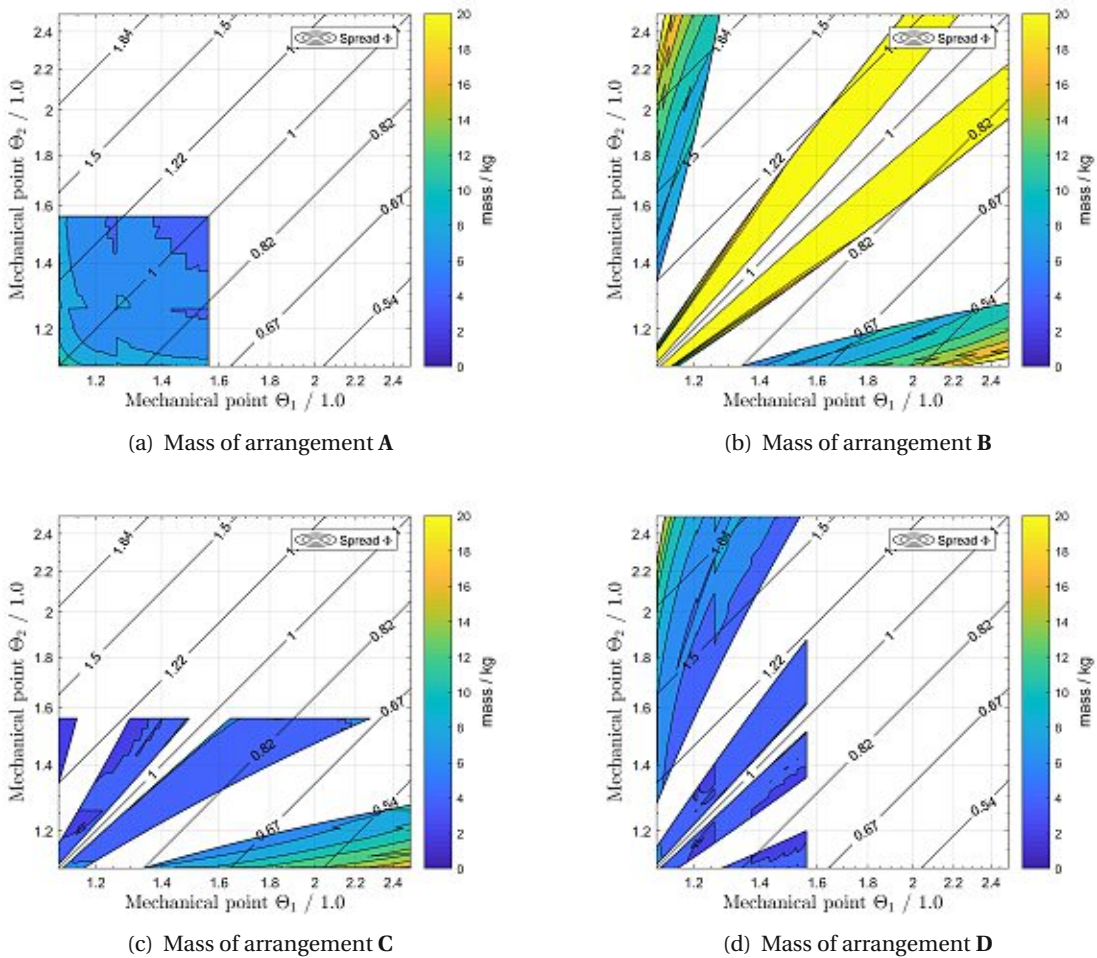


Figure 3.3.: Mass of the four Compound-Split arrangements according to figure 2.7

nominal speed) – i.e., a transmission spread of $\Phi = 1.5$ resp. $\Phi = 0.67$ – is required. As explained in

section 2.2.3, $\Phi = 0.67$ will be neglected to avoid circulating power flow in the mechanical path. It can be seen that arrangement **A** does not have a solution for these spreads. All other arrangements can be implemented. Design **D** offers the lightest solution in the analysed range.

3.4.2. Rotational speeds

From (2.23) it follows that for a given (Θ_1, Θ_2) only four different epicyclic gear ratios i_{abc} , i_{abd} , i_{acd} and i_{cbd} occur. As a consequence, only four planetary ratios $i_{12}(i_0)$ according to (2.1) have to be considered. The rotational speed of shaft a is 5750 min^{-1} and the speeds of b , c and d are determined by k_{ab} and (2.24). From these, rotational speeds of the sun gear, the ring gear and the carrier shaft can be calculated by (3.5) and (3.6). The relative speed of the planet gears is

$$\omega_{\text{pl,rel}} = \frac{\omega_1 - \omega_C}{u} \quad (3.12)$$

with u according to (3.8). The resulting maximum absolute values of the relative rotational speeds

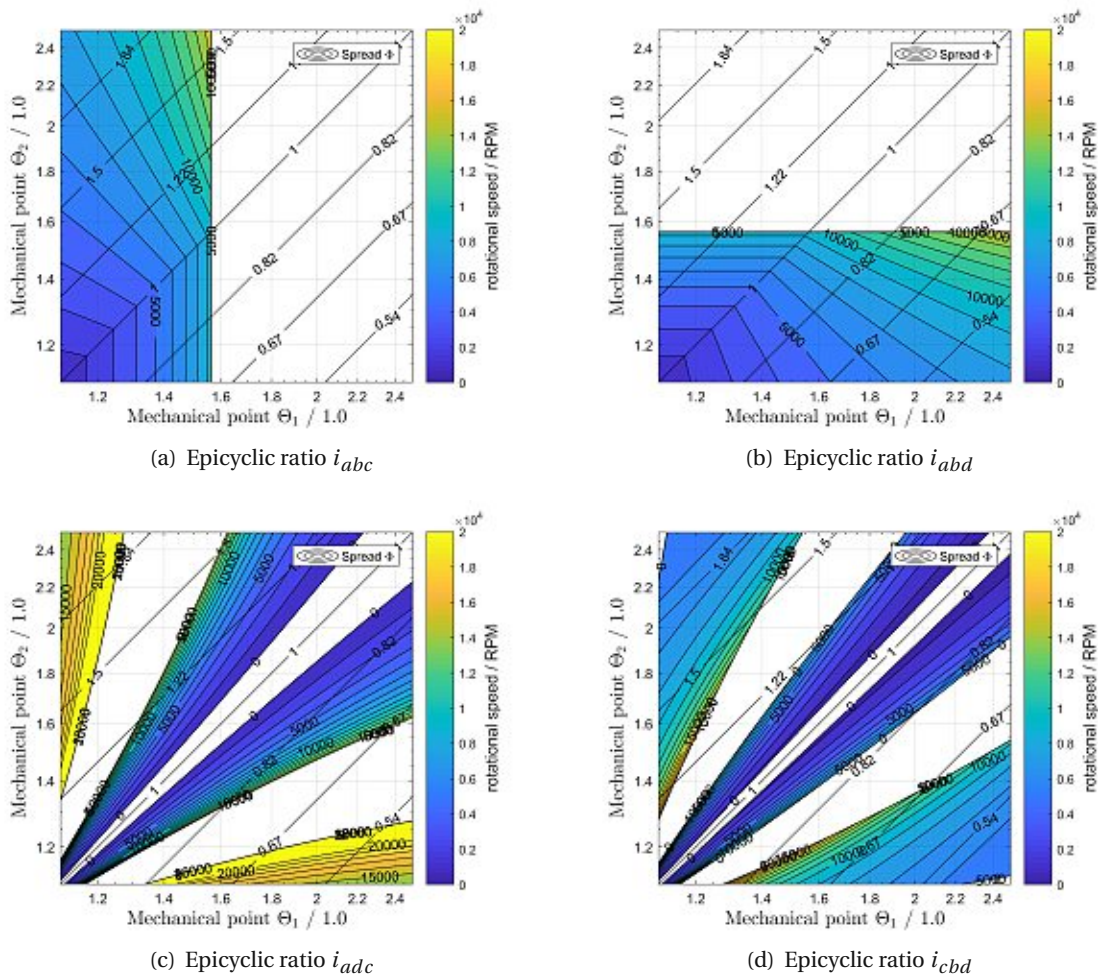


Figure 3.4.: Maximum rotational speeds of the planet gears (absolute values)

of the planetary gears for the four epicyclic gear ratios are depicted in figure 3.4. The speed levels

3. Basic Architecture

are colour-coded in 1000 RPM steps from 0 to 20000 RPM. The latter was assumed as an upper boundary for the bearings of the planet gears. Where no i_{12} could be found for the respective i_0 , the figure is blank. Arrangement **A** consists of i_{abc} and i_{abd} and since neither for $\Phi = 1.5$ nor for $\Phi = 0.67$ both epicyclic ratios have a corresponding planetary ratio i_{12} , this arrangement is ruled out. For i_{adc} the relative speed of the planetary gears is above 16000 RPM for the required spreads, except for an area where neither **B** nor **C** have a solution. For arrangement **D**, consisting of i_{abc} and i_{cbd} there are sections along the $\Phi = 1.5$ line where the relative speeds of both planetary gear sets are below 10000 RPM. Hence it was decided to analyse arrangement **D**.

3.5. Resulting arrangement of CS modules and drivetrain

From figure 3.4 it can be seen, that the searched combination of mechanical points (Θ_1, Θ_2) is located in the area $[1.1, 1.4] \times [1.6, 2.1]$. The final parameters have to be defined in the design process. For this thesis, the following values are set:

$$\begin{aligned} \Theta_1 &= 1.3, & i_{abc} &= 1.3, & i_{12C} &= -3.33, & q_C &= 5, \\ \Theta_2 &= 1.95, & i_{cbd} &= -2.17, & i_{12D} &= -2.17, & q_D &= 7. \end{aligned} \quad (3.13)$$

With equations (2.10) and (2.23), the principal architecture of the CS module depicted in figure 3.5

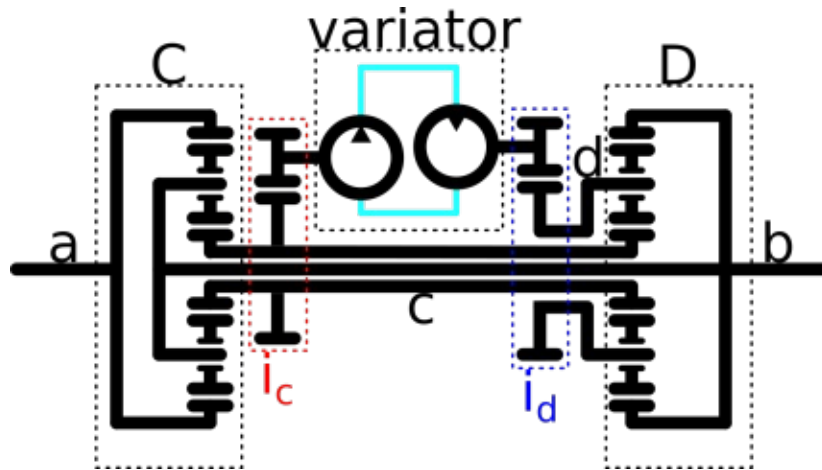


Figure 3.5.: Sketch of the final arrangement D

is obtained. The input shaft a is connected to the ring gear of the first planetary gear set C . Shaft c , which carries the pump take-off, connects the sun gears of the two planetary gear set and d , carrying the motor input, is the carrier of PGS D . The common output shaft b connects the carrier of C and ring gear of D . With these results, the maximum rotational speeds (absolute values) of shafts c and d can be calculated:

$$\begin{aligned} n_{c,\max} &= n_c(\Theta_2) = \frac{n_a(1 - \frac{\Theta_1}{\Theta_2})}{1 - \Theta_1} \approx -6388 \text{ RPM} \\ n_{d,\max} &= n_d(\Theta_1) = \frac{n_a(1 - \frac{\Theta_2}{\Theta_1})}{1 - \Theta_2} \approx 3026 \text{ RPM}. \end{aligned} \quad (3.14)$$

3.5. Resulting arrangement of CS modules and drivetrain

These results show that the carriers of *C* and *D* rotate at a maximum speed of $n_{b,max} \approx 4423$ RPM resp. $n_{d,max} \approx 3026$ RPM and therefore no unacceptably high stresses caused by the centrifugal forces of the planet gears are to be expected.

Figure 3.6 gives a rough idea of the available assembly space for the CS module. The pitch circle diameter of the ring gear of 653.9 mm [80, p. 2] can serve as a comparative value. With the results of chapter 6, the installation option can be rated.

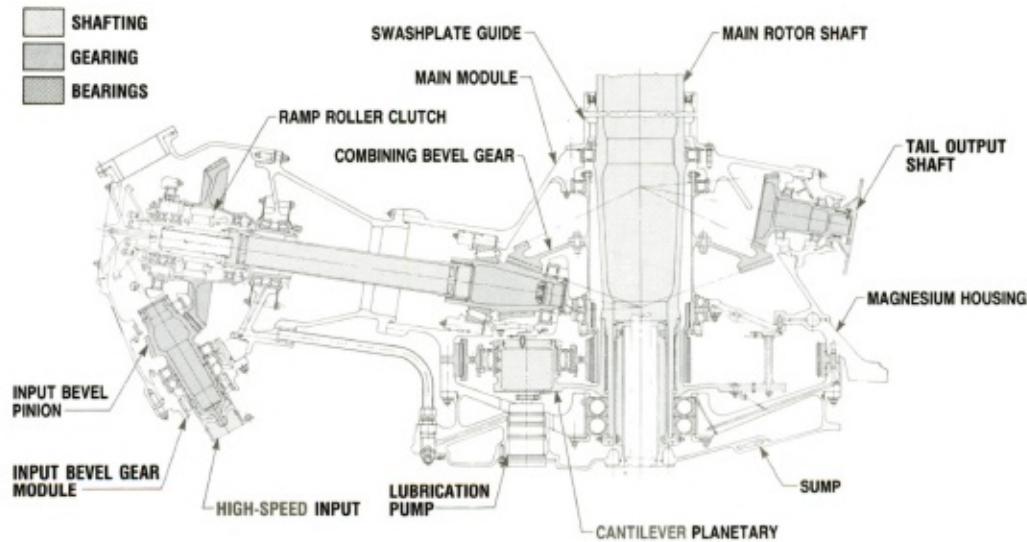


Figure 3.6.: Sketch of UH-60 transmission system (taken from [74])

The resulting drivetrain architecture is depicted in figure 3.7. As stated in the definition of architecture II, the parts comprising the turboshaft engines, free-wheeling units and accessories (not shown) are not changed compared to the baseline drivetrain. The first important change is that the tail rotor take-off is arranged immediately after the free-wheeling units on each side of the rotorcraft. From there, the TR power is transmitted to a combining bevel gear stage and further to the TR (*green*), which rotates at 1090 RPM (*pink*).

The following parts of the drivetrain are the CS-modules, which transform the input speed of 5750 RPM into a variable output speed of 2950 RPM to 4425 RPM, corresponding to a transmission spread of $\Phi = 1.5$. This value was chosen based on the finding that a variation between 70 % to 110 % of the baseline MR speed is desirable[46]. Each CS-module consists of two nested epicyclic gear sets, labelled *C* and *D*, and the variator. The input and output shafts of the variator are connected to the epicyclic gear sets via helical gear stages with transmission ratios i_c and i_d . The ring gear of *C* is driven by the input shaft of the CS-module. The sun gears of both EGS are connected via a shaft (*blue*) and the carrier of *C* along with the ring gear of *D* form the output shaft (*red*). The variator pump is connected to the two sun gears while the motor drives the carrier of EGS *D*.

After being transformed, the propulsive power of each turboshaft engine is transmitted to a combining bevel gear stage similar to the one in the baseline drivetrain and further to a planetary gear set and the main rotor (*dark green*).

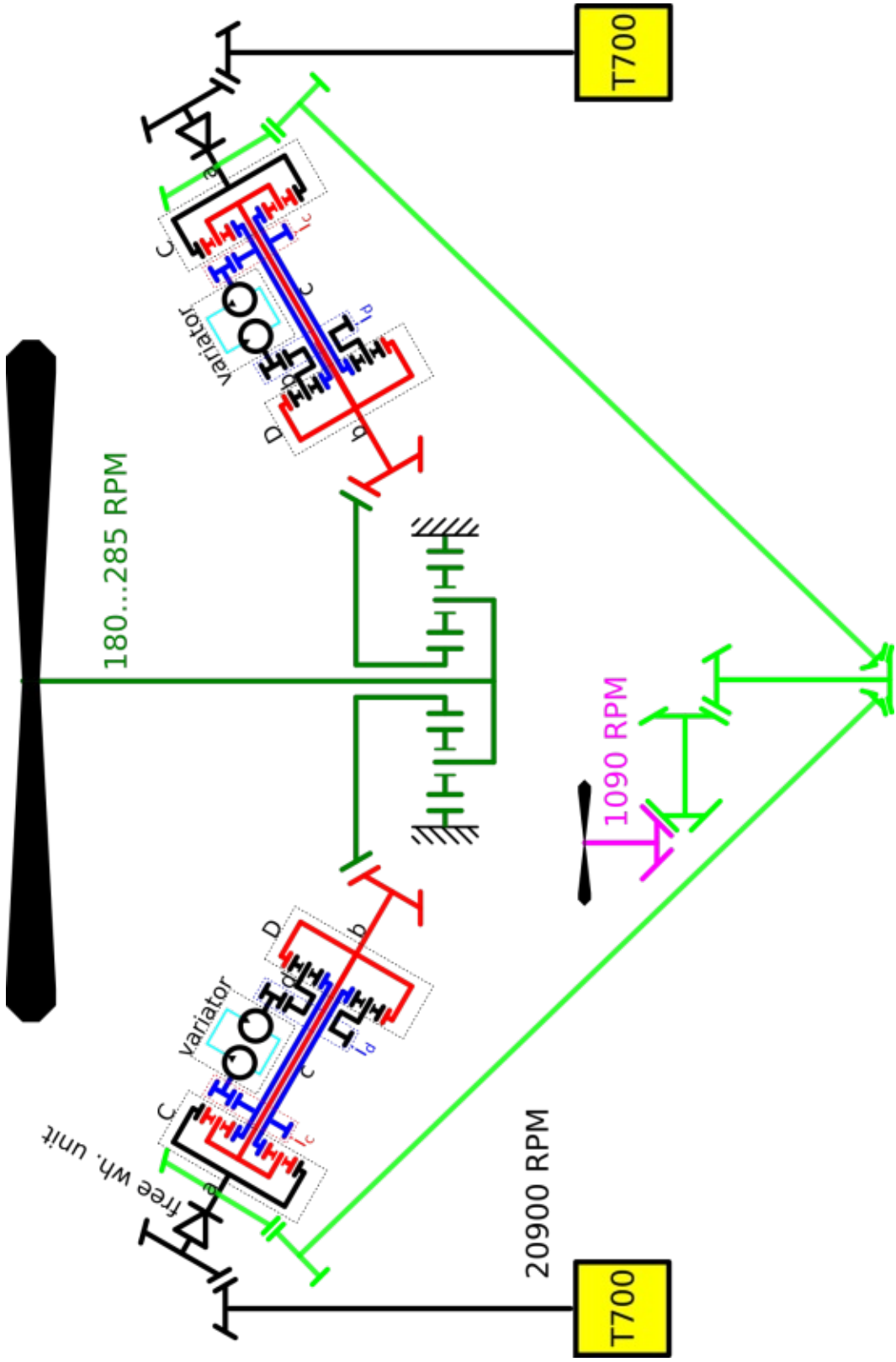


Figure 3.7.: Sketch of transmission layout

4. The Variator

The properties of the machines forming the variator have a strong influence on the characteristics of a drivetrain with one or more CS modules. Rough estimation of the machine size for the UH-60 transmission system based on the known properties of Compound-Split transmissions – especially the power to be transmitted via the variator path, cf. e.g. [129, p. 277] – gives rise to the assumption that an electric variator with state-of-the-art electric machine technology (cf. [64]) is much too heavy and therefore not viable. A study on the applicability of hybrid electric propulsion in rotorcraft [69] came to similar conclusions. Therefore, the present thesis will concentrate on hydrostatic variators – more precisely, such comprising variable displacement axial piston motors.

In this chapter, approximations of the key parameters based on catalogue data published by a manufacturer of axial piston motors with variable displacement are derived. The findings will be used for the further development of the transmission architecture. Parts of the information presented have been published in [83].

4.1. Axial piston motors with variable displacement

4.1.1. Principle layout

The basic design of axial piston motors with variable displacement is depicted in figure 4.1 which is taken from Bosch Rexroth [126]. The references are explained below.

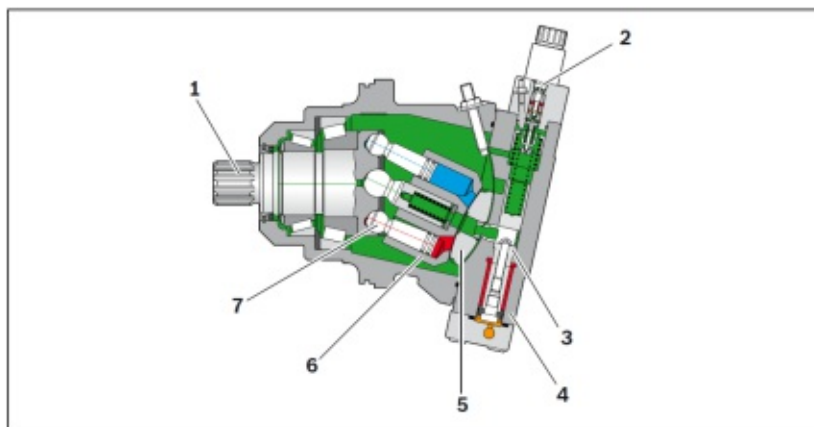


Figure 4.1.: Layout of A6VE axial piston motors (taken from [126, p. 18/60])

- | | | | |
|------------------|-----------------|--------------|----------|
| 1 Drive shaft | 3 Stroke piston | 5 Lens plate | 7 Piston |
| 2 Control piston | 4 Port plate | 6 Cylinder | |

4. The Variator

The axial piston unit depicted in figure 4.1 is of bent-axis design, an alternative principle is the swash-plate design. Bent-axis design means that there is an angle (swivel angle), denoted as $\tilde{\alpha}$, between the axis of the drive shaft (1) and the one of the cylinder (6). This arrangement forces the pistons (7) to execute a stroke when the shaft is rotated (pump operation) resp. a stroke of the pistons leads to rotation of the cylinder (6) and the shaft (motor operation). The cylinder with bores for the pistons slides on the lens plate (5) which is connected to the hydraulic system via the port plate (4). The swivel angle of the bent-axis rotary group is continuously variable. It is controlled hydraulically by the stroke piston (3). Movement of the stroke piston leads to a movement of lens plate, cylinder and pistons and as a consequence to a change of displacement. [126, p. 18/60 sq.]

The mathematical relationship between displacement V_g and the swivel angle $\tilde{\alpha}$ is given by (cf. [43, p. 306])

$$V_g(\tilde{\alpha}) = Z \cdot A_{\text{piston}} \tilde{h} = Z \cdot A_{\text{piston}} D_{\text{piston}} \sin(\tilde{\alpha}). \quad (4.1)$$

Here Z is the number of pistons, A_{piston} is the cross-section area of one piston, \tilde{h} is the stroke and D_{piston} is the pitch diameter of the circle on which the pistons are connected to the shaft.

As described below, axial piston machines can be principally used as pump or motor. However, there are differences between these two operation conditions which will be addressed in the following.

4.1.2. Pump and motor operation

When an axial piston unit is operated as pump, it transforms mechanical power into hydraulic flow. Therefore, the input parameters are angular velocity and torque and the output is a hydraulic flow q_v at a given pressure difference Δp . The pump operation is described by

$$\begin{aligned} q_v &= \frac{1}{2\pi} V_g(\tilde{\alpha}) \omega \eta_v \\ \Delta p &= \frac{2\pi Q}{V_g(\tilde{\alpha})} \eta_{\text{hm}} \\ P_{\text{hydr}} &= q_v \Delta p = Q \omega \underbrace{\eta_v \eta_{\text{hm}}}_{=: \eta_t}. \end{aligned} \quad (4.2)$$

Here also the volumetric efficiency η_v and the hydraulic-mechanical efficiency η_{hm} are taken into account. Their product is the total efficiency η_t of the hydraulic machine. When the hydraulic machine works as motor, the situation is the other way around, i.e., hydraulic flow and pressure are converted into rotation and torque. The related equations are

$$\begin{aligned} \omega &= 2\pi \frac{q_v}{V_g} \eta_v \\ Q &= \frac{V_g}{2\pi} \Delta p \eta_{\text{hm}} \\ P_{\text{mech}} &= Q \omega = \Delta p q_v \underbrace{\eta_v \eta_{\text{hm}}}_{=: \eta_t}. \end{aligned} \quad (4.3)$$

These are similar to (4.2), but the efficiencies act the other way round, in the positive sense of power flow. I shall be stressed, that η_v and η_{hm} are not necessarily the same for pump and motor

operation. In fact, they depend on several parameters, such as angular velocity, pressure and also the properties of the hydraulic fluid. A detailed description of these factors will be given in section 5.1.

4.1.3. Open and closed circuits

There are two main types of hydraulic circuits; open and closed ones. The former are characterised by a reservoir where the fluid is taken from by the pump and further transferred to the motor or other consumers such as hydraulic cylinders. From there, the fluid flows back into the reservoir. In contrast, closed circuits do not have a reservoir but the fluid coming from the motor goes directly back to the inlet of the pump. Of course, also closed circuits need to compensate for leakage and therefore special feed pumps, which are usually much smaller than the main pump, are added to the system. An important advantage of closed circuits is that the hydraulic system can be operated in reverse, i.e., the motor acting as pump and the pump converting hydraulic into mechanical power. Usually, closed circuit systems are used for hydraulic transmissions and this will be the case for this study as well.

4.2. Requirements on hydraulic machines

The characteristic curves of hydraulic motors are depicted in figure 4.2 as solid lines in blue (torque) and red (power). The figure and the notation are based on [123, 124, 125]. From standstill of the motor shaft at $\omega = 0$ to the nominal rotational speed ω_{nom} , the maximum deliverable torque Q_{max} is constant and therefore the machine power is directly proportional to the machine speed. For speeds between ω_{nom} and ω_{max} , the deliverable maximum power P_{max} is constant and therefore the torque decreases. At ω_{max} the motor can deliver the torque Q_x . Above ω_{max} the motor can rotate up to an angular velocity of $\omega_{\text{max},0}$, but without load, i.e., the torque is zero. For a short time overload, the permissible torque can be increased by a factor of approximately 1.1, the corresponding curves are plotted as dashed lines in figure 4.2. By varying the swivel angle $\tilde{\alpha}$ and/or the pressure difference Δp , every torque below the (dashed) blue line can be adjusted (cf. (4.3)). When using rotational speed in RPM instead of the angular velocity; n_{nom} , n_{max} and $n_{\text{max},0}$ can be defined analogously. The characteristics of hydraulic motors also apply if the motor is used as a pump. With (2.31) the required maximum power P_{hydr} to be transmitted hydraulically via the variator path can be written as

$$P_{\text{hydr,max}} = P_{\text{input}} \frac{\sqrt{\frac{\Theta_2}{\Theta_1}} - 1}{\sqrt{\frac{\Theta_2}{\Theta_1}} + 1} = P_{\text{input}} \frac{\sqrt{\Phi} - 1}{\sqrt{\Phi} + 1}. \quad (4.4)$$

If efficiency is neglected, it is determined by the input power and the spread. However, hydraulic machines directly connected to shafts c and d also have to fulfil

$$\begin{aligned} \omega_{\text{max},c} &\geq |\omega_c(\Theta_2)| \\ Q_{\text{max},c} &\geq |Q_c(\Theta_1)| \\ \omega_{\text{max},d} &\geq |\omega_d(\Theta_1)| \\ Q_{\text{max},d} &\geq |Q_d(\Theta_2)|. \end{aligned} \quad (4.5)$$

4. The Variator

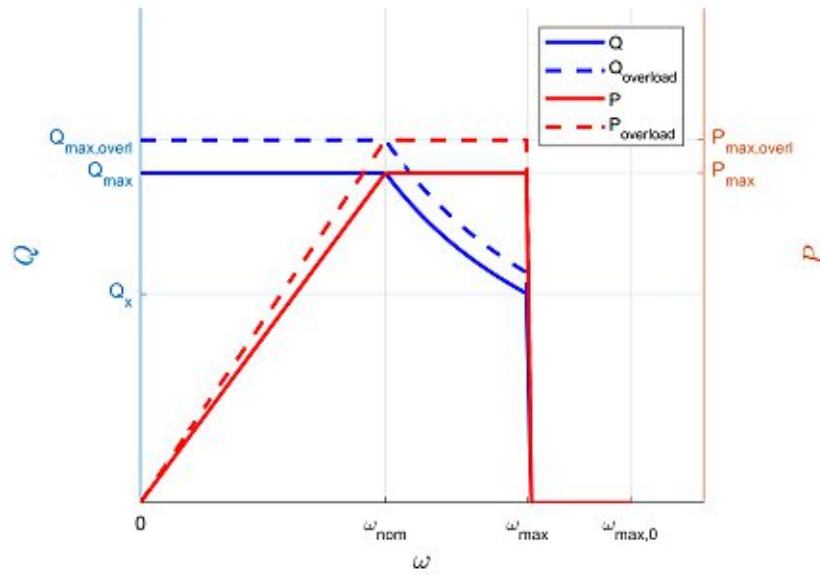


Figure 4.2.: Characteristic curves of variable displacement axial piston motors

If they are connected to shafts c and d via fixed-ratio gear stages with transmission ratios

$$\begin{aligned} i_c &:= \frac{\omega_{\text{motor},c}}{\omega_c} \\ i_d &:= \frac{\omega_{\text{motor},d}}{\omega_d} \end{aligned} \quad (4.6)$$

as defined in figure 3.5, they have to fulfil

$$\begin{aligned} \omega_{\max,c} &\geq |i_c \omega_c(\Theta_2)| \\ Q_{\max,c} &\geq \left| \frac{1}{i_c} Q_c(\Theta_1) \right| \\ \omega_{\max,d} &\geq |i_d \omega_d(\Theta_1)| \\ Q_{\max,d} &\geq \left| \frac{1}{i_d} Q_d(\Theta_2) \right|. \end{aligned} \quad (4.7)$$

Combining the equations for each shaft and using equations (2.24) and (2.26) leads to

$$\begin{aligned} \omega_{\max,c} Q_{\max,c} &\geq |\omega_c(\Theta_2) Q_c(\Theta_1)| \\ &= \left| \frac{\omega_a(1 - \frac{\Theta_1}{\Theta_2})}{1 - \Theta_1} Q_a(\Theta_1 - 1) \frac{\Theta_1 - \Theta_2}{\Theta_1 - \Theta_2} \right| \\ &= \left| P_a \left(\frac{1}{\Phi} - 1 \right) \right| \\ \omega_{\max,d} Q_{\max,d} &\geq |\omega_d(\Theta_1) Q_d(\Theta_2)| \\ &= \left| \frac{\omega_a(1 - \frac{\Theta_2}{\Theta_1})}{1 - \Theta_2} Q_a(\Theta_2 - 1) \frac{\Theta_1 - \Theta_2}{\Theta_1 - \Theta_2} \right| \\ &= |P_a(\Phi - 1)|. \end{aligned} \quad (4.8)$$

The product $\omega_{\max} Q_{\max}$ is called the *corner power* P_{corner} of a hydraulic machine and although it cannot be delivered, it is an important characteristic parameter. The required corner powers for $P_{\text{in}} = P_a = 1151 \text{ kW}$ and $\Phi = 1.5$ are

$$\begin{aligned} P_{\text{corner},c} &= 383.67 \text{ kW} \\ P_{\text{corner},d} &= 575.50 \text{ kW}. \end{aligned} \tag{4.9}$$

From (4.4) and (4.8) it follows that the machine size is a function of the required spread and the input power. Although both machines face the same requirements regarding maximum power, the demand with respect to the corner power is different. The ratio of the required corner power and the required maximum power for machines *c* and *d* is given as

$$\begin{aligned} \frac{P_{\text{corner},c}}{P_{\text{hydr,max}}} &= \left| \frac{P_a \left(\frac{1}{\Phi} - 1 \right)}{P_a \frac{\sqrt{\Phi}-1}{\sqrt{\Phi}+1}} \right| \\ &\stackrel{\Phi > 0}{=} \frac{\left(\sqrt{\Phi} + 1 \right)^2}{\Phi} =: \zeta_c \\ \frac{P_{\text{corner},d}}{P_{\text{hydr,max}}} &= \left| \frac{P_a (\Phi - 1)}{P_a \frac{\sqrt{\Phi}-1}{\sqrt{\Phi}+1}} \right| \\ &\stackrel{\Phi > 0}{=} \left(\sqrt{\Phi} + 1 \right)^2 =: \zeta_d. \end{aligned} \tag{4.10}$$

These ratios will be denoted as ζ and they are characteristic for a given machine. For the required spread $\Phi = 1.5$ (4.10) yields 3.30 and 4.95. For ratios of a given machine between 1.0 and the ones derived in (4.10), the corner power is the decisive criterion. Otherwise, the required maximum power determines the machine size. These considerations are illustrated in figure 4.3. Depicted

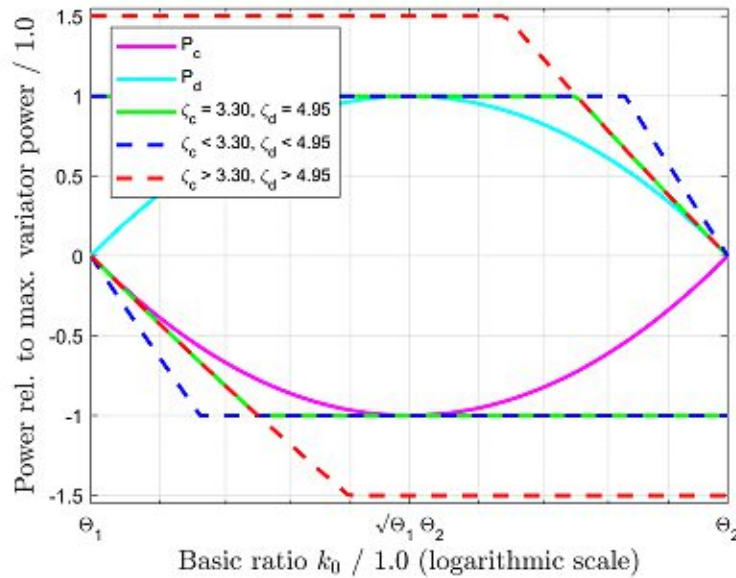


Figure 4.3.: Power transferred via variator path and characteristic curves of different hydraulic machines

4. The Variator

are the power demand of the shafts c and d and the deliverable power of hydraulic machines with different characteristics in dependence of the basic ratio k_0 . As defined earlier, the range of k_0 is limited to $[\Theta_1, \Theta_2]$. It is assumed that the variator machines are connected to the shafts c and d by fixed-ratio gear stages in such a way that the pump operates at ω_{\max} at Θ_2 and the motors operates at ω_{\max} at Θ_1 . The green lines pertain to hydraulic machines with $\zeta_c = 3.30$ and $\zeta_d = 4.95$, i.e., that maximum and corner power both exactly meet the requirements of the Compound-Split transmission. This can be easily understood because the curves' extrema are just the required maximum powers and their slope is tangential to the power demand curves of c and d in the mechanical points where the maximum torque has to be delivered. Since in that case the lightest machines are to be expected, it would be the most desirable case. However, usually this is not the case. The blue dashed lines show the characteristics of hydraulic machines with $\zeta_c > 3.30$ and $\zeta_d > 4.95$, i.e., that for both machines the maximum power is the limiting factor. In this case, the slope of the curves of the hydraulic machines is steeper than the one of the required powers. The red dashed lines belong to machines with $\zeta_c < 3.30$ and $\zeta_d < 4.95$. If this is the case, machine size is determined by the corner power. This is, as will be discussed in the following section, the case for the hydraulic machines that will be studied in detail in this thesis.

4.3. Approximation of hydraulic machine data

For further analysis of a Compound-Split transmission for the UH-60, the relationship of the characteristic variables of hydraulic motors is needed. Therefore, an estimation based on machine data published by **Bosch Rexroth AG** [123, 124, 125] is made. The relevant machine data is summarized in tables 4.1, 4.2 and 4.3. The first column contains the type of motor and the different variables. In the second column the series is denoted and the physical units of the variables can be found. In the remaining columns the values for the different nominal sizes of the motors are given. The variables listed are the maximum displacement $V_{g,\max}$ of the motor, the different characteristic speeds, the nominal pressure p_{nom} and the maximum pressure p_{max} . Also, maximum torque, maximum power, corner power, the ratio ζ and the mass are shown. The ratio ζ is between 1.0 and 3.30 for all studied motors and therefore, the corner power is the decisive criterion.

A6VE	Series 63	NG 28	NG 55	NG 80	NG 107	NG 160	NG 250
$V_{g,\max}$	cm ³	28.1	54.8	80	107	160	200
n_{nom}	RPM	5550	4450	3900	3550	3100	2700
n_{max}	RPM	8750	7000	6150	5600	4900	3600
$n_{\text{max},0}$	RPM	10450	8350	7350	6300	5500	3600
Δp_{nom}	bar	400	400	400	400	400	350
Δp_{max}	bar	450	450	450	450	450	400
Q_{max}	Nm	179	349	509	681	1019	1391
P_{max}	kW	104.0	162.6	207.9	253.2	330.8	393.3
P_{corner}	kW	164.0	255.8	327.8	399.4	522.9	524.4
ζ	1.0	1.58	1.57	1.58	1.58	1.58	1.33
m	kg	16	26	34	47	64	90

Table 4.1.: Data of A6VE Series 63 variable displacement axial piston motors (cf. [123])

To be able to interpolate between the nominal sizes of the motors, curve fits were derived. They are

A6VE	Series 65	NG 55	NG 80	NG 107	NG 160	NG 200
$V_{g,max}$	cm ³	54.8	80	107	160	200
n_{nom}	RPM	4450	3900	3550	3100	2900
n_{max}	RPM	7000	6150	5600	4900	4600
$n_{max,0}$	RPM	8350	7350	6300	5500	5100
Δp_{nom}	bar	400	400	400	400	400
Δp_{max}	bar	450	450	450	450	450
Q_{max}	Nm	349	509	681	1019	1273
P_{max}	kW	162.6	207.9	253.2	330.8	386.6
P_{corner}	kW	255.8	327.8	399.4	522.9	613.2
ζ	1.0	1.57	1.58	1.58	1.58	1.59
m	kg	28	36	46	62	78

Table 4.2.: Data of A6VE Series 65 variable displacement axial piston motors (cf. [124])

A6VE	Series 71	NG 60	NG 85	NG 115	NG 170	NG 215
$V_{g,max}$	cm ³	62.0	85.2	115.6	171.8	216.5
n_{nom}	RPM	4450	3900	3550	3100	2900
n_{max}	RPM	7200	6800	6150	4900	4800
$n_{max,0}$	RPM	8400	8350	7350	5750	5500
Δp_{nom}	bar	450	450	450	450	450
Δp_{max}	bar	500	500	500	500	500
Q_{max}	Nm	444	610	828	1230	1550
P_{max}	kW	206.9	249.1	307.8	399.3	470.7
P_{corner}	kW	334.8	434.4	533.3	631.1	779.1
ζ	1.0	1.62	1.75	1.73	1.58	1.66
m	kg	28	36	46	62	78

Table 4.3.: Data of A6VE Series 71 variable displacement axial piston motors (cf. [125])

based on the assumption that the used material is the same for all nominal sizes of a series. This means, in particular, that density, Young's modulus E , shear modulus G and permissible stresses are constant. Therefore, the mass of a hydraulic machines depends on a characteristic length L as follows

$$m \propto L^3. \quad (4.11)$$

Furthermore, the shear stress τ_t is calculated by

$$\tau_t = \frac{Q r_{max}}{J_T}, \quad (4.12)$$

where r_{max} and J_T denote the maximum radius and the torsional constant and the torsion constant of a shaft section. Since the maximum allowable shear stress is assumed to be constant and $r_{max} \propto L$ respectively $J_T \propto L^4$ apply,

$$Q \propto L^3 \quad (4.13)$$

4. The Variator

follows. The torque is connected to pressure via

$$Q = \Delta p V_g. \quad (4.14)$$

Since both, Q and V_g are proportional to L^3 , the pressure is the same for all nominal sizes of a hydraulic motor. Forces are usually proportional to torque divided by a characteristic length. Since surfaces and cross sections are proportional to L^2 , it follows that a torque according to (4.13) will yield the same stresses in the hydraulic machines for every nominal size of a series. Another important characteristic of a hydraulic machine are the velocities, for example sliding velocities of the pistons or the rolling velocities on the bearings. Since $v = r \omega$,

$$n_{\max} = \frac{30}{\pi} \omega_{\max} \propto L^{-1} \quad (4.15)$$

applies. As a consequence of (4.13) and (4.15) the relation between the corner power and a characteristic length is

$$P_{\text{corner}} \propto L^2. \quad (4.16)$$

Since the corner power is the decisive factor for the Compound-Split transmission, equations (4.11), (4.13) and (4.15) are transformed to

$$\begin{aligned} m &\propto P_{\text{corner}}^{3/2} \\ Q_{\max} &\propto P_{\text{corner}}^{3/2} \\ n_{\max} &\propto \frac{P_{\text{corner}}}{Q_{\max}}. \end{aligned} \quad (4.17)$$

The proportionality of the rotational speed indicates that the approximation was obtained from the curve fit of the torque and the given corner power instead of fitting it to machine data. The reason is, that this approach conserves corner power.

In figure 4.4, mass as a function of corner power of all motors of the A6VE type is depicted. Data points of series 63 are *blue*, of series 65 are *red* and of series 71 are *green*. For each series of motors a curve fit for the mass was derived with MatLab [66] and added to figure 4.4 in the colour of the respective data points. The data of the A6VE series 63 NG 250 is labelled in brackets and not included in the curve fits because it has a lower nominal pressure than all other motors of its series. The found curve fits are

$$\begin{aligned} m_{63}(P_{\text{corner}}) &= 0.005635 P_{\text{corner}}^{3/2} & (R_{63}^2 = 0.9701) \\ m_{65}(P_{\text{corner}}) &= 0.005358 P_{\text{corner}}^{3/2} & (R_{65}^2 = 0.9504) \\ m_{71}(P_{\text{corner}}) &= 0.003760 P_{\text{corner}}^{3/2} & (R_{71}^2 = 0.9701). \end{aligned} \quad (4.18)$$

The parameter R^2 (*R-squared*) in brackets is the coefficient of determination. For the purpose of this study, all found curve fits are sufficiently accurate. Figure 4.4 indicates, that for a given corner power (and therefore a given spread), hydraulic motors of the A6VE Series 71 have the lowest mass. The main reason for this is the higher pressure level ($\Delta p_{\text{nom}} = 450 \text{ bar}$ instead of 400 bar in the other series) for this type of machine. Therefore, they will be used as reference for hydraulic motors hereinafter. Another important result is that for the given machines and $\alpha > 1$

$$\alpha m_{71}(P_{\text{corner}}) < m_{71}(\alpha P_{\text{corner}}) = \alpha^{3/2} m_{71}(P_{\text{corner}}) \quad (4.19)$$

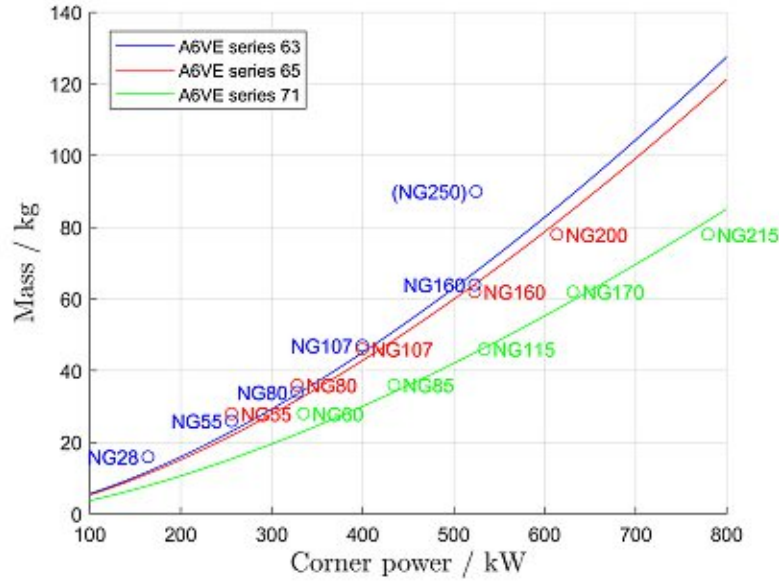


Figure 4.4.: Fit of mass as a function of corner power for A6VE motors Series 63, 65 and 71

applies. In particular, this means, that one large variator is heavier than two small ones. Referring to architectures I and II, this yields

$$\begin{aligned} m_{\text{I}} &= m_{71} (2 \cdot P_{\text{corner},c}) + m_{71} (2 \cdot P_{\text{corner},d}) \approx 226.75 \text{ kg} \\ m_{\text{II}} &= 2 \cdot m_{71} (P_{\text{corner},c}) + 2 \cdot m_{71} (P_{\text{corner},d}) \approx 160.33 \text{ kg}. \end{aligned} \quad (4.20)$$

This is another argument for the selection of architecture II.

In figure 4.5 the maximum torque and the maximum speed of A6VE Series 71 motors are plotted with added curve fits. The latter are given by

$$\begin{aligned} Q_{\text{max}}(P_{\text{corner}}) &= 0.07198 P_{\text{corner}}^{3/2} & (R_T^2 = 0.9839) \\ n_{\text{max}}(P_{\text{corner}}) &= \frac{30 \cdot 1000}{\pi} \frac{P_{\text{corner}}}{Q_{\text{max}}(P_{\text{corner}})} = 1.3267 \cdot 10^5 P_{\text{corner}}^{-1/2} & (R_n^2 = 0.8942). \end{aligned} \quad (4.21)$$

As already mentioned, $Q_{\text{max}}(P_{\text{corner}})$ was obtained by fitting machine data and $n_{\text{max}}(P_{\text{corner}})$ by dividing the corner power by the torque fit and multiplying with $\frac{30000}{\pi}$. Again, the values of R^2 are satisfactory and justify the use of the approximations for further study. With this knowledge, the data for the pump and the motor can be calculated. Based on the required corner powers (4.9) the results listed in table 4.4 are obtained. The nominal rotational speed n_{nom} was obtained from n_{max} by dividing by 1.74 (cf. [125, p. 8]). Now the ratio of the gear stages connecting shafts c and d to pump resp. motor can be calculated as

$$\begin{aligned} i_c &:= - \left| \frac{\omega_{\text{pump},c}}{\omega_{c,\text{max}}} \right| = - \frac{6773}{6388} \approx -1.06 \\ i_d &:= - \left| \frac{\omega_{\text{motor},d}}{\omega_{d,\text{max}}} \right| = - \frac{5530}{3026} \approx -1.83. \end{aligned} \quad (4.22)$$

4. The Variator

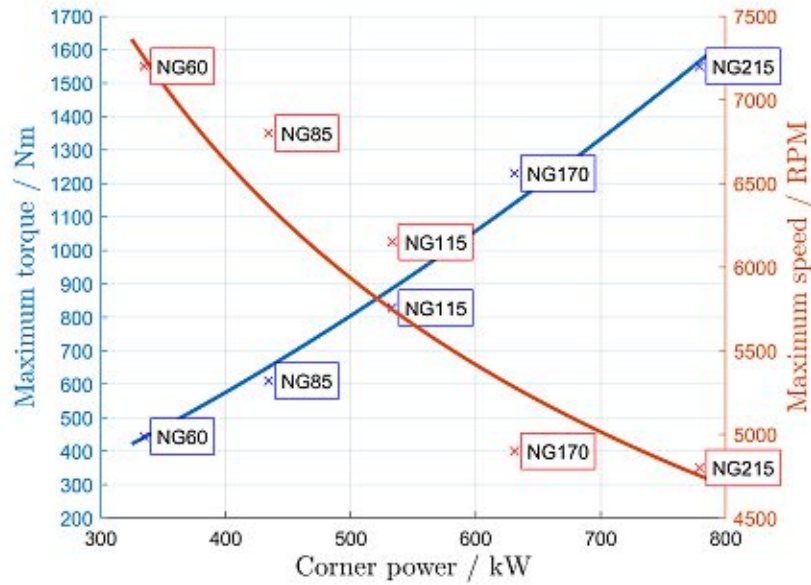


Figure 4.5.: Fit of characteristic variables as a function of corner power for A6VE Series 71 motors

A6VE Series 71	P_{corner} kW	Q_{max} Nm	n_{max} RPM	n_{nom} RPM	Δp_{nom} bar	mass kg	V_{max} cm ³
pump	383.67	540.9	6773	3893	450	28.26	75.5
motor	575.5	993.7	5530	3178	450	51.91	138.8

Table 4.4.: Approximated data of the required hydraulic motors

A serious disadvantage of hydraulic transmissions compared to mechanical ones is the lower efficiency. Although in a Compound-Split design only a portion of the propulsive power has to be transmitted hydraulically, a significant drop in drivetrain efficiency has to be reckoned with. With the basic architecture derived in the previous chapter and the information on the variator machines gathered above, an evaluation of the efficiency of the transmission system depicted in figure 3.7 can be carried out. The following chapter is dedicated to the used simulation approach, the made assumptions and the results of this evaluation.

5. Assessment of drivetrain efficiency

5.1. Efficiency of hydraulic motors

A major drawback of hydraulic transmissions is the low efficiency compared to gear drives. Although only a portion of the total propulsive power is transmitted via the variator, this perhaps unduly reduces the overall efficiency of the drivetrain. For this reason, a simulation of the overall efficiency of a transmission system containing two CS modules with hydraulic variators is carried out here. Parts of the results have already been published in [83].

Schlösser [97, 98] presented a method for estimating the efficiency of hydraulic machines, which will be used in the following. According to this, the total efficiency η_t of hydraulic machines is the product of the volumetric η_v and the hydraulic-mechanical efficiency η_{hm} . First, the non-dimensional parameters λ and σ are defined as

$$\lambda := \frac{\mu \omega}{\Delta p}$$

$$\sigma := \frac{\omega \sqrt[3]{\frac{V_g}{2\pi}}}{\sqrt{\frac{2\Delta p}{\rho}}}, \quad (5.1)$$

wherein μ is the dynamic viscosity of the hydraulic fluid and ρ is its density. V_g , ω and Δp denote the geometric displacement per revolution, the angular velocity of the shaft and the differential pressure. Based on the optimum range of the kinematic viscosity $\nu = 16 \text{ mm}^2/\text{s}$ to $36 \text{ mm}^2/\text{s}$ (cf. [125]) and usual values of mineral oils,

$$\mu = 0.0308 \text{ Pas}, \quad \rho = 856 \text{ kg/m}^3. \quad (5.2)$$

is set. With these parameters and the loss factors C_{pv} , C_{st} , C_{sv} , C_{tv} and C_{vv} , the efficiencies are determined by

$$\eta_v = \frac{1}{1 + \frac{C_{sv}}{\lambda} + \frac{C_{st}}{\sigma}}$$

$$\eta_{hm} = 1 - C_{pv} - C_{vv} \lambda - C_{tv} \sigma^2$$

$$\eta_t = \eta_{hm} \cdot \eta_v \quad (5.3)$$

for motor operation and by

$$\eta_v = 1 - \frac{C_{sv}}{\lambda} - \frac{C_{st}}{\sigma}$$

$$\eta_{hm} = \frac{1}{1 + C_{pv} + C_{vv} \lambda + C_{tv} \sigma^2}$$

$$\eta_t = \eta_{hm} \cdot \eta_v \quad (5.4)$$

5. Assessment of drivetrain efficiency

Loss factor	unit	description	typical range
C_{pv}	1.0	Loss factor taking the mechanical and hydraulic losses dependent on Δp into account	$0.01 \dots 0.1 \cdot 10^{-8}$
C_{st}	1.0	Loss factor taking the volumetric losses dependent on ρ into account	$0.5 \cdot 10^{-4} \dots 2.8 \cdot 10^{-4}$
C_{sv}	1.0	Loss factor taking the volumetric losses dependent on μ into account	$0.5 \cdot 10^{-8} \dots 2.0 \cdot 10^{-8}$
C_{tv}	1.0	Loss factor taking the mechanical losses dependent on ρ into account	100...250
C_{vv}	1.0	Loss factor taking the hydraulic losses dependent on μ into account	$0.2 \cdot 10^5 \dots 0.8 \cdot 10^5$

Table 5.1.: Loss factors (taken from [97])

for pump operation. The definitions of the loss factors and their ranges as specified in [97] are given in table 5.1. The ranges of loss factors were defined in the late 1960s, based on state-of-the-art axial piston motors of that time. Probably modern machines will reach better values. However, since the characteristics of the variator machines are not known in detail, three different calculations of overall efficiency, the first with best-case, the second with worst-case and the third one with average (arithmetic mean) case values of the loss factors according to Schlösser, will be performed. The first two cases are borderline cases, because "high values of C_{sv} usually coincide with low values of C_{vv} " [97, p. 9]. In all simulations an efficiency factor of $\eta_p = 0.99$ taking pressure losses in the pipes between the pump and the motor into account is assumed. It is expected that the results, although not completely precise, will be sound enough to allow deciding whether the Compound-Split technology is not only a possible, but also a satisfactorily efficient solution for rotorcraft with variable rotor speed.

5.2. Efficiency of A6VE Series 71 hydraulic motors

To be able to rate the assumptions made in Schlösser's model and get reference values for the efficiency of the machines forming the variator, the total efficiencies for the axial piston units defined in table 4.4 were calculated for a given pressure level $\Delta p = 450$ bar and their respective ranges of operation. The results are depicted figure 5.1. The related volumetric and hydraulic-mechanical efficiencies as well as shaft torques and powers can be found in figures A.1, A.2, A.3 and A.4 in Appendix A.1. It has to be pointed out, that according to [97, p. 9] the range of V_g is limited to $[10 \text{ cm}^3, 50 \text{ cm}^3]$ and therefore the displacements of the studies machines are not covered by the model. However, since the calculation is intended as a rough estimation only, the use of Schlösser's model seems reasonable. The three subfigures in the left column of figure 5.1 show the total efficiency of the pump, whereas the ones in the right column are related to the motor. The subfigures are based on best-, worst- and average case of the loss factors. The speed range of a hydraulic machine is laid on the x -axis and the displacement is laid on the y -axis. It shall be

stressed that the scales are not the same for pump and motor. The levels of total efficiency are colour-coded in 0.025 (2.5 %) steps between 0.0 and 1.0. In addition, the lines of maximum torque as defined in table 4.4 are plotted. Apparently, these lines lie within the nominal range of speeds and displacements for pump operation but are outside for motor operation. This phenomenon can be explained with equations (4.2) and (4.3). For a given pressure level of $\Delta p = 450$ bar, the total efficiency leads to an increased demand for mechanical input power – i.e., torque – of the pump, which lies above the maximum input torque for some operation conditions. For the motor, the situation is the other way around and the losses prevent the output torque from reaching its maximum value for a given pressure level. To be able to show the line of maximum nominal torque for the motor, the range of the y -axis has been extended and a dashed black line is plotted for the maximum displacement.

In subfigure (a) the total efficiency of the pump is depicted for best-case of loss factors. It can be seen that the maximum efficiency is about 0.95 at medium speed and low displacement. For rotational speed below 2000 RPM the total efficiency is nearly independent of the displacement and decreases significantly for very low speeds below about 500 RPM. This is mainly due to the volumetric efficiency as can be seen in subfigure A.1 (a) in Appendix A.1. Combinations of high speeds and big displacements yield satisfactory results. As mentioned earlier, the line of maximum nominal power lies within the nominal ranges of speed and displacement and therefore limits the operation of the pump.

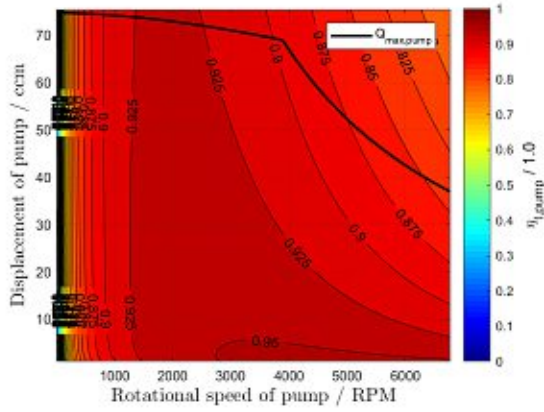
The worst-case for the pump is shown in subfigure (c). The overall appearance of the efficiency map is similar to the best-case, but the values of the total efficiency drop significantly. As a consequence, the maximum torque line is at lower displacements compared to the best-case. The maximum value is only about 0.75. Below speeds of about 1000 RPM, the efficiency decreases strongly towards standstill of the pump. The white areas indicate operation conditions where Schlösser's model even yields negative values of the total efficiency. This has no physical meaning, but it rather shows the limits of the model which was presumably not developed for these operating conditions.

Subfigure (e) shows the efficiency map for the average case. As could be expected, the results lie somewhere in between the ones for best- and worst-case. The maximum value of total efficiency is about 0.85 and below 1000 RPM it decreases strongly with the rotational speed and also shows areas where no physically meaningful solution was obtained.

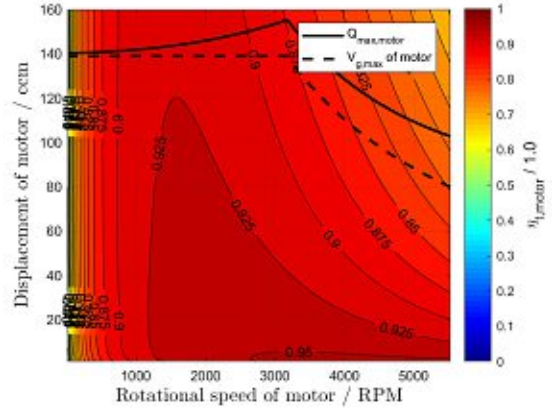
Turning to the results for the motor and subfigure (b), it can be seen, that the efficiency map is similar to the one of the pump depicted in subfigure (a). The maximum value is also about 0.95 and occurs at medium to high rotational speeds and low displacements. For low speeds, the total efficiency is nearly independent of the displacement, but very poor near standstill of the motor. The solid black line marking operation conditions at maximum nominal shaft torque lies above the dashed line for the maximum displacement limits of the motor. This is caused by the fact that the losses reduce the actual output torque compared to the nominal values, which were defined without considering efficiency. Combined with the inverse behaviour of the pump, the cyan and pink line in figure 4.3 will be shifted downwards and the sum of mechanical powers taken off EGS C and added to EGS D will not be zero. This means, that the pump has to contribute more torque for balancing the transmission system.

The worst-case for the motor is shown in subfigure (d). The resulting values are significantly lower than the ones of the pump. Near standstill of the motor no white areas marking operation conditions with no reasonable results occur. The maximum shaft torque line is even higher com-

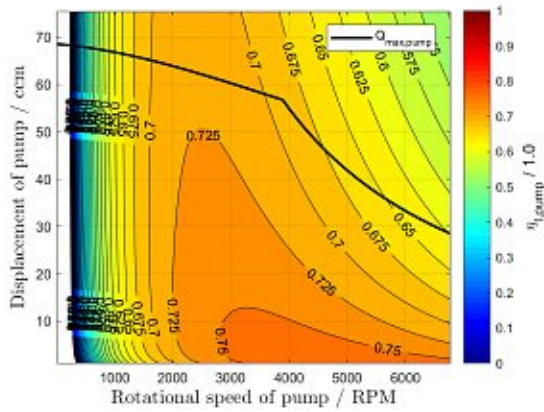
5. Assessment of drivetrain efficiency



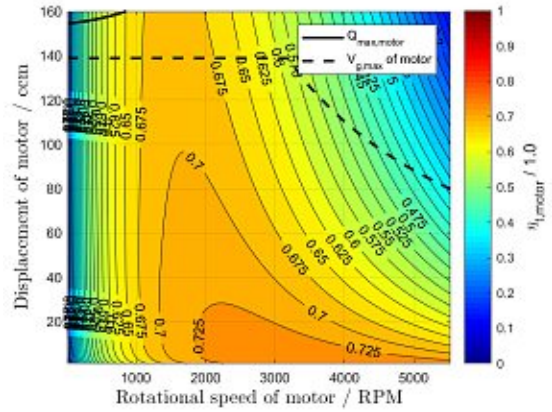
(a) Total efficiency of hydraulic pump, best-case



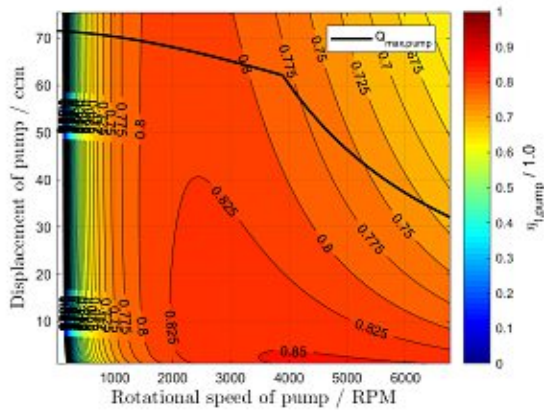
(b) Total efficiency of hydraulic motor, best-case



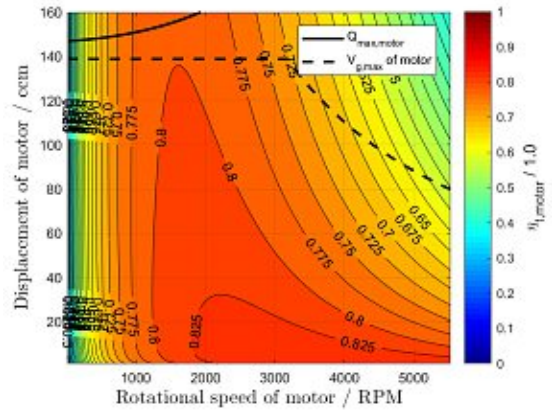
(c) Total efficiency of hydraulic pump, worst-case



(d) Total efficiency of hydraulic motor, worst-case



(e) Total efficiency of hydraulic pump, average case



(f) Total efficiency of hydraulic motor, average case

Figure 5.1.: Total efficiency of hydraulic machines of the A6VE Series 71 type in pump and motor operation

pared to the best-case, which means that the stress of the mechanical parts of the machine will be even lower than in that case.

As expected, the results for the average case loss factors depicted in subfigure (f) lie in between the previous two evaluations.

5.3. Efficiency of gear stages

To be able to assess the efficiency of the proposed transmission system, a reference value for the baseline UH-60 has to be calculated. Only the efficiency of gears will be taken into account whereas other sources of losses, such as bearings, will be neglected. The losses of gear stages consist of load dependent and load independent parts. Based on [79, p. 219 sqq.], the former are considered to be 1.5% of the input power P , i.e., $L_{l.i.} := 0.015P$. This applies for spur, helical and bevel gears, independent of the direction of the power flow. The latter are determined according to [79, p. 223] by

$$\begin{aligned} L_{l.d.} &= L_{l.i.} \delta_V \\ &= L_{l.i.} \frac{1.5 v_t}{100} \\ &= \frac{2.25 v_t}{10^4} P, \end{aligned} \quad (5.5)$$

where v_t is the tangential speed of the mesh. The angular velocities of all gears can be calculated as described in chapter 3 and the pitch diameters are taken from [74, 80] respectively are calculated with (3.7) for $b/d = 0.88$ (cf. [79, p. 267]). This leads to a total efficiency of a gear stage of

$$\begin{aligned} \eta_{\text{tot}} &= \frac{1}{P} (P - L_{l.d.} - L_{l.i.}) \\ &= 0.985 - \frac{2.25 v_t}{10^4}. \end{aligned} \quad (5.6)$$

Since the pitch power in planetary gear sets has to pass two meshes, the efficiency for this power flow is the product of the efficiencies of the two meshes. It should be noted that for planetary gear sets only the pitch power is assumed to be lossy, but not the coupling power. Losses of the coupling power, for example, windage losses of the carrier, are neglected. The terms for the efficiency of planetary gear sets considering only the pitch power flow are determined – as well as in (5.10) for the planetary gear stages of the CS module – as described in [77, p. 250 sqq.]. For the baseline fixed-ratio drivetrain of the UH-60, these assumptions yield a total efficiency of

$$\eta_{\text{tot, baseline}} = 91.73\%. \quad (5.7)$$

5.4. Drivetrain efficiency

The expected efficiency of the proposed UH-60 transmission system is calculated with the assumptions regarding power supply and demand as summarized in table 5.2. A full load as well as a partial load condition will be considered, each with the best-, average and the worst-case scenario of the variator. The two states are defined by the propulsive power of the two turboshaft engines and the power consumption of the tail rotor and the accessories. The values for the latter were taken from

5. Assessment of drivetrain efficiency

device	full load / kW	partial load / kW	note
turboshaft eng. (2x)	1151	575.5	-
accessories (2x)	-51	-51	incl. losses
tail rotor (TR)	-450	-112.5	incl. losses
main rotor (MR)	remaining power	remaining power	-

Table 5.2.: Assumptions regarding power supply and demand

[70, p. 86]. Since the last two are not affected by the CS module and the power has to pass as much gear meshes as in the basic UH-60 drivetrain, they are presumed to already contain the gearing losses. Therefore, in the simulation only the losses of the power flow to the main rotor will be taken into account. The overall efficiency is

$$\eta_{\text{overall}} = \frac{P_{\text{MR}}}{2 \cdot P_{\text{turboshaft eng.}} - P_{\text{TR}} - 2 \cdot P_{\text{accessories}}}. \quad (5.8)$$

The lossy transmission system can be described by a system of non-linear equations of the type $F(\underline{x}) = \underline{0}$. In this study, the efficiency is calculated for full and partial load in best-, average and worst-case for combinations of the displacement of the pump $V_{\text{pump}} \in [0, V_{\text{max,pump}}]$ and the basic transmission ratio $k_{ab} \in [\Theta_1, \Theta_2]$. Since the rotational speed of shaft a is assumed to be constant at 5750 RPM, all rotational speeds (angular velocities) are determined by k_{ab} . In addition, the input power and the torque of the CS modules are known:

$$\begin{aligned} P_a &= \left(P_{\text{turboshaft eng.}} - \frac{1}{2} \cdot P_{\text{TR}} - P_{\text{accessories}} \right) \eta_{\text{gear}} \\ Q_a &= \frac{P_a}{\omega_a}. \end{aligned} \quad (5.9)$$

With the other parameters defined so far, $F(x)$ can be written as

$$F \begin{pmatrix} P_{MR} \\ Q_b \\ Q_c \\ Q_d \\ V_{motor} \\ p_{pump} \\ p_{motor} \\ \lambda_{pump} \\ \lambda_{motor} \\ \sigma_{pump} \\ \sigma_{motor} \\ \eta_{v,pump} \\ \eta_{v,motor} \\ \eta_{hm,pump} \\ \eta_{hm,motor} \end{pmatrix} := \begin{pmatrix} 2 Q_b \omega_b \eta_{tot,cb} \frac{i_{12,UH-60} \eta_{tot,PGS} - 1}{i_{12,UH-60} - 1} - P_{MR} \\ \frac{1}{-i_{12C} \eta_{tot,C}^{-1}} Q_a + \frac{1}{i_{12D} \eta_{tot,D}^{-1}} Q_d - Q_c \\ \left(\frac{1}{i_{12C} \eta_{tot,C}^{-1}} - 1 \right) Q_a + \left(\frac{1}{i_{12D} \eta_{tot,D}^{-1}} - 1 \right) Q_d - Q_b \\ V_{pump} \eta_{v,pump} \eta_{v,motor} \omega_c |i_c| + \omega_d |i_d| V_{motor} \\ V_{motor} \frac{\eta_{hm,pump} \eta_{hm,motor} \eta_p Q_c \eta_{tot,c}}{|i_c|} - \frac{Q_d}{\eta_{tot,d} |i_d|} V_{pump} \\ \frac{V_{pump}}{2\pi} p_{pump} - \eta_{hm,pump} Q_c \frac{\eta_{tot,c}}{|i_c|} \\ \frac{V_{motor}}{2\pi} p_{motor} \eta_{hm,motor} - \frac{Q_d}{\eta_{tot,d} |i_d|} \\ \frac{\mu(-\omega_c |i_c|)}{p_{pump}} - \lambda_{pump} \\ \frac{\mu \omega_d |i_d|}{p_{motor}} - \lambda_{motor} \\ (-\omega_c |i_c|) \sqrt{\frac{3}{2} \frac{V_{pump}}{p_{pump}}} - \sigma_{pump} \\ \omega_d |i_d| \sqrt{\frac{3}{2} \frac{V_{motor}}{p_{motor}}} - \sigma_{motor} \\ 1 - \frac{C_{sv}}{\lambda_{pump}} - \frac{C_{st}}{\sigma_{pump}} - \eta_{v,pump} \\ 1 / \left(1 + \frac{C_{sv}}{\lambda_{motor}} + \frac{C_{st}}{\sigma_{motor}} \right) - \eta_{v,motor} \\ \frac{1}{1 + C_{pv} + C_{vv} \lambda_{pump} + C_{tv} \sigma_{pump}^2} - \eta_{hm,pump} \\ 1 - C_{pv} - C_{vv} \lambda_{motor} - C_{tv} \sigma_{motor}^2 - \eta_{hm,motor} \end{pmatrix}, \quad (5.10)$$

where the indices ib , cb , C , D , c , d , and PGS denote input and combining bevel gear stages, the stages depicted in figure 3.5 and the final planetary gear stage of the transmission system. The first term describes the relation between torque at the output shafts of the CS modules and MR power. The following two consider the equilibrium of torques of the lossy planetary gear sets. The fourth and fifth terms deal with the transmission ratio in the variator path. The following two consider the relation between the torques at the shafts c and d and the displacements and pressures at the hydraulic machines. The remaining terms determine the efficiency of the variator path.

The power at the main rotor is calculated with Matlab's nonlinear solver `fsolve` [67] and the overall efficiency is calculated according to (5.8). The resulting efficiencies are depicted in figure 5.2 and the pressure levels at the pump are shown in figure 5.3. The area of permissible solutions is limited by the short-time overload pressure (500 bar) and a minimum overall efficiency of 0.75. In addition, the maximum displacement of the motor is plotted as a solid black line (black patterns in the images occur around points for which the solver could not find a valid solution). On the left of the maximum displacement line, the required displacement is lower whilst on the right of it, the motor is not able to convert the flow delivered by the pump at the given speed level. Also, for some combinations of parameters – especially in the worst-case scenarios –, the simulation reaches the limits of Schlösser's model. For example, near the mechanical points at $k_{ab} = 1.3$ resp. $k_{ab} = 1.95$ one of the variator shafts c and d has very low speed and as a consequence, the parameters λ and σ become very low and division by them leads to numerical problems. However, it can be seen from figure 5.2 that in the best-case of hydraulic efficiency for the full load case as well as for the partial load case, solutions for nearly the whole range of k_{ab} could be found. Beyond the mechanical

5. Assessment of drivetrain efficiency

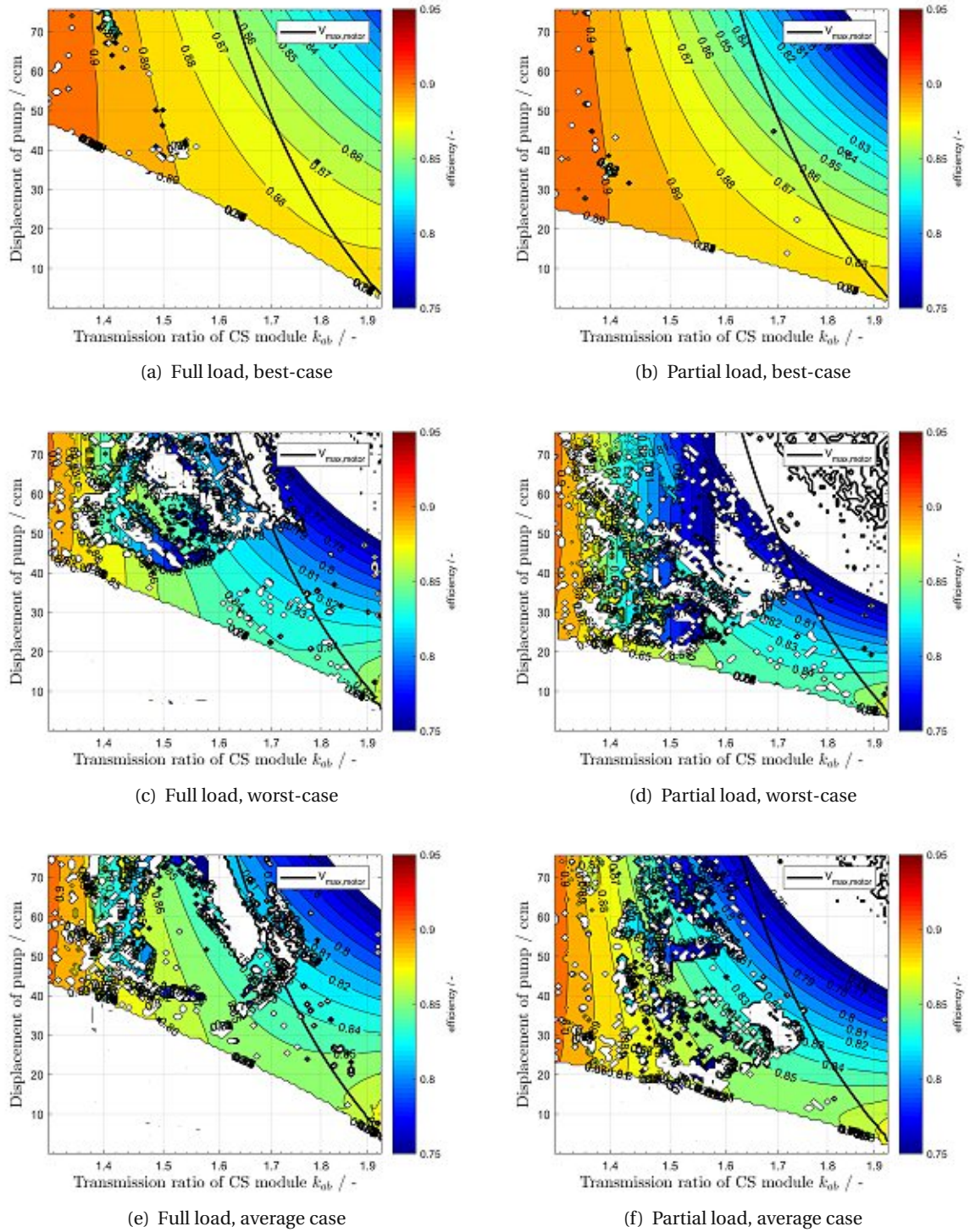


Figure 5.2.: Overall drivetrain efficiency η_{overall}

points, a minimum overall efficiency of 0.88 can be obtained. Compared to the basic transmission system with an estimated overall efficiency of 0.917, this is a significant reduction.

The worst-case scenarios yield even lower efficiencies and the results show numerical difficulties in solving (5.10). The minimum value in these cases is about 0.84. Subfigures 5.2 (e) and (f) show the results for the average case of machine efficiency. As could be expected, the calculated overall efficiencies are between the ones of best- and worst-case. The minimum value in the transmission range is about 0.85.

Another important finding is, that although the pump defined in table 4.4 is able to deliver the required flow in all operation conditions, the motor reaches the limits of possible displacement near the mechanical point Θ_2 . This is caused by the fact that the losses 'help' the pump to provide the torque at shaft *c* while reducing the torque resulting from the displacement and the pressure for the motor resp. shaft *d*. Therefore, in the final design the size of the pump and the motor have to be adapted to the losses. With a more detailed and validated loss model of the machines, this can be achieved by iteratively varying the maximum displacement of both machines until a satisfactory safety margin for the transferable power is reached in every operation condition. In any case an experimental assessment of the variator is indispensable. Turning to figure 5.3, one notices that the highest efficiencies are obtained for high pressure levels. This is an important finding for the control of the variator, since it is possible to define a nominal system pressure, which is kept constant by the pump while the motor adjusts the speed. Nevertheless, the control of a variable-ratio transmission system for the UH-60 poses a challenging task.

5. Assessment of drivetrain efficiency

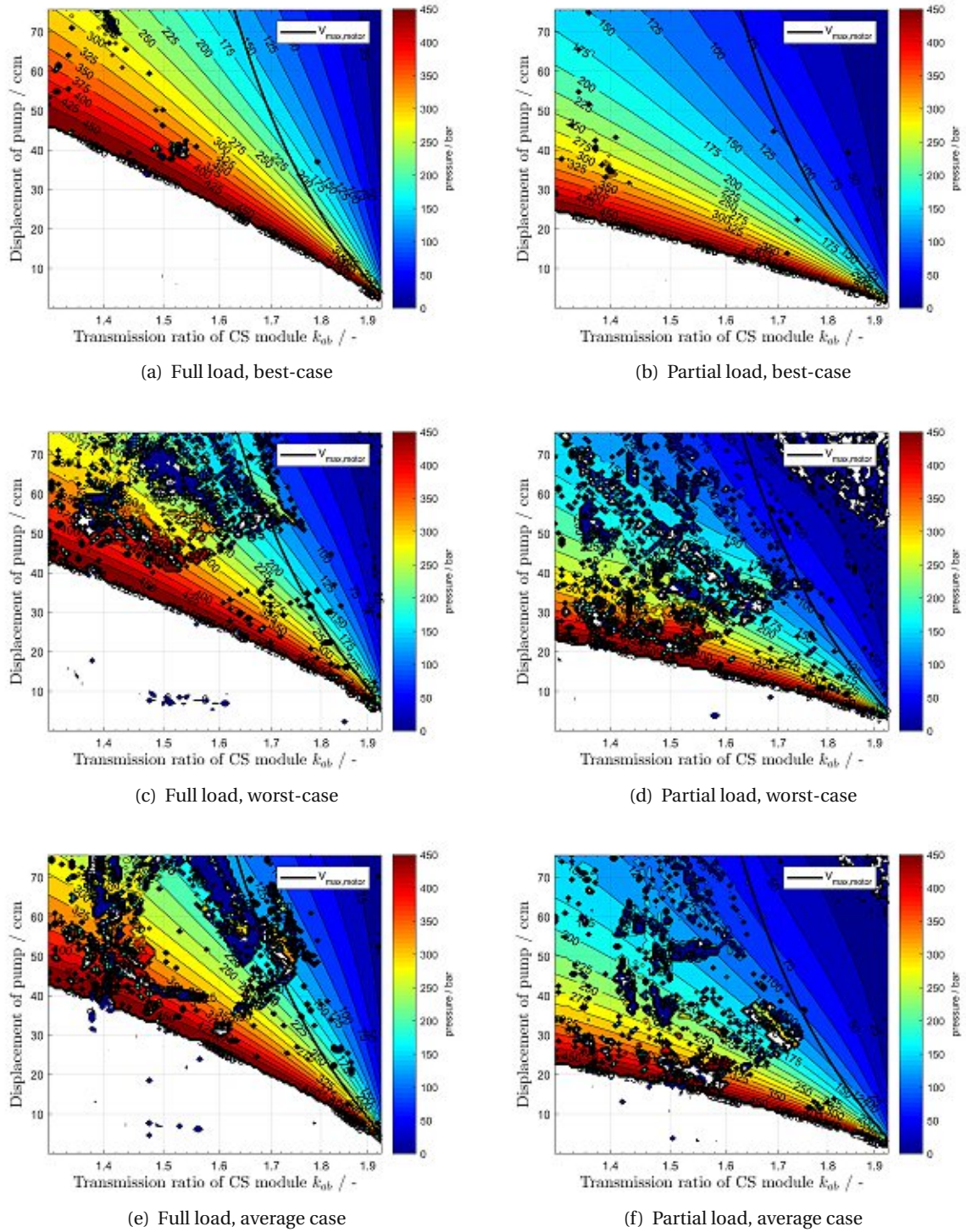


Figure 5.3.: Pressure level at the pump

6. Design

The basic properties of a variable-ratio transmission system comprising two Compound-Split modules for the UH-60 have been described in the previous chapters and also detailed information on the machines forming the variator could be gained. However, to be able to set up a dynamic simulation model of the drivetrain, additional design parameters have to be defined. In the following sections the considerations leading to the design data of the gears are described. The approach was the same as used in [82], but due to slightly changed parameters and restrictions, the results differ. However, both designs have similar dimensions and therefore the influence of the different parameters on the dynamic simulation is negligible.

6.1. Compound-Split modules

6.1.1. Definition of possible combinations of numbers of teeth

The required epicyclic and planetary ratios of the planetary gear sets C and D are given in (3.13). To find appropriate combinations of numbers of teeth of sun, planet and ring gears, all possible combinations of sun gears with 17 to 100 teeth and planet gears with numbers of teeth in the same range were searched. The number of teeth of the ring gear has to be close to $-(z_1 + 2z_{p1})$ (note the negative sign). When using profile shift, there can be a deviation of one or two teeth. These are not fixed limits but depend on the manufacturing process and several other restrictions described, for example, in [2, 3, 4, 5]. Especially for high numbers of teeth of the sun and planet gears, there is even more flexibility in the number of ring gear teeth. However, the allowed combinations of numbers of teeth \underline{z} for the scope of this thesis can be written as a set \mathcal{Z} defined as

$$\mathcal{Z} := \left\{ \underline{z} := [z_1, z_{p1}, z_2] \mid z_1, z_{p1} \in \{17, \dots, 100\} \wedge z_2 \in \{-((z_1 + 2z_{p1}) + 2), \dots, -((z_1 + 2z_{p1}) - 1)\} \right\}. \quad (6.1)$$

The set \mathcal{Z} contains 28224 vectors describing the numbers of teeth of sun, planet and ring gears. To reduce this number, every element which did not fulfil

$$\gcd(z_1, z_{p1}) \stackrel{!}{=} 1 \quad (6.2)$$

$$\gcd(z_1, z_2) \stackrel{!}{=} 1 \quad (6.3)$$

$$\gcd(z_{p1}, z_2) \stackrel{!}{=} 1 \quad (6.4)$$

was removed from the set. With this constraint set, every tooth of a gear mates with each tooth of the mating gear and not only with a subset. The aim of this measure is to reduce the influence of unfavourable overlap of production deviations and also a positive influence on the emission of noise is anticipated. In the design of a drivetrain for series production, these restrictions may be overruled by other requirements, for example, assembly space. Furthermore, according to [77, p. 237] planetary gear sets with q equally spaced planets have to fulfil

$$(z_1 - z_2) \bmod q \stackrel{!}{=} 0. \quad (6.5)$$

6. Design

For every element of \mathcal{Z} , the maximum number of planet gears was calculated according to (3.10). If the numbers of teeth and the calculated number of planets satisfied (6.5), the number of planets was added to the element, otherwise the element was removed from the set. The resulting set of vectors containing numbers of teeth and planets is denoted as \mathcal{Z}' . This set was used as basis for the dimensioning of suitable planetary gear sets for usage in the CS modules. In the next step the elements of \mathcal{Z}' which correspond to the required planetary ratios of the PGS C and D had to be found. This was obtained by using (3.8) and removing elements which yielded a planetary ratio i_{12} deviating more than 1 % from the target values given in (3.13). The remaining sets are denoted \mathcal{Z}''_C and \mathcal{Z}''_D . The full mathematical definitions are given by

$$\mathcal{Z}''_C := \left\{ [z_1, z_{p1}, z_2, q] \left| \begin{array}{l} z_1, z_{p1} \in \{17, \dots, 100\} \\ z_2 \in \{-((z_1 + 2z_{p1}) + 2), \dots, -((z_1 + 2z_{p1}) - 1)\} \\ \gcd(z_1, z_{p1}) = 1 \wedge \gcd(z_1, z_2) = 1 \wedge \gcd(z_{p1}, z_2) = 1 \\ q = \left\lfloor \frac{\pi}{1.10 \arcsin(\frac{u}{u+1})} \right\rfloor \\ (z_1 - z_2) \bmod q = 0 \\ \frac{z_2}{z_1} \in [-3.33 \cdot 0.99, -3.33 \cdot 1.01] \end{array} \right. \right\} \quad (6.6)$$

for planetary gear set C and

$$\mathcal{Z}''_D := \left\{ [z_1, z_{p1}, z_2, q] \left| \begin{array}{l} z_1, z_{p1} \in \{17, \dots, 100\} \\ z_2 \in \{-((z_1 + 2z_{p1}) + 2), \dots, -((z_1 + 2z_{p1}) - 1)\} \\ \gcd(z_1, z_{p1}) = 1 \wedge \gcd(z_1, z_2) = 1 \wedge \gcd(z_{p1}, z_2) = 1 \\ q = \left\lfloor \frac{\pi}{1.10 \arcsin(\frac{u}{u+1})} \right\rfloor \\ (z_1 - z_2) \bmod q = 0 \\ \frac{z_2}{z_1} \in [-2.17 \cdot 0.99, -2.17 \cdot 1.01] \end{array} \right. \right\} \quad (6.7)$$

for PGS D .

6.1.2. Calculation of strength

In the next step, designs with sufficient strength were derived for each element of \mathcal{Z}''_C and \mathcal{Z}''_D . A main parameter defining a gearing is the normal module m_n . The Deutsches Institut für Normung (DIN) standards collection defines a set of preferred values of the normal module in [6, 7]. From this list, the following set of values was chosen to be used in the calculation process:

$$m_n / 1 \text{ mm} \in \{1, 1.125, 1.25, 1.375, 1.5, 1.75, 2, 2.25, 2.5, 2.75, 3, 3.5, 4, 4.5, 5, 5.5, 6, 7, 8, 9, 10\}. \quad (6.8)$$

Of course, for application with highest demands on the transmission system – such as is rotorcraft – tailored tools with normal modules deviating from these values could be used. However, for the purpose of this study the distance between the standard values is sufficiently small. The reference profile according to [8] which was used for sun and planet gears of the planetary gear sets C and D is given in table 6.1. Since the tooth geometry and the manufacturing of the ring gears is subjected to additional restrictions, the final profile of the ring gears was determined on a case-by-case basis by the calculation software. The related absolute values of addendum, dedendum, tip clearance and root fillet radius of the basic rack are denoted h_{aP} , h_{fP} , c_P and ρ_{fP} .

The selection of the profile shift coefficients is not straightforward, since the used software does

Parameter	Symbol	Phys. dimension	Value
addendum-factor	h_{aP}^*	1.0	1.00
dedendum-factor	h_{fP}^*	1.0	1.25
Tip clearance-factor	c_P^*	1.0	1.25
Root fillet radius-factor	ρ_{fP}^*	1.0	1.0
pressure angle	α	deg	20

Table 6.1.: Reference profile for gears of planetary gear sets C and D

not offer an optimization based on the given parameters. To be able to conduct a variety of calculations, the profile shift coefficients of sun and planet gears, x_1 and x_{p1} , were chosen according to [9] to obtain a balanced mesh. The set values are given below.

$$(x_1, x_{p1}) = \begin{cases} (0.05, 0.00) & \text{for } z_2 = -(z_1 + 2 z_{p1}) + 1 \\ (0.25, 0.20) & \text{for } z_2 = -(z_1 + 2 z_{p1}) \\ (0.35, 0.30) & \text{for } z_2 = -(z_1 + 2 z_{p1}) - 1 \\ (0.35, 0.30) & \text{for } z_2 = -(z_1 + 2 z_{p1}) - 2 \end{cases} \quad (6.9)$$

The profile shift coefficient of the ring gear x_2 , which is a function of x_1 and x_{p1} , was calculated by the software. Because of the relatively low values of x_1 and x_{p1} , the resulting profile shift coefficients of the ring gears satisfy the limits defined in [4].

To be able to carry out strength calculations, some information on the used material, manufacturing and lubricant is needed. The assumed data is listed in tables 6.2, 6.3 and 6.4. According to [10], gears in power transmissions of aerospace applications are usually manufactured from steel which is case hardened either by nitriding or carburizing. Weden et al. [131] and Coy et al. [33] state that the commonly used material in US helicopter transmissions is AISI 9310, a carburizing steel. Therefore, the data of the gear material of sun and planet gears was selected from [11] for carburized steel of quality ME. The latter is the highest quality grade and to meet its requirements, a large number of measures have to be taken. These are defined in [11, p. 32 sqq.] and include; amongst others; chemical analysis, requirements on grain size, ultrasonic examination and crack inspection. The strength values given in [11] are valid for a probability of failure of 1 %. According to [10, p. 44], a reliability of three standard deviations has been used for highly reliable aerospace design in the past. With the statistic information given there, this is equivalent to a reliability of 99.875 % and the strength values presented in [11] have to be reduced by a factor of $\frac{0.7}{0.7674}$, which corresponds to reliability factors K_R and C_R of approximately 1.0963. In table 6.2 the strength values for 99 % and 99.875 % reliability are summarized. To avoid an excess of indices, the latter are not identified with the corresponding reliability. Gears for aerospace applications are usually shot peened or coated to increase the strength of the material. It is assumed that the influence of such measures is already taken into account in the values listed in table 6.2.

Depending on the application, ring gears are sometimes only quenched and tempered. For higher requirements on strength they are ground and nitrided afterwards. Only in exceptional cases, the grinding process is carried out after nitriding. Ring gears for high stress applications are sometimes carburized, hardened and ground. [96, p. 876]

For the scope of this thesis, it is assumed that all gears are manufactured from the same material.

6. Design

Parameter	Symbol	Phys. dimension	Value
description	-	-	AISI 9310
material quality	-	-	ME
reliability	-	%	99.875
probability of damage	-	%	0.125
reliability factor	-	1.0	1.0963
data source	-	-	[11, Figures 9 & 10]
type	-	-	carburized steel
Young's modulus	E	N/mm ²	206000
Poisson's ratio	ν	1.0	0.3
surface hardness	-	HV	660
core hardness	-	HV	370
allowable stress number (contact, 99 %)	$\sigma_{H,lim,99}$	N/mm ²	1700
nominal stress number (bending, 99 %)	$\sigma_{F,lim,99}$	N/mm ²	550
allowable stress number (bending, 99 %)	$\sigma_{FE,99}$	N/mm ²	1100
allowable stress number (contact, 99.875 %)	$\sigma_{H,lim}$	N/mm ²	1550
nominal stress number (bending, 99.875 %)	$\sigma_{F,lim}$	N/mm ²	500
allowable stress number (bending, 99.875 %)	σ_{FE}	N/mm ²	1000

Table 6.2.: Gear material

Surface quality and roughness have a big influence on the formation of the lubricating films. This affects the efficiency of the transmission system and the threat of some damage types, especially scuffing and micropitting. The assumed values of surface roughness on the flanks and the root fillet are summarized in table 6.3. In addition, the cold working treatment and finishing process are indicated. These are only informative, their influence is taken into account in the values of material strength and roughness. The gear quality according to DIN 3961 [12] was set 5.

Parameter	Symbol	Phys. dimension	Value
cold working process	-	-	all gears shot peened
final processing	-	-	all gears superfinished
arithmetic mean roughness (flank)	Ra_H	μm	0.3
mean peak-to-valley roughness (flank)	Rz_H	μm	(1.8)
arithmetic mean roughness (root)	Ra_F	μm	0.3
mean peak-to-valley roughness (root)	Rz_F	μm	(1.8)
Gear tooth quality DIN 3961	-	-	5

Table 6.3.: Manufacturing and finishing

As lubricant a synthetic oil fulfilling the requirements of [13] was assumed. The information on the load stage has been extrapolated from tests of oils fulfilling this specification. These tests were performed at the *Institute of Engineering Design and Logistics Engineering (TU Wien)*. The oil temperature was taken from [120, D-11].

Parameter	Symbol	Phys. dimension	Value
description	-	-	helicopter transmission oil
data source	-	-	[13]
type	-	-	synthetic
Kinematic viscosity at 40 °C	ν_{40}	mm ² /s	23
Kinematic viscosity at 100 °C	ν_{100}	mm ² /s	5 (4.90 – 5.40)
FZG load stage (A/8.3/90)	-	-	11
FZG load stage micropitting (C/8.3/90)	-	-	10
estimated temperature	-	°C	71

Table 6.4.: Lubricant data

Besides geometry, material and lubricant, the strength of a gear mesh depends on the operating data. Information on the assumed power, rotational speed and service life is given in table 6.5. Since no detailed information is available or – as in the case of the time slice of rotational speeds – do not exist for the UH-60, the chosen values are estimations on the safe side. The input power represents the intermediate power of one T700 turboshaft engine (cf. [121]). Tail rotor power and the demand of the accessories are not subtracted. The assumed service life of 10 000 h is a common value for helicopter transmissions. However, high speed parts with high numbers of load cycles are usually designed fatigue durable. Usually, helicopter transmissions are designed for a given load spectrum. This information is not open to the public and therefore no calculation of service life under variable load could be carried out and instead the life time factors Z_N and Y_N are both set 0.85. The load capacity of PGS *C* and the fixed-ratio stage driving the pump are calculated for a standstill of the pump shaft because this yields the maximum torques. For PGS *D* and the fixed-ratio stage driven by the hydraulic motor, the other mechanical point, i.e., a standstill of the motor shaft, is used.

Parameter	Symbol	Phys. dimension	Value
service life	-	h	10000
input power at shaft <i>a</i>	P_{in}	kW	1151
input speed	$n_a (\omega_a)$	RPM (rad/s)	5750 (602.14)

Table 6.5.: Operating data

6.1.3. Calculation method

Based on the assumptions made so far, a strength calculation was performed for each element of \mathcal{Z}''_C resp. \mathcal{Z}''_D in order to find the minimum normal module – and therefore the minimum diameters – in combination with which the minimum safety factors defined in table 6.6 are met. The first two factors are the results of the pitting resistance resp. bending calculation acc. to ISO 6336 [14, 15, 16]. The safety factors for scuffing were determined acc. to DIN 3990 part 4 [17]. In addition, the bending strength of the ring gears considering the influence of the rim was rated in conformity with one method developed by Verein Deutscher Ingenieure (VDI) [18] and two procedures published by Forschungsvereinigung Antriebstechnik (FVA) [50, 99, 102]. The threat of micropitting was calculated with FVA 54 [100]. The calculation was carried out by using a script within

6. Design

the FVA-Workbench (FVA-Wb) [45], a calculation software for machine elements and transmission applications.

Damage type / safety factor	Symbol	Phys. dimension	Value
pitting (ISO 6336)	S_H	1.0	1.1
root (ISO 6336)	S_F	1.0	1.4
scuffing (DIN 3990, integral temperature)	$S_{int S}$	1.0	1.8
scuffing (DIN 3990, contact temperature)	S_B	1.0	2.0
root (VDI 2737, ring gear only)	$S_{EVDI 2737}$	1.0	1.4
root (FVA 389, ring gear only)	$S_{FVA 389}$	1.0	1.4
root (FVA 45, ring gear only)	$S_{FVA 45}$	1.0	1.4
threat of micropitting (FVA 54)	λ/λ_{crit}	1.0	1.0

Table 6.6.: Required minimum safety factors for the planetary gear sets within the CS modules

To be able to run the calculations, some additional specifications have to be made. For example, assumptions on the influence of the application, internal dynamics and load sharing had to be made. The load sharing factor (mesh load factor) K_γ was taken from ANSI/AGMA 6123-B06 [1, Table 8] for application level 3:

$$K_{\gamma,C} = 1.19 \quad (6.10)$$

$$K_{\gamma,D} = 1.23. \quad (6.11)$$

For accurate determination of the other load factors detailed information regarding a multitude of parameters is needed. At the time, this data is not available. Therefore, for K_A , K_{AS} , K_v , $K_{H\beta}$, $K_{H\alpha}$, $K_{F\beta}$, $K_{F\alpha}$, $K_{B\beta}$ and $K_{B\alpha}$ the following assumptions were made:

$$K_A = 2 \quad (6.12)$$

$$K_{AS} = 2 \quad (6.13)$$

$$K_v, K_{H\beta}, K_{H\alpha}, K_{F\beta}, K_{F\alpha}, K_v, K_{B\beta}, K_{B\alpha} = 1. \quad (6.14)$$

Since the compared transmissions are quite similar to each other, it is expected that these assumptions – even if not yielding exact solutions for a given mesh – may be reasonable for comparing their strength.

For reasons of space, the variator cannot be placed in-between the two epicyclic gear sets as depicted in figure 3.5. To limit the required centre distance for the helical gear stages i_c and i_d and also to reduce the centrifugal forces acting on the planet bearings, high values value of b/d_1 resp. b/d_{p1} – whichever is greater – are preferable. In [79, Tafel 22.1/5], guideline values of this parameter are given for spur and helical gears. An example of a planetary gear is described at [79, pp. 364 sqq.]. Here a value of $b/d = 0.8$ was chosen for the smallest gear. This value was set for the layout of the planetary gear sets of the two CS modules.

The planetary gear stage in the baseline drivetrain of the UH-60 consists of spur gears. High-speed meshes and even the final (non-epicyclic) stages of helicopter transmissions comprise helical gears. The helix angles of sun, planet and ring gears in epicyclic gear sets of motor vehicles and hybrid

electric cars are usually different from zero (cf. [78]). In several studies; e.g., [51, 94, 95]; it has been shown, that for gears without modifications, whole-number values of the overlap ratio ε_β lead to reduced noise emission. Therefore, the helix angle β was chosen so that overlap ratios of 1.0, 2.0, 3.0 and 4.0 were obtained, unless the helix angle exceeded 25° .

Besides the parameters described so far, some additional input has to be provided to the calculation software. This information is listed in the echoprint of input data in the result files which can be found in the supplementary. The used FVA-Wb model and the script setting the parameters, starting the calculations and saving the results have also be added to the supplementary.

6.1.4. Final parameters of planetary gear sets *C* and *D*

The results of the calculations are tables listing possible combinations of parameters satisfying the set conditions. The full tables for *C*, *D* and the fixed-ratio stages can be found in the supplementary. From the multitude of results, one was chosen for each planetary gear set. These are not necessarily the ones with the smallest diameter, but the ones offering good overall properties at small diameters. The selected gearing data and resulting safety factors are shown in tables 6.7 and 6.8.

All of the geometric parameters of PGS *C* are common in helicopter drivetrains at the given speed and torque level. Especially, none of the is at a boundary of the permitted parameter range, which would indicate that the optimum is outside this area. With a helix angle of 20.5° an overlap ratio of about 2.0 is achieved. If the resulting axial forces lead to unacceptably high loads on the bearings, this value has to be reduced. The working pitch diameter of the sun gear ($d_{w,2} = -242.441$ mm) is smaller than the diameter of the input bevel gear (~ 340 mm) (cf. [74, 80]). Therefore, the diameter is no limiting factor concerning assembly space (see figure 3.6 and section 3.5). The resulting safety factors are far above the minimum values defined in table 6.6. The reason for this is the threat of micropitting, which required an increase of the normal module though the other safety factors were already sufficient.

Turning to table 6.8, we see that the selected normal module for PGS *D* is smaller than the one for PGS *C* whilst the numbers of teeth are higher. As a consequence, the overlap ratio of 2.0 is obtained with a smaller helix angle of 16.5° . The resulting working pitch diameters are smaller than the ones of PGS *C*. The main reason for this is the fact that only a portion of the propulsive power has to be transmitted via *D*. The calculated safety factors are closer to the minimum values but are also more than sufficient.

6. Design

Parameter	Symbol	Phys. dimension	Value
number of teeth sun gear	z_1	1	23
number of teeth planet gears	z_{Pl}	1	26
number of teeth ring gear	z_2	1	-77
planetary ratio	i_{12}	1.0	-3.3478
number of planets	q	1	5
normal module	m_n	mm	3
profile shift coefficient sun	x_1	1.0	0.35000
profile shift coefficient planet	x_{Pl}	1.0	0.30000
profile shift coefficient ring	x_2	1.0	0.13368
working pitch diameter sun	$d_{w,1}$	mm	75.373
working pitch diameter planets	$d_{w,Pl}$	mm	85.205 / 81.863
working pitch diameter ring	$d_{w,2}$	mm	-242.441
face width sun / planet / ring	b_1	mm	55.8 / 55.8 / 55.8
helix angle	β	°	20.5
overlap ratio sun-planet	ϵ_β	1.0	1.999
overlap ratio planet-ring	ϵ_β	1.0	1.999
Damage type / safety factor	Symbol	Phys. dimension	Value
pitting (ISO 6336) sun / planet / ring	S_H	1.0	1.82 / 1.82 / 2.96
root (ISO 6336) sun / planet / ring	S_F	1.0	9.61 / 6.66 / 7.45
scuffing (DIN 3990, integral temperature)	$S_{int S}$	1.0	2.50 / 3.18
scuffing (DIN 3990, contact temperature)	S_B	1.0	2.43 / 5.29
root (VDI 2737, ring gear only)	$S_{FVDI 2737}$	1.0	8.23
root (FVA 389, ring gear only)	$S_{FFVA 389}$	1.0	7.12
root (FVA 45, ring gear only)	$S_{FFVA 45}$	1.0	8.12
threat of micropitting (FVA 54)	$\lambda > \lambda_{crit} \Rightarrow$ no expectation of micropitting damage !		

Table 6.7.: Chosen parameters and resulting safety factors for planetary gear set C

Parameter	Symbol	Phys. dimension	Value
number of teeth sun gear	z_1	1	51
number of teeth planet gears	z_{p1}	1	29
number of teeth ring gear	z_2	1	-110
planetary ratio	i_{12}	1.0	-2.1569
number of planets	q	1	5
normal module	m_n	mm	1.5
profile shift coefficient sun	x_1	1.0	0.35000
profile shift coefficient planet	x_{p1}	1.0	0.30000
profile shift coefficient ring	x_2	1.0	-0.39884
working pitch diameter sun	$d_{w,1}$	mm	80.970
working pitch diameter planets	$d_{w,p1}$	mm	46.042 / 45.474
working pitch diameter ring	$d_{w,2}$	mm	-172.486
face width sun / planet / ring	b_1	mm	35.2 / 35.2 / 35.2
helix angle	β	°	16.5
overlap ratio sun-planet	ϵ_β	1.0	2.001
overlap ratio planet-ring	ϵ_β	1.0	2.001
Damage type / safety factor	Symbol	Phys. dimension	Value
pitting (ISO 6336) sun / planet / ring	S_H	1.0	1.47 / 1.47 / 2.13
root (ISO 6336) sun / planet / ring	S_F	1.0	4.11 / 2.93 / 3.37
scuffing (DIN 3990, integral temperature)	S_{intS}	1.0	2.53 / 3.29
scuffing (DIN 3990, contact temperature)	S_B	1.0	2.55 / 4.76
root (VDI 2737, ring gear only)	$S_{F,VDI 2737}$	1.0	3.15
root (FVA 389, ring gear only)	$S_{F,FVA 389}$	1.0	2.79
root (FVA 45, ring gear only)	$S_{F,FVA 45}$	1.0	3.24
threat of micropitting (FVA 54)	$\lambda > \lambda_{crit} \Rightarrow$ no expectation of micropitting damage !		

Table 6.8.: Chosen parameters and resulting safety factors for planetary gear set D

6.2. Fixed-ratio helical gear stages connecting the variator to the mechanical path

To define sets of possible numbers of teeth for the gears of the helical gear stages connecting the mechanical path to the variator machines, an approach similar to the one for the planetary gear sets was chosen. The number of teeth of the pinion was varied between 17 and 100 and multiplied with i_c resp. i_d according to (4.22). If the transmission ratio of the rounded results deviated less than 1 % from the target value, the combination of numbers of teeth was added to the sets of permissible input for the calculation, denoted \mathcal{Z}_{hC} and \mathcal{Z}_{hD} . These are given by

$$\mathcal{Z}_{hC} := \left\{ [z_1, z_2] \left| \begin{array}{l} z_1 \in \{17, \dots, 100\} \\ z_2 \mid -1.06 \cdot z_1 \mid \\ \frac{z_2}{z_1} \in [-1.06 \cdot 0.99, -1.06 \cdot 1.01] \end{array} \right. \right\} \quad (6.15)$$

for the helical gear stage connected to the pump and

$$\mathcal{Z}_{hD} := \left\{ [z_1, z_2] \left| \begin{array}{l} z_1 \in \{17, \dots, 100\} \\ z_2 \mid -1.83 \cdot z_1 \mid \\ \frac{z_2}{z_1} \in [-1.83 \cdot 0.99, -1.83 \cdot 1.01] \end{array} \right. \right\} \quad (6.16)$$

for the one connected to the hydraulic motor. It shall be pointed out, that the index 1 denotes the pinion, i.e., the smaller of the two gears of the mesh, and not the driving gear.

The sum of profile shift coefficients $x_1 + x_2$ is set to 0.8 (high flank and root strength), which is split automatically according to [9] by the software. Material, manufacturing and lubricant data for the two helical gear stages is the same as for the planetary gear stages *C* and *D* (cf. tables 6.2, 6.3 and 6.4). The operating conditions have already been discussed in section 6.1 (cf. table 6.5). To reduce the axial length of the mechanical part of the CS modules and to reach large enough centre distances so that the hydraulic machines can be placed besides the PGS, the common face width of the helical gear stages were preset to 20 mm and 30 mm. Whole-number values for the overlap ratios were strived. As for the planetary gear sets, all possible combinations of parameters were checked on compliance with the set requirements. If accepted, the minimum normal module, so that the minimum safety factors were met, was searched. The resulting tables for the fixed-ratio stages i_c and i_d can be found in the supplementary. The selected final design parameters as well as the resulting safety factors are presented in tables 6.9 and 6.10.

The chosen values for i_c are quite common, none are at the end of the permissible range. The small face width combined with a minimum overlap ratio of 1.0 result in comparable high numbers of teeth and a normal module of 2 mm. The resulting centre distance is big enough to place the pump besides the ring gear of *C*. The face width of 24.3 mm and 22.3 mm result from small changes to achieve a whole-number overlap ratio, a $1 \times 45^\circ$ chamfer at the tip and a 2 mm wider pinion. Due to the low b/d ratio, an overlap ratio of only 1.0 could be achieved with a helix angle of 18° . The safety factors meet the requirements. However, for the threat of micropitting no reasonable rating is possible, because the strength calculation is based on the mechanical points and high torque at standstill as well as low torque at high-speed are difficult operation conditions to be examined.

For the fixed-ratio helical gear stage i_d , the same general comments apply. Due to the higher torque at the motor shaft in standstill, the resulting working pitch diameters are larger although the common face width is increased by 50 % compared to i_c .

6.2. Fixed-ratio helical gear stages connecting the variator to the mechanical path

Parameter	Symbol	Phys. dimension	Value
number of teeth pinion	z_1	1	76
number of teeth wheel	z_2	1	81
normal module	m_n	mm	2
profile shift coefficient pinion	x_1	1.0	0.40541
profile shift coefficient wheel	x_2	1.0	0.39459
working pitch diameter pinion	$d_{w,1}$	mm	161.325
working pitch diameter wheel	$d_{w,2}$	mm	171.938
face width pinion	b_1	mm	24.3
face width wheel	b_2	mm	22.3
helix angle	β	°	18
overlap ratio	ϵ_β	1.0	0.998
Damage type / safety factor	Symbol	Phys. dimension	Value
pitting (ISO 6336) pinion / wheel	S_H	1.0	1.26 / 1.26
root (ISO 6336) pinion / wheel	S_F	1.0	1.44 / 1.56
scuffing (DIN 3990, integral temperature)	S_{intS}	1.0	3.69
scuffing (DIN 3990, contact temperature)	S_B	1.0	15.5
threat of micropitting (FVA 54)	Near standstill no reasonable rating is possible.		

Table 6.9.: Chosen parameters and resulting safety factors for helical gear stage i_c

Parameter	Symbol	Phys. dimension	Value
number of teeth pinion	z_1	1	44
number of teeth wheel	z_2	1	81
normal module	m_n	mm	3
profile shift coefficient pinion	x_1	1.0	0.44387
profile shift coefficient wheel	x_2	1.0	0.35613
working pitch diameter pinion	$d_{w,1}$	mm	140.420
working pitch diameter wheel	$d_{w,2}$	mm	258.500
face width pinion	b_1	mm	34.5
face width wheel	b_2	mm	32.5
helix angle	β	°	18
overlap ratio	ϵ_β	1.0	1.000
Damage type / safety factor	Symbol	Phys. dimension	Value
pitting (ISO 6336) pinion / wheel	S_H	1.0	1.12 / 1.12
root (ISO 6336) pinion / wheel	S_F	1.0	1.62 / 1.47
scuffing (DIN 3990, integral temperature)	S_{intS}	1.0	3.63
scuffing (DIN 3990, contact temperature)	S_B	1.0	13.59
threat of micropitting (FVA 54)	Near standstill no reasonable rating is possible.		

Table 6.10.: Chosen parameters and resulting safety factors for helical gear stage i_d

6.3. Changes to combining bevel gear stage and main planetary gear stage

The changes made to the baseline drivetrain to obtain a continuously variable transmission system affect the Combining Bevel Gear Stage (CBGS) and the Main Planetary Gear Stage (MPGS) in three ways. First, the Compound-Split modules have a minimum transmission ratio of 1.3 at MP I (Θ_1), which increases the overall ratio. If no changes are applied to the final stages, the range of rotor speed would be 132 RPM to 198 RPM. Second, the maximum main rotor speed shall be 180 RPM to 258 RPM. Therefore, even for $\min(\Theta_1, \Theta_2) = 1$, the transmission ratios of combining bevel and main planetary gear stage would have to be adapted. The third – but probably most important – influence is the increased torque when the rotor is operated at speeds below the nominal value.

To address the first two points, the numbers of teeth of the affected gears have to be changed. The values for the baseline transmission system were taken from [74] and are shown in table 6.11. To reduce the numbers of indices, none were added to the symbols. If the same symbol is used for different parameters, it is apparent from the context which one is meant. The overall transmission

parameter	Symbol	Phys. dimension	Value
number of teeth bevel pinion	z_1	1	17
number of teeth bevel gear	z_2	1	81
transmission ratio bevel gear stage	i_{CBGS}	1.0	4.765
number of teeth sun gear	z_1	1	62
number of teeth planet gears	z_{p1}	1	83
number of teeth ring gear	z_2	1	-228
planetary ratio	$i_{12,\text{MPGS}}$	1.0	-3.677
transmission ratio	$i_{1s,\text{MPGS}}$	1.0	4.677
number of planets	q	1	5

Table 6.11.: Data of combining bevel gear and main planetary gear stage (cf. [74, p. 7])

ratio of the two stages is $i = 22.287$. To reach the maximum main rotor speed at $k_{ab} = \Theta_1$, this value has to be reduced to $\tilde{i} = i/1.1/1.3 = 15.585$. As for the planetary gear sets *C* and *D*, a set of possible combinations of numbers of teeth was defined for the main PGS. Again, there should be as little changes as possible to achieve the required transmission ratios. This leads to the following assumptions:

1. The required change of transmission ratio shall be evenly divided among the two stages.
2. The number of teeth of the gear of CBGS is 81 and will be kept unchanged.
3. The number of planets shall stay the same.
4. Since for the numbers of teeth of the baseline main PGS $z_1 + 2 z_{\text{p1}} = -z_2$ applies, this condition is required for the new design as well.
5. The number of teeth of the planet gears shall stay the same.
6. The numbers of teeth of the gears of CBGS shall not have a common divisor different to 1.
7. No pair of numbers of teeth of the gears of MPGS shall have a common divisor different to 1.

6.4. Remarks on the design of the variable-ratio drivetrain

The values of the selected modification of the two stages satisfying these requirements are given in table 6.12. To take the influence of the increased torques into account is more challenging since

parameter	Symbol	Phys. dimension	Value
number of teeth bevel pinion	\tilde{z}_1	1	20
number of teeth bevel gear	\tilde{z}_2	1	81
transmission ratio bevel gear stage	\tilde{i}_{CBGS}	1.0	4.050
number of teeth sun gear	\tilde{z}_1	1	87
number of teeth planet gears	\tilde{z}_{p1}	1	83
number of teeth ring gear	\tilde{z}_2	1	-253
planetary ratio	$\tilde{i}_{12,\text{MPGS}}$	1.0	-2.908
transmission ratio	$\tilde{i}_{1s,\text{MPGS}}$	1.0	3.908
number of planets	\tilde{q}	1	5

Table 6.12.: Data of modified combining bevel gear and main planetary gear stage

no information on the design load spectrum is publicly available. As a rough estimate,

$$\frac{Q}{V_{\text{spur gear}}} \propto \frac{Q}{d^2 b} = \text{const.} \quad (6.17)$$

can be assumed. Since for constant maximum power MR speed will be reduced to 70 %, a torque increase by 42.9 % is expected. If b/d is kept constant, this yields

$$\tilde{d} = \sqrt[3]{1.429} d \approx 1.126 d \quad (6.18)$$

$$\tilde{b} = \sqrt[3]{1.429} b \approx 1.126 b. \quad (6.19)$$

For the combining bevel gear stage this factor is probably covered by the increased number of teeth of the pinion. Since the planet gears are probably the critical parts in the main planetary gear stage, the normal module and the face width of sun, planet and ring gears will be increase by a factor of 1.126.

6.4. Remarks on the design of the variable-ratio drivetrain

In this chapter some design data of the Compound-Split modules as well as of the remaining drivetrain was derived. This information is needed to be able to estimate the dimensions of the modifications compared to the UH-60's baseline transmission system. It will also be used in the dynamic simulation of the propulsion system, where transmission ratios and estimated moments of inertia (based on gear geometry data) will have a mayor influence on the results. It shall be stressed, that the found solution is only valid for the given assumptions and restrictions and therefore appropriate for a demonstrator rather than a serially produced helicopter.

The design parameters selected for the mechanical path of the CS modules are limited to the gears. Shafts and bearings were not considered in detail, because there are lots of unknown parameters and especially the given assembly space is not known in detail. The lubrication for the CS modules poses a challenging task, since the cooling of the high speed parts will be a core function of such a system. Due to the special operation conditions of the fixed-ratio helical gear stages i_c and i_d ,

6. Design

they are probably at risk of micropitting. To face this threat a comprehensive examination of the gear stages; including operating conditions, materials, surface treatments and lubrication, has to be done. However, based on the gearing data, it is assumed, that engineering will find satisfying solutions to these problems.

The needed data of the two hydraulic machines has already been defined in chapter 4. As mentioned there, these machines are COTS products for mobile applications. The properties of tailored solutions for the use in rotorcraft transmission systems may strongly differ from the values in chapter 4. However, a working hydraulic transmission needs far more than pump and motor. First of all, they have to be connected by hydraulic lines consisting of pipes and hoses. To obtain a CVT, some control mechanism has to be implemented to change the displacements. During operation, the hydraulic fluid warms up and is contaminated by debris and the products of ageing and other chemical processes. To ensure safe and efficient operation of the transmission system, oil coolers and filters are needed. As described in section 5.1, volumetric losses occur at the hydraulic machines by the very principle of power transformation. To compensate for these losses and supply hydraulic fluid, feed pumps, which do not stand still in any operation condition, are needed. Furthermore, some kind of reservoir or tank for a minimum of hydraulic fluid has to be included. To counter a malfunction of any device in the hydraulic circuit, valves have to be installed. For example, the system pressure has to be limited and in case of a clogged filter, a by-pass has to be opened. Similar to the lubrication system of the UH-60, a by-pass of the oil cooler could be designed to ease run-up and increase system efficiency (cf. [120, p. D-11]). Perhaps, an oil heating system is required to enable operations in extreme climate. Additional measuring devices for pressure, temperature, oil flow, etc. – especially if connected to the cockpit or a Health and Usage Monitoring System (HUMS) system – may further increase safety.

Due to a lack of measured data, the reliability of the hydraulic system cannot be rated quantitatively at present. However, certification requirements and demands of operators (especially in the military sector) put emphasis on the safety of the system. It is possible that redundant hydraulic systems are required for both CS modules, i.e. two pumps and two motors on each side of the drivetrain. If (4.19) applies for the final variator machines, redundant systems may decrease variator weight.

To sum up, it can be said that the design, manufacturing and testing of the proposed type of continuously variable transmission system is a challenging and fascinating task. Unfortunately, it is far beyond the scope of this study and the related project VARI-SPEED and therefore remains as a subject for follow-up projects.

Part III.

Dynamic Simulation



Die approbierte gedruckte Originalversion dieser Dissertation ist an der TU Wien Bibliothek verfügbar.
The approved original version of this doctoral thesis is available in print at TU Wien Bibliothek.

7. Modelling

To show the feasibility of a transmission system containing two Compound-Split modules for the use in rotorcraft, a dynamic simulation was carried out. The model was built up in Simulink [103], making extensive use of the Simscape Multibody toolbox. In this chapter, the models of the main components of the propulsion system of the UH-60 are described. For the main rotor and the two turboshaft engines it is relied on models found in the literature. The drivetrain model consists of a multi-body system combined with basic modelling of the hydraulic system.

7.1. T700 turboshaft engine

The model of the two General Electric T700 turboshaft engines is based on the simplified open-loop dynamic model developed by Duyar et al. [40]. It has been obtained by linking linear state space models which were derived from detailed nonlinear engine simulations [40, p. 62]. The five operating points used are shown in table 7.1. The first two lines show the power turbine speed relative to nominal speed $\%N_P$ and the fuel flow W_F . These two values form the control vector \underline{u} of the T700 model, i.e.,

$$\underline{u} := \begin{pmatrix} \%N_P \\ W_F \end{pmatrix}. \quad (7.1)$$

The output vector \underline{y} , defined by

$$\underline{y} := \begin{pmatrix} \%N_G \\ Q_S \\ T_{45} \\ P_{S3} \end{pmatrix}, \quad (7.2)$$

consists of the relative gas generator speed, the engine shaft torque multiplied by the transmission ratio of the main gear box (i.e., the torque acting on the MR shaft), the interturbine gas temperature and the static pressure at station 3. The values of these parameters at the five operating points are summarized in lines three to six in table 7.1. For illustration, the corresponding values affecting the dynamic model of the drivetrain – i.e., engine shaft speed, torque and power – are presented below. To be able to use the numerical values given in the paper, the original operating points and units are used in the Simulink model and only the resulting torque, which acts on the power turbine shaft, is converted to Nm.

For each operating point $j \in \{1, 2, 3, 4, 5\}$, a set of matrices $\underline{\underline{D}}_j$, $\underline{\underline{E}}_j$, $\underline{\underline{F}}_j$, $\underline{\underline{G}}_j$ and $\underline{\underline{Z}}_j$ determining the linear model

$$\underline{x}(k+1) = \underline{\underline{D}}_j \underline{x}(k) + \underline{\underline{E}}_j \underline{u}(k) + \underline{\underline{F}}_j \quad (7.3)$$

$$\underline{y}(k) = \underline{\underline{C}}_j \underline{x}(k) + \underline{\underline{Z}}_j \quad (7.4)$$

7. Modelling

Operating point			1	2	3	4	5
rel. power turbine speed	$\%N_P$	%	100	100	100	100	100
fuel flow	W_F	lb/s	0.0884	0.1170	0.1456	0.1742	0.2028
rel. gas generator speed	$\%N_G$	%	87.5	91.4	94.5	96.7	98.5
engine shaft torque (at MR)	Q_S	ft-lb	9369.0	15309.0	21443.0	27303.0	32619.0
interturbine gas temperature	T_{45}	degR	1472.0	1578.0	1675.0	1778.0	1896.0
static pressure at station 3	P_{S3}	psi	132.0	161.7	188.9	212.3	231.5
engine shaft speed	n_{TSE}	Nm	20900	20900	20900	20900	20900
engine shaft torque	Q_{TSE}	Nm	156.8	256.2	358.9	457.0	545.9
engine power	P_{TSE}	kW	343.0	560.4	785.0	999.5	1194.1

Power turbine design speed = 20900 RPM / Gas generator design speed = 44 700 RPM

Table 7.1.: Operating points of turboshaft engine model (cf. [40, p. 64])

is given in [40]. Here \underline{x} denotes the engine model state vector. To cover the whole operating range of the T700 engine, an interpolation between the point models based on the gas generator speed is possible (cf. [40, p. 66]). However, it turned out to be favourable to prescribe the operation points in the model based on preliminary results. The sampling time of the models is 0.1 s [40, p. 65]), i.e., 0.1 seconds pass between the states k and $k+1$. To obtain a more dynamic model for the simulation of the transmission system, a linear interpolation in the time step can be performed. The state vector at $t + \Delta t$, with $\Delta t \leq 0.1$, is then given by

$$\underline{x}(t + \Delta t) = \underline{x}(t) + \frac{\Delta t}{0.1} \left(\underline{D}_j \underline{x}(t) + \underline{E}_j \underline{u}(t) + \underline{F}_j - \underline{x}(t) \right). \quad (7.5)$$

Since the power turbine shaft is considered as a part of the transmission system and therefore is affected by changes of power demand of the rotors, the sampling time can be reduced by using (7.5) to be able to model highly dynamic processes. However, due to the low level of detail of the turboshaft engines' speed controllers, the sampling time was kept unchanged for this study to reduce simulation effort.

7.2. Main rotor

The main rotor is modelled with classical Blade Element Momentum Theory (BEMT). As the name suggests, BEMT is a combination of blade element and momentum theory. The latter is used to determine the induced velocity at the discrete elements of the blades. With knowledge of the inflow, the forces acting on the blade elements can be determined by using lookup tables available in the literature.

7.2.1. Blade model

The main rotor of the UH-60 comprises four identical blades. The planform with the sections of the two used airfoils SC1095 and SC1094 R8 is shown in figure 7.1.

From 0.0 to 0.1925 R , the blade was assumed non-aerodynamic, i.e., no lift and drag forces were calculated. Outboard from this point, the section with airfoil SC1095 starts. Between 0.4658 R and

0.4969 R there is a linear transition to SC1094 R8. Its section ranges from 0.4969 R to 0.8230 R . After another transition, SC1095 is used from 0.8540 R to the blade tip. [28]

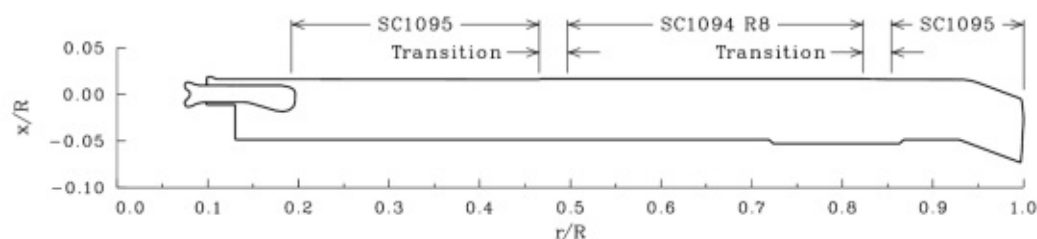


Figure 7.1.: Main rotor blade of UH-60 (taken from [28, p. 6])

The four blades of the UH-60's main rotor are modelled by sixteen elements per blade. Information on blade geometry and mass distribution was taken from [28, 32, 35, 133, 134]. The properties of the blade sections are summarized in table 7.2. The length of one section was set to 5 % of the main rotor radius R , except for the first one, which covers the remaining distance at the inner end of the airfoil sections. The generic radial position from the hinge \tilde{r} is defined as the ratio of the radial position minus the hinge offset e to the main rotor radius. It is equivalent to the parameter r used in [70]. The blade chord was assumed to be constant, the trim tab at 0.7316...0.8629 R and the form of the tip section, which is swept by 20° (cf. [28, p. 6]), were not considered in the simulation.

#	rad. pos. of center r m	$\tilde{r} := \frac{r-e}{R}$ 1.0	length L_{bl} m	area A_{bl} m^2	mass m_{bl} kg	twist ϑ_{tw} deg	airfoil -
1	1.810	0.175	0.470	0.248	4.826	11.5	SC1095
2	2.249	0.228	0.409	0.215	4.176	10.5	SC1095
3	2.658	0.278	0.409	0.215	4.215	9.5	SC1095
4	3.067	0.328	0.409	0.215	4.228	8.5	SC1095
5	3.476	0.378	0.409	0.215	4.228	7.5	SC1095
6	3.885	0.428	0.409	0.215	4.301	6.5	SC1095
7	4.293	0.478	0.409	0.215	4.293	5.5	SC1094 R8
8	4.702	0.528	0.409	0.215	4.285	4.5	SC1094 R8
9	5.111	0.578	0.409	0.215	4.501	3.5	SC1094 R8
10	5.520	0.628	0.409	0.215	4.977	2.5	SC1094 R8
11	5.929	0.678	0.409	0.215	5.377	1.5	SC1094 R8
12	6.338	0.728	0.409	0.215	5.348	0.5	SC1094 R8
13	6.747	0.778	0.409	0.215	5.754	-0.5	SC1094 R8
14	7.156	0.828	0.409	0.215	6.916	-1.5	SC1095
15	7.565	0.878	0.409	0.215	6.975	-2.5	SC1095
16	7.974	0.928	0.409	0.215	3.496	-3.5	SC1095

MR radius $R=8.178$ meter / chord $c=0.527$ meter

Table 7.2.: Data of UH-60's main rotor blades (based on [32, 35])

7. Modelling

7.2.2. Lift and drag forces

The lift and drag coefficients C_L and C_D of the SC1095 and SC1094 R8 airfoils were simulated as functions of Angle of attack (AoA) α and the Mach number Ma :

$$C_L = f(\alpha, Ma) \quad (7.6)$$

$$C_D = f(\alpha, Ma). \quad (7.7)$$

The dependences were taken from [101, Appendix B], transferred to lookup tables and interpolated linearly. The resulting lift and drag forces F_L and F_D of a blade element can be determined by

$$F_L = C_L \frac{\rho_{\text{air}}}{2} V_{AS}^2 A_{bl} \quad (7.8)$$

$$F_D = C_D \frac{\rho_{\text{air}}}{2} V_{AS}^2 A_{bl}, \quad (7.9)$$

where ρ_{air} and V_{AS} denote the air density and the airfoil section speed in flow axis. The former was assumed to be 1.0 kg/m^3 . The flow conditions at a blade element are sketched in figure 7.2. The notation has been taken from [70, p. 65]. It can be seen, that V_{AS} consists of the tangential speed in

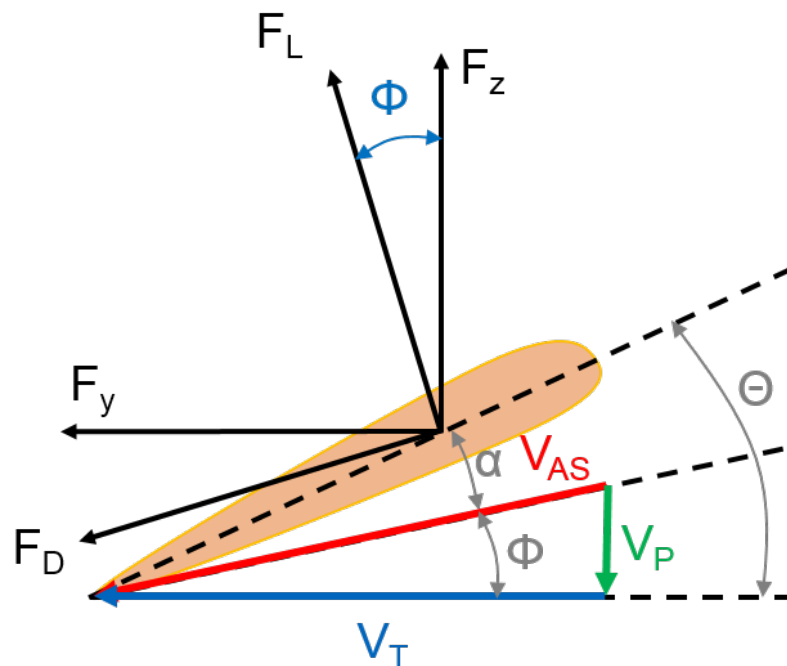


Figure 7.2.: Lift and drag forces at a blade section (cf. [70, p. 65])

wind axes V_T and the perpendicular speed in wind axes V_P . The radial component of the flow V_R will be neglected in this study. The velocities are determined by (cf. [70, p. 65]¹)

$$\frac{V_T}{\Omega R} = \xi + \tilde{r} \cos(\beta) + \mu \sin(\Psi) \quad (7.10)$$

$$\frac{V_P}{\Omega R} = \lambda \cos(\beta) + \frac{\tilde{r} \dot{\beta}}{\Omega} + \mu \sin \beta \cos \Psi \quad (7.11)$$

$$V_{AS} = \sqrt{V_T^2 + V_P^2}. \quad (7.12)$$

Here β denotes the flapping angle and $\dot{\beta}$ is its time derivative. The relative hinge offset ξ is the ratio of hinge offset to main rotor radius and the advance ratio μ is defined as forward speed V divided by the blade tip speed ΩR . The blade azimuthal angle Ψ is zero when the blade is pointing to the rear of the helicopter and increases with the rotation of the main rotor. The tangential velocity can be calculated with knowledge of the main rotor geometry, its angular velocity Ω , the blade azimuthal angle and the forward speed of the helicopter. All these parameters are known resp. can be determined in every time step of the simulation. For the calculation of the airfoil perpendicular speed in wind axes V_P the induced inflow parameter λ has to be known. It will be obtained by using a linear inflow model developed by Glauert² [48, 70]. The details are described in the following section.

7.2.3. Induced inflow model

The information on Glauert's model was taken from [48, 70]. To obtain the inflow parameter λ , the system of equations (7.13) has to be solved:

$$\begin{aligned} \lambda_i &= \lambda_{i0} (1 + (\xi + \tilde{r} \cos(\beta)) K_x \cos(\Psi)) \\ \lambda_{i0} &= \frac{c_T}{2\sqrt{\mu^2 + (\lambda_{i0} + \mu \tan(\alpha_{MR}))}} \\ \lambda &= \mu \tan(\alpha_{MR}) + \lambda_i \\ K_x &= \frac{15\pi}{23} \tan\left(\frac{\chi}{2}\right) \\ \chi &= \arctan\left(\frac{\mu}{\lambda_i}\right). \end{aligned} \quad (7.13)$$

Here, c_T denotes the thrust coefficient defined by main rotor thrust T and rotor disc area A_{MR} as

$$c_T := \frac{T}{\rho_{\text{air}} A_{MR} (\Omega R)^2}. \quad (7.14)$$

The parameter α_{MR} is the tilt angle of main rotor relative to waterline. Since (7.13) is a non-linear system of equations, it has to be solved iteratively. Because of the huge computing cost and resulting simulation times, it was not possible to solve the systems for all 64 blade elements in each time step. Therefore, the system was solved for sets of values of the parameters $\tilde{r} \cos(\beta)$, c_T , μ , Ψ and α_{MR} with Matlab's nonlinear solver `lsqnonlin` [67] once. During the simulation, λ was obtained by linearly interpolating these results.

¹In formula (3.8) of [70], the factor $1/\Omega$ is missing at $r \dot{\beta}$.

²Hermann Glauert (1892-1934), British aerodynamicist

7. Modelling

In figure 7.3 the resulting induced velocity parameters on the rotor disc are depicted for different advance ratios at reference rotor speed. As parameters $c_T = 0.0082$ and $\alpha_{MR} = 3^\circ$ – which corresponds to a tilt of the fuselage to waterline level α_{WL} of 0° – were set. Subfigure (a) represents hover flight. For hover condition ($\mu = 0.0$), the value of the induced velocity parameter is 0.0641 all over the rotor disc. This corresponds to

$$\lambda = \sqrt{\frac{c_T}{2}}, \quad (7.15)$$

which is yielded by basic momentum theory. When the forward speed increases, the distribution of the inflow parameter across the rotor disc changes. The values of λ are higher at the rear section of the rotor ($|\Psi| < 90^\circ$). The higher the forward speed resp. μ gets, the lower are the values of λ . This is consistent with the expectation that the induced Power P_i , defined by

$$P_i := T V_i, \quad (7.16)$$

decreases with forward speed (cf., for example, [27, p. 103 sqq.] and [128, p. 328 sqq.]).

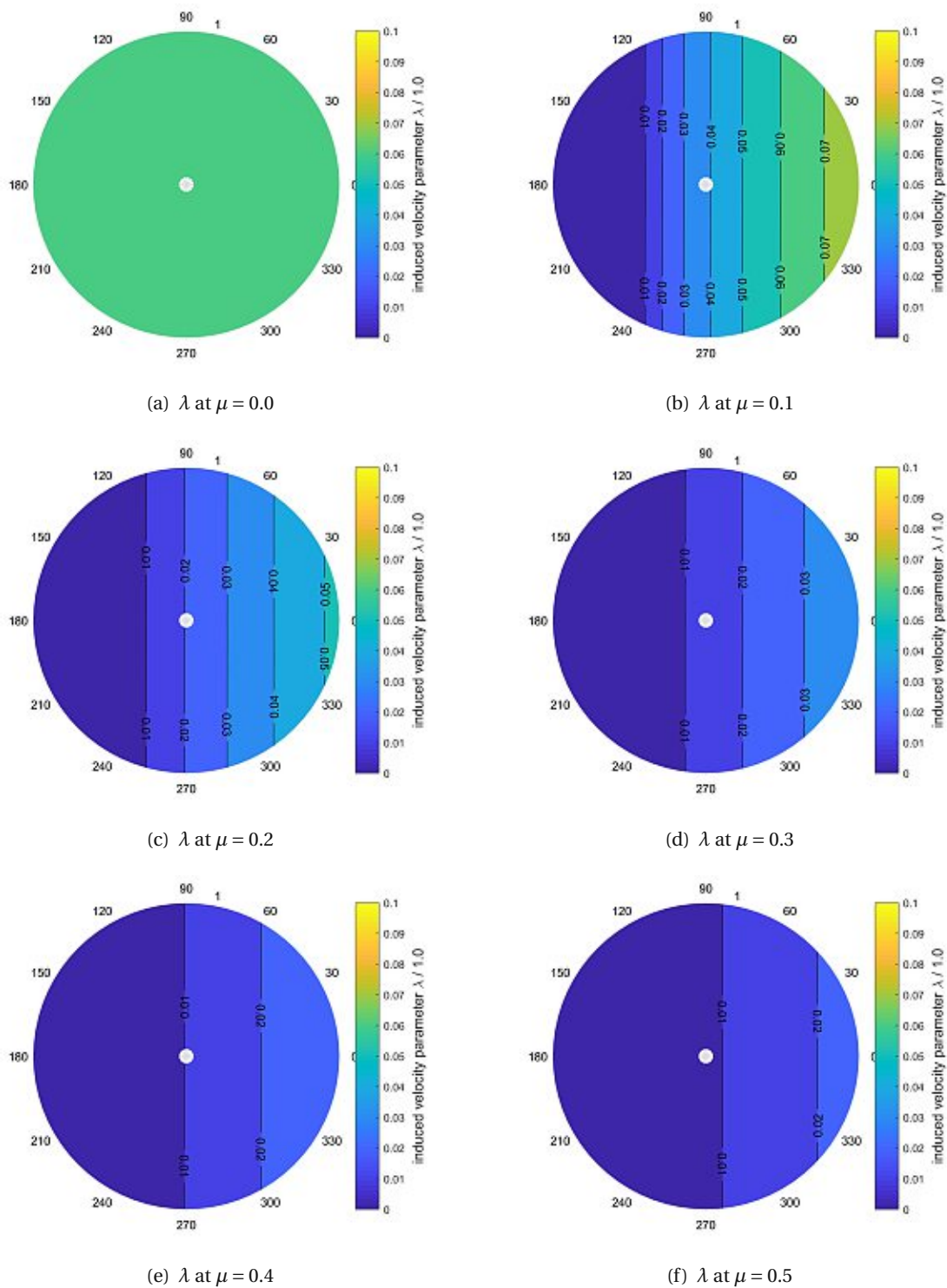


Figure 7.3.: Induced velocity parameter λ at different advance ratios μ

7.3. Tail rotor

Although it would have been possible to set up a tail rotor model in the same way as it has been done for the main rotor, the simulation was done with a simpler model. The reason for this was the reduced simulation time. Furthermore, the involvement of a fixed-speed tail rotor in the simulation model would not have yielded any additional insight into the operation of a helicopter with a variable-ratio transmission connecting engines and main rotor.

The simplified tail rotor model consists of a force acting on the fuselage in direction of the TR axis at the position of the TR hub. This TR thrust T_{TR} is controlled by a PID controller so that the yaw angle of the fuselage is kept at 0° . Using momentum theory for hover conditions, the power demand of the TR P_{TR} is calculated by

$$P_{TR} = \frac{1}{FM} \sqrt{\frac{T_{TR}^3}{2 \rho_{air} A_{TR}}}, \quad (7.17)$$

where A_{TR} is the disc area of the tail rotor and the value of the Figure of Merit (FM) was set 0.7 acc. to [128, p. 122].

7.4. Fuselage

The UH-60's fuselage is simulated as a rigid body connected to rotors and transmission system via revolute joints. Information on mass, inertia and Center Of Gravity (COG) is taken from [52]. The aircraft mass m_{ac} is specified as 16400.0 lbs, which corresponds to 7438.9 kg. Lift and drag forces of the fuselage were calculated according to the formulae published in [70, 134]. In [52] also a damping model for the fuselage is included. This has been added to the Simulink model. With introduction of the rotor solidity σ

$$\sigma := \frac{N c R}{A_{MR}}, \quad (7.18)$$

where N is the number of blades; an important comparative figure can be defined. The blade loading is given by $\frac{c_T}{\sigma}$. For hover condition, this yields

$$\frac{c_T}{\sigma} = \frac{T A_{MR}}{\rho_{air} A_{MR} (\Omega R)^2 (N c R)} \approx \frac{m_{ac} g}{\rho_{air} (\Omega R)^2 (N c R)} \approx 0.0868. \quad (7.19)$$

In forward flight, thrust and blade loading increase due to the drag of the fuselage. The resulting values are summarized in table 7.3. The parameter $\frac{c_T}{\sigma}$ will be important in the evaluation of the

forward speed	advance ratio μ	blade loading $\frac{c_T}{\sigma}$
0 m/s	0.000	0.0868
20 m/s	0.091	0.0868
40 m/s	0.181	0.0864
60 m/s	0.272	0.0854

Table 7.3.: Blade loading for different advance ratios μ

simulation results, because all conclusions are restricted to it.

The modelled fuselage has four degrees of freedom: three translational and one rotational across MR axis. Initially, it had been intended to use all six DOFs and the results presented in [82] were obtained with these constraints. However, it turned out that due to the high cost of computation and the simple control system included in the model, less DOFs are preferable. In addition, the limited model is more stable and the results are sufficient for a rating of the proposed transmission system. However, comprehensive analysis and simulation with more DOFs is inevitable before a prototype helicopter equipped with a drivetrain containing Compound-Split modules is to fly. However, this task is beyond the scopes of the project VARI-SPEED and this thesis, and therefore it is left for future research.

Since there are no DOFs, roll and pitch attitude of the fuselage depending on the advance ratio μ are taken from [133, p. 258 sq.]. The data was calculated resp. measured for a weight coefficient c_W ,

$$c_W := \frac{W}{\rho_{\text{air}} A_{\text{MR}} (\Omega R)^2}, \quad (7.20)$$

of 0.0065. This corresponds to a gross mass of 6787.3 kg. The roll attitude is set 0° for all advance ratios, whilst the values of the pitch attitude can be found in table 7.4. Although the gross weights for

forward speed	advance ratio μ	pitch attitude α_{WL}	roll attitude
0 m/s	0.000	-4°	0°
20 m/s	0.091	-2°	0°
40 m/s	0.181	0°	0°
60 m/s	0.272	2°	0°

Table 7.4.: Attitude of fuselage (cf. [133])

which roll and pitch attitude were determined slightly differs from the mass set in the Simulink model, it is assessed sufficiently accurate for the purpose of this study. Furthermore, the chosen values were used for all main rotor speeds. Since the study is not focussed on the attitude of the fuselage and the influence on the transmission system is expected to be negligible, these assumptions seem to be justified.

7.5. Transmission system

7.5.1. Variator and hydraulic system

The hydraulic system of the proposed drivetrain consists of the two axial piston hydraulic machines, hydraulic fluid, connecting lines, possibly required hydraulic accumulators and different kinds of valves. Not all of these are included in the simulation model.

In Simulink, motors and pumps are represented by *Variable-Displacement Motor* blocks, which are provided in the Simulink library. This type of block includes information on maximum stroke and displacement as well as contains a tabulated efficiency model. All this information has been obtained in chapters 4 and 5. As discussed in section 5.1, Schlösser's model reaches its limits for low rotational speeds or loads. Therefore, a minimum efficiency of 5 % was set for both hydraulic machines to avoid non-physical results. It is assumed, that this minimum efficiency can be achieved

7. Modelling

by real-life axial piston hydraulic motors in nearly all operating conditions. However, the actual efficiencies of the variator need to be determined by testing. The parameters regarding motor-pump transition have been set to very low values. However, in the following simulation runs, no transition of operation mode occurs and therefore, these parameters have no influence on the results. The actual stroke is controlled by a PID controller, cf. section 7.6. The properties of the hydraulic fluid were set acc. to section 5.1.

Since much of the design data of the hydraulic system is not yet specified, it was kept very simple in the Simulink model. The whole system is represented by a *Hydraulic Pipeline* block taken from the Simulink library. Some parameters were chosen based on the information given in [126], others had to be estimated. Since the hydraulic pipeline model has flexible diameters, it works as a kind of accumulator. There are no additional hydraulic accumulators in the system. Furthermore, all valves were neglected. The reasons for this are twofold: firstly, the poor data situation and the resulting unreliable results and, secondly, the high computational costs of simulating valve actuation, which are not justified because the focus of the study is not on this topic.

As all other parts of the Simulink model used in this study, the hydraulic system can be easily adapted to a more sophisticated variator system when detailed information is available. Especially some safety issues, which will be discussed in part IV in detail, will require comprehensive analysis of the elaborated variator system.

7.5.2. Multi-body system

The simulation model of the transmission system was built up in Simulink's Simscape Multi-body [103]. The gear data was taken from chapter 6. Information on shaft inertia was derived³ from [44, 74, 80]. The inertia of the power turbine shaft of the T700 engine, which is considered as part of the transmission system (cf. [40, p. 63]), was found in [127]. Bearings were added to the multi-body system only as revolute joints to enable the rotation of the parts of the transmission system, but no masses or inertias were taken into account. The inertia of the main rotor is summarized in table 7.2. Since a tail rotor drive has not been designed in chapter 6, it was simply simulated by two torques acting at the position of the TR power take-off (cf. figure 3.7) which take off half the TR power (7.17) each.

As illustration of the multi-body system, the display of the model in Simulink's Mechanics Explorer is depicted in figure 7.4. It is easy to distinguish four crucial parts of the model: main rotor, tail rotor (hub), fuselage and drivetrain. Each of the four blades of the main rotor consist of 16 rigidly connected sections (cf. table 7.2) and a massless bar connecting the hinges (not displayed) to the blades. In the model, only flapping and lead/lag hinges are taken into account. The modelling of flap and lead/lag damping is based on published data [35, 133].

As discussed earlier, the tail rotor is not simulated in detail but only by its hub, which can be found in the upper left corner of figure 7.4. For future simulations, the main rotor model can be copied to this hub and by adapting the parameters and the inflow model, a fully working tail rotor model can be obtained.

The fuselage is not represented by a realistic body in Mechanics Explorer but by a simple ball at the center of gravity (centre bottom of figure 7.4). This ball carries all of the mass properties of the fuselage, which is assumed to be rigid. The drivetrain is located in the centre of figure 7.4 just below

³This work was carried out by Valentin Zadrazil as part of a project thesis.

the rotor. Since all gears are rigid bodies with just one rotational degree of freedom and no tooth stiffness is considered, the transmission system in total has two kinematic degrees of freedom. In the yellow box the Compound-Split module is pointed out.

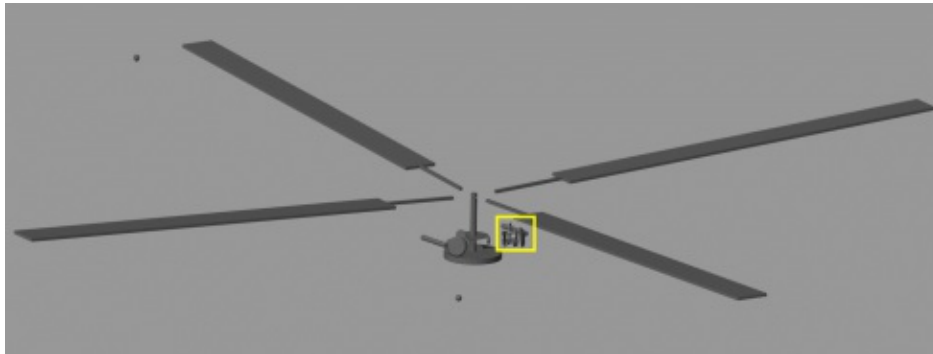


Figure 7.4.: Display of multi-body system in Simulink Mechanics Explorer

In figure 7.5 this detail is magnified to show the composition of this crucial part of the drivetrain. The long shaft which is partly covered by gears represents the input shaft and the power turbine shaft. Due to the complex design of the latter, its geometry has been simplified, but still the inertial properties represent the physical system. At the end of this shaft is the input bevel pinion, which mates with the input bevel gear. As discussed in previous chapters, this stage has the same properties as in the baseline UH-60. However, the gears are depicted as truncated cones instead of gears, because the import of CAD models would not have added additional information and thus would not have justified the effort. The shaft connecting the CS module and the input bevel gear is not depicted. Its inertia is included in the gears. The accessories and the tail rotor take-off, which are located on this shaft are neglected as well as is the free-wheeling unit. The CS module has already been sketched in figure 3.5. The Simulink model is based on this principal structure and the parameters derived in chapter 6. Due to the lack of data and the low expected influence on the simulation results, bearings and shafts of the CS module are neglected. The variator and hydraulic lines are also not displayed, because they are simulated by forces acting on the respective gears. The output shaft of the CS module is connected to the connecting bevel pinion from where the propulsive power is transmitted to the main rotor via a planetary gear stage.

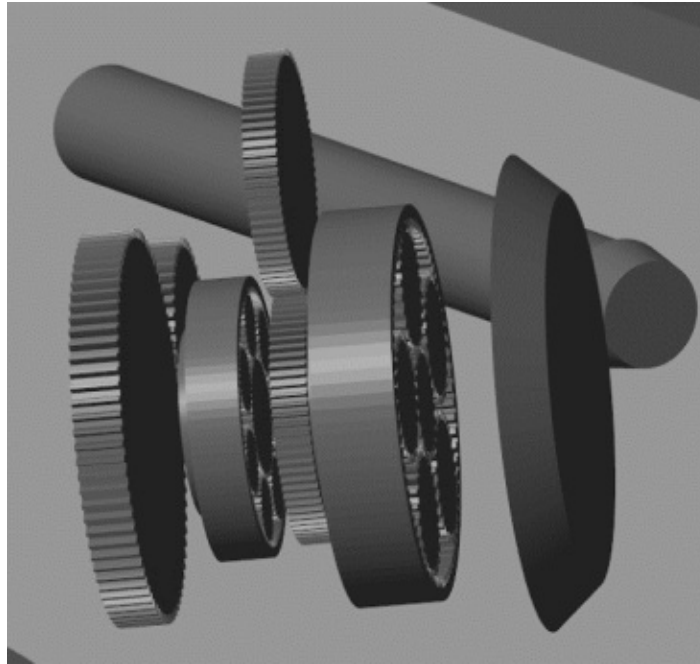


Figure 7.5.: Detail view of Compound-Split in Simulink Mechanics Explorer

7.6. Controls

To keep the system in the desired operation condition – i.e., forward, lateral and climb speed; yaw angle and main rotor speed –, five different types of PID controllers are included in the Simulink model. One adapts the collective angle ϑ_0 depending on the climb rate whilst two vary the cyclic pitch angles ϑ_{1c} and ϑ_{1s} in order to obtain the required forward and lateral speeds. There are two blocks each of the fourth and fifth type of PID controllers, one in the power path of each turboshaft engine. The fourth type adjusts the fuel flow W_F of both turboshaft engines to keep the power turbine speed constant. The fifth type changes the stroke of both hydraulic machines at a given ratio to pertain a hydraulic system pressure of 450 bar. When the angular velocity of the main rotor is to be changed, the target value of the ratio is adjusted.

7.7. Simulation runs

With the model described in the previous sections, several simulation runs were carried out. The used parameters are summarized in table 7.5. The values pose initial resp. target values, the simulation results might differ and some runs terminated before reaching the required simulation time (cf. chapter 8).

The first four runs represent forward flight at 0, 20, 40 and 60 m/s with the transmission system operating at mechanical point I. The duration is 60 s. It was expected – and affirmed by the results – that this is enough time for the simulation to reach a sufficiently stable state after the abatement of transient processes. The same was carried out for MP II. It has to be pointed out, that for these eight simulation runs, the pump resp. motor shafts had been locked and the hydraulic system was

neglected. The reason is, that near mechanical points no proper results for the hydraulic path can be expected and therefore, the higher computation costs are not justified.

After the mechanical points, twelve operating points with flow of hydraulic fluid in the variator were searched. The target angular velocities of the main rotor were 27, 23.7 and 20.8 rad/s which represent the reference speed, the angular velocity with (theoretically) maximum variator power and the transmission ratio, so that 23.7 rad/s is the geometric mean of the other two.

Of special interest are acceleration and deceleration of the main rotor and parts of the drivetrain. Operations of this kind were examined in the last six simulation runs. Since transient processes occur not only at the beginning of the simulations but also throughout the variation of MR speed and after the target values are reached, the simulation time was increased to 80 s. It has to be pointed out, that only main rotor angular velocities in the range of 20.8 rad/s to 27 rad/s were considered. Again, the lack of a valid efficiency model was the reason for this decision. Speed variation was only simulated for combinations of forward speeds and between MR speeds for which the simulation numbers 9 to 20 have lasted the full 60 s.

The choice of the numeric solver was left to the software, i.e., in the solver options type and solver were set *Variable-step* and *auto* (*Automatic solver selection*). For the models without hydraulic system, Simulink chose *ode45* (*Dormand-Prince*) whilst for the ones with a detailed variator model *ode23t* (*mod. stiff/Trapezoidal*) was used.

Of course, several initial conditions and starting values of different parameters had to be chosen in the model. They were set based on experience and estimations but also taken from the literature, e.g., from [133], and improved several times after preliminary simulation results were available. For reasons of space, they are not discussed in this context in detail, but can be found in the Simulink model resp. in the Simulink.SimulationInput objects (see section A.3).

7. Modelling

#	forward speed	advance ratio μ	duration	MR angular velocity Ω_{MR}	comment
1	0 m/s	0.000	60 s	29.7 rad/s	MP I
2	20 m/s	0.091	60 s	29.7 rad/s	MP I
3	40 m/s	0.181	60 s	29.7 rad/s	MP I
4	60 m/s	0.272	60 s	29.7 rad/s	MP I
5	0 m/s	0.000	60 s	18.9 rad/s	MP II
6	20 m/s	0.091	60 s	18.9 rad/s	MP II
7	40 m/s	0.181	60 s	18.9 rad/s	MP II
8	60 m/s	0.272	60 s	18.9 rad/s	MP II
9	0 m/s	0.000	60 s	27.0 rad/s	reference speed
10	20 m/s	0.091	60 s	27.0 rad/s	reference speed
11	40 m/s	0.181	60 s	27.0 rad/s	reference speed
12	60 m/s	0.272	60 s	27.0 rad/s	reference speed
13	0 m/s	0.000	60 s	23.7 rad/s	max. variator power
14	20 m/s	0.091	60 s	23.7 rad/s	max. variator power
15	40 m/s	0.181	60 s	23.7 rad/s	max. variator power
16	60 m/s	0.272	60 s	23.7 rad/s	max. variator power
17	0 m/s	0.000	60 s	20.8 rad/s	$\Omega_{MR} = \frac{23.7^2}{27.0}$
18	20 m/s	0.091	60 s	20.8 rad/s	$\Omega_{MR} = \frac{23.7^2}{27.0}$
19	40 m/s	0.181	60 s	20.8 rad/s	$\Omega_{MR} = \frac{23.7^2}{27.0}$
20	60 m/s	0.272	60 s	20.8 rad/s	$\Omega_{MR} = \frac{23.7^2}{27.0}$
21	0 m/s	0.000	80 s	27.0 rad/s → 20.8 rad/s	change of MR speed
22	0 m/s	0.000	80 s	20.8 rad/s → 27.0 rad/s	change of MR speed
23	20 m/s	0.091	80 s	27.0 rad/s → 20.8 rad/s	change of MR speed
24	20 m/s	0.091	80 s	20.8 rad/s → 27.0 rad/s	change of MR speed
25	40 m/s	0.181	80 s	27.0 rad/s → 23.7 rad/s	change of MR speed
26	40 m/s	0.181	80 s	23.7 rad/s → 27.0 rad/s	change of MR speed

Table 7.5.: Main parameters of the different simulation runs

8. Results

In this chapter, the results of the 26 simulation runs are summarized and discussed. The first section is dedicated to the validation of the simulation model. To this end, some core results of the flight simulation at the reference speed of 27.0 rad/s will be compared to data available in the literature, more precisely in [40] and [133]. The subsequent sections contain results of all simulation runs which will be described and used to evaluate, if the proposed transmission system is feasible for the use in rotorcraft of CS-29 class.

8.1. Validation of model at reference rotor speed

8.1.1. Main rotor speed and power coefficient

The calculated actual angular velocities of the main rotor at different forward speeds are depicted in figure 8.1. The target value for all four simulations is the reference speed of 27.0 rad/s. After the abatement of transient processes – which are mainly caused by the pressure build-up in the hydraulic system – the angular velocities of the main rotor are quite constant for all forward speeds. The results relative to the target value are presented in figure 8.2. It can be seen, that the maximum

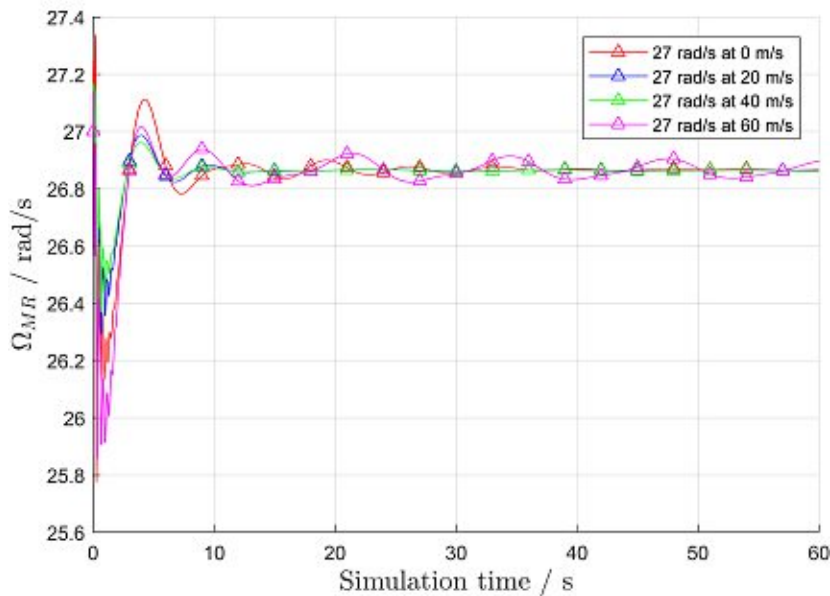


Figure 8.1.: Angular velocity of main rotor

absolute rel. deviation is less than 1.0%. Based on the findings at [40, p. 68], this outcome is satisfactory. The deviation from the reference value of about 0.5% is mainly caused by losses in the variator system.

8. Results

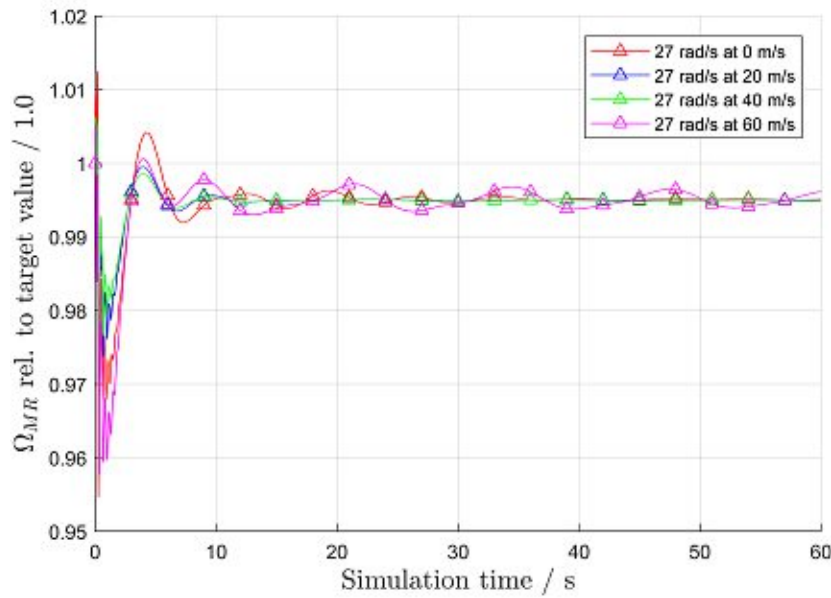


Figure 8.2.: Angular velocity of main rotor rel. to target value

The next parameter to be validated is the power coefficient c_P , defined by

$$c_P := \frac{P_{MR}}{\rho_{air} A_{MR} (\Omega R)^3}. \quad (8.1)$$

Reference data is provided at [133, p. 253] for $c_W = 0.0065$ (6787.3 kg) and $c_W = 0.0074$ (7727.1 kg). The weight coefficient used in the simulation is 0.0071, so it is expected that the results lie in-between the reference data. Figure 8.3 summarizes the information. For forward speeds of 20 and 40 m/s, the calculated values of c_P lie at the lower boundary of the reference data or slightly below. Hence, the power demand is under-estimated whilst for 60 m/s it is slightly over-predicted. For the hover case no flight test data is available, but if the given data is extrapolated to $\mu = 0.0$, the simulation result fits well into.

8.1.2. Control angles

Figure 8.4 shows the calculated time series of the collective pitch angles. The resulting values for 60 m/s exhibit minor fluctuations, which are presumably caused by the operation of the speed controllers. The collective angles for hover and fast forward flight are about 7.3° , whilst for low and moderate forward speeds they are approximately 5.2° . In figure 8.5 the results are compared to [133, p. 255]. The collective pitch angles are under-predicted for the whole range of advance ratios. A possible reason could be the influence of blade tip losses and radial flow, which were neglected in the used rotor model.

The resulting lateral cyclic angles are shown in figure 8.6. All four courses show decreasing transient behaviour which lasts till the end of the simulation time. According to figure 8.7, the values show good compliance with reference data for 20 m/s only. In general, the values in figure 8.7 are lower

8.1. Validation of model at reference rotor speed

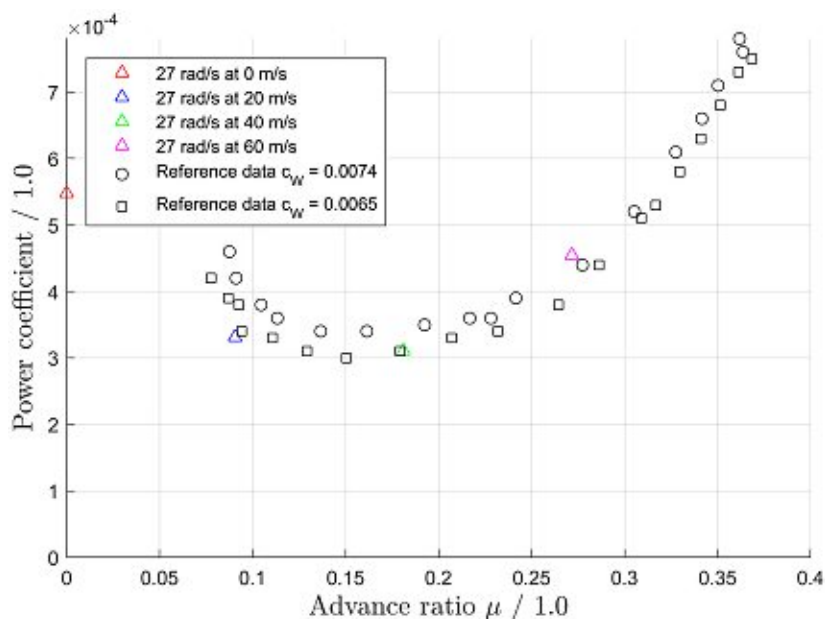


Figure 8.3.: Main rotor power coefficient compared to reference data

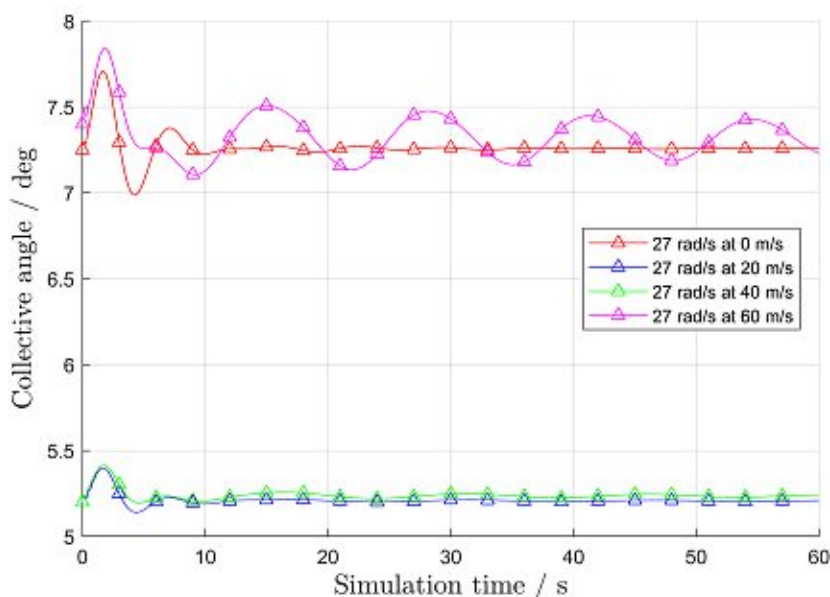


Figure 8.4.: Collective angle

than the measured results but show a similar course with a minimum between $\mu = 0.1$ and $\mu = 0.2$. The deviation might be explained by the fact, that the roll motion is locked and as a consequence, no lateral tilt of the MR axis is possible. However, even CAMRAD II yielded significant deviations to the measured results and also under-predicts the actual values [133, p. 255].

The longitudinal cyclic angles (figures 8.8 and 8.9) show good agreement with the reference data.

8. Results

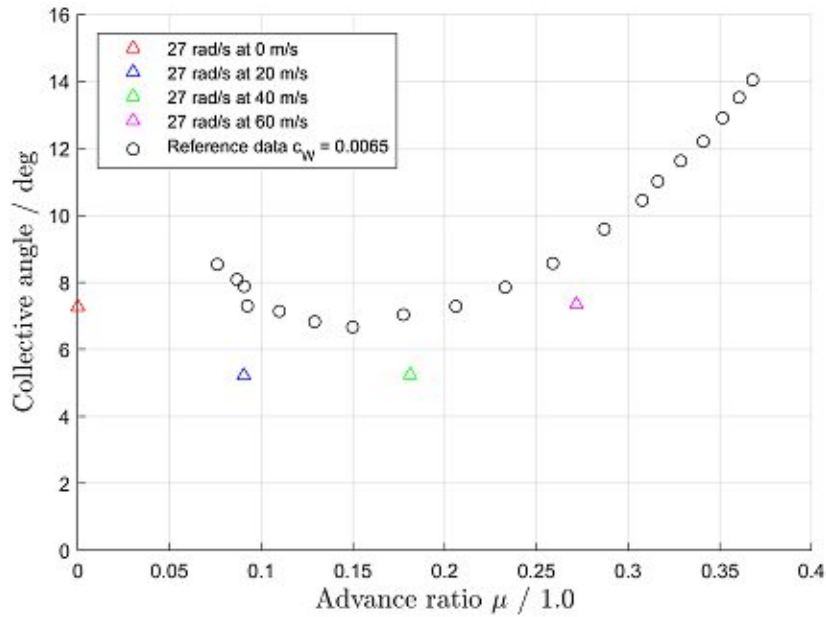


Figure 8.5.: Mean collective angle compared to reference data

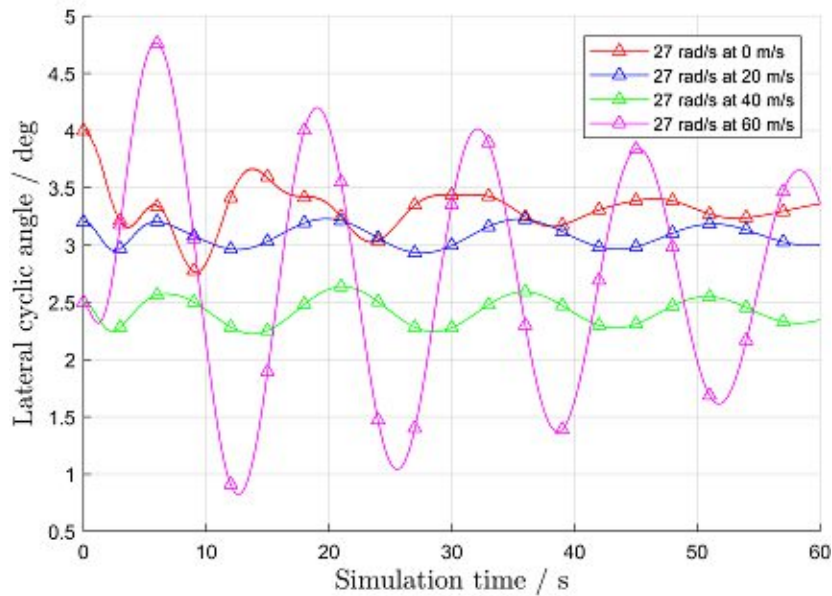


Figure 8.6.: Lateral cyclic angle

Again, the calculated θ_{1s} for 20 m/s matches the results of the flight test data best. At higher forward speeds, the absolute value of the control angle is under-predicted. If the reference data is extrapolated linearly to $\mu = 0.0$, the value obtained by the Simulink model seems reasonable. As for the lateral control angle, the deviations may be caused by the locking of the pitch DOF of the fuselage. An improved Simulink model, either by adapting the pitch attitude or allowing 6-DOF movement of the fuselage might yield better results.

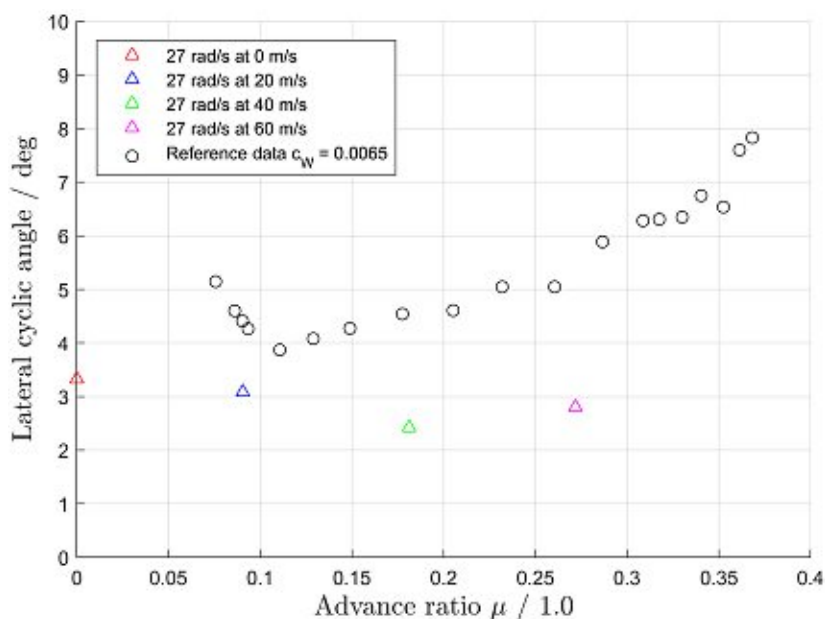


Figure 8.7.: Mean lateral cyclic angle compared to reference data

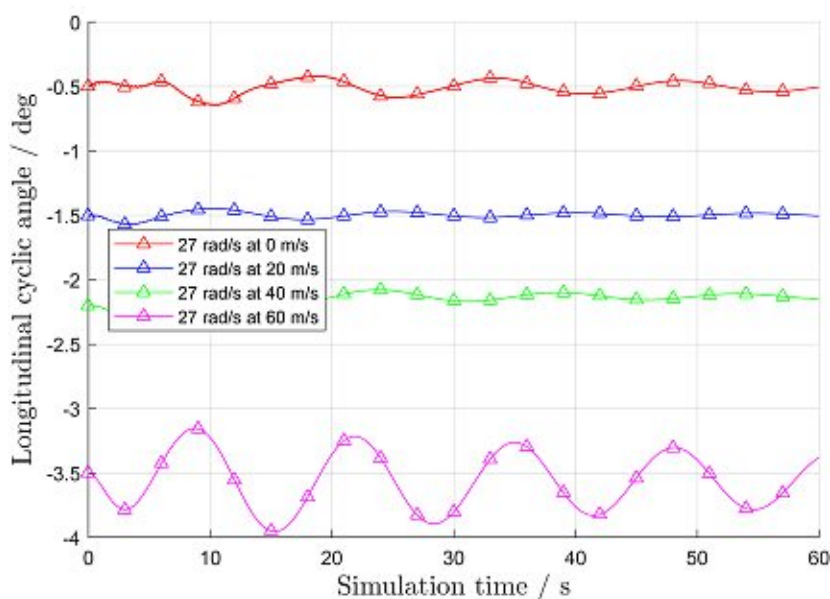


Figure 8.8.: Longitudinal cyclic angle

8.1.3. Reaction moments

A particularity of the used Simulink model is the fact, that pitch and roll attitudes of the fuselage are prescribed. As mentioned earlier, this may lead to deviations from measured results. In particular, non-physical reaction moments occur at the fuselage. To be able to assess the error caused by this constraint, the resulting moments for pitch and roll motion rel. to maximum main rotor torque (74 kNm) are depicted in figures 8.10 and 8.11. The normalization was chosen to get a feeling, how

8. Results

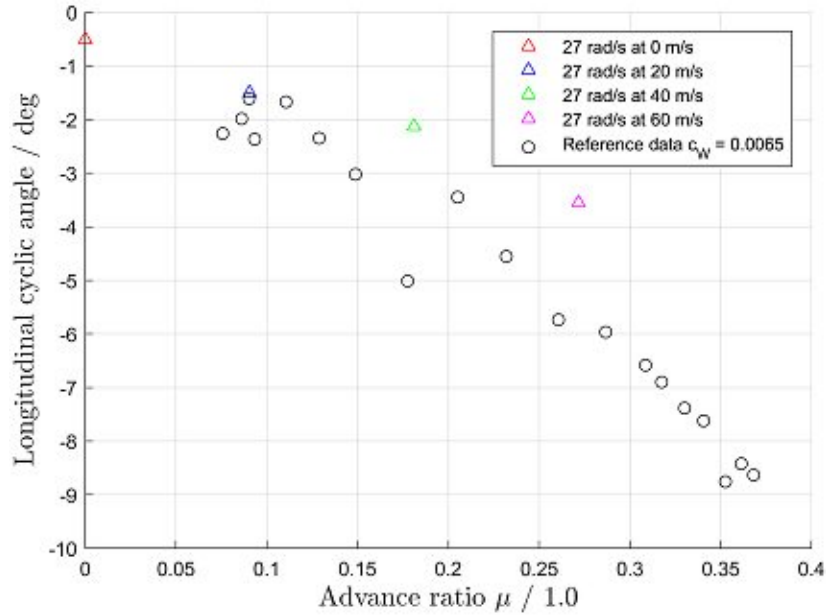
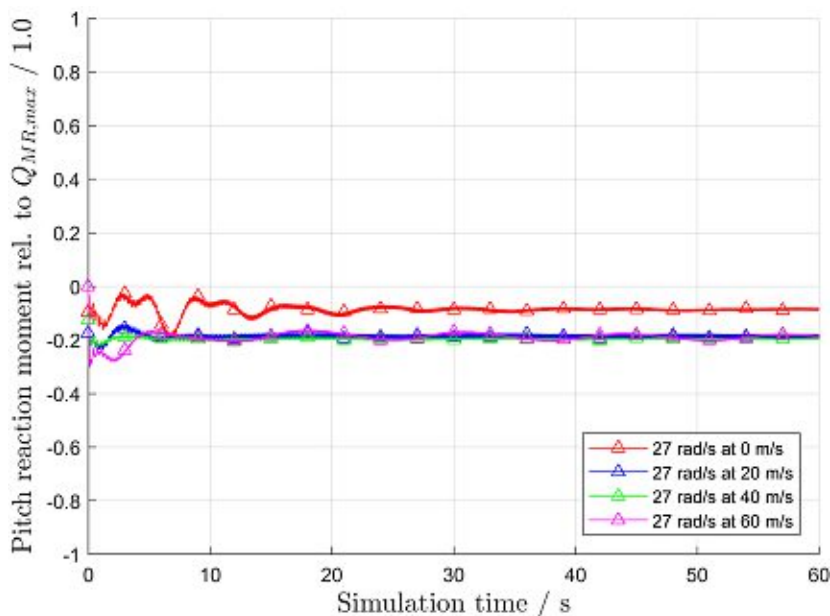
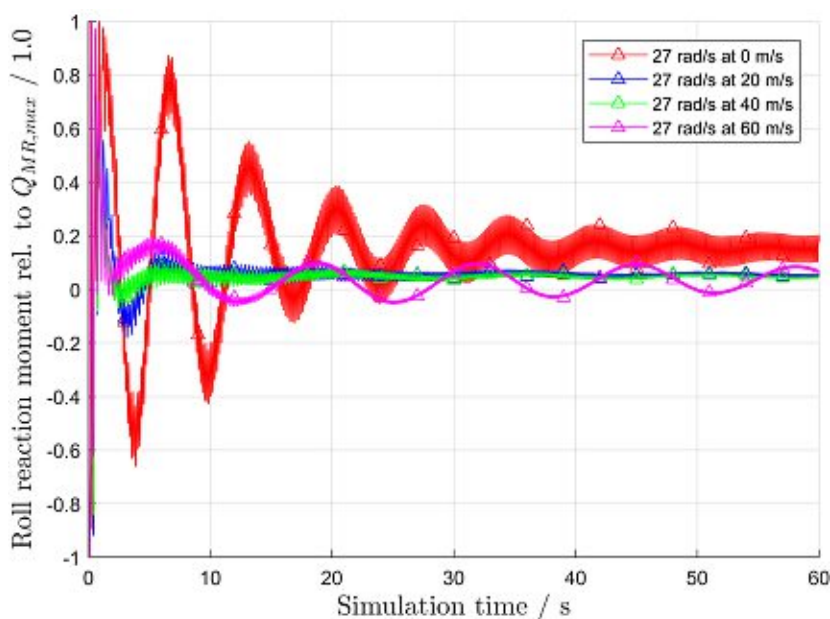


Figure 8.9.: Mean longitudinal cyclic angle compared to reference data

large the moments are and how they will affect the model. The courses of moments show very limited fluctuation ranges for all forward speeds. The mean absolute and relative values of the reaction moments after the abatement of transient processes are summarized in table 8.1. For all studied flight conditions except hover, the mean pitch moments exceed the values of the roll moments. This can be explained by the fact, that the pitch attitude together with the tilt of the tip path plane control the forward speed of the rotorcraft. Therefore, high forces and moments are involved which lead to high reaction torques if the prescribed pitch attitude differs from the actual equilibrium of the fuselage. For hover, this effect is not as distinct. As a consequence, in real-life flight, larger pitch angles (absolute values) and roll angles different to zero will set. Although the reaction moments have high absolute values, they are not expected to have a significant influence on the transmission system – an assumption that is supported by the good agreement of c_p . For the aim of this study, the accuracy is considered sufficient.

forward speed	advance ratio μ	pitch axis		roll axis	
		absolute	rel. to $Q_{MR,max}$	absolute	rel. to $Q_{MR,max}$
0 m/s	0.000	6.458 kNm	8.72 %	11.659 kNm	15.74 %
20 m/s	0.091	13.804 kNm	18.64 %	4.012 kNm	5.42 %
40 m/s	0.181	14.573 kNm	19.67 %	3.518 kNm	4.75 %
60 m/s	0.272	13.998 kNm	18.90 %	3.193 kNm	4.31 %

Table 8.1.: Mean reaction moments at fuselage

Figure 8.10.: Reaction torque in pitch axis rel. to $Q_{MR,max}$ Figure 8.11.: Reaction torque in roll axis rel. to $Q_{MR,max}$

8.1.4. Flapping and lead/lag motion

In figure 8.12 the flapping motion is depicted over a period of 3 s. The courses show the expected behaviour with a period of about 0.232 s. The amplitudes of hover and fast forward flight are higher than the ones for low and moderate speeds. In figure 8.13 the coning angles are plotted and compared to reference data found at [133, p. 256]. For all flight conditions, the coning angles are over-predicted by the Simulink results. However, it has to be kept in mind that the reference

8. Results

data was measured for a smaller gross weight of the rotorcraft. The higher lift forces required to counteract the weight may lead to an increase of the coning angles. Furthermore, the influence of flapping hinge stiffness was neglected in the Simulink model. In the following figure 8.14 the maximum flapping angles, i.e., the maximum absolute deviation from the mean value, are depicted. The reference data was obtained from [133, p. 256] by combining the information on longitudinal and lateral flapping angles. These values show good agreement with the measurements. The course with a minimum around $\mu = 0.11$ is close to the one of the flight test data. The higher amplitudes for hover and 60 m/s correspond to the reference data.

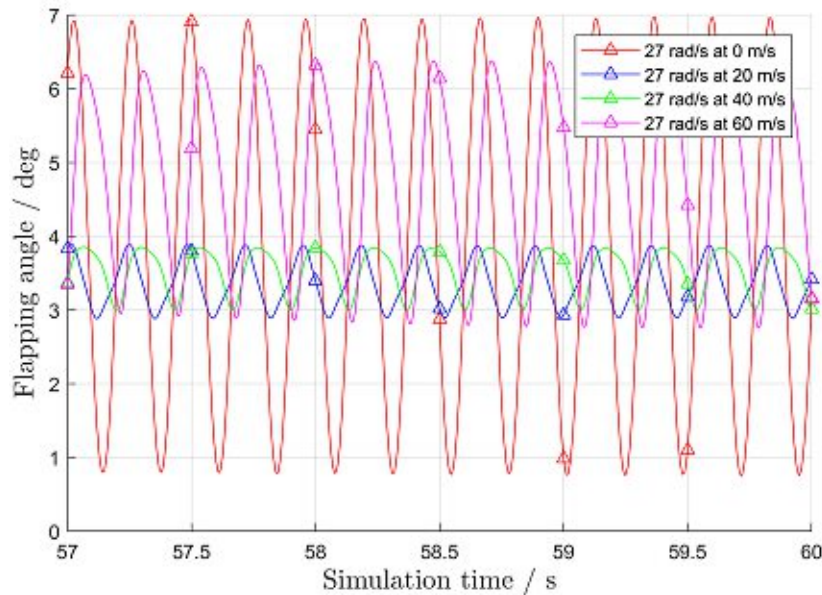


Figure 8.12.: Flapping angle

After analyzing the flapping angles, the same was done for the lead/lag motion of the rotor blades. The four courses of lag angles for 0, 20, 40 and 60 m/s are shown in figure 8.15. For all forward speeds they show oscillation with the expected period of 0.232 s. The course for hover condition is not as harmonic as for the others, which can be explained with the low advance ratio which leads to changing excitation of the lead/lag motion. For all studied flight conditions except hover, the mean values (figure 8.16) show reasonable agreement with the data presented in [133]. The absolute deviations are smaller than for the flapping angles. For hover condition, the mean lag angle is far smaller, than an extrapolation of the flight test data would indicate. However, for the lead/lag motion the excitation caused by forward speed is the major influence. Therefore, the actual values for advance ratios of $\mu = 0.0$ to $\mu = 0.07$ may show a different course than indicated by extrapolation of the given values. For the oscillation of the lag angle, no information is given in the source of reference data. It can be assumed that the lead/lag motion will not adversely affect the results obtained for the transmission system.

The model of the main rotor used in this study is not focussed on its vibratory behaviour. A study of these phenomena would require a much more sophisticated model. It has to include at least flexible blades with structural damping and a proper model of air damping. However, the vibratory behaviour of a helicopter rotor operated at different angular velocities has to be

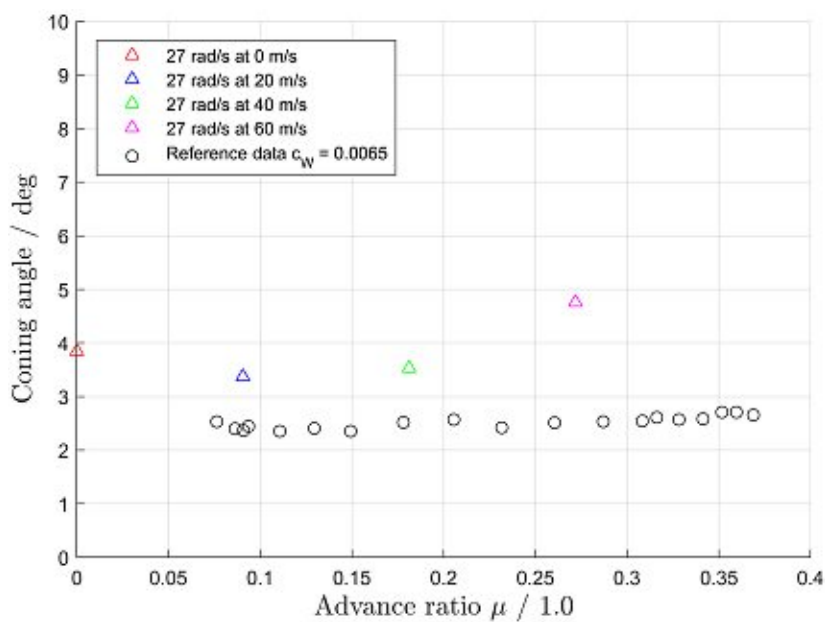


Figure 8.13.: Coning angle compared to reference data

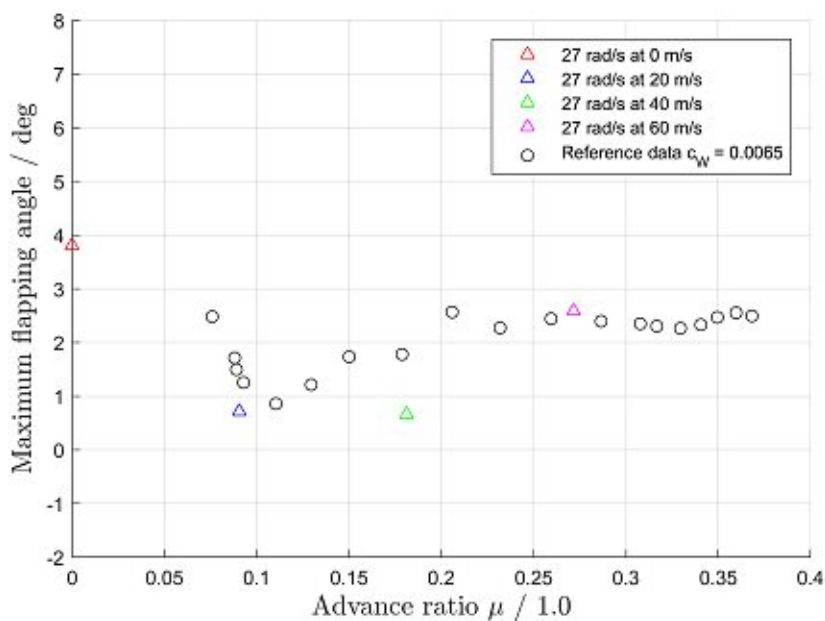


Figure 8.14.: Maximum flapping angle compared to reference data

addressed by further studies. From today's view, operation at different main rotor speeds will require a completely new design of the whole rotor system. Possible design methods for different types of rotorcraft have already been developed and tested; see, for example, [58, 59].

8. Results

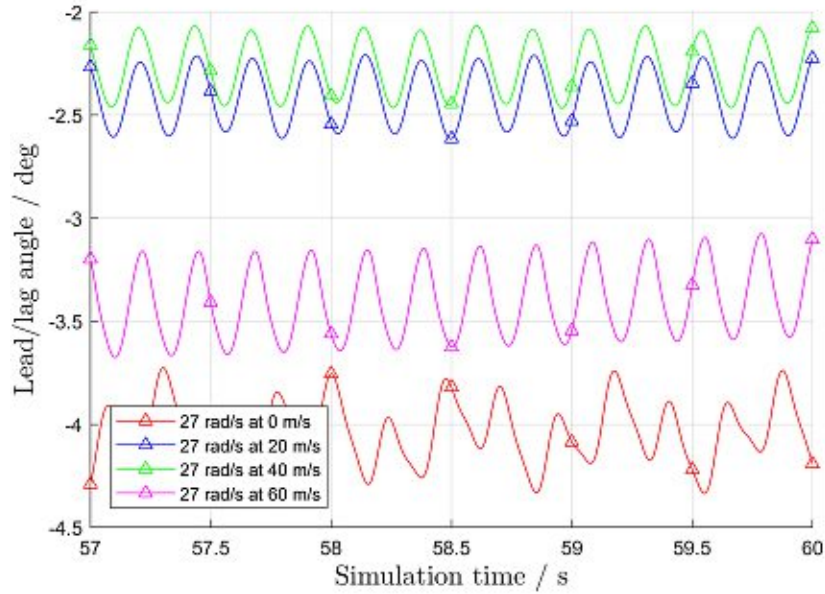


Figure 8.15.: Lead/lag angle

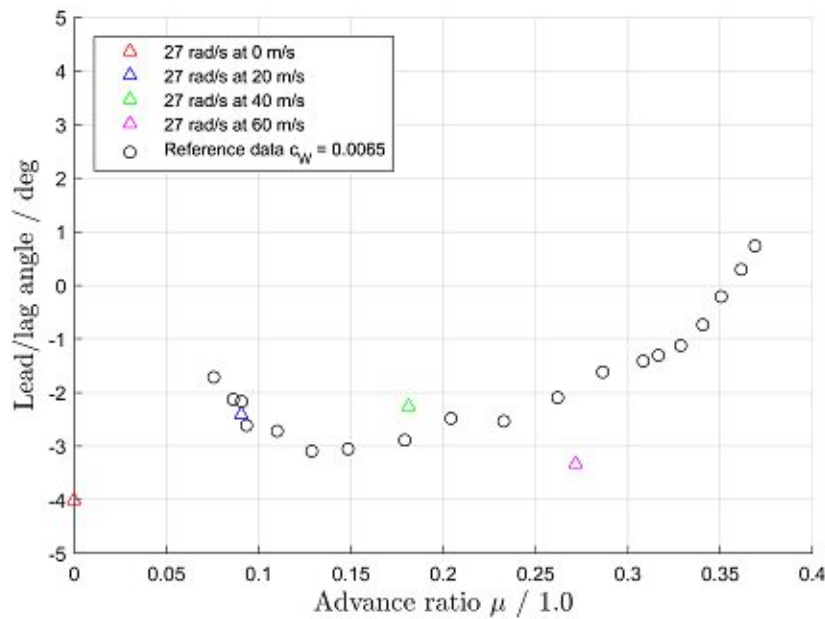


Figure 8.16.: Mean lead/lag angle compared to reference data

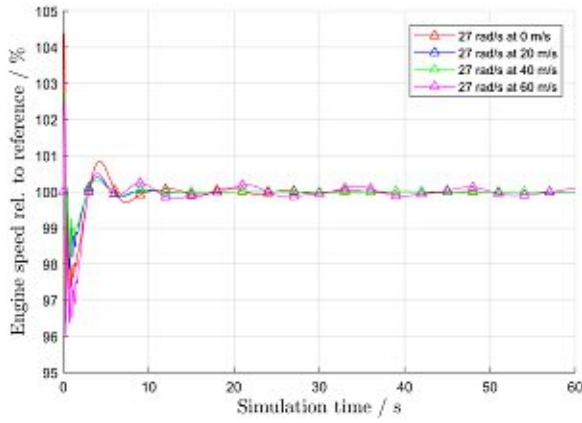
8.1.5. Turboshaft engines

In addition to the results discussed so far, figure 8.17 contains the results of the turboshaft engine parameters for the four validation runs. In subfigure (a) the power turbine speed relative to the target value of 20900 RPM is shown. The speed is maintained satisfactory during the whole simulation time. In subfigure (b) the shaft power of one engine is plotted. As expected, the power is high for hover and decreases for slow forward flight. At higher speeds, the power demand of the rotor

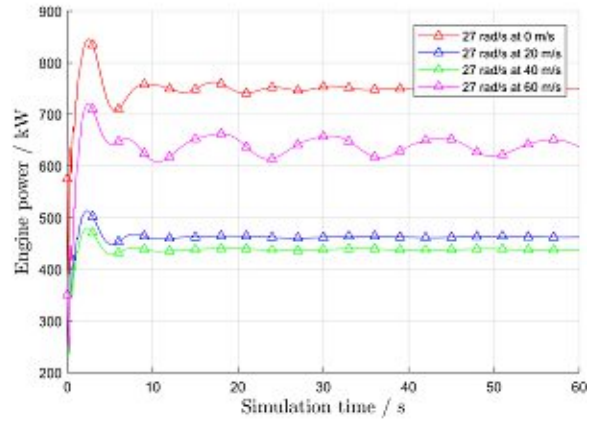
8.1. Validation of model at reference rotor speed

increases and therefore the shaft power provided by the engines is also higher. The next subfigure shows the fuel flow W_F . Since the fuel consumption for a forward speed of 60 m/s is higher than for hover, it can be concluded that the T700 engine is operated at higher fuel efficiency in hover condition. In principle, the remaining parameters – gas generator speed, interturbine gas temperature and static pressure at station 3 (subfigures (d), (e) and (f)) – show the same characteristics as the engine power.

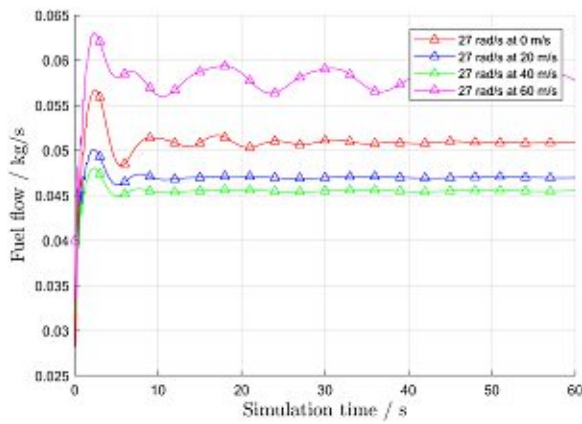
8. Results



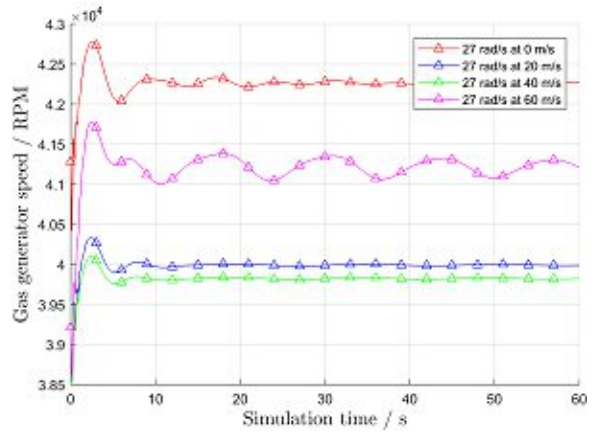
(a) Power turbine speed rel. to reference



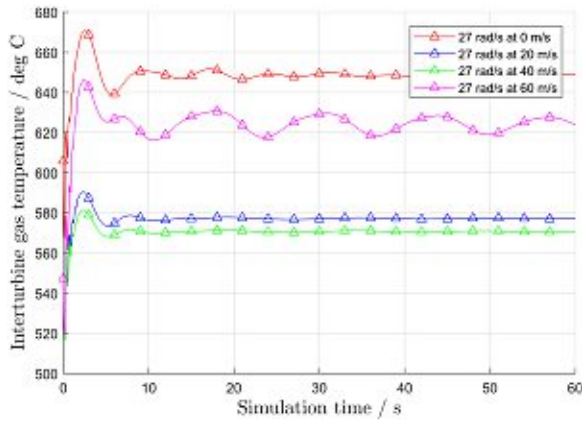
(b) Engine power



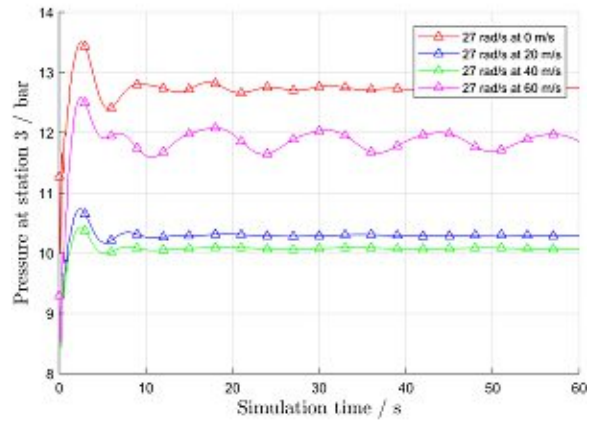
(c) Fuel flow W_F



(d) Gas generator speed



(e) Interturbine gas temperature T_{45}



(f) Static pressure at station 3 P_{S3}

Figure 8.17.: Operation parameters of turboshaft engines at 27 rad/s

8.1.6. Summary of model validation

Although there are some deviations from measured data, the mean values of all parameters show sufficient agreement with the reference data. Especially the calculated power coefficient c_p delivers good predictions compared to the values found in the literature. Even though there is considerable uncertainty caused by the fact, that for a rotorcraft intended to be operated at different main rotor speeds a completely new rotor system needs to be developed, the validation gives reason to believe that the simulation results will sufficiently accurately predict the operation parameters. This is especially true for the transmission system, because of the good agreement of the prediction of the transferred power.

8.2. Results for different flight conditions

In this section results of the different simulation runs described in table 7.5 are discussed. For the operation at mechanical points, it is focussed on the maintaining of the flight states whilst for operation at main rotor speeds between MP I and MP II and especially for changes of MR speed additional parameters – such as flow of hydraulic fluid and pressure – are of special interest. A flight state is defined by five parameters:

- Forward speed
- Lateral speed
- Climb rate
- Yaw angle
- Main rotor speed.

In addition, the deviation of the actual MR speed from the target value is also plotted for all simulation runs.

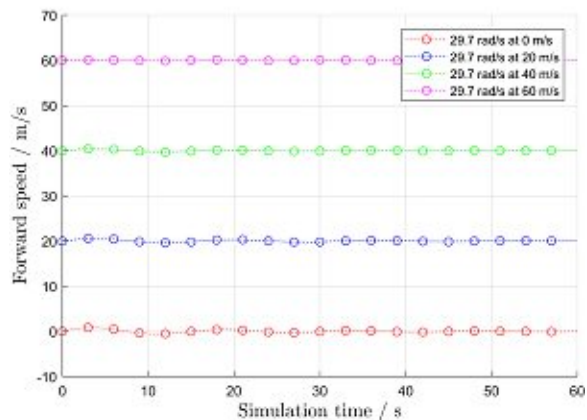
8.2.1. Mechanical point I

In figure 8.18 the flight conditions for the simulation runs at MP I are depicted. Subfigure (a) shows the forward speeds. The target values are 0, 20, 40 and 60 m/s. For all four simulation runs the speed is maintained sufficiently. Around a simulation time of 10 s, there is a drop in hover and slow forward flight. At first glance, the lateral speed plotted in subfigure (b) seems to exhibit strong fluctuations. In fact, the absolute lateral speeds are always below 1.0 m/s, which is noticeable and possibly unpleasant for occupants, but does not adversely influence the simulation results. The same applies for the climb rate, whose absolute values are even lower. The parameter plotted in subfigure (d) is the yaw angle. The thrust of the tail rotor is controlled in order to keep this angle at 0.0 rad. This works satisfactorily, although some oscillation is present during the whole time of simulation. The lower two subfigures show the course of MR speed as absolute value and relative to the initial target value of 110 % of the nominal speed, i.e., 29.7 rad/s. At all studied advance ratios, the calculated angular velocities are below the target value. Since the transmission ratio of the drivetrain is fixed for simulations at MP I, this can only be caused by deviations made in the design process of the transmission system; e.g., through the choice of discrete numbers of teeth.

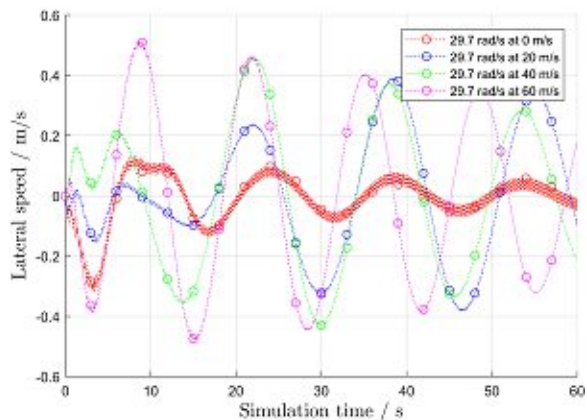
8. Results

The related engine performance is summarized in figure A.5 in appendix A.2. The values oscillate more than for the reference case studied in the previous section, but the general behaviour is as it would be expected.

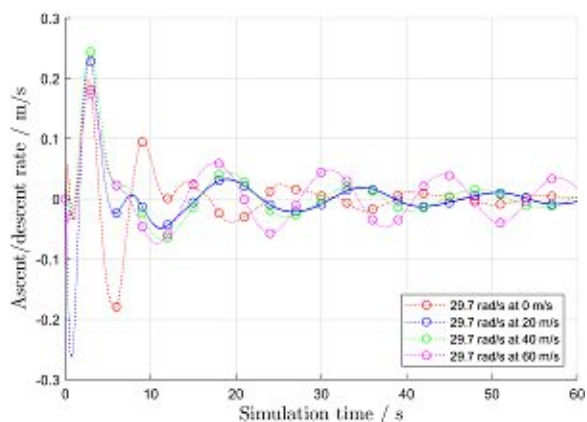
8.2. Results for different flight conditions



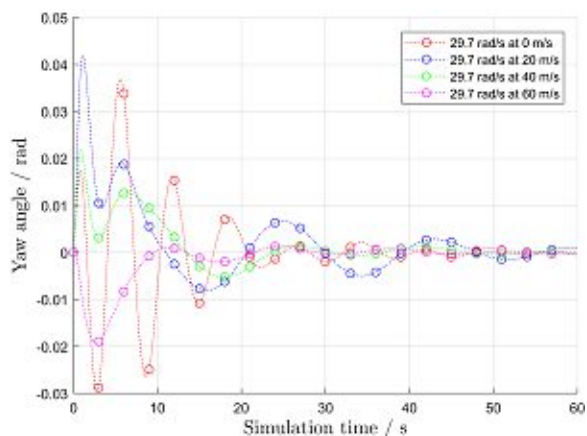
(a) Forward speed



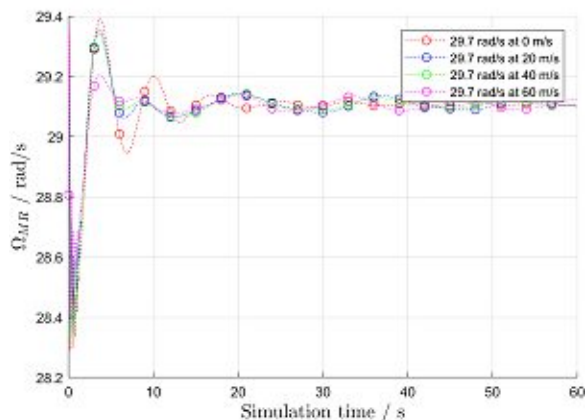
(b) Lateral speed



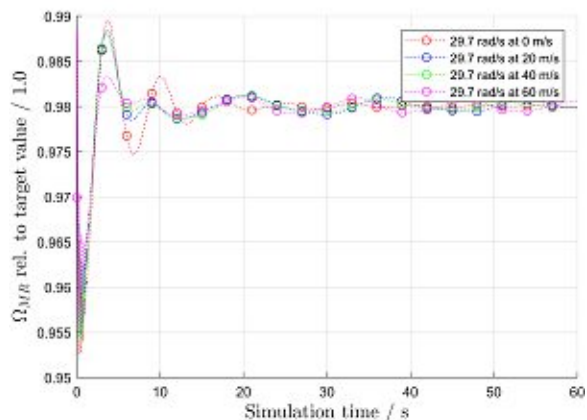
(c) Climb rate



(d) Yaw angle



(e) Angular velocity of main rotor



(f) Angular velocity of main rotor rel. to target value

Figure 8.18.: Speeds and yaw angle at MP I

8. Results

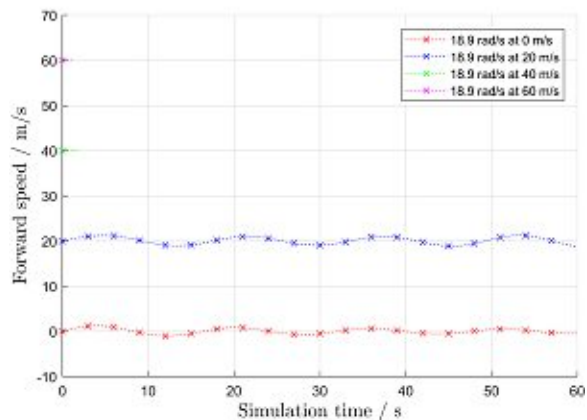
8.2.2. Mechanical point II

The flight states for operation at Mechanical Point II are shown in figure 8.19. The arrangement of subfigures is the same as for MP I. The target values also stay the same, except for the main rotor's angular velocity which is now 18.9 rad/s.

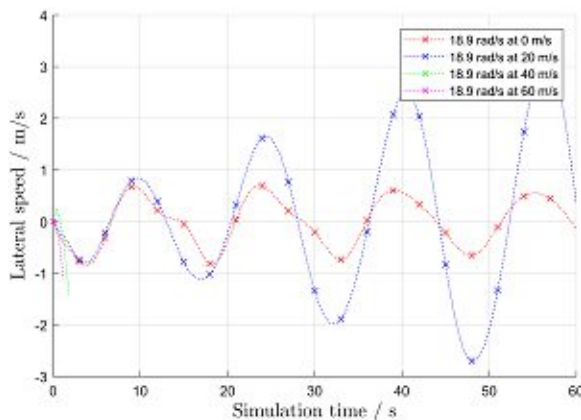
One important result is immediately apparent in subfigure (a), namely the fact that the simulation runs with target values of 40 and 60 m/s terminated prematurely. Both of them did not even last five seconds, whereby the simulation of the moderate speed lasted a little bit longer. This is in good agreement with the results presented at [111, p. 50]. The reason for this will become clear by the discussion of power demands in section 8.3. The lateral speed is oscillating around the target value of 0.0 m/s. Maxima and minima exceed the values calculated for operation in MP I and for a forward speed of 20 m/s, an increasing amplitude is apparent. For the studied simulation time, the influence can be neglected, but for longer-lasting simulations it might be a problem. The ascent rate is maintained very well – except for the cases that ended prematurely – and the amplitudes do not increase for any forward speed. The yaw angles shown in subfigure (d) have higher amplitudes than in MP I, but still are within the acceptable range. For moderate and high forward speeds, the turboshaft engines are not able to provide the demanded power for main and tail rotor. As a consequence, the yaw angles decrease until the simulations finally terminated. The angular velocity of the main rotor is maintained satisfactory for hover and slow forward flight, for 40 and 60 m/s the lack of propulsive power leads to a significant decrease of MR speed in the first seconds of the simulations. As can be seen in subfigure (f), the MR angular velocities stay above the target value for the simulations which lasted the full 60 s. Again, the reason is the choice of number of teeth, which does not perfectly match the calculated transmission ratios.

Engine performance data can be found in figure A.6 in appendix A.2. In subfigure (a) the strongly increasing fuel consumption of the turboshaft engines in the prematurely terminated flight conditions can be seen. However, the engines are not able to provide the power demanded by the rotors, which leads to numerical issues in the simulation and finally to a termination of the affected simulation runs.

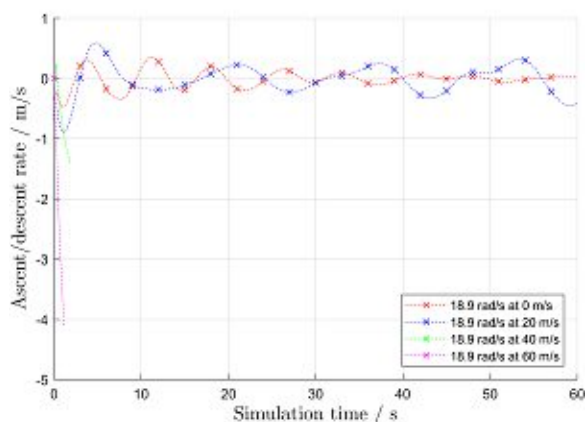
8.2. Results for different flight conditions



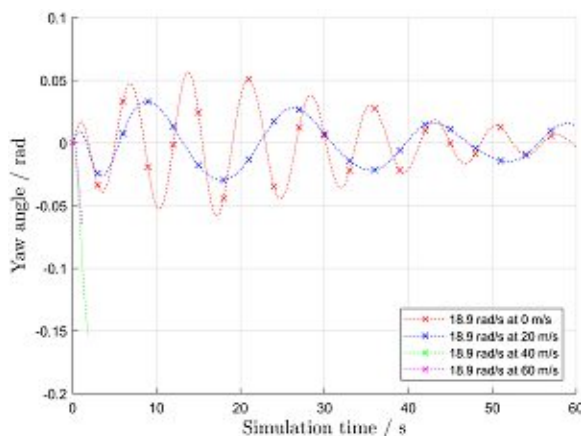
(a) Forward speed



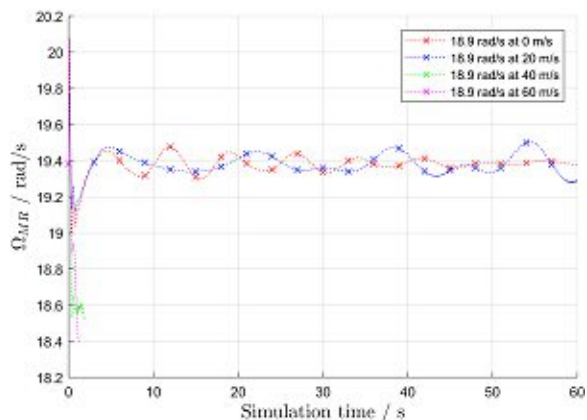
(b) Lateral speed



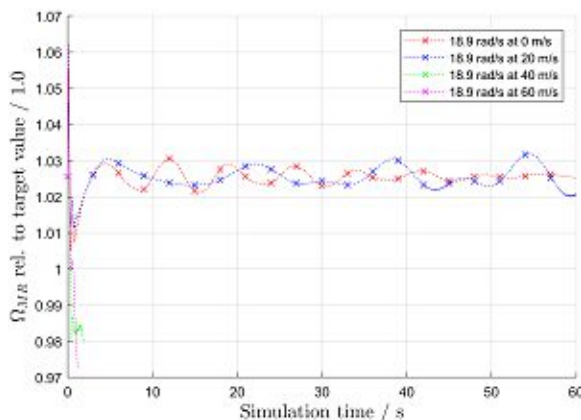
(c) Climb rate



(d) Yaw angle



(e) Angular velocity of main rotor



(f) Angular velocity of main rotor rel. to target value

Figure 8.19.: Speeds and yaw angle at MP II

8.2.3. Operation with hydraulic power transmission

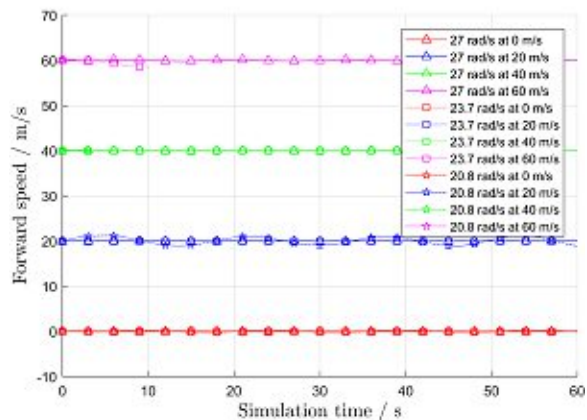
During operation in mechanical points one shaft of the variator was blocked and the hydraulic system omitted. In this section, flight conditions with a working variator, i.e., with hydraulic flow, are studied. Altogether, twelve different flight states are studied. The details can be found in table 7.5. As for the mechanical points, the maintenance of the target flight conditions is discussed, see figure 8.20. The forward speeds are close to the target values for the whole simulation time, except for the three cases which terminated prematurely. These are 23.7 rad/s at 60 m/s respectively 20.8 rad/s at 40 and 60 m/s. Again, it can be stated that these conditions are close to the expected boundaries of the flight envelope (cf. [111, p. 50]). The lateral speeds (subfigure (b)) are in an acceptable range around 0.0 m/s, but for slow forward flight at low MR speed an increasing amplitude occurs as it does at MP II. The courses of ascent rate and yaw angle are satisfactory. As could be expected, the early terminated cases exhibit fast descents and decreasing yaw angles. Subfigure (e) summarizes the angular velocities of the MR. For flight conditions with sufficient engine power – i.e., no drop in MR speed – the angular velocity is maintained well by the speed controller. The target values are met closely for 23.7 and 27 rad/s. For the low target value of 20.8 rad/s, a significant deviation of about 5 % occurs. It is caused by the poor efficiency of the hydraulic variator in this operation condition. However, this does not pose a problem at all, because for a real-life helicopter the MR speed will be adapted by a controller whilst in the Simulink model simply the variator ratio was set.

Information on the operation parameters of the turboshaft engines can be found in figure A.7 in appendix A.2. The characteristics are similar to the ones for the operation in the two mechanical points. The courses for operation at low main rotor speed and slow forward flight (20.8 rad/s at 20 m/s) show significant oscillation. However, this is assessed as an artefact caused by the simple design of the speed controller. Similar to the flight conditions at moderate and fast forward flight, three simulations did not last the full 60 s as well. As could be expected, these are cases at comparatively high forward flight speed and low MR angular velocity.

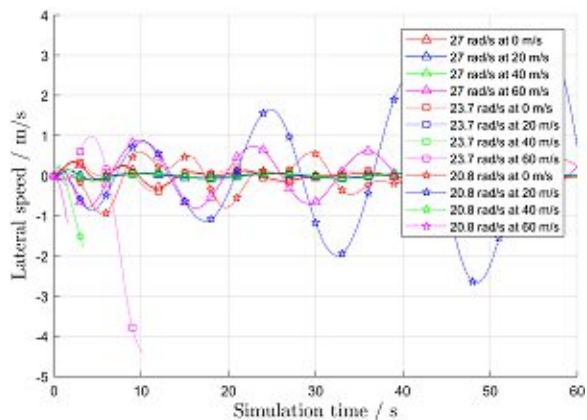
The simulation results of the variator system are summarized in figures 8.21, 8.22 and 8.23. The first important parameter is the system pressure. The target value is 450 bar with a maximum value of 500 bar (cf. chapter 4). After (non-physical) transient processes in the beginning of the simulation, the system pressure is maintained satisfactory by the pressure controller. For a MR angular velocity of 20.8 rad/s at 20 m/s beat-like phenomena, which show increasing amplitudes, occur approximately every 12 s. At the moment, no explanation can be given for this phenomenon, but it is expected, that the damping characteristics of a real hydraulic fluid will make them disappear. Whether this assumption is true has to be shown by a more detailed simulation of the variator system and test runs. The maximum value of system pressure is exceeded only in cases in which the power demand of the rotor exceeds the engine limits, i.e., the ones that did not run the full simulation time. Although these flight conditions have to be considered as beyond the limits of the permissible flight envelope, it has to be noted, that during operation of the rotorcraft shocks, which lead to pressure peaks in the variator, can occur. Pressure relief valves have to be installed to avoid damages to the hydraulic system.

In figure 8.22 the flow of hydraulic fluid in the variator is depicted. Since the system pressure is quite the same for all flight conditions, a higher flow means higher power transfer in the variator. As could be expected, the highest powers have to be transmitted in hover conditions, when the power demand of the main rotor is comparatively high. At low and moderate forward speeds, the

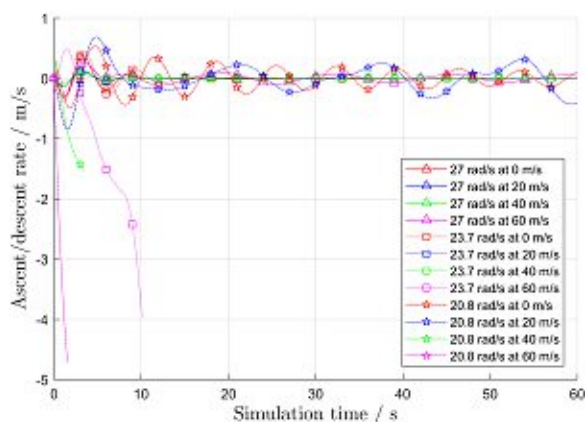
8.2. Results for different flight conditions



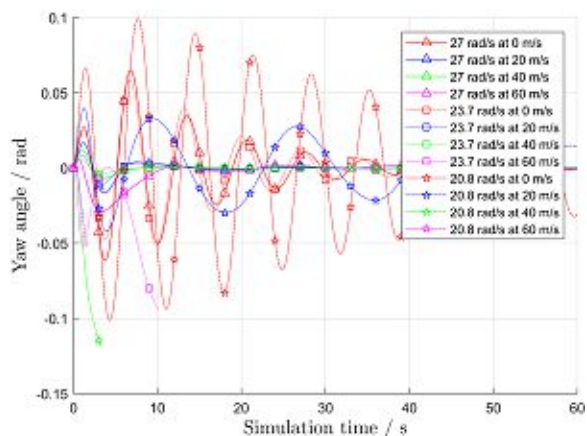
(a) Forward speed



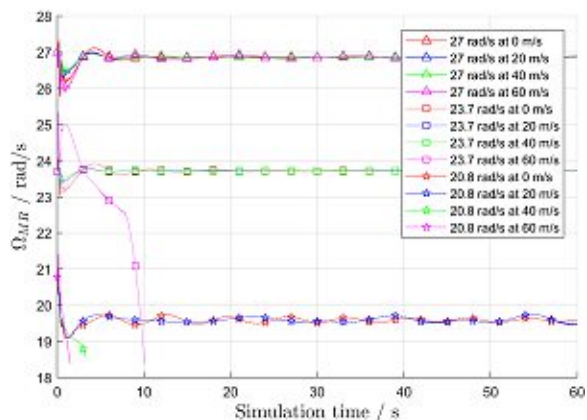
(b) Lateral speed



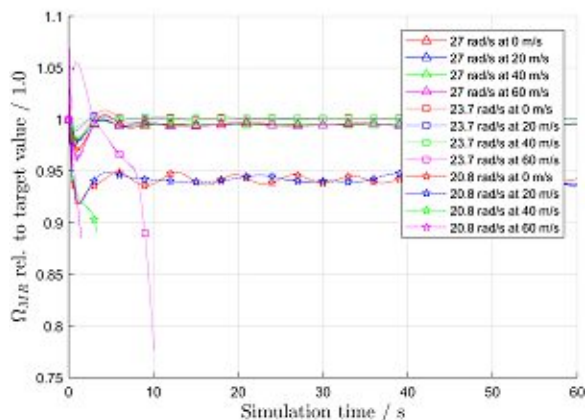
(c) Climb rate



(d) Yaw angle



(e) Angular velocity of main rotor



(f) Angular velocity of main rotor rel. to target value

Figure 8.20.: Speeds and yaw angle with hydraulic power transmission

8. Results

transmitted hydraulic power is lower. The values of the only fast forward flight which lasted 60 s lie in-between.

As discussed earlier, the poor efficiency of a hydraulic transmission system is its major drawback. In figure 8.23 the resulting efficiencies of the variator system, based on the mechanical shaft powers at pump and motor shaft, are depicted. At the reference MR speed of 27 rad/s, the resulting efficiencies are about 48 % to 49 %. Since engine and main rotor speed are the same for all of these flight states, also the speeds of the variator shafts are (nearly) equal. With the system pressure of 450 bar and the negligible influence of the displacement (cf. (5.1)), the resulting efficiencies are nearly the same for all forward speeds. At a main rotor speed of 23.7 rad/s, when the power flow in the variator relative to engine power is at a maximum, the efficiency of the hydraulic system is higher, approximately 57 % to 58 %. For the third main rotor speed (20.8 rad/s), i.e., the operation condition with the slowest rotational speed of the hydraulic motor shaft, the efficiency drops significantly to values between 6 % to 7 %. As stated earlier, at low speeds of the hydraulic machines, it is inadmissible to use Schlösser's model. Actually, the hydraulic motor is operated close to the set efficiency minimum of 5 % (cf. section 7.5.1) in these cases. Again, only full-scale tests of the variator system will provide a final answer to the issue of the hydraulic efficiency at different operation conditions. In conclusion, the Simulink model yielded no better information on hydraulic efficiency to the findings of chapter 5 because the same loss model was used. However, it enabled to rate the efficiency for a given flight condition, which broadens the previous findings.

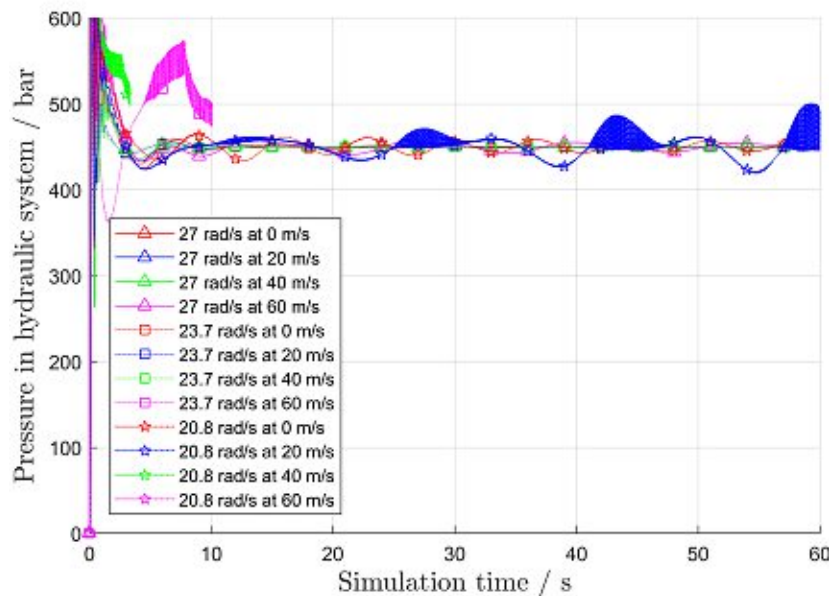


Figure 8.21.: Pressure in hydraulic system

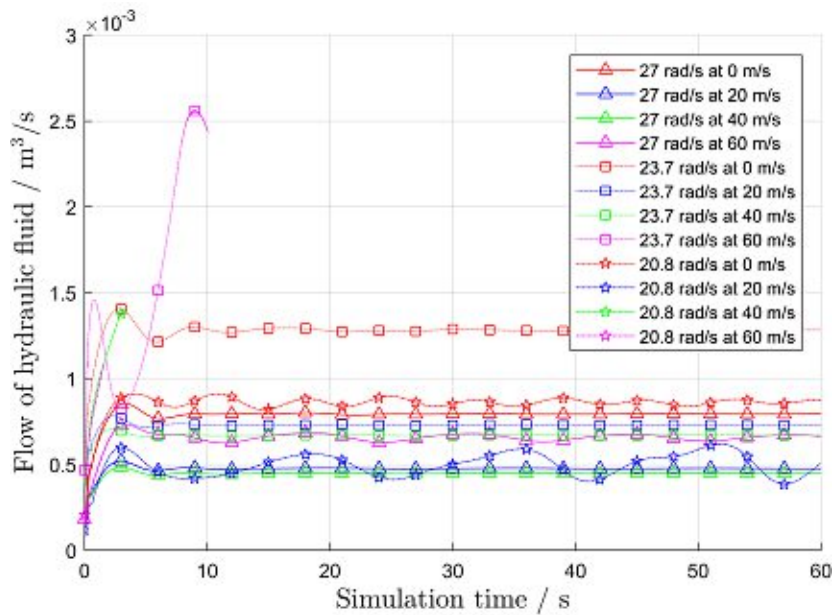


Figure 8.22.: Flow of hydraulic fluid

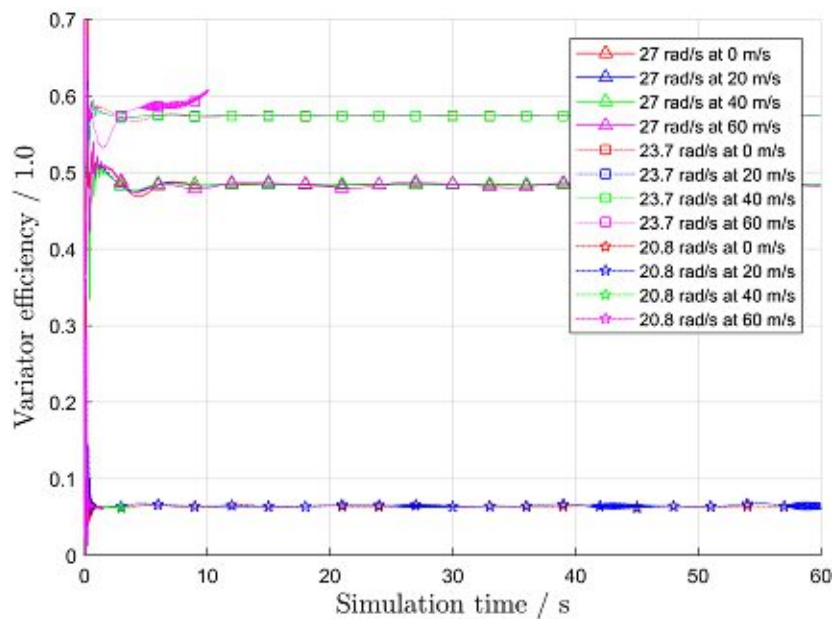


Figure 8.23.: Variator efficiency

8.2.4. Change of main rotor speed

In the previous three sections flight conditions with constant main rotor speed were studied. Although it is of course possible to predefine a target value before take-off and operate the rotorcraft at this MR angular velocity for the whole duration of the mission, the possibility to adapt it during flight offers overwhelming advantages. To show that the derived transmission system is able to achieve this goal, six simulation runs with varying MR speeds were performed (cf. table 7.5). The

8. Results

results are presented in the same way as in section 8.2.3, i.e., with one figure summarizing the flight sates and three pictures dealing with the variator performance.

Figure 8.24 provides six subfigures containing the time series of velocities, yaw angle and MR speed. For the first ten seconds, the simulation yields the same courses as in figure 8.20, because the same parameters and boundary conditions were used. This time is needed for transient processes to abate and to allow the start of the change of the MR angular velocity at a steady flight condition. Afterwards, the angular velocity of the main rotor is changed to the target value during a period of 50 s and the last 20 s are used to obtain a steady operational state again.

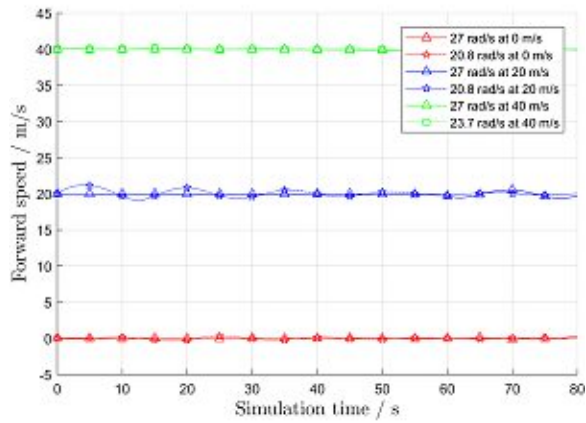
The forward speed is not apparently affected by the adaptation of the MR speed to a new target value and also the lateral speed does not exceed the values that occurred for operations at constant MR speed. For some flight conditions, especially hover at low MR speed and slow forward flight at reference MR speed, oscillations of the climb rate (subfigure (c)) occur at the beginning and the end of the speed transition phase. However, the calculated values do not exceed the permissible range and abate after some ten seconds. Therefore, these phenomena are not assessed as critical for the operation of the rotorcraft. The same applies for the oscillations of the yaw angle (subfigure (d)).

The most interesting outcome of the six simulation runs, the time-courses of angular velocities, is depicted in subfigures (e) and (f). The curvature of the courses is caused by the method of speed change, which is done by adapting the transmission ratio in the variator linearly. For simulations starting at the reference speed of 40 s, the time-courses are nearly identical during the first 40 s of speed change (50 s of simulation time). Afterwards, the target value of 23.7 rad/s is maintained very well whilst MR speeds further decreases to the target value of 20.8 rad/s. In the last few seconds, the speed change rate is very high. This is due to the fast decrease of variator efficiency in these operation condition. As mentioned earlier, the latter is not reached exactly due to the influence of the variator's efficiency. However, the set angular velocity is maintained well enough for the purpose of this study. Of course, it is much easier to reduce main rotor speed during flight than to increase it. To prove that the designed transmission system is capable of both operations – within the limits of the turboshaft engines – the acceleration of the MR to the reference value was shown for three different starting points. Reversed to the results for deceleration, there is a strong increase of MR speed in the first few seconds of transition from 20.8 rad/s. For the higher starting angular velocity of 23.7 rad/s this characteristic is not that distinct. After the target value is reached, the speed of the main rotor is kept within a small range around it.

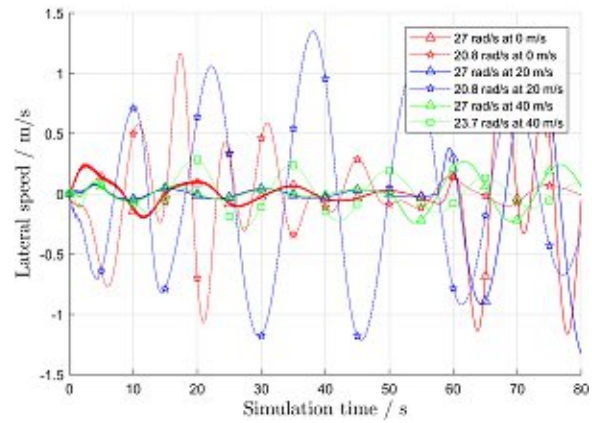
The related engine parameters can be found in figure A.8 in appendix A.2.

Figures 8.25, 8.26 and 8.27 summarize the parameters of the variator path during the change of main rotor angular velocity. In the first figure, the system pressure is depicted. There are small oscillations around the target value of 450 bar. As could be expected, peaks occur at the start of acceleration and at the end of deceleration of the main rotor. The maximum system pressure is exceeded in the latter cases. The related flows of hydraulic fluid are shown in figure 8.26. Again, oscillations occur at the beginning and the end of the MR speed change process, but in general, the time-courses do not exhibit inadmissible behaviour. Consequently, it is assessed that the – very simple – control system of the variator is working satisfactory. The last figure of this section shows the course of variator efficiency during shift operation. As discussed earlier, the efficiency determined by the used model is very poor for low MR speeds and reaches only 50 % to 60 % for medium and reference angular velocity. During transition from 23.7 rad/s to 27.0 rad/s and the other way around, the variator efficiency changes slowly and at the end of the simulation time, the

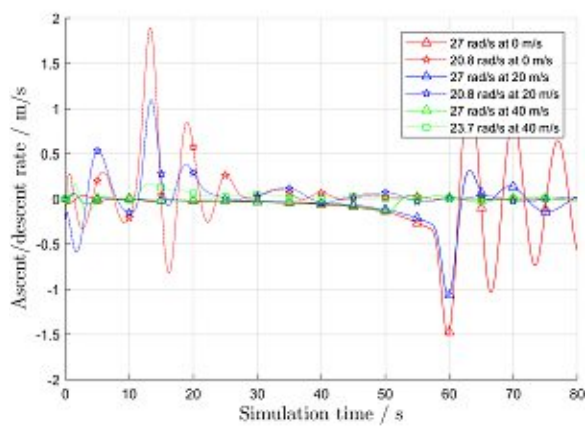
8.2. Results for different flight conditions



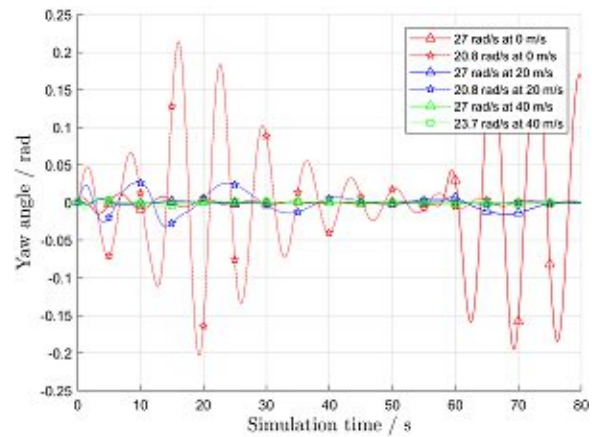
(a) Forward speed



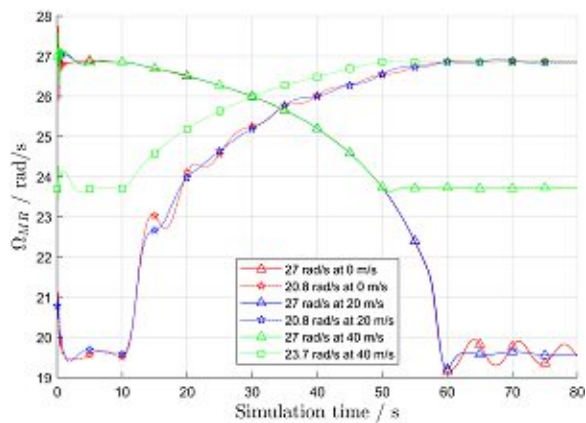
(b) Lateral speed



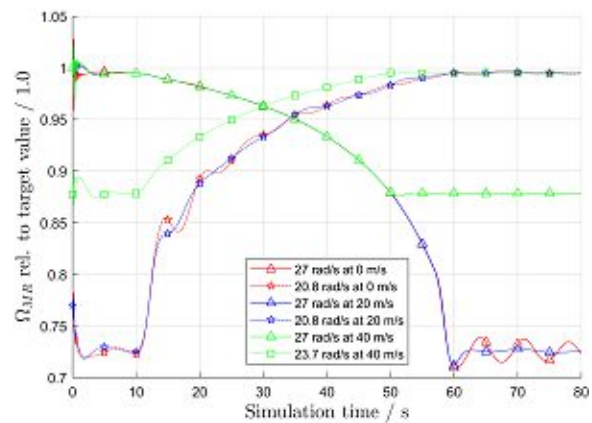
(c) Climb rate



(d) Yaw angle



(e) Angular velocity of main rotor



(f) Angular velocity of main rotor rel. to baseline speed

Figure 8.24.: Speeds and yaw angle during change of main rotor speed

8. Results

values have switched places. If the starting or end value of the MR speed is 20.8 rad/s, the behaviour is different and shows a very steep ascent/descent of efficiency at low MR speeds. This is caused by the used efficiency model (cf. section A.1) but is considered as a non-physical phenomenon which has to be addressed in future test campaigns. At medium main rotor speeds, the calculated efficiency also lies in the range of 50 % to 60 %.

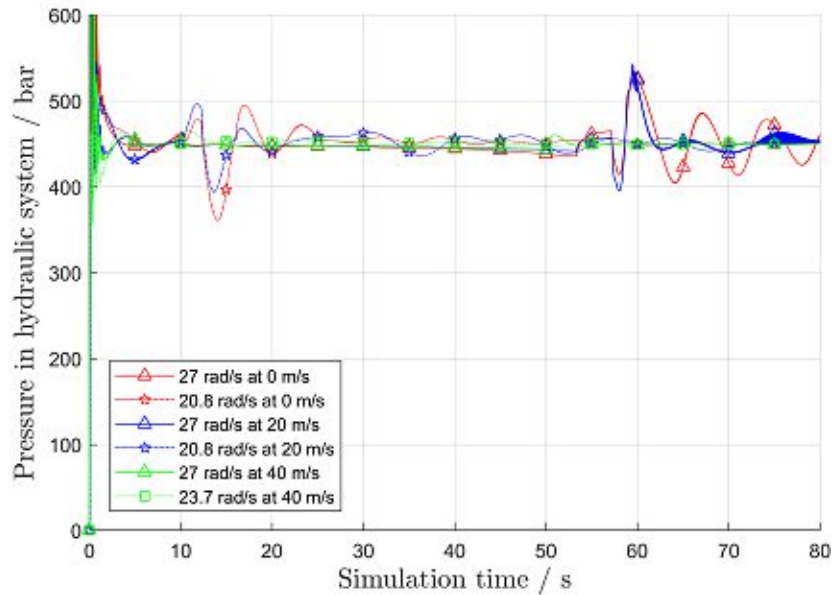


Figure 8.25.: Pressure in hydraulic system

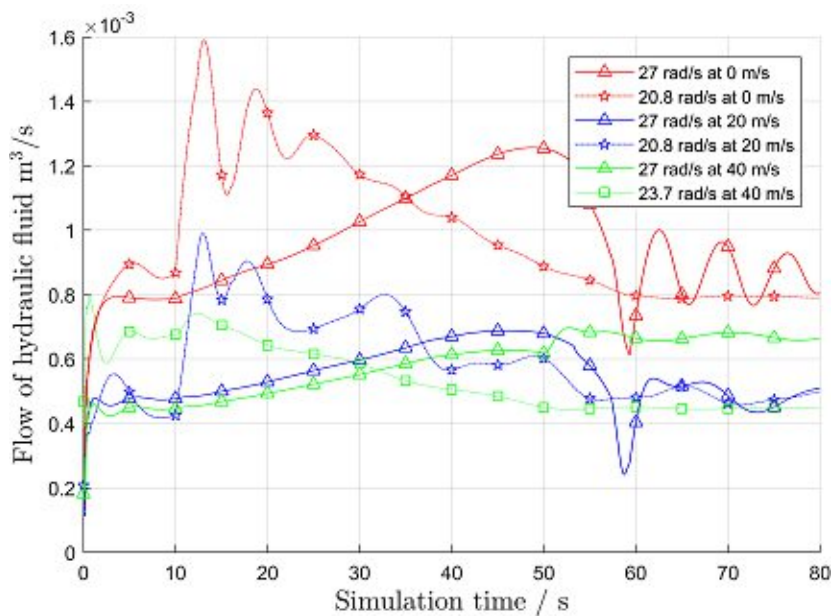


Figure 8.26.: Flow of hydraulic fluid

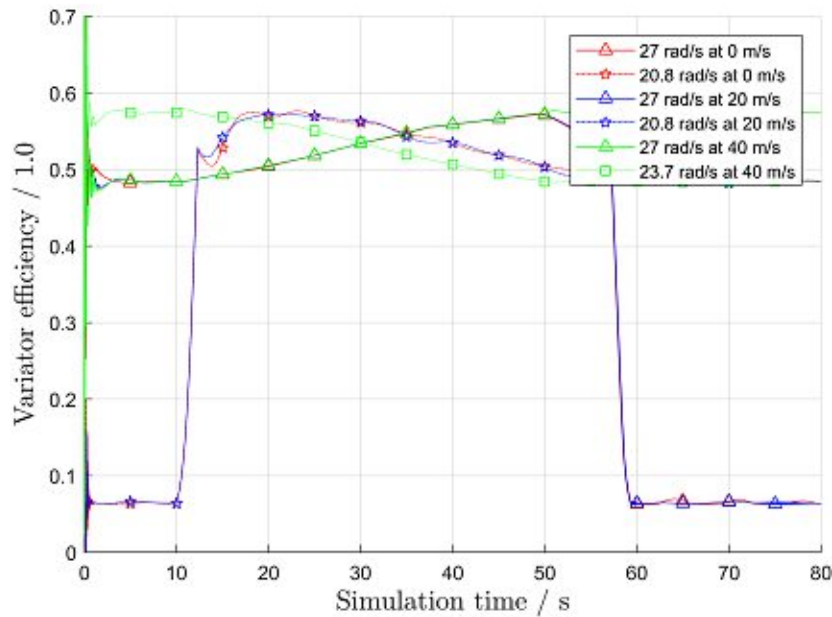


Figure 8.27.: Variator efficiency

8.3. Power demand

One of the major motivations to study variable main rotor speeds of helicopters is the expected reduction of power demand and consequently of fuel consumption. The mean power demands of the UH-60's main rotor for different flight states at different – but constant – RPM are depicted in figure 8.28. The coloured geometrical figures indicate the power demand. The connecting dotted lines are just to make it easier to find the related points (i.e., the ones with the same MR RPM) but have no physical meaning. It can be seen, that for all flight states a reduction of MR angular velocity would lead to a reduced power demand of the main rotor. In hover, the minimum demand is not at the minimum MR speed but at 20.8 rad/s. At all other advance ratios, the minimum angular velocity of the main rotor coincides with the minimum power demand. These results correspond to the findings in [46]. The power demands relative to the demand at reference speed are summarized in figure 8.29. It can be seen, that for hover and low to moderate speeds the main rotor power can be reduced by up to 13 %. At a flight speed of 60 m/s all simulations with MR speeds below the reference speed failed to finish. Therefore, no reduction of the power demand can be expected at this advance ratio.

Of course, the power demand of the rotorcraft is not determined by the main rotor alone. A reduction of MR speed may lead to increased torque, which requires an increase of tail rotor thrust and thus of tail rotor power. By comparing the engine powers for different flight states, the power demand of both rotors and the losses in the variators can be taken into account. In figures 8.30 and 8.31, the absolute and relative power demands are presented. As for the main rotor, a reduction of the angular velocity compared to the reference case of 27.0 rad/s is advantageous, but now 'the lower, the better' applies. This means, that the lowest available MR speed yielded the lowest power demand of the helicopter. The results presented in figure 8.31 can be compared to [46, Figures 8 & 9]. According to this source, for the simulated values of $\frac{c_T}{\sigma}$ (cf. table 7.3), the opti-

8. Results

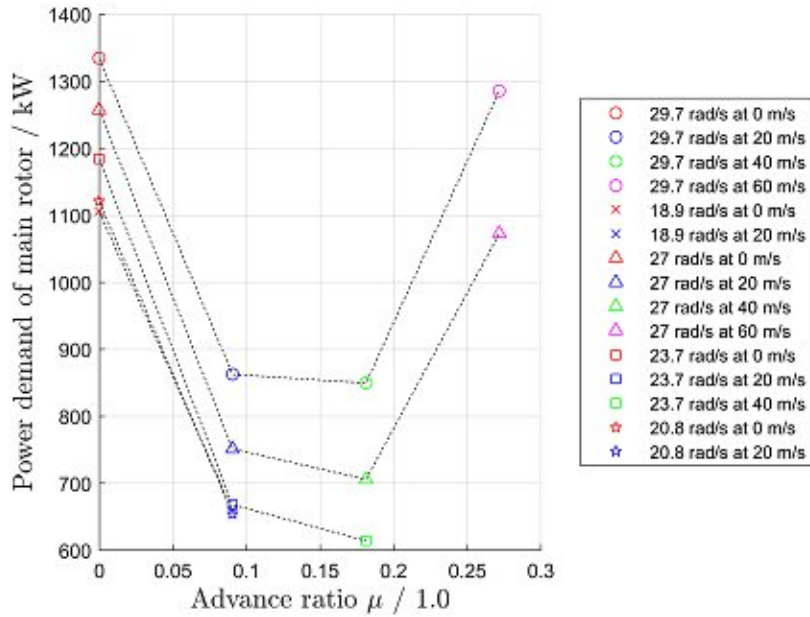


Figure 8.28.: Main rotor power demand

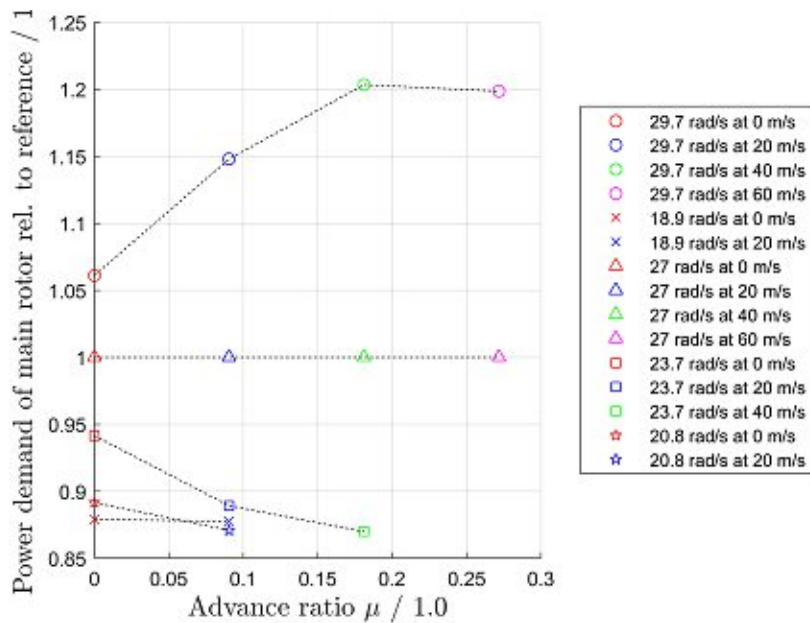


Figure 8.29.: Main rotor power demand rel. to reference speed

imum main rotor speed is between 85 % (hover) and about 100 % ($\mu = 0.272$). Therefore, in hover condition the optimum speed (70 % of reference speed) seems to be too low whilst for the other flight conditions, the simulation results show good agreement with the literature. The possible reductions of power demand in the studied range of parameters are quantified as 0 % to 3 % in [46, Figures 8]. As can be seen in figure 8.31, the study on hand over-predicts the advantages of lower MR speeds considerably compared to the chosen reference data. However, [73, Figure 8] supports

the simulation results for a gross mass of 16000 lb at sea level. Again, only extensive flight tests can answer the question for the exact reduction of power demand conclusively.

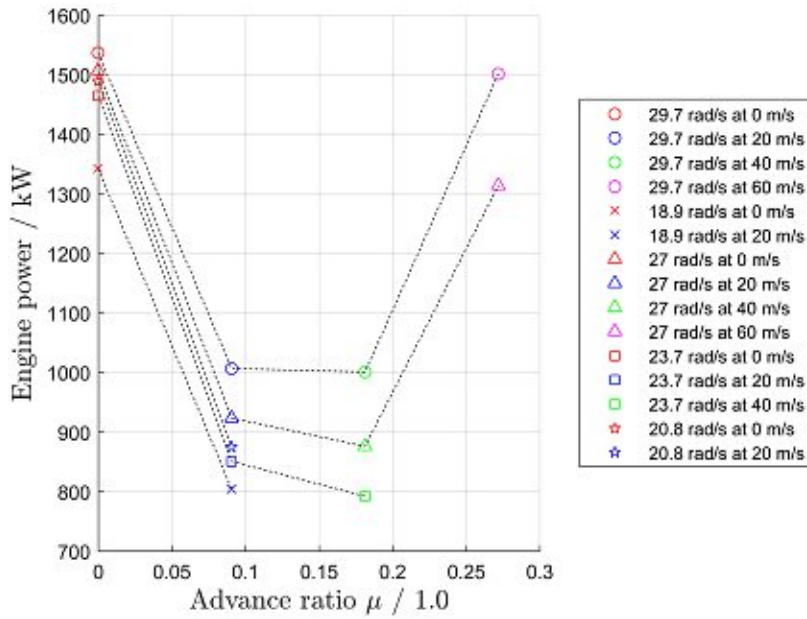


Figure 8.30.: Engine power

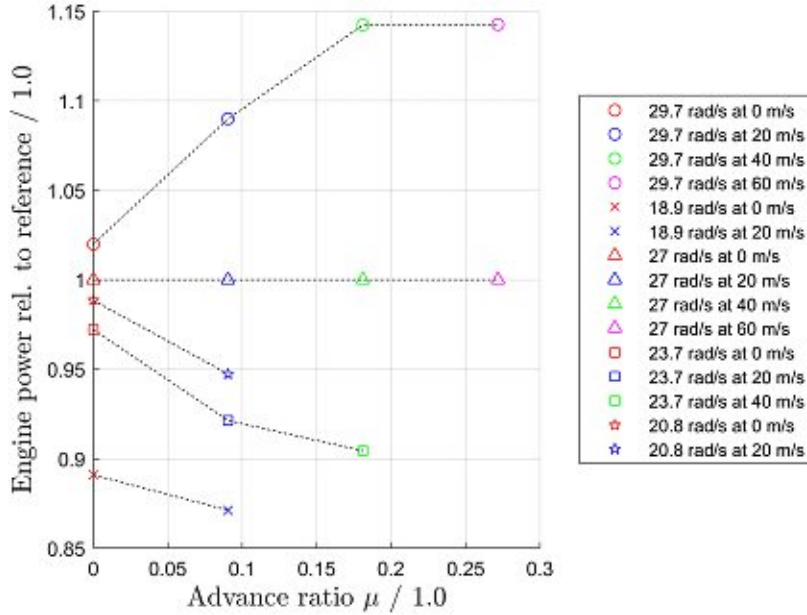


Figure 8.31.: Engine power rel. to reference speed

8.4. Main rotor torque

Another important aspect of a variable main rotor speed is the change of torque due to speed variation and resulting changes in power demand. In figures 8.32 and 8.33 the absolute values respectively the values relative to the torque at reference speed are depicted. The results in the first illustration show, that the main rotor torque at reference speed is always at the lower boundary of possible results. In figure 8.33, this becomes even clearer. In hover, only the operation in MP I yielded a lower torque than operation at the reference value. The lower MR speeds lead to significant increases in main rotor torque, the maximum increase of about 22 % occurs at 18.9 rad/s (MP II). At slow forward flight, the torque at high MR speed increases relative to the value at reference speed. A possible reason is the influence of incident flow on the advancing and retreating blades. The main rotor torques for low angular velocities rel. to the reference case stay quite the same as in hover whilst a moderate reduction of MR speed would yield a significant reduction of power demand at a negligible increase of MR torque. At a forward flight speed of 40 m/s the trends prevail and MR (target) angular velocity of 23.7 rad/s would lead to a reduction of both, power and torque – an absolutely preferable situation. At fast forward flight, no angular velocity below the reference speed yielded simulation results and the increased MR speed would cause a significant increase in both, power demand and shaft torque. Therefore, the reference speed is the right choice for this flight condition, which is not surprising, since it is presumably close to the design point of the UH-60.

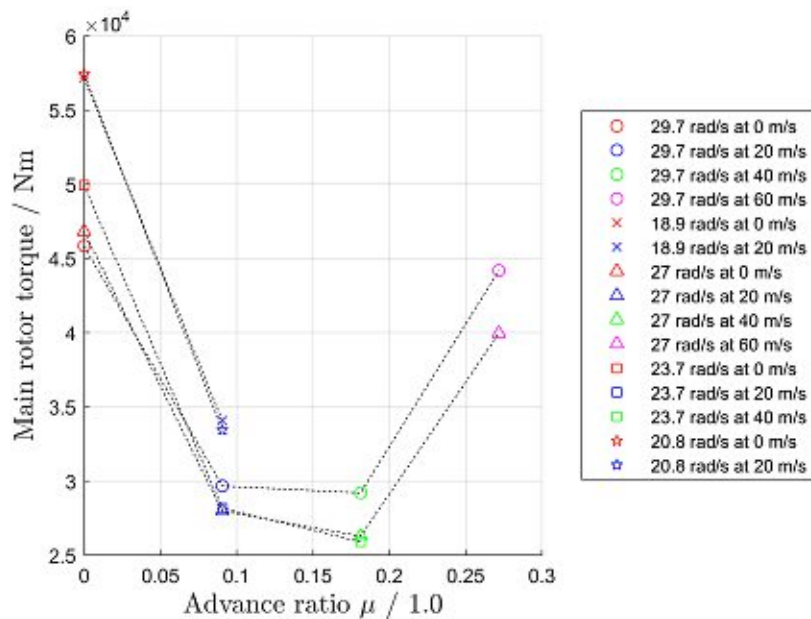


Figure 8.32.: Main rotor torque

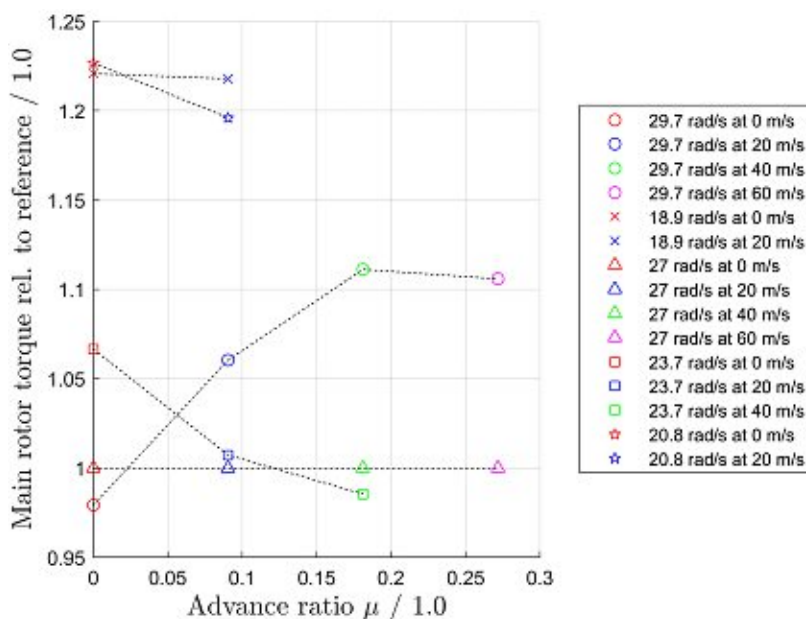


Figure 8.33.: Main rotor torque rel. to reference speed

8.5. Tail rotor power

As already mentioned in the discussion of the overall power demand of the rotorcraft, the power consumption of the tail rotor is not independent of the operation condition of the main rotor. Therefore, the impacts of different MR angular velocities on the tail rotor are discussed hereafter with the aid of figures 8.34 and 8.35. As in the sections before, the former depicts the absolute power demand whilst the latter shows the value relative to the one of the operation at MR reference speed. Since TR speed is assumed to be constant, figure 8.35 is also corresponding to the relative torques at the tail rotor shaft. As could be expected, the principal courses of TR power in figure 8.34 show similar characteristics as the MR torques depicted in figure 8.32. However, since the tail rotor thrust T_{TR} is directly proportional to main rotor torque but tail rotor power and thrust are interconnected via (7.17), the relative position of the data points to each other is skewed in figure 8.34.

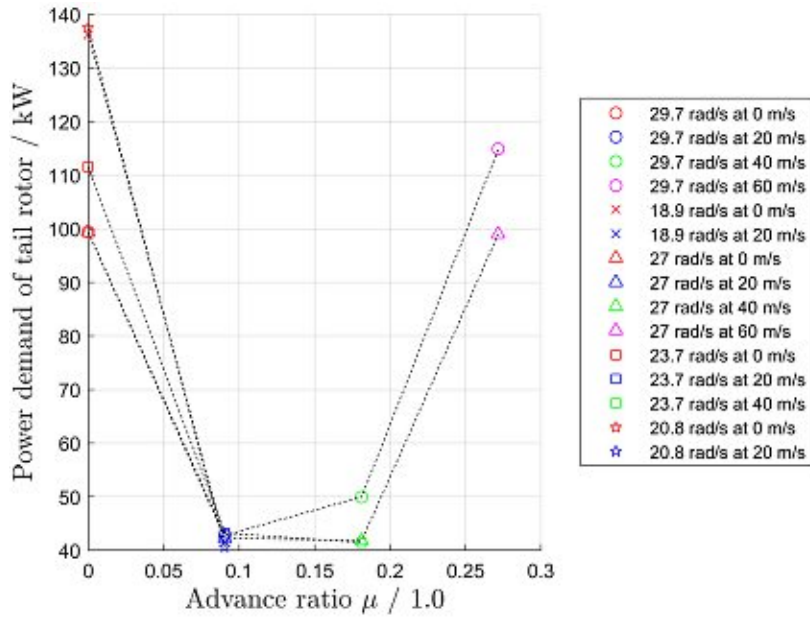


Figure 8.34.: Tail rotor power demand

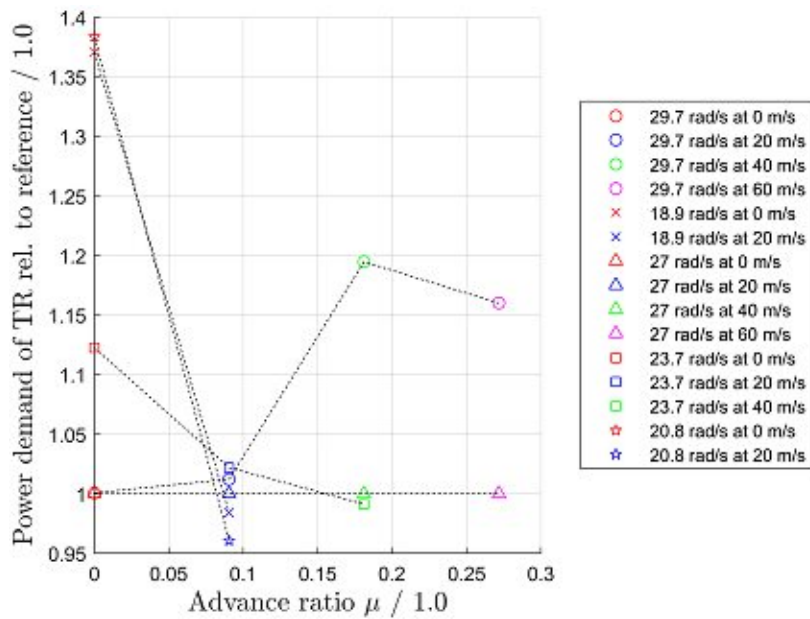


Figure 8.35.: Tail rotor power demand rel. to reference speed

8.6. Variator power

The main advantage of a Compound-Split transmission compared to the Input- respectively Output-Split is the smaller percentage of propulsive power which has to be transmitted via the variator path. This has already been discussed in section 2.2 and the results for the Compound-Split can be found in equation (2.27) and figure 2.8. However, these findings are based on loss-free operation of

all parts of the transmission system, which chapter 5 showed to be a very unrealistic assumption. The actual powers at pump and motor shaft, as determined by the Simulink model, are depicted as a function of the main rotor (target) angular velocity in figure 8.36. The coloured lines are just to make it easier to find the related points and have no additional meaning. As defined by the setup of the simulation models, the mechanical power taken off resp. supplied by pump and motor at mechanical points ($\Omega_{MR} = 18.9, 29.0$ rad/s) is zero. Between the MPs, the power transmitted hydraulically increases and has its maximum – as expected – at 23.7 rad/s. However, it is obvious that the sum of motor and pump power is not zero for operation of the CS module with hydraulic power transmission. Compared to the ideal, loss-free case the values are shifted downwards. This means that more power is taken off by the pump than re-supplied by the motor – a direct consequence of the hydraulic efficiency. For the same reason, the ratio of pump to motor power is closer to 1.0 at 27.0 rad/s, where the variator efficiency is high, than at 20.8 rad/s, where the efficiency is very poor.

In figure 8.37 pump and motor power are compared to the respective input power in the flight case. It can be seen, that despite of different operation conditions and variator efficiencies, the resulting ratios lie close together for all main rotor speeds. In general, a maximum of about 12 % of the input power is taken off by the pumps whilst the motors re-supply maximum about 8 %. For comparison, calculation under assumption of perfect efficiency using equation (2.31) yields a maximum value of 11.25 % for both hydraulic machines.

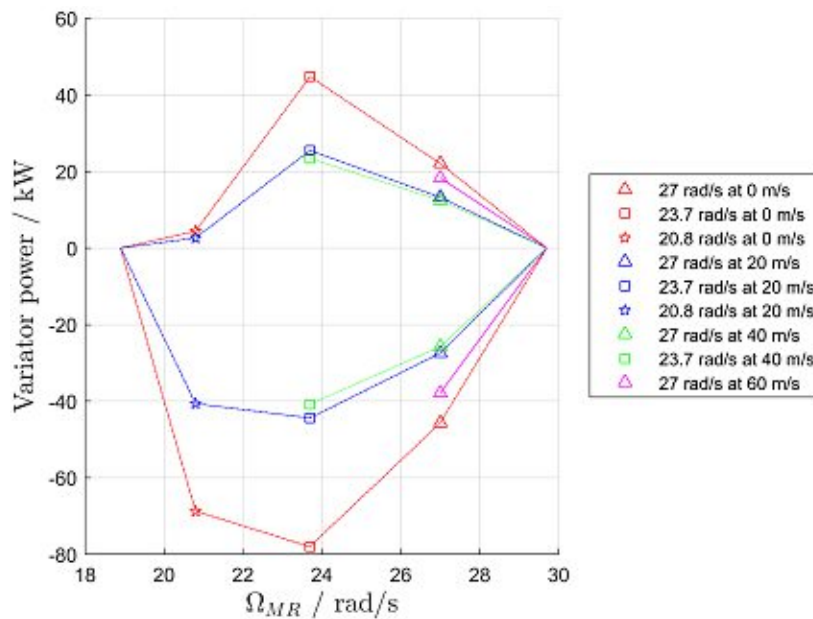


Figure 8.36.: Power flow in variator

8. Results

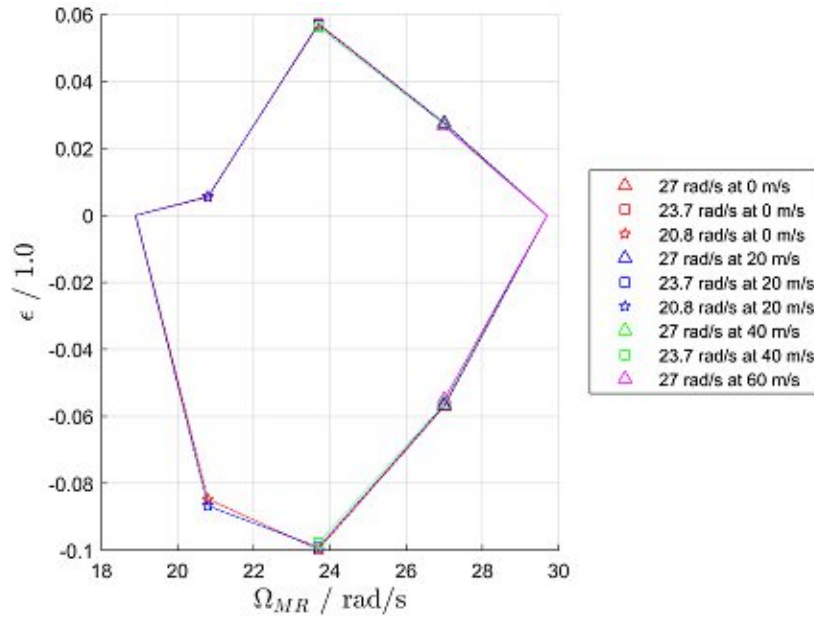


Figure 8.37.: Power flow in variator rel. to engine power

8.7. Summary of simulation results and discussion

The simulation of different flight states in combination with various angular velocities of the main rotor respectively a changing MR speed yielded several interesting results. First of all, the validation of the model at the reference MR speed of 27.0 rad/s showed, that it is suitable to represent the physical phenomena of interest for this study. An important finding is the fact, that the calculation model is able to maintain a given flight state at several MR angular velocities satisfactory. Also, combinations of parameters which lie outside the permissible flight envelope were identified in good agreement with the literature. In the previous sections the core results of the simulation runs of different Simulink models have been presented and discussed. All time-courses of parameters show a reasonably low level of oscillation and the resulting values correspond to the expectations. Regarding the main objective of MR speed variation, the reduction of power consumption, the literature is divided on the question of the possible savings. The results obtained in this study lie in-between. The simulation runs also showed the proper function of a lossy hydraulic variator system under the set boundary conditions. In summary, the simulations with changing main rotor speed were successful because the results show that it is possible to vary the speed within a wide range. However, there is still a lot of simulation and validation work to be done to find a helicopter design ready for series production.

Part IV.

Certification & Safety Aspects



Die approbierte gedruckte Originalversion dieser Dissertation ist an der TU Wien Bibliothek verfügbar.
The approved original version of this doctoral thesis is available in print at TU Wien Bibliothek.

9. Certification according to CS-29

The objective of this chapter is to discuss how the implementation of the proposed transmission system will affect the certification according to the Certification Specification (CS) CS-29 [42] issued by the European Aviation Safety Agency (EASA). The certification process is a complex procedure to show compliance with the regulations of the aviation authorities. It involves the definition of measures to prove the suitability of the rotorcraft and its sub-components. These can include several tests or computer simulations. Some common measures are summarized as Acceptable Means of Compliance (AMC) in CS-29 [42, Book 2]. In the previous chapters only the basic layout of a helicopter drivetrain containing Compound-Split modules has been developed. A lot of design data has not yet been defined. Furthermore, the concept has not been discussed with an aviation authority in detail. Therefore, the remarks in this chapter can only be a short overview of possible issues and measures and certainly pose no final assessment of all aspects of certification.

9.1. Certification requirements

9.1.1. Applicability

In CS 29.1, the scope of CS-29 is defined as large rotorcraft, for which two categories, designated A and B, are introduced. The UH-60 falls under category A, because its maximum weight is greater than 9072 kg (20000 lbs) and it can carry more than ten passengers.

9.1.2. Weight limits

The implementation of a transmission system with Compound-Split modules for the UH-60 will affect the total mass and especially the mass distribution of a rotorcraft. Maximum and minimum weight must be established accordingly and the limitations for the centre of gravity have to be adapted (cf. CS 29.21 to CS 29.29).

9.1.3. Main rotor speed range

Of course, one of the main issues arising is the definition of a range of main rotor speeds. An important regulation thereto is paragraph CS 29.33, which deals with main rotor speed and pitch limits. Item CS 29.33 (a) requires the establishment of a range of main rotor speeds that:

- (1) "With power on, provides adequate margin to accommodate the variations in rotor speed occurring in any appropriate manoeuvre, and is consistent with the kind of governor or synchroniser used; and
- (2) With power off, allows each appropriate autorotative manoeuvre to be performed throughout the ranges of airspeed and weight for which certification is requested." [42, p. 1-B-2]

9. Certification according to CS-29

It is an evident requirement, that the demands on a rotorcraft with fixed MR speed also apply for one with variable MR speed at every permissible speed. Beyond that, the significantly higher acceleration/deceleration of the rotor during RPM changes may lead to broader margins at the maximum and minimum permissible MR speeds.

The two requirements affect the whole propulsion and control system of the rotorcraft. The operation is affected by the interdependencies between engines, Full Authority Digital Engine Control (FADEC), transmission system (especially the variators), the devices controlling the transmission ratio and the flight control input in any permissible manoeuvre. At the moment, too many issues concerning these systems and the interaction between them are unsolved and so it can only be stated, that they have to be addressed during the design process.

Compliance with demand (2) strongly depends on the properties of the main rotor, especially its inertia. It has to be assured, that even at the lowest rotor speed occurring in normal operation – i.e., 180 RPM or 70 % of baseline speed in the proposed system – the kinetic energy stored in the rotating MR is high enough to allow the pilot an adequate reaction in case of loss of propulsive power.¹

Sub-paragraphs CS 29.33 (b), (c) and (d) deal with the establishment of main rotor pitch limits (high and low), which are intended to ensure that the defined minimum main rotor speed does not significantly fall below the defined minimum speed in any flight condition. The requirements on a low speed warning for the MR are described in sub-paragraph CS 29.33(e). For a rotorcraft with a variable-ratio transmission system, it is probably desirable to implement a warning not only if MR speed falls below the minimum permissible speed, but also, if the current target speed of the MR – regardless of whether specified by the pilot or a special device – cannot be maintained.

9.1.4. One Engine Inoperative (OEI) resp. one engine disconnected by loss of variator

As has already been discussed in section 3.3, the addition of Compound-Split modules to the transmission system of a two (or more) engine helicopter has an influence on the reliability of the propulsion system. In the system derived in this study (see figure 3.7), the failure of one CS module (without blocking) disrupts the power flow from one input bevel gear stage to the combining bevel gear stage. However, the affected engine is still connected to the MR via the tail rotor drive. It can be assumed, that the power transmitting capacity of the TR drive is limited and so the power supply to the MR is reduced, but probably higher than in case of an effective engine failure, a so-called One Engine Inoperative (OEI) condition. This additional operation mode may be addressed during the certification process. For example, the five OEI conditions defined in CS-29 [42, pp. 1-G-3 sq.];

- 2½-minute OEI
- 30-minute OEI
- Continuous power OEI
- Rated 30-second OEI
- Rated 2-minute OEI;

¹At this point the author wants to express special thanks to Dr. Richard Markiewicz (Defence Science and Technology Laboratory (DSTL)) for bringing up the issue in a discussion at the 44th European Rotorcraft Forum.

could be expanded by operations in which power is transferred via the TR drive. Of course, the related permissible power ratings of both engines have to be defined accordingly.

A failure of one engine resp. the significant reduction of available propulsive power by malfunction of a CS module is especially unfavourable during take-off. Paragraph CS 29.53 demands the determination and scheduling of the take-off performance so that a safe return to and stop at the take-off site is possible or the manoeuvre can be continued. CS 29.59 demands that the take-off capability of the rotorcraft after the Take-Off Decision Point (TDP) in case of an engine failure is shown by a flight test. In addition to these requirements, CS 29.67 defines demands on the climbing speed in OEI operation.

The requirements for landing of the helicopter are similar to the ones for take-off. In case of failure of the critical engine – i.e., the one whose failure would most adversely affect the performance or handling abilities of the rotorcraft – the helicopter can be either landed safely or the landing manoeuvre can be aborted and height gained.

It has to be stressed that definitions of the MR speed have to be made for the take-off/landing procedures and all other flight conditions for which certification is requested. A broad range of permissible speeds and especially the possible change during a manoeuvre will strongly increase the certification efforts and costs – especially when flight tests are explicitly required. In addition, height-velocity envelopes would have to be established for different MR speeds which would complicate the handling of these important documents for the flight crews. Therefore, it might be reasonable to limit MR RPM in take-off and landing manoeuvres to a nominal speed.

9.1.5. Flight and handling characteristics

The demands on the flight characteristic of a rotorcraft to be certified according to CS-29 can be found in paragraphs CS 29.141 to CS 29.181 (cf. [42, p. 1-B-8 sqq.]).

The very principle of helicopter propulsion and control involves a strong influence of the main rotor speed on controllability and manoeuvrability. Of course, CS-29 demands permissible flight characteristics in all operating conditions for which certification is requested. Again, the wide range of main rotor speeds and the possibility of changes during manoeuvre extend the multitude of operating conditions enormously. If OEI modes are extended as suggested, this number further increases.

Vibrations of the rotorcraft are excited by varying loads, some of which are caused by the varying angular velocity of the main rotor and drivetrain components. To avoid impermissible stresses of structural components, the vibrations of a helicopter equipped with a transmission containing CS modules have to be studied and tested comprehensively. In case of ground operation, a fixed RPM could be prescribed to avoid ground resonances.

Due to the low Technology Readiness Level (TRL) of rotorcraft transmission systems with Compound-Split modules, no final evaluation of the influence on the flight characteristics can be made. Therefore, most questions concerning the certification of this topic have to be left open for future research.

9.1.6. Strength requirements

General

Needless to say, all parts of a rotorcraft have to fulfil certain strength requirements. To prove compliance with the certification specification, limit loads covering all permissible flight conditions have to be defined. In particular, the main rotor RPM range (power on / power off) has to be established (cf. CS 29.309 (b) & CS 29.1509). Since the operating speed of the two turboshaft engines is the same for the proposed drivetrain as for the baseline transmission system, the engine torque specifications (cf. CS 29.361) will probably stay the same. If the installed engine power shall be used at all main rotor speeds achievable with the proposed transmission system, the acting torques and forces will increase compared to the baseline rotorcraft in parts of the drivetrain. In addition, the vibrational level may increase in some operation conditions (and decrease in others). As a consequence, the limit loads can be expected to be higher than for the baseline UH-60. In addition, it may pose a challenge to analyse all possible combinations of flight manoeuvres and MR speed. As a proof of structure (cf. CS 29.307) several tests have to be performed. Regarding structural analysis, CS 29.307 reads

"Structural analysis (static or fatigue) may be used only if the structure conforms to those for which experience has shown this method to be reliable." [42, p. 1-C-1]

Since for a CS module in a helicopter drivetrain no operational data is available, extensive load testing is a must.

Fatigue

According to CS 29.571 (a),

"A fatigue tolerance evaluation of each Principal Structural Element (PSE) must be performed, and appropriate inspections and retirement time or approved equivalent means must be established to avoid Catastrophic Failure during the operational life of the rotorcraft." [42, p. 1-C-11]

Principal Structural Elements (PSEs) are defined as "structural elements that contribute significantly to the carrying of flight or ground loads and the fatigue failure of which could result in catastrophic failure of the rotorcraft" [122, Page C-101]. Most parts of the transmission system have to be considered as PSEs. As a consequence, in-flight measurements of the fatigue loads of these parts have to be executed to be able to derive appropriate load spectra as a basis for a fatigue assessment of each PSE. Furthermore, "[t]he effect of damage on stiffness, dynamic behaviour, loads and functional performance must be considered" [42, p. 1-C-12].

Because of the lack of test and service experience with Compound-Split transmissions comprising hydraulic variators in rotorcraft, the fatigue analysis of the proposed transmission system will be a very time and resource consuming process. For safety reasons, the aviation authority may require short inspection intervals or some kind of HUMS for some components of the drivetrain (cf. CS 29.1465). Important aspects of HUMS for hydraulic pumps in helicopters have been summarized and discussed in [86].

9.1.7. General aspects of design and construction

Paragraph CS 29.601 requires that

- (a) "The rotorcraft may have no design features or details that experience has shown to be hazardous or unreliable.
- (b) The suitability of each questionable design detail and part must be established by tests." [42, p. 1-D-1]

Since the properties of hydraulic fluids strongly depend on the temperature (cf. CS 29.603 (c)) and the very principle of power conversion in axial piston motors with variable displacement includes leakage, the hydraulic variator may be rated as a questionable design detail and therefore has to be tested extensively.

The important term of Critical Parts is defined in paragraph CS 29.602:

"A critical part is a part, the failure of which could have a catastrophic effect upon the rotorcraft, and for which critical characteristics have been identified which must be controlled to ensure the required level of integrity." [42, p. 1-D-1]

The proposed design of the transmission system adds several critical parts to the baseline design. These have to be included into the critical parts list and procedures assuring compliance with the certification requirements have to be established.

Further demands of SUBPART D – DESIGN AND CONSTRUCTION affect the used materials and the manufacturing processes. A challenging design task will be to ensure the accessibility of parts requiring recurring inspection. Due to the layout of the nested epicyclic gear sets of a Compound-Split module, inspection may require special equipment, such as endoscopes. To ensure safe operation, special factors may be established for some parts of the transmission system (cf. CS 29.619).

Fire is a great danger for a rotorcraft and its occupants. Therefore, special means for fire protection are required by CS-29. The choice of a hydraulic fluid poses a conflict of objectives, since it has to fulfil demands on power transmitting capability, ageing resistance, fire protection and environmental sustainability. From the safety aspect, a flame-retardant oil seems preferable. Paragraph CS 29.863 lists several demands on the fire protection of flammable fluids which have to be kept in mind when designing the hydraulic system of the Compound-Split.

9.1.8. Rotor drive system

In Subpart E of CS-29 [42], one chapter is dedicated to the rotor drive system. The most important points concerning the certification of a transmission system with CS modules are discussed in the following section.

Design of the rotor drive system

By definition,

"[t]he rotor drive system includes any part necessary to transmit power from the engines to the rotor hubs. This includes gearboxes, shafting, universal joints, couplings,

9. Certification according to CS-29

rotor brake assemblies, clutches, supporting bearings for shafting, any attendant accessory pads or drives, lubricating systems for drive system gearboxes, oil coolers and any cooling fans that are a part of, attached to, or mounted on the rotor drive system." [42, p. 1-E-2]

Therefore, the whole transmission system developed in the previous chapters of this thesis is part of the rotor drive system. Acc. to CS 29.917 (c), a Design Assessment for the rotor drive system is mandatory. It must include a detailed failure analysis to identify failures that rule out a safe flight or landing. In chapter 10, a basic failure analysis of the proposed transmission system is presented. It includes a risk assessment of each possible failure, potential countermeasures and re-evaluation of the risks based on the anticipated effectiveness of the countermeasures.

Some requirements on the arrangement are listed in paragraph CS 29.917 (c). Item (1) demands that in case of an engine failure all rotors necessary for safe flight and control are driven by the remaining ones. For the UH-60 this means that both, main and tail rotor, must be able to be driven by one engine. As already discussed in section 9.1.4, a failure of one variator has similar consequences as the failure of one engine. Main and tail rotor are driven as long as one CS module works properly and the transmission is not obstructed from rotating, e.g., by a blocked variator machine. In addition, the rotor drive system must contain a device to automatically disengage a failed engine from the rotors. This is usually done by free-wheeling units. Perhaps a disconnection of a failed variator is also desirable, but because of the reverse power flow in autorotation, free-wheeling units may not be used. To avoid catastrophic consequences of a blocked variator, defined breaking points may be provided to allow unimpeded rotation of the mechanical path of the Compound-Split modules.

Rotor drive system and control mechanism tests

To ensure the proper function of the transmissions system, mandatory tests are established in CS 29.923 [42, p. 1-E-3]. The tests have to be carried out on the rotorcraft and include

- Take-off run
- Maximum continuous run
- Endurance tests at 60 %, 80 % and 90 % of MCP
- Engine malfunctioning run
- Overspeed run
- Tests of rotor control positions
- Clutch and brake engagements
- OEI power runs
- Special tests
- Tests of operating lubricants.

Some of the tests include OEI operations. When testing a variable-ratio transmission system, the remarks made in section 9.1.4 apply. Engine malfunction tests are intended to ensure that no dangerous dynamic behaviour occurs in the drivetrain if one or more engines do not work properly. Due to the systems added to the baseline transmission system, these tests gain even more importance since the operation in a range of MR speed strongly affects the dynamic behaviour of the rotor drive system.

Special tests are defined by:

"Each rotor drive system designed to operate at two or more gear ratios must be subjected to special testing for durations necessary to substantiate the safety of the rotor drive system." [42, p. 1-E-5]

In cooperation with the aviation authorities, the manufacturer seeking certification of a variable-ratio drivetrain will have to define at which main rotor speeds resp. speed changing rates tests are demanded. Since every test run has to last at least 200 h, a strong increase in time and cost effort can be anticipated in any case.

The arrangement of the two nested epicyclic gear sets and the relatively high rotational speeds of their gears pose a great challenge concerning lubrication and cooling. Therefore, a focus has to be laid on the qualification of the lubrication/cooling system during the certification process. The mandatory tests are defined in item CS 29.923 (p). Because of the changed power flow and resulting losses at different transmission ratios, the lubrication tests will also require more effort than in case of certification of a fixed-ratio transmission system.

Additional tests

Additional tests include runs with engine overtorque and verifications of any torque limiting devices. Of particular importance is the proof of safe operation in case of a failure of the lubrication system. For Category A rotorcraft, a 30 minute endurance after the loss of any pressurized lubrication system is required. Also, runs at overspeed and transient speeds are required. Since the hydraulic machines forming the variator are lubricated and cooled by the hydraulic fluid, the supply of it has to be considered as well.

9.1.9. Hydraulic systems

The requirements on hydraulic systems in rotorcraft are established in paragraph CS 29.1435. Of course, every component has to be designed so that the operational loads may not cause any inadmissible or permanent deformation. To prove the capability of transmitting the hydraulic power, tests with a system pressure of 1.5 times the nominal pressure have to be performed. Since both pump and motor will be operated at different rotational speeds, the tests have to be performed for a multitude of speeds, especially at or near standstill. It is also important to show that a change of rotational speed at the maximum permissible rate has no negative influence on operation safety of the variator and the transmission system. Furthermore, means for pressure indication and limitation have to be installed. Finally, it is recalled that hydraulic systems using flammable fluids must be designed acc. to the requirements discussed in section 9.1.7.

9.1.10. Powerplant limitations

To ensure that the powerplant loads do not exceed the limits for which the engines are type certified, additional limits have to be established. These must include maximum values of

- rotational speed
- turbine inlet and outlet gas temperature
- engine torque and power
- engine and transmission oil temperatures

9. Certification according to CS-29

and corresponding time limits. For the rotational speed, also minimum values have to be defined. Of course, the maximum allowable temperature of the hydraulic fluid has to be added to this list when a hydraulic variator is used. In addition, a maximum ambient atmospheric temperature below which the cooling systems are sufficient has to be specified. These requirements apply in particular to the OEI cases.

9.1.11. Emergency landing

The redesign of the UH-60's drivetrain will lead to additional mass above the cockpit and the passenger compartment. In case of an emergency landing, this poses a risk to the helicopter's occupants and crew. For approval of the rotorcraft design, the demands of paragraphs CS 29.561 sqq. [42, pp. 1-C-9 sqq.] have to be fulfilled. Maybe the structure has to be strengthened to obtain these goals.

The high-pressure hydraulic system and the potential flammable fluid in the transmission system pose another threat. In the transmission design proposed in this thesis, no storage of hydraulic energy is used and therefore the high pressure is restricted to the short connection between pump and motor plus hydraulic elements, such as accumulators, which are needed for a proper operation of the variator. However, actions have to be taken to minimize the risk and giving "each occupant every reasonable chance of escaping serious injury in a crash landing" [42, p. 1-C-9]. This could include automatically and/or pilot-controlled pressure release devices. The topic of fire protection has already been discussed in section 9.1.7. In addition to the remarks there, it shall be pointed out that a crash or hard landing may also affect the fire protection measures and that the mixture of fuel, lubrication and hydraulic oil as a consequence of breakage of the fluid lines may lower the flash point of the oils and increase the fire hazard.

9.1.12. Additional considerations

The topics discussed so far have to be addressed in the flight manual to ensure the correct handling of the rotorcraft by the flight and ground crews. Additional markings and placards (cf. CS 29.1541) may be used to avoid operational errors.

During operation it is important that the pilot has a complete overview of the operating conditions of the most important components of the helicopter. Therefore, additional powerplant instruments will have to be installed. Details of the requirements on powerplant instruments are summarized in CS 29.1305 and CS 29.1337. Special requirements apply for lines carrying flammable fluids under pressure, as it is the case in the variator's hydraulic system. Another important aspect is the indication of the oil quantity, both for fluids lubricating/cooling the drivetrain and such transmitting power.

To identify damage or wear of ferromagnetic parts of the transmission system at an early stage, the drivetrain has to be equipped with chip detectors. It may turn out to be a tricky task to make sure that particles are transported to the chip detectors by the lubrication fluid rather than being enclosed in the planetary gear sets of the Compound-Split.

9.2. Acceptable Means of Compliance

In Book 2 of CS-29 Acceptable Means of Compliance are established for some paragraphs. The most important ones affecting the transmission system will be discussed in this section.

9.2.1. Loss of lubrication tests

Paragraph AMC 29.917 provides additional information to supplement Advisory Circular (AC) 29-2C [122] published by the Federal Aviation Administration (FAA). Therefore, it should be used in conjunction with this document. Although the paragraph explicitly addresses lubrication systems, the hydraulic system of the variators will be discussed with respect to it, because the failure modes are similar. Also, some effects of failure; e.g., increasing friction and temperature following inadequate lubrication; are comparable. However, since the main function of the hydraulic fluid is not lubrication and cooling, but the transmission of power and these two aspects cannot be considered independently. Therefore, it seems reasonable to separate the analysis and test of the lubrication system from the one of the hydraulic system even if one affects the safety of the rotorcraft significantly stronger. Again, this leads to increased effort for the certification of the rotorcraft.

For all lubrication systems of the rotor drive system a safety assessment should be carried out. Usually this is done by a Failure Mode and Effect Analysis (FMEA). On a very basic level, this will be done in the following chapter 10. One of the outcomes of the safety assessment is the establishment of a *most severe failure*, i.e., the one "that results in the shortest duration of time in which the gearbox should be able to operate following the indication to the flight crew of a *normal-use lubrication system* failure." [42, pp. 2-56 sqq.]. This failure mode is the one to be represented in the loss of lubrication test(s) (cf. CS 29.927(c)). The compliance with the requirements on safe power transmission after loss of lubrication may rely on an *auxiliary lubrication system*. The baseline UH-60 does not have an auxiliary lubrication system, but the special demands of the nested epicyclic gear sets in the Compound-Split modules may require the installation of one. In this case, it should be sufficiently independent from the normal-use lubrication system. An auxiliary lubrication system may counteract the threat of seizure of the pistons in the hydraulic machines in case of loss of supply with hydraulic fluid but may not recover the power transmitting capacity. This can only be achieved by using redundant systems – an idea worth following up on.

A detailed description of the procedure of the loss of lubrication test(s) is given in AMC 29.927 [42, pp. 2-58 sqq.]. This also includes the possible establishment of a maximum period of operation following loss of lubrication of more than 30 minutes.

9.2.2. Vibration health monitoring system

It can be expected, that the advantages of Health and Usage Monitoring Systems including Vibration Health Monitoring (VHM) will lead to a widespread use in helicopters in the future and will become mandatory for category A rotorcraft one day. The additional risks of a variable-ratio transmission system as proposed in this study may demand the use of VHM anyway. The AMCs concerning such systems are defined in AMC 29.1465 [42, pp. 2-76 sqq.]. The list of assemblies, components and VHM indicators given in Table 1 [42, p. 2-79] may be extended with hydraulic machines and their shafts, bearings, swashplates and pistons.

9.3. Concluding remarks on certification

Due to the low Technology Readiness Level of the presented transmission system, no comprehensive discussion of its certification could be done in this chapter – and doing so would have been

9. Certification according to CS-29

far beyond the scope of this thesis. However, some aspects could be pointed out. Perhaps, the most important finding is that the time and cost efforts for certification will significantly increase because compliance has to be proven for a wide range of main rotor speeds. Since the MR speed affects vibration and controllability, the outcome of some tests or simulations may require a re-design of the drive system – including engines, transmission and rotors. Another issue is raised by the additional mass above the cockpit and the passenger compartment and the high-pressure hydraulic system. At some points, the certification specifications may be extended to cover special issues raised by the new drivetrain.

10. Design/Safety Assessment

A basic design/safety assessment of a Compound-Split module in rotorcraft is carried out in this chapter. The results are based on the ones presented at the 43rd European Rotorcraft Forum (ERF) [84]. However, they were adapted to take the transmission layout, which was not yet known then, into account. This results in different ratings of failure modes.

10.1. Functional FMEA

As method for the assessment of possible failures and countermeasures, a functional FMEA acc. to SAE ARP4761 [110], a standard published by the Society of Automotive Engineers (SAE), was chosen. This standard provides methodology for conducting a comprehensive safety analysis for aircraft and airborne equipment, comprising Failure Hazard Analysis (FHA), Preliminary System Safety Assessment (PSSA) and System Safety Assessment (SSA). The basic types of FMEA as described in [110] are functional and piece-part FMEA. Due to the low TRL of the transmission system to be analysed, only a functional FMEA could be performed. As already stated in section 3.3, the data situation for hydraulic machines used as part of a transmission system and also for planetary gear sets in three-shaft operation in rotorcraft is very poor. Therefore, the study is limited to a qualitative FMEA. However, the required maximum failure rates acc. to AC 29-2C [122] were added as a guideline.

10.1.1. Definition of functions

First of all, the core functions of the different aggregates have to be identified. The study will focus on variable displacement axial piston motors/pumps and planetary gear sets. The functions identified are:

- **pump:** transforms mechanical power (ω, Q) into hydraulic power ($q_v, \Delta p$)
- **motor:** transforms hydraulic power ($q_v, \Delta p$) into mechanical power (ω, Q)
- **planetary gear set:** transmits mechanical power and maintains a given ratio between angular velocities of the shafts.

"Combinations of failures are not usually considered as part of the FMEA" [110, p. 135] and their analysis would require more information on the design of the drivetrain and the reliability of all parts. Therefore, this task is left for future studies.

10.1.2. Possible failures, failure effects and severity

As possible failures of a function, no or disturbed output was identified. The failure effects of each failure mode were evaluated on the aircraft level. According to its effect on the rotorcraft, every failure mode was assigned to one of these five failure effects. The severity of each failure

10. Design/Safety Assessment

effect was rated according to AC 29-2C [122]. The definitions and permissible allowable qualitative and quantitative probabilities of failure are summarized in table 10.1. The possible failure effect

DESCRIPTION	SEVERITY OF FAILURE EFFECT	ALLOWABLE QUALITATIVE PROBABILITY	ALLOWABLE QUANTITATIVE PROBABILITY
Minor			
"Failure conditions which would not significantly reduce rotorcraft safety, and which involve crew actions that are well within the crew capabilities. Minor failure conditions may include, for example, a slight reduction in safety margins or functional capabilities, a slight increase in crew workload, such as routine flight plan changes, or some inconvenience to occupants." (AC 29-2C, p. C-47)	Minor	Reasonably probable	1.0E-3 to 1.0E-5
Major			
"Failure conditions which would reduce the capability of the rotorcraft or the ability of the crew to cope with adverse operating conditions to the extent that there would be, for example, a significant reduction in safety margins or functional capabilities, a significant increase in crew work load or in conditions impairing crew efficiency, or discomfort to occupants, possibly including injuries." (AC 29-2C, p. C-47)	Major	Remote	1.0E-5 to 1.0E-7
Hazardous			
"Failure conditions which would reduce the capability of the rotorcraft or the ability of the crew to cope with adverse operating conditions to the extent that there would be -- (i) A large reduction in safety margins or functional capabilities. (ii) Physical distress or higher workload such that the flight crew cannot be relied upon to perform their tasks accurately or completely. (iii) Serious or fatal injury to a relatively small number of the occupants. (iv) Loss of ability to continue safe flight to a suitable landing site." (AC 29-2C, p. C-47)	Hazardous	Extremely Remote	1.0E-7 to 1.0E-9
Catastrophic			
"Failure conditions which would prevent a safe landing." (AC 29-2C, p. C-47)	Catastrophic	Extremely Improbable	< 1.0 E-9

Table 10.1.: Severity of failure modes acc. to AC 29-2C (cf. [122])

categories have already been used in [84] in a similar form. They are:

1 Limited power transfer

description: This failure effect is characterized by the fact, that the power transfer in the variator path is limited. The transmission ratio can either be changed only in a certain region due to the lack of power or the transferable power is limited. But the rotorcraft can still be operated because the main power flow is on the mechanical path.

occurrence: This failure effect occurs for the failure modes *low output parameter* and in the

failure mode *high rotational speed* of the function **hydraulic motor**.

severity: It is defined as a *major* failure of the system.

2 No power transfer

description: In this failure effect, there is a cut-off of the power transfer from one turboshaft engine to the rotor. All parts are free to rotate and power from the second engine is still transmitted to main and tail rotor.

occurrence: This failure effect occurs in the failure modes *no output parameter* except for the failure mode *no rotational speed* of the function **hydraulic motor**. Also, for the failure mode *breakage of any shaft* of the function **planetary gear set**, this failure effect occurs.

severity: It is defined as a *hazardous* failure of the system.

3 No power transfer and damage on drive train

description: A cut-off of the power transfer from one turboshaft engine to the rotors occurs. But in this effect, at least one shaft is not free to rotate. As a consequence, additional damage to the drivetrain and a possible prevention of safe landing occur.

occurrence: This failure effect occurs in the function **planetary gear set** if the failure modes *driven shaft, driving shaft or gear set gets stucked*.

severity: It is defined as a *catastrophic* failure of the system.

4 Poor efficiency

description: This failure effect decreases the efficiency of the variator path but beyond that has no influence on the functionality of the Compound-Split.

occurrence: This failure effect occurs for the failure modes *high output parameter* except in the failure mode *high rotational speed* of the function **hydraulic motor**.

severity: It is defined as a *minor* failure of the system.

5 Fixed transmission ratio

description: The Compound-Split loses its ability to change the transmission ratio from the turboshaft engine to the rotor. Therefore, the system is working like a transmission system with fixed ratio.

occurrence: This failure effect occurs in the failure mode *no rotational speed* of the function **hydraulic motor**. Also, the failure mode *variator shaft gets stucked* of the function **planetary gear set** leads to this failure effect.

severity: It is defined as a *hazardous* failure of the system.

10.2. Results of FMEA

The FMEA was performed using the worksheet provided in [110, p. 139] as a baseline. Columns containing possible countermeasures were added and a re-evaluation under consideration of them was carried out. The results for the hydraulic machines and for the planetary gear sets are summarized in

Table 10.2.: Design assessment of hydraulic machines (see p. 142)

Table 10.3.: Design assessment of planetary gear sets (see p. 143)

For the pump two basic failure modes were identified. These are inadequate output pressure and flow. The possible causes and consequences of both basic failures are similar and in many cases

they will occur coincident. However, they are not fully equivalent and therefore will be discussed separately. A comprehensive analysis of the failure modes based on tests and operating experience will lead to a better understanding of the failure modes and provide an improved base for the FMEA.

Each failure mode can occur as low and high values or a complete lack of the output quantity. The effect severities on the rotorcraft level range from hazardous to minor. A loss of pressure or flow prevents the transmission of power resp. the counteraction of the torques acting on the Compound-Split module. This leads to a disconnection of the input bevel gear stage and the combining bevel gear stage in the power path of one turboshaft engine, which is equivalent to an undefined transmission ratio. As already stated, a portion of power may be transferred via the tail rotor drive, but basically, the consequences are the same as in OEI case. Therefore, these failure modes are rated as *hazardous*. Loss of flow or pressure can be easily detected by pressure or flow indicators, which are common in rotorcraft, e.g., in the lubrication system. Possible failure causes are problems with the displacement control – the functional principle and design of which is not yet determined – or leakage. To limit the effects of the failure, overrunning clutches resp. brakes can be installed between pump or motor shaft and the housing to block the rotation of one of them and be able to operate the drivetrain in a mechanical point. If this countermeasure works reliably, the severity of loss of pressure or flow may be reduced to *major*.

The failure modes of too high resp. too low output values are similar to and may have the same causes as a total loss. Their severity strongly depends on the remaining power which can be transmitted from the turboshaft engine to the main rotor by the Compound-Split module. In case that it is sufficient to continue the flight state in which the failure occurred (or is detected by the crew), the severity of low values is probably *major* whilst high values can be rated as *minor* incidents – otherwise, the failure may be treated as a loss of the output quantity. The reason for the rating of the high value cases is the fact that working safety valves may prevent any dangerous increase of pressure. As compensating actions an adjustment of the drivetrain management or an operation with a limited range of transmission ratios are possible. For low as well as for high output values, these measures may reduce the severity of an incident by one category.

The failure analysis of the hydraulic motor follows the same pattern as described for the pump. The output quantities are angular velocity and torque. The effects of a loss of one of them is an undefined transmission ratio. The countermeasures are the same as for the pump: overrunning clutches or brakes. With the possibility of flight with a transmission ratio fixed to one of the mechanical points, the severity of such an incident may be *major* instead of *hazardous*. However, a reliable system blocking one of the variator shafts is another complex system which would have to be added to the drivetrain and which also requires tests and certification. Furthermore, it will increase the drivetrain mass and lead to increased costs for inspection and maintenance. Therefore, a consequent minimization of the probability of failure may be the better way to fulfil the certification requirements.

The failure modes representing too low resp. too high angular velocities/torques are all rated as *minor* resp. *major* failures. To counter the effects of low/high output, the drivetrain management could be adapted – automatically or by the pilot. As for the other cases, overrunning clutches may limit the transmission range. With this measure, the severity ratings may be reduced. However, because of additional technical and safety issues as well as because of additional mass and costs, highly reliable variator systems in Compound-Split modules seem far preferable.

The third function to be analysed is the planetary gear set. Its input and output are not as straight forward as for the hydraulic machines. In principle, its functionality is to fulfil the Willis equation (2.1) and to bear and transmit the resulting torques. The least severe failure poses the blocking of one of the two variator – i.e., pump or motor – shafts. In that case, the rotorcraft can be still operated at a fixed transmission ratio in a mechanical point or in an OEI mode. However, since the blocking of a variator shaft is not comparable to the intended operation in a MP and the shaft may break or start rotating again, the incident is to be considered as *hazardous*. If the stucked shaft is blocked with an additional device, such as an overrunning clutch or a brake, the severity rating may be reduced. The breakage of any shaft without blocking the transmission system entails another *hazardous* failure mode. To counteract the resulting undefined transmission ratio and restore power transfer from the affected engine, the clutch/brake system can be used.

In difference to the two functions of the hydraulic variator, the PGS involves catastrophic failure modes preventing a safe landing of the rotorcraft. Those occur if the rotation of the rotors is hindered or blocked by a failed part of the mechanical path of the Compound-Split module. Of course, this is the case when input or output shaft cannot rotate freely or the relative motion of the gears in the PGS is hindered, e.g., by a broken off tooth. The only way to limit the consequences of such an incident would be a device to disconnect the blocked part from the rotors. For example, clutch systems or defined breaking points could be designed. However, the machine elements involved in a PGS in three-shaft operation have been used in rotorcraft for decades and pose proven solutions. The most challenging part will probably be the lubrication system and the operation of the transmission system after a failure of it.

10.3. Concluding remarks of the Design/Safety Assessment

Due to the low Technology Readiness Level, the FMEA used for a design and safety assessment has to stay rudimentary. Nevertheless, the most important risks caused by a Compound-Split module with hydraulic variator could be identified and rated. They have been systematically recorded and assigned to one of five failure effects on rotorcraft level. As could be expected, malfunctions of the transmission system pose significant danger to the rotorcraft. Consequently, nine out of seventeen failure modes were rated as hazardous or even catastrophic. To mitigate the effects of failure, countermeasures were proposed. They involve additional complex devices and raise further issues concerning the certification. If, however, a clutch or brake is installed to relieve the hydraulic path during operation in a mechanical point anyway, it may be used to counteract failures and increase safety.

FUNCTION NAME	FAILURE MODE	FAILURE EFFECT	FAILURE EFFECT CATEGORY	DETECTION METHOD	POSSIBLE CAUSE	SEVERITY OF FAILURE EFFECTS (AC 29-2C)	ALLOWABLE QUALITATIVE PROBABILITY (AC 29-2C)	ALLOWABLE QUANTITATIVE PROBABILITY (AC 29-2C)	COMPENSATING ACTIONS	Severity of failure after compensation action
Hydrostatic pump	loss of pressure	no power transfer, undefined transmission ratio	2	pressure indicator	e.g., failure of displacement control, leakage	Hazardous	Extremely Remote	1.0E-7 to 1.0E-9	overrunning clutch between shaft and housing or energy storage	Major
	low pressure	limited power transfer and range of transm. ratios, poor efficiency	1	pressure indicator	e.g., failure of displacement control, leakage	Major	Remote	1.0E-5 to 1.0E-7	adjustment of drivetrain management, operation with limited transm. ratio	Minor
	high pressure	poor efficiency, increase of temperature	4	pressure indicator	e.g., failure of displacement control	Minor	Reasonably probable	1.0E-3 to 1.0E-5	adjustment of drivetrain management, operation with limited transmission ratio, pressure valve	No effect
	no flow rate	no power transfer, undefined transmission ratio	2	flow display	e.g., failure of displacement control, leakage	Hazardous	Extremely Remote	1.0E-7 to 1.0E-9	overrunning clutch between shaft and housing	Major
	low flow rate	limited power transfer and range of transm. ratios, poor efficiency	1	flow display	e.g., failure of displacement control, leakage	Major	Remote	1.0E-5 to 1.0E-7	adjustment of drivetrain management, operation with limited transmission ratio	Minor
	high flow rate	poor efficiency, increase of temperature	4	flow display	e.g., failure of displacement control	Minor	Reasonably probable	1.0E-3 to 1.0E-5	adjustment of drivetrain management, operation with limited transmission ratio, pressure valve	No effect
Hydrostatic motor	no rotational speed (stucked)	fixed transmission ratio	5	RPM counter	e.g., seizure, bearing damage	Hazardous	Extremely Remote	1.0E-7 to 1.0E-9	overrunning clutch between shaft and housing	Major
	low rotational speed	limited power transfer and range of transm. ratios, poor efficiency	1	RPM counter	e.g., failure of displacement control	Major	Remote	1.0E-5 to 1.0E-7	overrunning clutch between shaft and housing	Minor
	high rotational speed	limited power transfer and range of transm. ratios, poor efficiency	1	RPM counter	e.g., failure of displacement control	Major	Remote	1.0E-5 to 1.0E-7	overrunning clutch between shaft and housing	Minor
	no torque	no power transfer, undefined transmission ratio	2	torque meter	e.g., failure of displacement control, shaft broken	Hazardous	Extremely Remote	1.0E-7 to 1.0E-9	overrunning clutch between shaft and housing or energy storage	Major
	low torque	limited power transfer and range of transm. ratios, poor efficiency	1	torque meter	e.g., failure of displacement control	Major	Remote	1.0E-5 to 1.0E-7	adjustment of drivetrain management, operation with limited transmission ratio	Minor
	high torque	poor efficiency, increase of temperature	4	torque meter	e.g., failure of displacement control	Minor	Reasonably probable	1.0E-3 to 1.0E-5	adjustment of drivetrain management, operation with limited transmission ratio	No effect

FUNCTION NAME	FAILURE MODE	FAILURE EFFECT	FAILURE EFFECT CATEGORY	DETECTION METHOD	POSSIBLE CAUSE	SEVERITY OF FAILURE EFFECTS (AC 29-2C)	ALLOWABLE QUALITATIVE PROBABILITY (AC 29-2C)	ALLOWABLE QUANTITATIVE PROBABILITY (AC 29-2C)	COMPENSATING ACTIONS	Severity of failure after compensation action
Epicyclic gear set	driving shaft gets stucked	no power transfer from TSE to rotor, consequential damages to drivetrain	3	RPM counter	e.g., seizure, bearing damage	Catastrophic	Extremely Improbable	< 1.0 E-9	predetermined breaking point	Hazardous
	driven shaft gets stucked	no power transfer from TSE to rotor, consequential damages to drivetrain	3	RPM counter	e.g., seizure, bearing damage	Catastrophic	Extremely Improbable	< 1.0 E-9	predetermined breaking point	Hazardous
	variator shaft gets stucked	fixed transmission ratio	5	RPM counter	e.g., seizure, bearing damage	Hazardous	Extremely Remote	1.0E-7 to 1.0E-9	overrunning clutch/brake between shaft and housing	Major
	gear set gets stucked	no power transfer from TSE to rotor, consequential damages to drivetrain	3	RPM counter	e.g., tooth break, bearing damage	Catastrophic	Extremely Improbable	< 1.0 E-9	predetermined breaking point	Hazardous
	breakage of any shaft	no power transfer, undefined transmission ratio	2	RPM counter, torque meter	shaft breakage	Hazardous	Extremely Remote	1.0E-7 to 1.0E-9	overrunning clutch/brake between shaft and housing	Major



Die approbierte gedruckte Originalversion dieser Dissertation ist an der TU Wien Bibliothek verfügbar.
The approved original version of this doctoral thesis is available in print at TU Wien Bibliothek.

Summary



Die approbierte gedruckte Originalversion dieser Dissertation ist an der TU Wien Bibliothek verfügbar.
The approved original version of this doctoral thesis is available in print at TU Wien Bibliothek.

11. Summary

In this concluding chapter, the findings of the study are summarized and compared to the aims defined in section 1.4. It is discussed, to what extent the research questions could be answered and what had to be left for follow-up studies. At the end, conclusions are drawn from the research work presented in this thesis. The core findings and their meaning for the development of a variable-ratio transmission system for rotorcraft will be pointed out. Finally, open questions, especially the ones which arose during the work on the research project VARI-SPEED, are summarized and an outlook for future research is given.

11.1. Results, discussion and conclusion

In the introduction of this thesis four main objectives of the research were stated. Each of them was addressed in a dedicated part of the thesis.

The first aim was to give a comprehensive summary of the fundamentals of epicyclic gearing, to state the basic equations and derive the mathematical relations which will be needed to find a suitable drivetrain concept in the subsequent chapters. Because of the sheer amount of available literature and the multitude of research fields – ranging from efficiency, manufacturing and damage analysis to acoustics – a choice of the topics to be discussed had to be made. The selected information and equations dealing with epicyclic gearing and power-split transmissions pose a viable basis for the further study and therefore, the aim of part is considered achieved.

Another main question of the study in hand was the one for a principal drivetrain architecture for a rotorcraft of CS-29 class, more precisely for the UH-60 Black Hawk. To reduce the literally infinite number of possible solutions and to avoid raising issues, which would lead beyond the scope of the study, some constraints had to be made. Because they are directly influencing the outcome of the whole study and also determine research questions for future studies, they are summarized again in the following.

1. The rotational speed of the tail rotor shall be kept constant at the value of the reference helicopter.
2. The two free-wheeling units shall be operated at the same speed and torque levels as in the baseline UH-60.
3. The accessories shall be driven at constant speed.

These constraints lead to two possible architectures, one containing one Compound-Split module and the other with two of them, one in the power path of each turboshaft engine. The decision between these two solutions was made based on an assessment of their respective reliability. Since the architecture with two CS modules is expected to provide a higher safety level, it was decided

11. Summary

to concentrate on it in the study in hand. Subsequently, the arrangement of the CS modules was chosen based on the expected mass of the planetary gear sets and the maximum relative speed of planet gears. With the decision for arrangement **D** and axial piston motors with variable displacement as variator machines, it was possible to derive the key parameters of the transmission system and study the expected overall drivetrain efficiency.

In the design part a promising drivetrain architecture could be derived and it could be shown, that its efficiency is, although lower than the one of the baseline helicopter, sufficient for the use in a rotorcraft with variable main rotor speed. It has to be stressed, that the found solution is not the only possible and that the complete new-design of a helicopter with variable rotor speed will probably yield a totally different arrangement. However, to show the feasibility of Compound-Split modules in rotorcraft drivetrains, the derived architecture is sufficient. A key aspect of transmission systems in rotorcraft is their mass. Although a basic design of the drivetrain has been developed in this study and an estimation of the variator mass has been derived, no viable assessment of the expected mass was made. The reason is again the low Technology Readiness Level. Too much parameters are unknown at the moment. However, based on the derived dimensions of the mechanical path and the variators, the transmission system may reduce the payload, but will be definitely light enough for flight. If it is economically justifiable, cannot be rated at the moment.

To prove that the proposed drivetrain is able to transmit the propulsive power and vary rotor speed in flight conditions, a dynamic simulation was carried out. First of all, a calculation model had to be built up in Simulink, using rotor and engine models found in the literature. The model was validated with flight test data and showed good agreement for constant main rotor speed. It was therefore concluded, that the simulation for different and varying rotor speeds pose a good approximation of the physical system. The results showed that the proposed transmission system is able to maintain a target MR speed for several flight conditions. The limits of operation, i.e., flight states which could not be maintained and lead to premature termination of the simulation, showed good agreement to the predictions of other studies, which identified stall at parts of the MR blades as the limiting factor. Therefore, it could be concluded that the reason for these phenomena is the main rotor system and not the powertrain. However, a series helicopter with variable main rotor speed will require a totally newly developed rotor system anyway.

The last aim of the thesis in hand was to discuss the implications of the proposed powertrain on the certification of a rotorcraft which is equipped with it. By the very nature of this question, no concluding answers could be expected, because the certification process would be completely new to aviation authorities and helicopter manufacturers. Furthermore, new requirements and specifications would have to be issued and appropriate means of compliance would have to be defined. However, some fundamental aspects could be pointed out, especially the fact that due to the increased demand for testing, the costs of the certification process of rotorcraft with variable main rotor speed will be significantly higher than for conventional helicopters. In addition, the conducted safety assessment of the Compound-Split module showed, that a failure of this system poses a great threat to the rotorcraft and its occupants. Some measures to limit the consequences of a failure could be found. However, the consequent minimization of failure rates of all components of the CS module seems to be the more promising approach – both from a technical as well as from an economic point of view.

To sum up, all four research questions could be answered satisfactorily. All results are sufficiently reliable to conclude that a drivetrain including two Compound-Split modules is in principle able to enable the variation of main rotor speed of the UH-60 during flight. Based on these findings, further research on Compound-Split transmissions for rotorcraft is justified. However, during the work a lot of questions arose. They will be discussed briefly in the following section.

11.2. Future research and engineering

The development of a ready-for-production rotorcraft transmission system is far beyond the scope of a PhD thesis. Therefore, a lot of research and engineering work still needs to be done. However, with the information gained in this study, the design process of a variable-ratio transmission system comprising Compound-Split modules with hydraulic variators could start. Clearly, the development will be an iterative process and findings from simulations and tests will require changes to the initial draft. Some main aspects, which have to be defined are discussed hereinafter.

- The *required spread* has to be established. Of course, this depends not only on the type of rotorcraft and its mission profile, but also on the rotors. Different designs of them may lead to different speed ranges.
- The main rotor design – including number of blades, blade length and chord, airfoils, twist and mass distribution – is crucial for the performance of the rotorcraft.
- If a MR/TR configuration is chosen, the operation of the *tail rotor* has to be specified. As discussed in section 3.2, constant and variable speed is possible. Of course, this decision has a direct impact on the transmission design.
- Besides the rotors, the *engines* have the most influence on the design of the drivetrain. For this study constant engine speed has been assumed, but a variation may offer additional benefits regarding fuel consumption, cf.[70].
- The analysis of the *variator* system in the thesis in hand is based on data of hydraulic motors designed for the use in mobile machines, such as trucks or excavators. A tailored development for the use in rotorcraft may have different properties, which will have an influence on the drivetrain design.

All of these issues affect the development of the transmission system. In addition, a completely new-design offers much more freedom for the drivetrain architecture, unlike the "minimally invasive" approach which was chosen in this study to limit the possible solutions.

These considerations show, that in principle, the next step of development will be the design of a (scaled) prototype to prove the feasibility of the technology in flight tests. From there, it is still a long way to the certification, series production and operation of a helicopter of CS-29 class with variable rotor speed.



Die approbierte gedruckte Originalversion dieser Dissertation ist an der TU Wien Bibliothek verfügbar.
The approved original version of this doctoral thesis is available in print at TU Wien Bibliothek.

Bibliography

- [1] ANSI/AGMA 6123-B06:2006, Design Manual for Enclosed Epicyclic Gear Drives.
- [2] DIN 3993-1:1981-08, Geometrische Auslegung von zylindrischen Innenradpaaren mit Evolventenverzahnung - Teil 1: Grundregeln.
- [3] DIN 3993-2:1981-08, Geometrische Auslegung von zylindrischen Innenradpaaren mit Evolventenverzahnung - Teil 2: Diagramme über geometrischen Grenzen für die Paarung Hohlrad-Ritzel.
- [4] DIN 3993-3:1981-08, Geometrische Auslegung von zylindrischen Innenradpaaren mit Evolventenverzahnung - Teil 3: Diagramme zur Ermittlung der Profilverschiebungsfaktoren.
- [5] DIN 3993-4:1981-08, Geometrische Auslegung von zylindrischen Innenradpaaren mit Evolventenverzahnung - Teil 4: Diagramme über die Grenzen für die Paarung Hohlrad-Schneidrad.
- [6] DIN 780-1:1977-05, Modulreihe für Zahnräder - Teil 1: Moduln für Stirnräder.
- [7] DIN 780-1:1977-05, Modulreihe für Zahnräder - Teil 2: Moduln für Zylinderschneckengetriebe.
- [8] DIN 867:1986-02, Bezugsprofile für Evolventenverzahnungen an Stirnrädern (Zylinderrädern) für den allgemeinen Maschinenbau und den Schwermaschinenbau.
- [9] DIN 3992:1964-03, Profilverschiebung bei Stirnrädern mit Außenverzahnung.
- [10] AGMA 911-A94:1994, Design Guidelines for Aerospace Gearing.
- [11] ISO 6336-5:2016-08, Calculation of load capacity of spur and helical gears - Part 5: Strength and quality of materials.
- [12] DIN 3961:1978-08, Toleranzen für Stirnradverzahnungen: Grundlagen.
- [13] DOD-PRF-85734A:2004-06, PERFORMANCE SPECIFICATION: LUBRICATING OIL, HELICOPTER TRANSMISSION SYSTEM, SYNTHETIC BASE.
- [14] ISO 6336-1:2006-09, Calculation of load capacity of spur and helical gears - Part 1: Basic principles, introduction and general influence factors.
- [15] ISO 6336-2:2006-09, Calculation of load capacity of spur and helical gears - Part 2: Calculation of surface durability (pitting).
- [16] ISO 6336-3:2006-09, Calculation of load capacity of spur and helical gears - Part 3: Calculation of tooth bending strength.
- [17] DIN 3990-4:1987-12, Tragfähigkeitsberechnung von Stirnrädern - Teil 4: Berechnung der Freßtragfähigkeit.
- [18] VDI 2737:2005-12, Berechnung der Zahnfußtragfähigkeit von Innenverzahnungen mit Zahnkranzeinfluss.

Bibliography

- [19] C. W. J. Acree and C Snyder. "Influence of Alternative Engine Concepts on LCTR2 Sizing and Mission Profile". In: *American Helicopter Society Future Vertical Lift Aircraft Design Conference*. San Francisco, CA, 2012.
- [20] Xiaolan Ai. "Two speed transmission with smooth power shift". Pat. US 7,044,877 B2. 2006.
- [21] Andree Altmikus and Manuel Kessler. "ELECTRICAL POWERED TAIL ROTOR OF A HELICOPTER". Patent Application Publication US 2013/0170985 A1. 2013.
- [22] H. Amri. "Variable Rotor Speed Drivetrain Investigation". PhD thesis. Institute of Engineering Design and Logistics Engineering, Vienna University of Technology, 2018.
- [23] H. Amri, K. Hartenthaler, and M. Weigand. "Mass and Kinematic Analysis of Compound Split with Simulation of the Shifting Process for Variable Rotor Speed". In: *AHS International 74th Annual Forum & Technology Display*. Phoenix, Arizona, USA, 2018.
- [24] H. Amri et al. "Possible Technologies for a Variable Rotor Speed Rotorcraft Drive Train". In: *42rd European Rotorcraft Forum 2016*. Lille, France, 2016.
- [25] Hanns Amri et al. "Übersetzungsvariable Getriebe für Drehflügler – Eine Notwendigkeit für künftige Hubschraubergenerationen?" In: *63. Deutscher Luft- und Raumfahrtkongress*. (In German). 2014.
- [26] Sylvester V. Ashok. "Variable Speed Transmission using Planetary Gear System for High Speed Rotorcraft Application". In: *American Helicopter Society 66th Annual Forum*. 2010.
- [27] Walter Bittner. *Flugmechanik der Hubschrauber - Technologie, das flugdynamische System Hubschrauber, Flugstabilitäten, Steuerbarkeit*. (In German). Springer-Verlag Berlin Heidelberg, 2014.
- [28] William G. Bousman. *Aerodynamic Characteristics of SC1095 and SC1094 R8 Airfoils*. NASA/TP 2003-212265. Moffett Field, California: Ames Research Center, 2003.
- [29] Frank Buyschaert et al. "The Ljungström turbine for aeronautical applications". In: *5th EUROPEAN CONFERENCE FOR AEROSPACE SCIENCES*. 2013.
- [30] Frank Buyschaert et al. "THE TDR HELICOPTER CONCEPT : DESIGN AND INTEGRATION OF THE LJUNGSTRÖM TURBINE". In: *41st European Rotorcraft Forum*. 2015.
- [31] Frank Buyschaert et al. "THE TURBINE DRIVEN ROTOR CONCEPT, A NEW VISION FOR HELICOPTER PROPULSION". In: *40st European Rotorcraft Forum*. 2014.
- [32] Robert T. N. Chen. *An Exploratory Investigation of the Flight Dynamics Effects of Rotor RPM Variations and Rotor State Feedback in Hover*. NASA/Technical Memorandum 83726. Moffett Field, California 94035-1000: NASA Ames Research Center, 1992.
- [33] John C. Coy, D. P. Townsend, and H. H. Coe. *Results of NASA/Army Transmission Research*. Tech. rep. COM-TR-87-C-3. U.S. Army Research and Technology Activity-AVSCOM Lewis Research Center, 1987.
- [34] Anubhav Datta, H. Yeo, and Thomas R. Norman. "Experimental Investigation and Fundamental Understanding of a Slowed UH-60A Rotor at High Advance Ratios". In: *American Helicopter Society 66th Annual Forum*. NASA Ames Research Center, Moffett Field, CA. Virginia Beach, VA, 2011.
- [35] S. Jon Davis. *Predesign Study For a Modern 4-bladed Rotor For the RSRA*. NASA Contractor Report 166155. SIKORSKY AIRCRAFT DIVISION UNITED TECHNOLOGIES CORPORATION, 1981.

- [36] Friedrich List Doblhoff. "JET-DRIVEN HELICOPTER ROTOR". Pat. US 2,667,226 (Hayes, Middlesex, England). 1954.
- [37] Friedrich List Doblhoff. "JET PROPULSION OF HELICOPTERS". Pat. US 2,818,223 (Hayes, Middlesex, England). 1957.
- [38] Friedrich List Doblhoff. "JET ROTATED ROTARY WING AIRCRAFT". Pat. US 2,540,190 (Hayes, Middlesex, England). 1951.
- [39] H. Dong and N.G. Barakos. "Variable Speed Tail Rotors for Helicopters with Variable Speed Main Rotors". In: *42nd European Rotorcraft Forum*. Lille, France, 2016.
- [40] Ahmet Duyar, Gu Zhen, and Jonathan S. Litt. "A Simplified Dynamic Model of the T700 Turboshaft Engine". In: *Journal of the American Helicopter Society* (1995), pp. 62–90.
- [41] Oroitz Elgezabal Gomez. "Heckrotoranordnung". Pat. DE 10 2011 054 849 B3 (51147, Köln, DE). 2013.
- [42] European Aviation Safety Agency. *Certification Specifications for Large Rotorcraft CS-29*. Amendment 5. 2018.
- [43] Dietmar Findeisen. *Ölhydraulik - Handbuch für die hydrostatische Leistungsübertragung in der Fluidtechnik*. Vol. 5. (In German). Springer-Verlag Berlin Heidelberg, 2006.
- [44] Harold Frint. *Automated Inspection and Precision Grinding of Spiral Bevel Gears*. Contractor Report Technical Report 4083. Stratford, Connecticut: Sikorsky Aircraft Division United Technologies Corporation, 1987.
- [45] FVA-Workbench EnterpriseMembersEdition. *5.0.1*. Lyoner Straße 18 60528 Frankfurt (Niederrad): Forschungsvereinigung Antriebstechnik e.V. (FVA), 2018.
- [46] W. Garre, T. Pflumm, and M. Hajek. "Enhanced Efficiency and Flight Envelope by Variable Main Rotor Speed for different Helicopter configurations". In: *42nd European Rotorcraft Forum 2016*. Lille, France, 2016.
- [47] W. Garre et al. "Helicopter Configurations and Drive Train Concepts for Optimal Variable Rotor Speed Utilization". In: *Deutscher Luft- und Raumfahrtkongress 2016*. Braunschweig, Germany, 2016.
- [48] A. Gessow and G. C. Myers. *Aerodynamics of the helicopter*. New York, NY : Ungar, 1978.
- [49] Bill Gunston and Jeff Batchelor. *Hubschrauber: 1900 - 1960*. Ed. by Christy Campbell. (In German). Wilhelm Heyne Verlag, 1977.
- [50] F Hantschack. *FVA-Forschungsvorhaben 389, Rationelle, genaue Analyse der Zahnfußbeanspruchung von Innenzahnradern unter Berücksichtigung des Kranzeinflusses und modifizierter Zahngrundgestaltung*. FVA-Heft 748. (In German). FVA, 2004.
- [51] Michael Karl Heider. "Schwingungsverhalten von Zahnradgetrieben: Beurteilung und Optimierung des Schwingungsverhaltens von Stirnrad und Planetengetrieben". (In German). PhD thesis. Fakultät für Maschinenwesen der Technischen Universität München, 2012.
- [52] Kathrin B. Hilbert. *A Mathematical Model of the UH-60 Helicopter*. NASA/Technical Memorandum 85890. Moffett Field, California: Aeromechanics Laboratory, US Army Research and Technology Laboratories - AVSCOM Ames Research Center, 1984.
- [53] Peter Hofmann. *Hybridfahrzeuge - Ein alternatives Antriebssystem für die Zukunft*. Vol. 2. (In German). Springer Wien Heidelberg New York Dordrecht London, 2014.

Bibliography

- [54] Marie-Laure Hopdjanian et al. "ELECTRICAL ARCHITECTURE FOR A ROTARY WING AIRCRAFT WITH A HYBRID POWER PLANT". Pat. US 8,757,542 B2 (Marignane Cedex (FR)). 2014.
- [55] W. Johnson, G. K. Yamauchi, and Michael E. Watts. "NASA Heavy Lift Rotorcraft Systems Investigation". In: *The 2nd International Basic Research Conference on Rotorcraft Technology*. NASA. Nanjing, China, 2005.
- [56] Jeffrey Frank Jones. *Eurocopter EC145 UH-72 Lakota Helicopter Flight Manual*. U.S. Department Of Defense. 2008.
- [57] A.L. Kapelevich and V.M. Ananiev. "Gear Transmission Density Maximization". In: *Proceedings of the ASME 2011 International Design Engineering Technical Conferences & Computers and Information in Engineering Conference*. 2011.
- [58] Abraham E. Karem. "OPTIMUM SPEED ROTOR". Pat. US 6,007,298. 1999.
- [59] Abraham E. Karem. "OPTIMUM SPEED TILT ROTOR". Pat. US 6,641,365 B2. 2003.
- [60] Nicholas D. Lappos et al. "Variable Speed Gearbox with independently Variable Speed Tail Rotor System". Pat. US 7,434,764 B2. 2008.
- [61] D. G. Lewicki. "Two-Speed Gearbox Dynamic Simulation Predictions and Test Validation". In: *American Helicopter Society 66th Annual Forum*. 2010.
- [62] D. G. Lewicki and Mark A. Stevens. *Testing of Two-Speed Transmission Configurations For Use In Rotorcraft*. Tech. rep. NASA/TM-2015-218816. Cleveland, Ohio: Glenn Research Center, 2015.
- [63] Jonathan S. Litt, Jason M. Edwards, and Jonathan A. DeCastro. *A Sequential Shifting Algorithm for Variable Rotor Speed Control*. NASA/Technical Memorandum 214842. Glenn Research Center, The Boeing Company, Rolls-Royce Corporation, 2007.
- [64] Cesar A. Luongo et al. "Next Generation More-Electric Aircraft: A Potential Application for HTS Superconductors". In: *IEEE Transactions on Applied Superconductivity* 19.3 (2009), pp. 1055–1068.
- [65] Rainer Marquardt. "Trägheitsarmer Direktantrieb hoher Leistungsdichte". Pat. DE 10 2007 013 732 B4 (85521 Riemerling, DE). 2011.
- [66] MATLAB. 9.3.0.713579 (R2017b). Natick, Massachusetts, USA: The MathWorks Inc., 2017.
- [67] *MATLAB Optimization Toolbox Version 8.0 (R2017b)*. The MathWorks, Natick, MA, USA. 2017.
- [68] P.H. Mellor et al. "ELECTRICAL MACHINE TECHNOLOGIES FOR AN ELECTRIC TAIL ROTOR DRIVE". In: *41st European Rotorcraft Forum*. Deutsche Gesellschaft für Luft- und Raumfahrt - Lilienthal-Oberth e.V. 2015.
- [69] Christian Mercier, Marc Gazzino, and Marc Mugnier. "State of the art of Helicopter Hybrid Propulsion". In: *41st European Rotorcraft Forum*. 2015.
- [70] Gianluigi Alberto Misté. "Variable Speed Rotor Helicopters: Optimization of Main Rotor Turboshaft Engine Integration". PhD thesis. Scuola di Dottorato di Ricerca in Ingegneria Industriale, 2015.

- [71] Gianluigi Alberto Misté and E. Benini. “Variable-Speed Rotor Helicopters: Performance Comparison between Continuously Variable and Fixed-Ratio Transmissions”. In: *Journal of Aircraft* 53.5 (2016), pp. 1189–1200.
- [72] Gianluigi Alberto Misté et al. “A Methodology for Determining the Optimal Rotational Speed of a Variable RPM Main Rotor/Turboshaft Engine System”. In: *Journal of the American Helicopter Society* 60.5 (2015), 032009–1 to 032009–11.
- [73] Mihir Mistry and Farhan Gandhi. “Helicopter Performance Improvement with Variable Rotor Radius and RPM”. In: *Journal of the American Helicopter Society* 59 (2014), 042010–10 to 42010–19.
- [74] Andrew M. Mitchell, Fred B. Oswald, and Harold H. Coe. *Testing of UH-60A Helicopter Transmission in NASA Lewis 2240-kW (3000-hp) Facility*. Technical Paper. NASA, 1986.
- [75] Richard E. Moore. “Helicopter Rotor Transmission System”. Pat. US 4,632,337 (Culver City, California). 1986.
- [76] Tim Moser. “Unbemanntes Luftfahrzeug und Antrieb dafür”. Pat. DE 10 2008 014 44 B4 (Niederndorf, CH). 2011.
- [77] Herbert W. Müller. *Die Umlaufgetriebe – Auslegung und vielseitige Anwendungen*. Ed. by G. Pahl. Vol. 28. Konstruktionsbücher. (In German). Springer, 1998.
- [78] Harald Naunheimer, Bernd Bertsche, and Gisbert Lechner. *Fahrzeuggetriebe – Grundlagen, Auswahl, Auslegung und Konstruktion*. 2nd ed. (In German). Springer, 2007.
- [79] Gustav Niemann and Hans Winter. *Maschinenelemente Band 2: Getriebe allgemein, Zahnradgetriebe - Grundlagen, Stirnradgetriebe*. 2nd ed. Vol. II. (In German). Springer, 2003.
- [80] Fred B. Oswald. *Gear Tooth Stress Measurements on the UH-60A Helicopter Transmission*. NASA Technical Paper 2698. NASA, 1987.
- [81] Peter Xavier Palcic, Todd Garcia, and Yuriy Gmirya. “Variable Speed Transmission for a Rotary Wing Aircraft”. Pat. US 7,628,355 B2 (Sikorsky Aircraft Corporation). 2009.
- [82] P. Paschinger and M. Weigand. “Simulation of a Compound-Split Transmission for the UH-60”. In: *44th European Rotorcraft Forum 2018*. Delft, Netherlands, 2018.
- [83] P. Paschinger and M. Weigand. “Study on possible solutions of a Compound-Split transmission system for the UH-60 helicopter”. In: *Mechanism and Machine Theory* 129 (2018), pp. 17–35. DOI: 10.1016/j.mechmachtheory.2018.07.004.
- [84] P. Paschinger et al. “Compound-Split Transmissions for Rotorcraft”. In: *43rd European Rotorcraft Forum 2017*. Milan, Italy, 2017.
- [85] Pierre Paschinger. “Analyse der Betriebsfestigkeit von Getriebestrukturen eines koaxialen Ultraleicht-Hubschraubers mit variabler Rotordrehzahl”. (In German). MA thesis. TU München, 2015.
- [86] Gregor Paulmann and Geneviève Mkadara. “Condition monitoring on hydraulic pumps - lessons learnt”. In: *43rd European Rotorcraft Forum*. 2017.
- [87] Gayle Plutrich. “FARNBOROUGH: Cutaway & technical description: Defying convention - Boeing A160 Hummingbird”. In: *Flightglobal* 178(5248) (2010), pp. 90–94.
- [88] K. Reif and K.E. Noreikat. *Kraftfahrzeug-Hybridantriebe*. Ed. by K. Boorgest. ATZ/MTZ-Fachbuch. (In German). Springer Vieweg, 2012.

Bibliography

- [89] Reliability Analysis Center. *NONELECTRONIC PARTS RELIABILITY DATA*. Dec. 1981.
- [90] M. Robuck and Y. Zhang. *Engine Power Turbine and Propulsion Pod Arrangement Study*. Tech. rep. NASA/CR-2014-216661. Philadelphia, Pennsylvania: The Boeing Company, 2014.
- [91] M. Robuck et al. “Design Study of Propulsion and Drive Systems for the Large Civil TiltRotor (LCTR2) Rotorcraft”. In: *American Helicopter Society 67th Annual Forum*. Virginia Beach, VA, 2011.
- [92] Mark Robuck et al. *The Effect of Rotor Cruise Tip Speed, Engine Technology and Engine/Drive System RPM on the NASA Large Civil Tiltrotor (LCTR2) Size and Performance*. Tech. rep. NASA NNA06BC41C Task Order 10 and NASA NNA09DA56C Task Order 2, 4 and 5. Philadelphia, PA; Indianapolis, IN: The Boeing Company, Rolls-Royce Corporation, 2012.
- [93] Ival O. Salyer. “AIRCRAFT USING TURBO-ELECTRIC HYBRID PROPULSION SYSTEM”. Pat. US 8,727,271 B2 (Flowery Branch, GA (US)). 2014.
- [94] K. Sattelberger. *FVA-Forschungsvorhaben 133 II, Sprungüberdeckung, Einfluss von Verzahnungsabweichungen und -korrekturen auf die Schwingungsanregung schrägverzahnter Getriebe*. FVA-Heft 459. (In German). FVA, 1995.
- [95] Klaus Sattelberger. “Schwingungs- und Geräuschanregung bei ein und mehrstufigen Stirnradgetrieben”. (In German). PhD thesis. Fakultät für Maschinenwesen der Technischen Universität München, 1997.
- [96] Berthold Schlecht. *Maschinenelemente: 2. Getriebe, Verzahnungen, Lagerungen*. 1st ed. Vol. II. (In German). Pearson Studium, 2010.
- [97] W.M.J. Schlösser. “The Overall Efficiency of Positive Displacement Pumps”. In: *Fluid Power Symposium*. Jan. 1969.
- [98] W.M.J. Schlösser. “Über den Gesamtwirkungsgrad von Verdrängerpumpen”. In: *Oelhydraulik und Pneumatik* 12.10 (1968). (In German), pp. 415–420.
- [99] W. Schmidt. *FVA-Forschungsvorhaben 45/I+II, Untersuchungen zur Grübchen- und Zahnfußtragfähigkeit geradverzahnter evolventischer Innenstirnräder*. FVA-Heft 165. (In German). FVA, 1985.
- [100] G. Schönnenbeck. *FVA-Forschungsvorhaben 54/II, Graufleckigkeit*. FVA-Heft 152. (In German). FVA, 1983.
- [101] Daniel P. Schrage et al. *The Assessment of the Capabilities and Limitations of the Flight-Lab Simulation Software in the Prediction of Rotorcraft Component Loads to Support Flight testing*. Contract Report N00421-94-M-3691. Georgia Institute of Technology, 1995.
- [102] M. Schubert. *FVA-Forschungsvorhaben 45/III, Einfluß der Radkranzabstützung und Radkranzdicke auf die Zahnfußspannung innenverzahnter Stirnräder*. FVA-Heft 379. (In German). FVA, 1993.
- [103] Simulink. *Version 9.0 (R2017b)*. Natick, Massachusetts, USA: The MathWorks Inc., 2017.
- [104] C Snyder. “Exploring propulsion system requirements for more and all-electric helicopters”. In: *ISABE-2015-20221*. 2015.
- [105] C. A. Snyder and C. W. Jun. Acree. “Preliminary Assessment of Variable Speed Power Turbine Technology on Civil Tiltrotor Size and Performance”. In: *American Helicopter Society 68th Annual Forum*. 2012.

- [106] C. A. Snyder et al. *Summary of the Large Civil Tiltrotor (LCTR2) Engine Gearbox Study*. NASA/Technical Memorandum 216908. Glenn Research Center, The Boeing Company, Rolls-Royce Corporation, 2010.
- [107] Christopher A. Snyder. *Defining Gas Turbine Engine Performance Requirements for the Large Civil TiltRotor (LCTR2)*. NASA/Technical Memorandum 218101. Cleveland, Ohio: Glenn Research Center, 2013.
- [108] Christopher A. Snyder et al. *Design Study of Propulsion and Drive Systems for the Large Civil TiltRotor (LCTR2) Rotorcraft*. NASA/Technical Memorandum 218102. Cleveland, Ohio: Glenn Research Center, The Boeing Company, Rolls-Royce Corporation, 2013.
- [109] Christopher A. Snyder et al. *Study and Sub-System Optimization of Propulsion and Drive Systems for the Large Civil TiltRotor (LCTR2) Rotorcraft*. NASA/Technical Memorandum 218102. Cleveland, Ohio: Glenn Research Center, The Boeing Company, Rolls-Royce Corporation, 2013.
- [110] Society of Automotive Engineers. *Aerospace Recommended Practice*. ARP4761. 1996.
- [111] Jason H. Steiner. "AN INVESTIGATION OF PERFORMANCE BENEFITS AND TRIM REQUIREMENTS OF A VARIABLE SPEED HELICOPTER ROTOR". MA thesis. The Pennsylvania State University The Graduate School Department of Aerospace Engineering, 2008.
- [112] M. A. Stevens and Robert F. Handschuh. *Variable/Multispeed Rotorcraft Drive System Concepts*. Technical Memorandum 2009-215456. NASA, 2009.
- [113] M. A. Stevens, Robert F. Handschuh, and D. G. Lewicki. *Concepts for Variable/Multi-Speed Rotorcraft Drive System*. Technical Memorandum 2008-215276. NASA, 2008.
- [114] Mark A. Stevens, Robert F. Handschuh, and David G. Lewicki. "Offset Compound Gear inline Two-Speed- Transmission". Pat. US 8,091,445 B1 (Washington, DC (US)). 2012.
- [115] K. Stickels et al. "ADVANCES IN HELICOPTER ELECTRIC TAIL ROTOR DRIVE". In: *43rd European Rotorcraft Forum*. 2017.
- [116] Johannes Stuhlberger et al. "Drive System for Helicopters". Pat. US 9,004,395 B2. 2015.
- [117] Johannes Stuhlberger et al. "Hybrid Drive and Energysystem for Aircraft". Pat. EP 2 571 763 B1. 2017.
- [118] Johannes Stuhlberger et al. "Hybrid Drive for Helicopters". Pat. EP 2 571 763 B1. 2017.
- [119] Ken Torrin, ed. *A guide to Sikorsky UH-60 Black Hawk, technical details, its manufacturer, operators, weaponry, and more*. ISBN:9781276184540. Webster's Digital Services, 2012.
- [120] *UH-60A STUDENT HANDOUT : UH-60A Powertrain/ Rotor System*. United States Army Aviation Warfighting Center. Fort Rucker, Alabama, 2008.
- [121] *UH-60A STUDENT HANDOUT : UH-60A T700 ENGINE*. United States Army Aviation Warfighting Center. Fort Rucker, Alabama, 2007.
- [122] U.S. Department of Transportation, Federal Aviation Administration. *Certification of Transport Category Rotorcraft AC 29-2C*. Change 4. 2014.
- [123] *Variable Plug-in Motor A6VE: Data sheet Series 63*. 06.2012. RE 91606/06.12. Bosch Rexroth AG Mobile Applications.
- [124] *Variable Plug-in Motor A6VE: Data sheet Series 65*. 05.2016. RE 91615/05.16. Bosch Rexroth AG Mobile Applications.

Bibliography

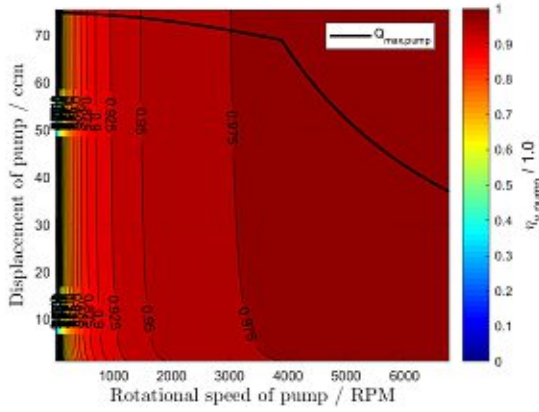
- [125] *Variable Plug-in Motor A6VE: Data sheet Series 71*. 05.2016. RE 91616/05.16. Bosch Rexroth AG Mobile Applications.
- [126] *Variable Plug-in Motor A6VE: Series 65 and 71*. 10.2014. RE 91616-01-B. Bosch Rexroth AG Mobile Applications.
- [127] Mahesh Kumar Varrey. "FEASIBILITY STUDY OF T700 ROTORCRAFT ENGINE ROTOR SUPPORTED BY HYBRID AIR FOIL BEARINGS". Master Thesis. The University of Texas at Arlington, 2011.
- [128] Berend Gerdes van der Wall. *Grundlagen der Hubschrauber-Aerodynamik*. (In German). Springer-Verlag Berlin Heidelberg, 2015.
- [129] Weihua Wang et al. "Analysis on compound-split configuration of power-split hybrid electric vehicle". In: *Mechanism and Machine Theory* 78 (2014), pp. 272–288.
- [130] Hans-Jürgen Warnecke. *Schiffsantriebe – 5000 Jahre Innovation*. (In German). Koehlers Verlagsgesellschaft mbH, 2005.
- [131] Gilbert W. Weden and John C. Coy. *Summary of Drive-Train Component Technology in Helicopters*. NASA/Technical Memorandum 83726. Cleveland, Ohio: Propulsion Laboratory AVSCOM Research and Technology Laboratories Lewis Research Center, 1984.
- [132] G. E. Welch. "Assessment of Aerodynamic Challenges of a Variable-Speed Power Turbine for Large Civil Tilt-Rotor Application". In: *American Helicopter Society 66th Annual Forum*. 2010.
- [133] H. Yeo and W. Johnson. "Comparison of Rotor Structural Loads Calculated Using Comprehensive Analysis". In: *31st European Rotorcraft Forum*. 2005.
- [134] H. Yeo and W. Johnson. "Performance Analysis of a Utility Helicopter with Standard and Advanced Rotors". In: *Journal of the American Helicopter Society* (2004), pp. 250–270.

A. Appendix

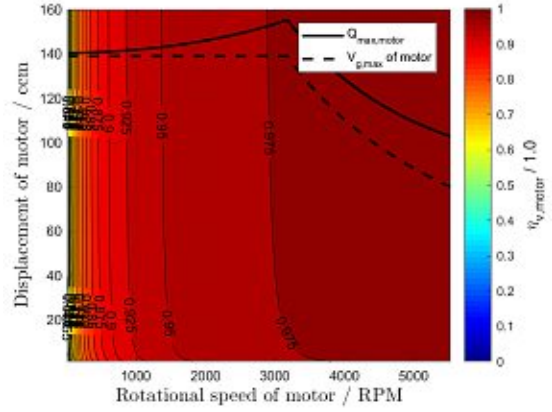
A.1. Characteristics of hydraulic machines

This section provides additional information on the hydraulic machines chosen to be used in the variators of the proposed transmission system.

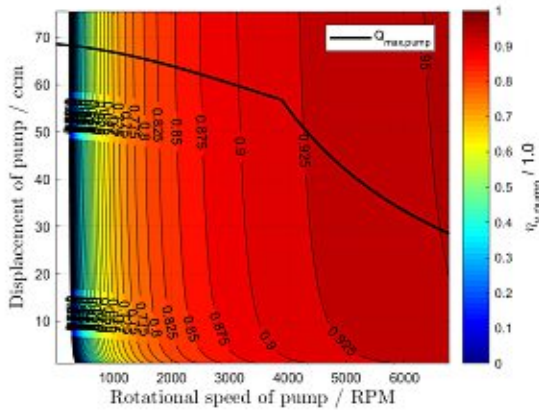
A. Appendix



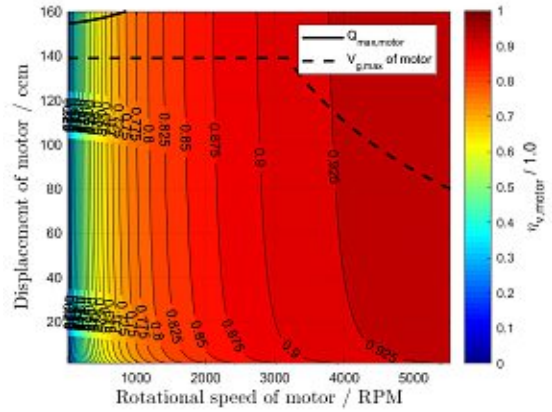
(a) Volumetric efficiency of hydraulic pump, best case



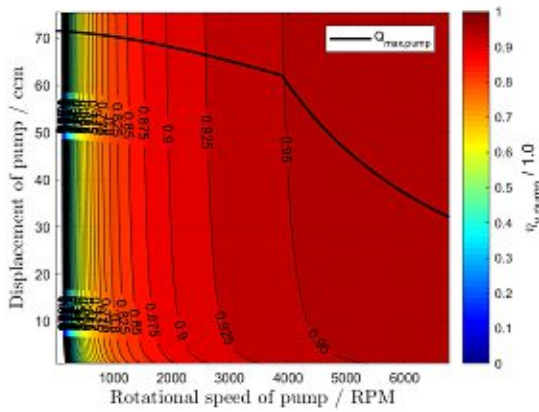
(b) Volumetric efficiency of hydraulic motor, best case



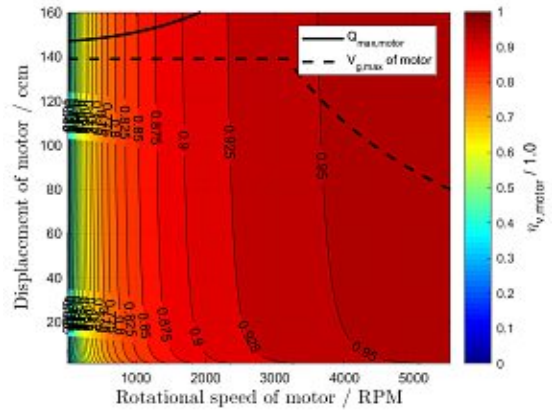
(c) Volumetric efficiency of hydraulic pump, worst case



(d) Volumetric efficiency of hydraulic motor, worst case



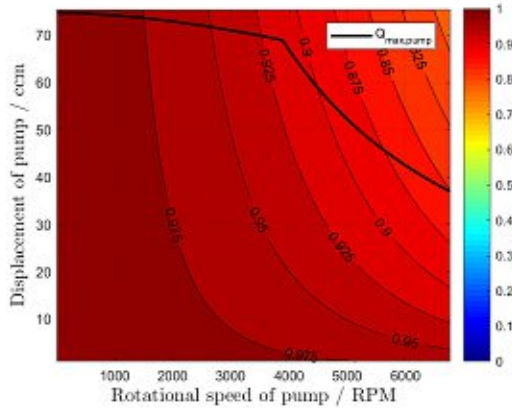
(e) Volumetric efficiency of hydraulic pump, average case



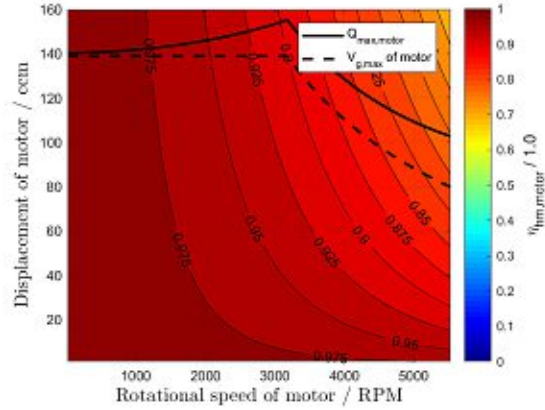
(f) Volumetric efficiency of hydraulic motor, average case

Figure A.1.: Volumetric efficiency of hydraulic machines of the A6VE Series 71 type in pump and motor operation

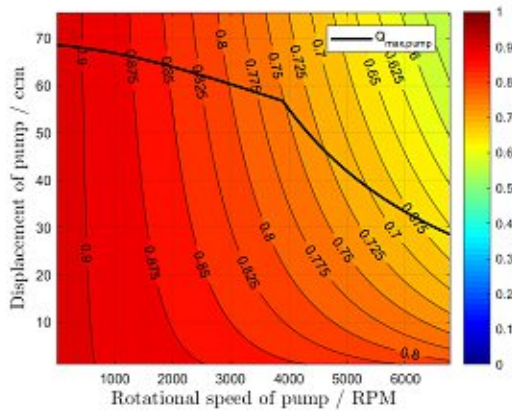
A.1. Characteristics of hydraulic machines



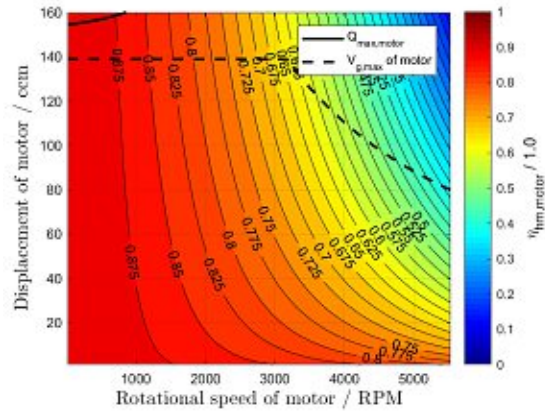
(a) Hydraulic-mechanical efficiency of hydraulic pump, best case



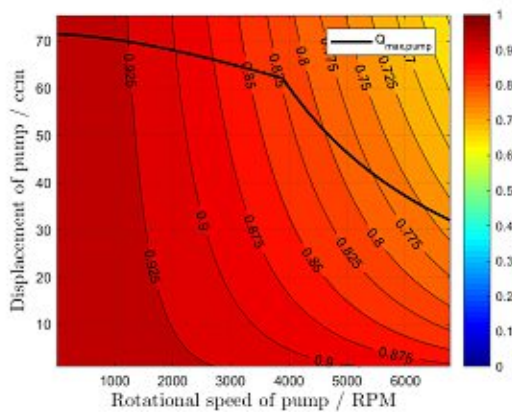
(b) Hydraulic-mechanical efficiency of hydraulic motor, best case



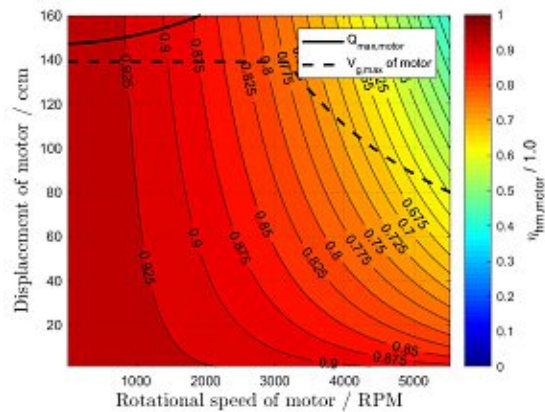
(c) Hydraulic-mechanical efficiency of hydraulic pump, worst case



(d) Hydraulic-mechanical efficiency of hydraulic motor, worst case



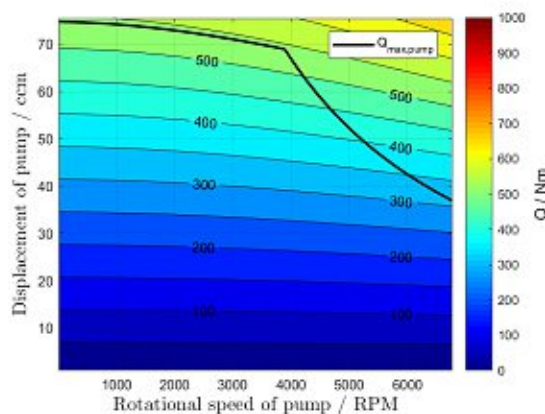
(e) Hydraulic-mechanical efficiency of hydraulic pump, average case



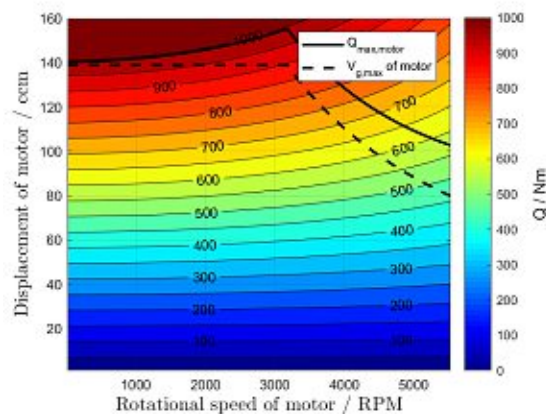
(f) Hydraulic-mechanical efficiency of hydraulic motor, average case

Figure A.2.: Hydraulic-mechanical efficiency of hydraulic machines of the A6VE Series 71 type in pump and motor operation

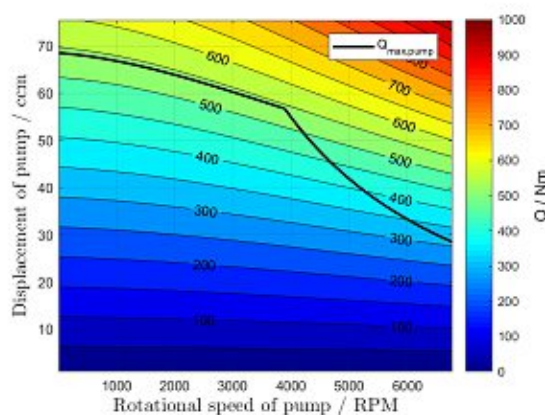
A. Appendix



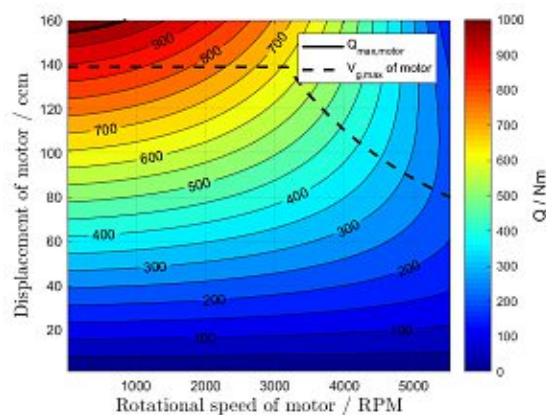
(a) Required torque at pump shaft, best case



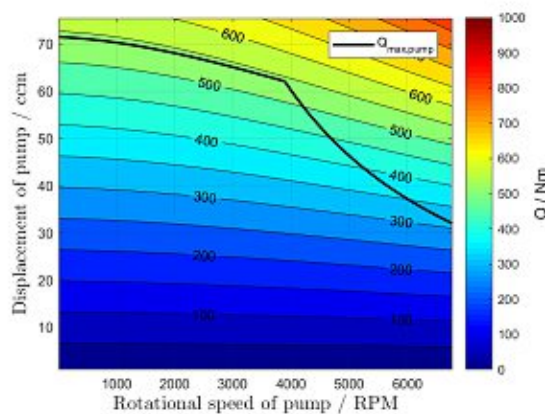
(b) Output torque at motor shaft, best case



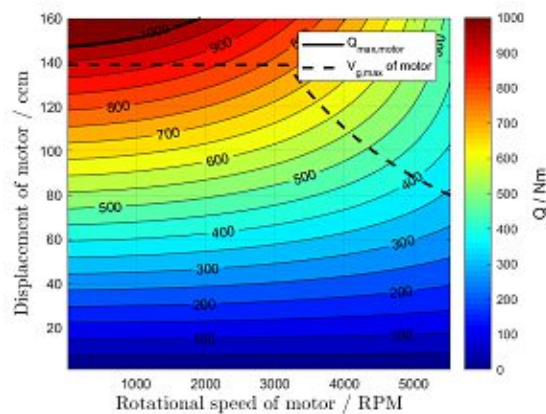
(c) Required torque at pump shaft, worst case



(d) Output torque at motor shaft, worst case

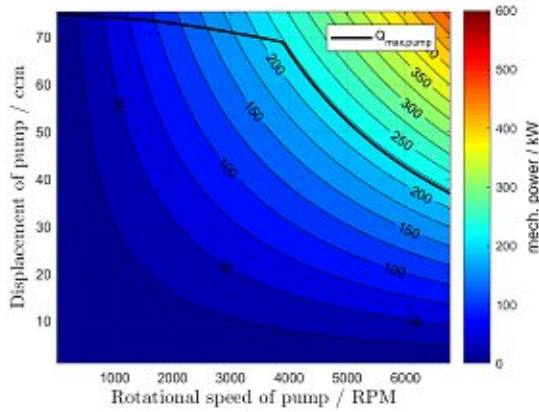


(e) Required torque at pump shaft, average case

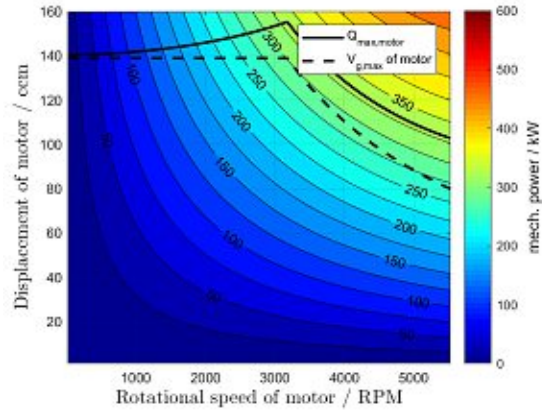


(f) Output torque at motor shaft, average case

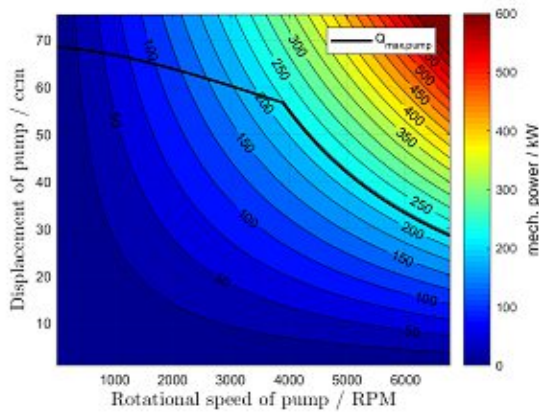
Figure A.3.: Torques of hydraulic machines of the A6VE Series 71 type in pump and motor operation



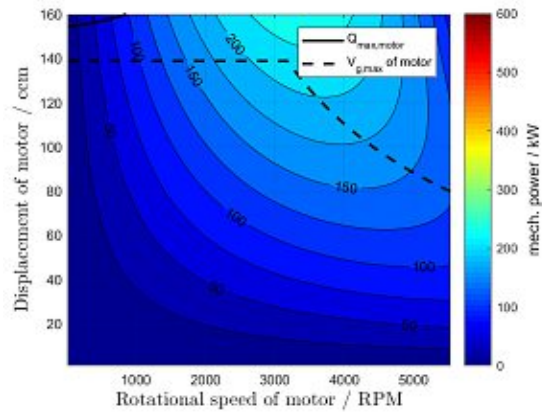
(a) Mechanical input power at pump shaft, best case



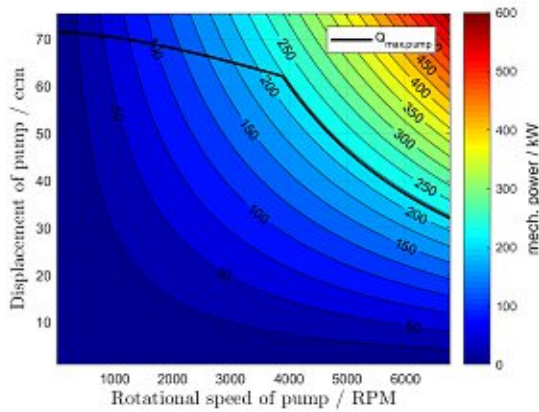
(b) Mechanical output power at motor shaft, best case



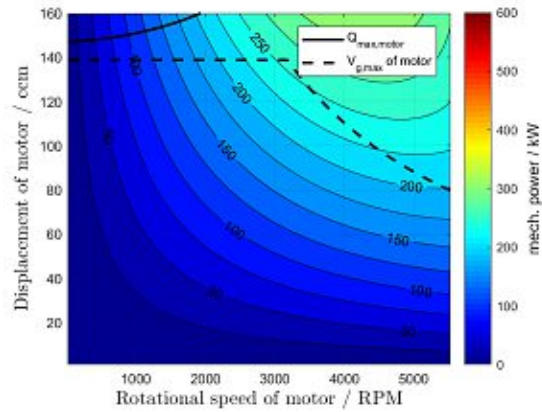
(c) Mechanical input power at pump shaft, worst case



(d) Mechanical output power at motor shaft, worst case



(e) Mechanical input power at pump shaft, best case



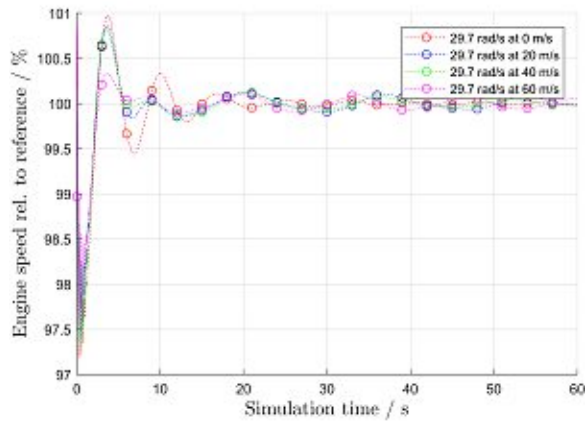
(f) Mechanical output power at motor shaft, average case

Figure A.4.: Mechanical powers of hydraulic machines of the A6VE Series 71 type in pump and motor operation

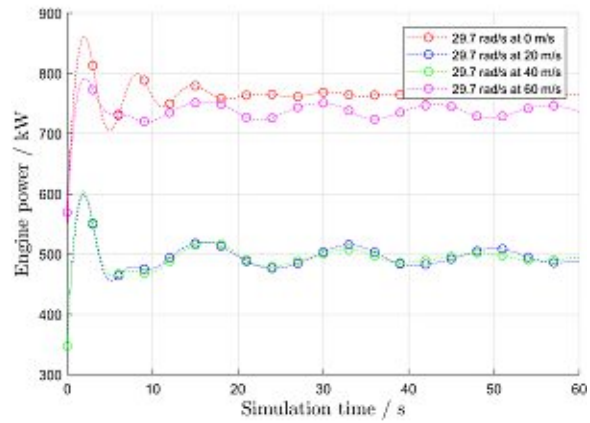
A.2. Additional results of turboshaft engines

This section provides additional information on the parameters of the T700 engines which were obtained by the dynamic simulations of the UH-60's powertrain.

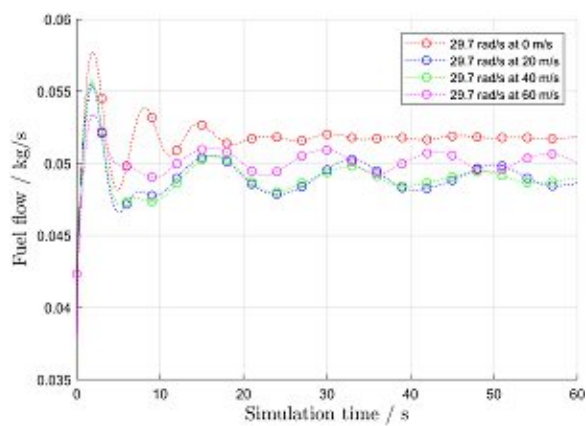
A.2. Additional results of turboshaft engines



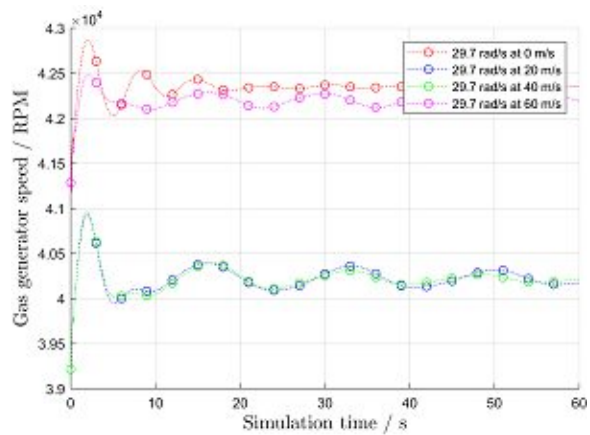
(a) Power turbine speed rel. to reference at MP I



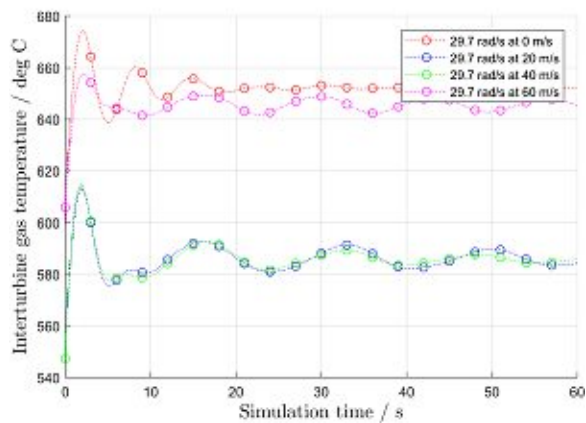
(b) Engine power at MP I



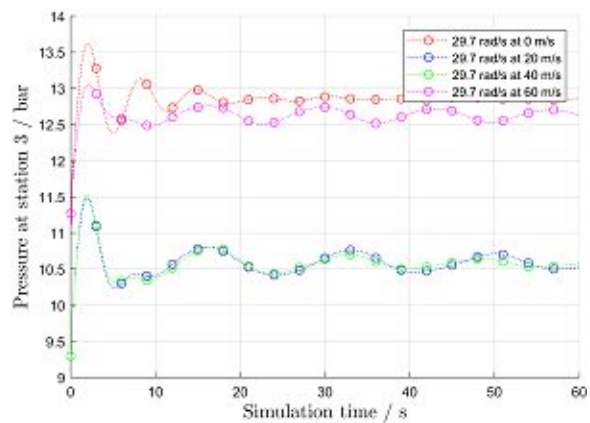
(c) Fuel flow W_F at MP I



(d) Gas generator speed at MP I



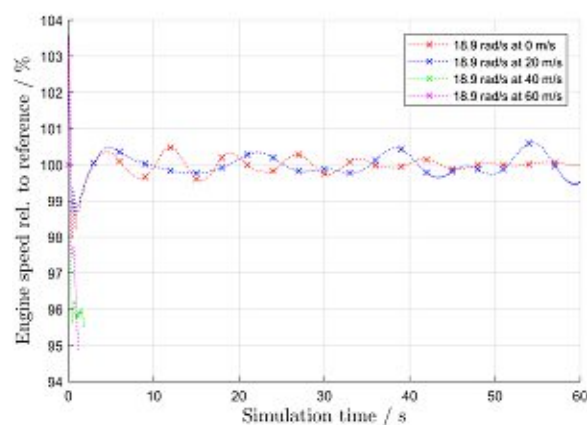
(e) Interturbine gas temperature T_{45} at MP I



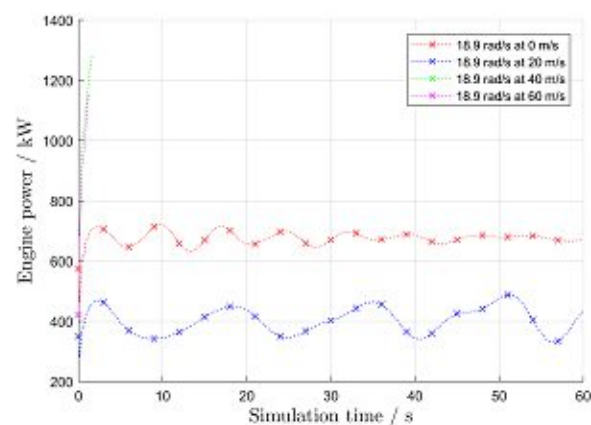
(f) Static pressure at station 3 P_{S3} at MP I

Figure A.5.: Operation parameters of turboshaft engines at MP I

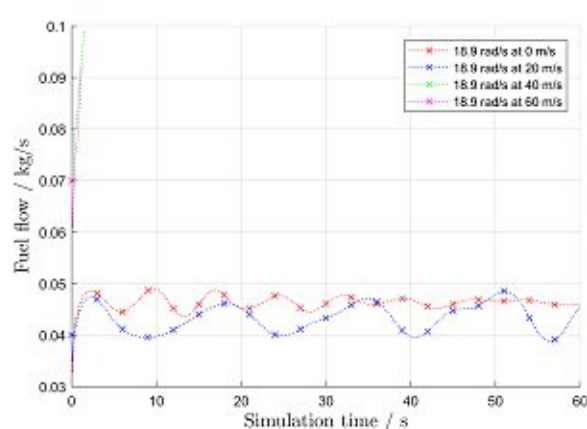
A. Appendix



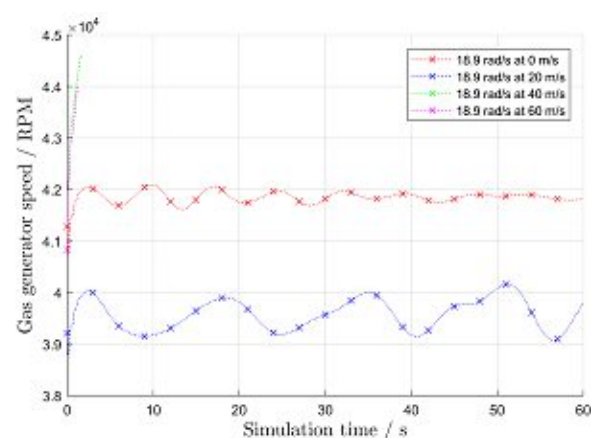
(a) Power turbine speed rel. to reference at MP II



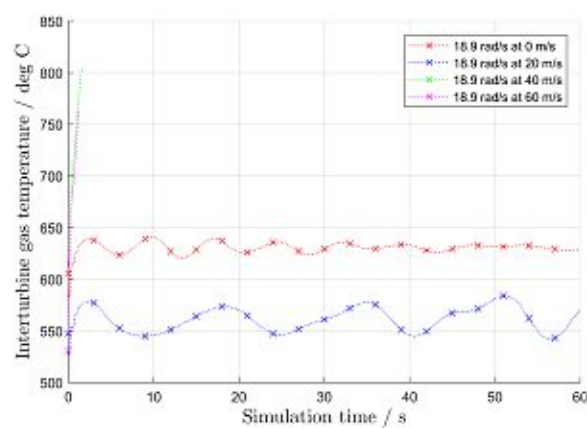
(b) Engine power at MP II



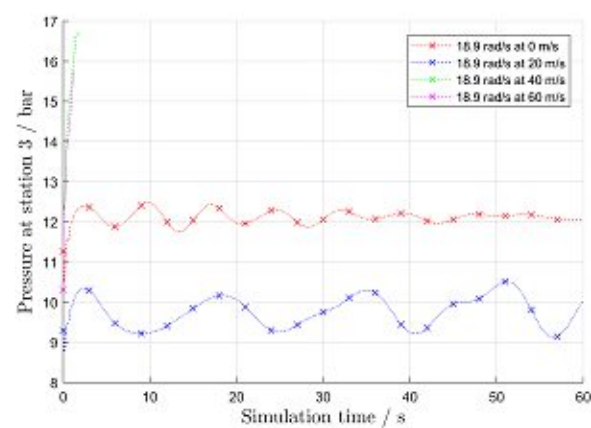
(c) Fuel flow W_F at MP II



(d) Gas generator speed at MP II



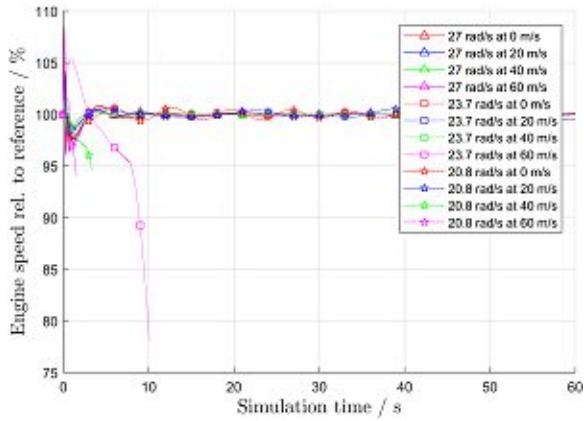
(e) Interturbine gas temperature T_{45} at MP II



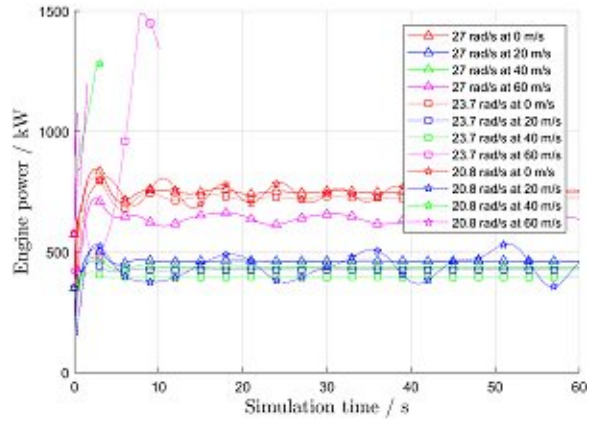
(f) Static pressure at station 3 P_{S3} at MP II

Figure A.6.: Operation parameters of turboshaft engines at MP II

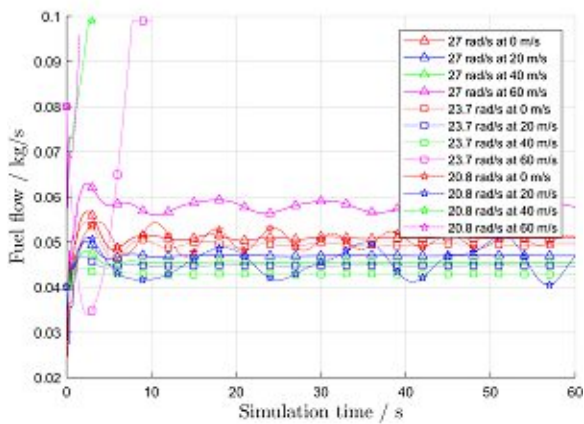
A.2. Additional results of turboshaft engines



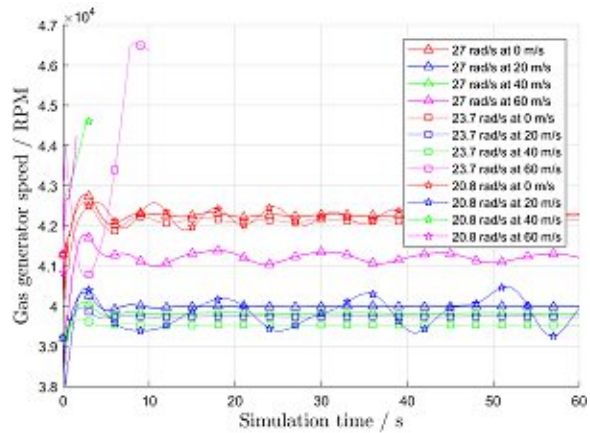
(a) Power turbine speed rel. to reference with hydraulic power transmission



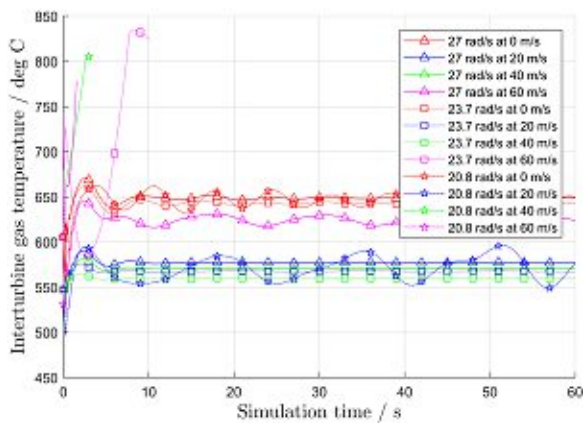
(b) Engine power with hydraulic power transmission



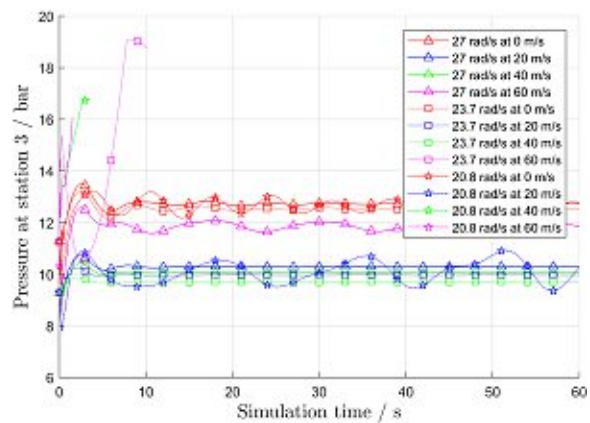
(c) Fuel flow W_F with hydraulic power transmission



(d) Gas generator speed with hydraulic power transmission



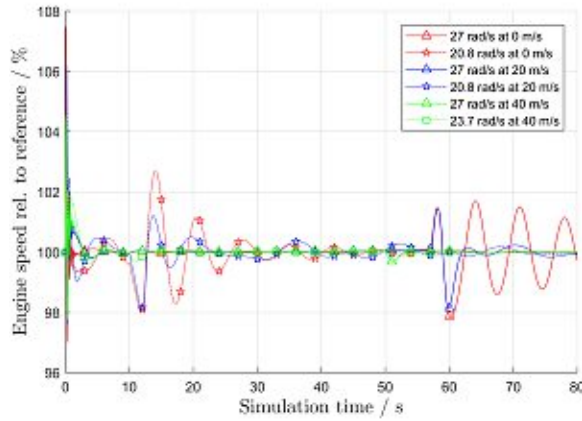
(e) Interturbine gas temperature T_{45} with hydraulic power transmission



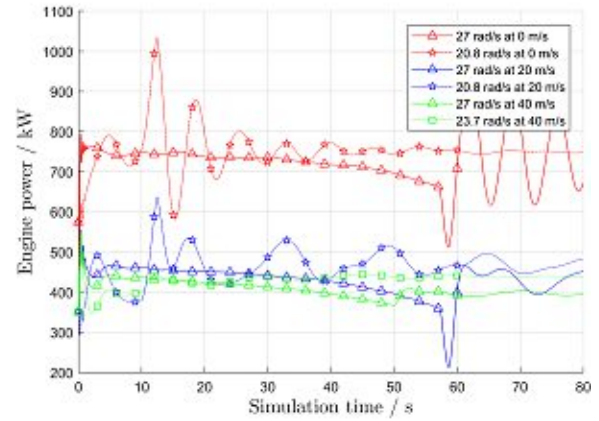
(f) Static pressure at station 3 P_{S3} with hydraulic power transmission

Figure A.7.: Operation parameters of turboshaft engines with hydraulic power transmission

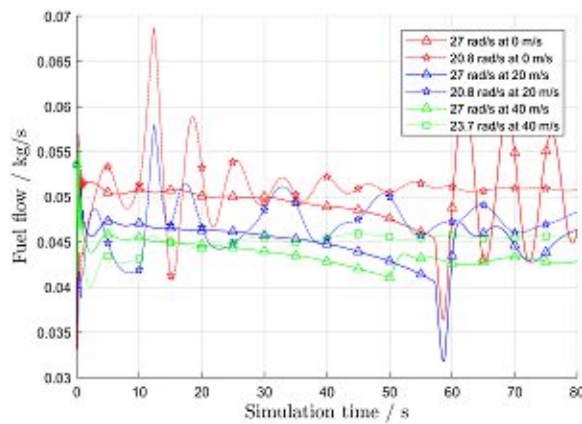
A. Appendix



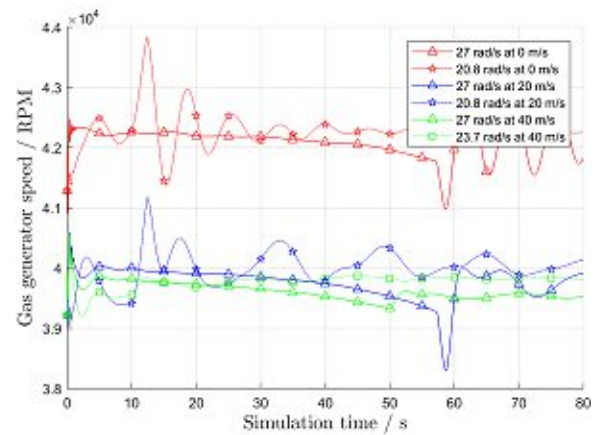
(a) Power turbine speed rel. to reference during change of main rotor speed



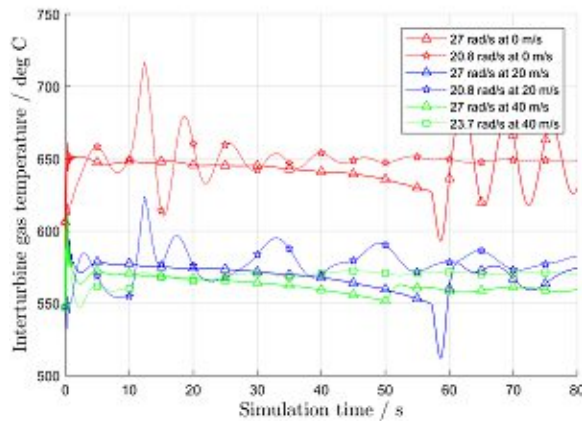
(b) Engine power during change of main rotor speed



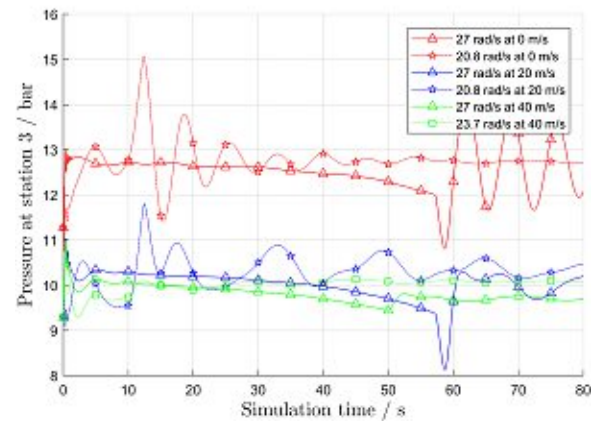
(c) Fuel flow W_F during change of main rotor speed



(d) Gas generator speed during change of main rotor speed



(e) Interturbine gas temperature T_{45} during change of main rotor speed



(f) Static pressure at station 3 P_{S3} during change of main rotor speed

Figure A.8.: Operation parameters of turboshaft engines during change of main rotor speed

A.3. Supplementary

The research work summarized in this thesis required a lot of information and software input which could not be described in detail in the text for reasons of space. To be able to provide these data and to enable an extension of the results, all files used for the study were brought together in a supplementary folder. It is available at the *Institute of Engineering Design and Product Development, TU Wien* or can be requested from the author¹.

The supplementary material is structured into two parts, one containing the material related to the design part and the other dedicated to the dynamic simulation. In the design folder, the FVA-Workbench model, the related scripts and results files can be found. With these files and the software used for the study in hand, all results of chapter 6 can be duplicated. The Simulink models, Matlab calculation of the inflow and input file for multiple simulations are included in the second part of the supplementary. Again, with these files the simulation results of chapter 8 can be reproduced and further flight cases can be studied by adapting the input files.

¹e-mail: ppaschinger@gmx.at



Die approbierte gedruckte Originalversion dieser Dissertation ist an der TU Wien Bibliothek verfügbar.
The approved original version of this doctoral thesis is available in print at TU Wien Bibliothek.

Index

- Addendum of the basic rack for cylindrical gears h_{aP} , 64
- Addendum-factor of the basic rack for cylindrical gears h_{aP}^* , 65
- Advance ratio μ , 83
- Air density ρ_{air} , 82
- Aircraft mass m_{ac} , 86
- Airfoil perpendicular speed in wind axes V_P , 83
- Airfoil SC1094 R8, 80
- Airfoil SC1095, 80
- Airfoil section speed in wind axes V_{AS} , 82
- Airfoil tangential speed in wind axes V_T , 83
- Angle of attack (AoA) α , 82
- Azimuthal blade angle Ψ , 83

- Basic ratio k_{12} , 11
- Basic ratio of epicyclic gear set k_0 , 13
- Bent-axis design, 44
- Blade Element Momentum Theory (BEMT), 80
- Blade element theory, 80
- Blade loading $\frac{c_T}{\sigma}$, 86
- Blade section
 - area, 81
 - length, 81
 - mass, 81
 - radial position, 81
 - twist, 81

- CAMRAD II, 95
- Certification Specification, 127
 - CS 29, 127
- Characteristic curve of hydraulic motors, 45
- Chip detector, 134
- Coefficient of determination R^2 , 50
- Collective pitch angle ϑ_0 , 90
- Compound-Split (CS), 14

- Continuously Variable Transmission (CVT), 14
- Control vector
 - of turboshaft engine model \underline{u} , 79
- Corner power P_{corner} , 47
- Critical part, 131
- Cross-section area of a piston A_{piston} , 44

- Dedendum of the basic rack for cylindrical gears h_{fP} , 64
- Dedendum-factor of the basic rack for cylindrical gears h_{fP}^* , 65
- Density of hydraulic fluid ρ , 53
- Design assessment, 132
- Displacement of axial piston motor V_g , 44
- Drag coefficient C_D , 82
- Drag force F_D , 82
- Dynamic viscosity μ , 53

- Efficiency factor of hydraulic lines η_p , 54
- Epicyclic gear set (EGS), 12
- Epicyclic ratio i_0 , 12
- European Aviation Safety Agency (EASA), 127
- European Rotorcraft Forum (ERF), 137

- Failure effects, 137
- Failure Hazard Analysis (FHA), 137
- Federal Aviation Administration (FAA), 135
- Figure of Merit (FM), 86
- Flapping angle β , 83
- Flapping hinge, 88
- Forschungsvereinigung Antriebstechnik, 67
- Forward speed V , 83
- Fuel flow W_F , 80
- FVA
 - 45, 67
 - 54, 67
 - 389, 67
- FZG load stage

INDEX

- A/8.3/90, 67
- C/8.3/90 (micropitting), 67
- General Electric T700 turboshaft engine, 31
- Generic radial position from hinge \tilde{r} , 81
- Glauert
 - Herrmann, 83
 - Linear inflow model, 83
- Hardness
 - core, 66
 - surface, 66
- Health and Usage Monitoring System (HUMS), 130
- Helix angle β , 69
- Hinge offset e , 81
- Hybrid electric vehicles (HEVs), 14
- Hydraulic flow q_v , 44
- Hydraulic-mechanical efficiency η_{hm} , 44
- Induced inflow parameter λ , 83
- Input-Split (IS), 14
- Interturbine gas temperature T_{45} , 80
- Kinematic viscosity at 100 °C ν_{100} , 67
- Kinematic viscosity at 40 °C ν_{40} , 67
- Lateral cyclic pitch angle ϑ_{1c} , 90
- Lead/lag hinge, 88
- Lens plate, 44
- Lift coefficient C_L , 82
- Lift force F_L , 82
- Load sharing factor K_γ , 37, 68
- Longitudinal cyclic pitch angle ϑ_{1s} , 90
- Loss factor
 - C_{pv} , 53
 - C_{st} , 53
 - C_{sv} , 53
 - C_{tv} , 53
 - C_{vv} , 53
- Lubrication system
 - auxiliary, 135
 - normal-use, 135
- Mach-number Ma , 82
- Mechanical point (MP), 18
- Mesh load factor, *see also* Load sharing factor
- Momentum theory, 80
- Non-dimensional parameter λ , 53
- Non-dimensional parameter σ , 53
- Normal module m_n , 64
- Number of blades N , 86
- Number of pistons Z , 44
- Oil
 - temperature, 67
- One engine inoperative (OEI), 128
- Output-Split (OS), 14
- Output vector
 - of turboshaft engine model \underline{y} , 79
- Overlap ratio ε_β , 69
- Pitch diameter of axial piston motor D_{piston} , 44
- Planetary gear set C , 40
- Planetary gear set D , 40
- Planetary gear set (PGS), 11
- Planetary ratio i_{12} , 11
- Poisson's number ν , 66
- Port plate, 44
- Power coefficient c_p , 94
- Power-Split Transmission (PST), 14
- Preliminary System Safety Assessment (PSSA), 137
- Pressure difference Δp , 44
- Principal Structural Element (PSE), 130
- Profile shift, 63
 - coefficient x , 64
- Relative gas generator speed $\%N_G$, 80
- Relative hinge offset ξ , 83
- Relative power turbine speed $\%N_P$, 80
- Reliability, 65
- Reliability factor
 - for bending strength K_R , 65
 - for pitting resistance C_R , 65
- Root fillet radius of the basic rack for cylindrical gears ρ_{fp} , 64
- Root fillet radius-factor of the basic rack for cylindrical gears ρ_{fp}^* , 65
- Rotor disc area A_{MR} , 83
- Rotor drive system tests
 - Additional, 133
 - Special, 132
- Rotor solidity σ , 86

- Rotor thrust c_T , 83
- SAE ARP4761, 137
- Safety factor
- pitting (ISO 6336) S_H , 68
 - root (FVA 389) $S_{EFVA\ 389}$, 68
 - root (FVA 45) $S_{EFVA\ 45}$, 68
 - root (ISO 6336) S_F , 68
 - root (VDI 2737) $S_{FVDI\ 2737}$, 68
 - scuffing (contact temperature) S_B , 68
 - scuffing (integral temperature) $S_{int\ S}$, 68
- Severity of a failure effect, 137
- Society of Automotive Engineers (SAE), 137
- Spread Φ , 15
- State vector of turboshaft engine model \underline{x} , 80
- Static pressure at station 3 P_{S3} , 80
- Stress number
- allowable (bending) σ_{FE} , 66
 - allowable (contact) $\sigma_{H,lim}$, 66
 - nominal (bending) $\sigma_{F,lim}$, 66
- Stroke of a piston \tilde{h} , 44
- Stroke piston, 44
- Swash-plate design, 44
- Swivel angle $\tilde{\alpha}$, 44
- System Safety Assessment (SSA), 137
- Tail rotor thrust T_{TR} , 86
- Take-off decision point (TDP), 129
- Thrust coefficient c_T , 83
- Tilt angle of fuselage relative to waterline
- α_{WL} , 84
- Tilt angle of main rotor relative to waterline
- α_{MR} , 83
- Tip clearance of the basic rack for cylindrical gears c_p , 64
- Tip clearance-factor of the basic rack for cylindrical gears c_p^* , 65
- Total efficiency of hydraulic machine η_t , 44
- Transmission ratio i_c , 41
- Transmission ratio i_d , 41
- Transmission spread, *see also* Spread
- Variator, 14
- VDI
- 2737, 67
- Verein Deutscher Ingenieure, 67
- Vibration health monitoring (VHM), 135
- Volumetric efficiency η_v , 44
- Weight coefficient c_W , 87



Die approbierte gedruckte Originalversion dieser Dissertation ist an der TU Wien Bibliothek verfügbar.
The approved original version of this doctoral thesis is available in print at TU Wien Bibliothek.

Curriculum vitae of the author

Education

Since 10/2015	Doctoral programme in Engineering Sciences
Since 10/2007	Bachelor's programme: Mathematics in Science and Technology Technische Universität Wien Bachelor thesis: Mathematical considerations on Density Functional Theory and Time-Dependent Density Functional Theory
09/2013 – 10/2015	Master's programme: Mechanical Engineering Technische Universität Wien / Technische Universität München Master thesis: Analysis of strength of gear box structures of a coaxial helicopter with variable rotor speed (In German)
10/2007 – 08/2013	Bachelor's programme: Mechanical Engineering – Management Technische Universität Wien Bachelor thesis: Design and calculation of a high-speed input module of a helicopter transmission (In German)
09/1998 – 06/2006	Secondary school (Realgymnasium) in Waidhofen/Thaya, Austria

Work experience

10/2015 – 06/2019	Project assistant Institute for Engineering Design and Logistics Engineering Technische Universität Wien
09/2015 – 10/2018	Project assistant Zoerkler Gears GmbH & Co KG
03/2015 – 09/2018	Undergraduate research assistant Forschungsstelle für Zahnräder und Getriebebau (FZG) Technische Universität München
10/2012 – 09/2014	Undergraduate project assistant Institute for Engineering Design and Logistics Engineering Technische Universität Wien
04/2012 – 09/2012	Senior Analyst at HQ of KFOR/KOSOVO Foreign deployment with Austrian Armed Forces
10/2006 – 09/2007	Military service